

**Identification of *Arabidopsis* genes involved in differential interaction
phenotype establishment by distinct *Verticillium* spp. and isolates**

Dissertation

zur Erlangung des mathematisch-naturwissenschaftlichen Doktorgrades

"Doctor rerum naturalium"

der Georg-August-Universität Göttingen

im Promotionsprogramm Biologie

der Georg-August University School of Science (GAUSS)

vorgelegt von

Dimitri Stepanets

geboren in

Shitomir, Ukraine

Göttingen 2018

Betreuungsausschuss

1. Betreuer: Prof. Dr. Volker Lipka

Abteilung Zellbiologie der Pflanze, Albrecht-von-Haller Institut für Pflanzenwissenschaften

2. Betreuer: PD Dr. Thomas Teichmann

Abteilung Zellbiologie der Pflanze, Albrecht-von-Haller Institut für Pflanzenwissenschaften

Mitglieder der Prüfungskommission

Referent: Prof. Dr. Volker Lipka

Abteilung Zellbiologie der Pflanze,
Albrecht-von-Haller Institut für Pflanzenwissenschaften

Korreferent: PD Dr. Thomas Teichmann

Abteilung Zellbiologie der Pflanze,
Albrecht-von-Haller Institut für Pflanzenwissenschaften

Weitere Mitglieder der Prüfungskommission

Prof. Dr. Gerhard Braus

Abteilung Molekulare Mikrobiologie und Genetik
Institut für Mikrobiologie und Genetik

Prof. Dr. Andrea Polle

Abteilung Forstbotanik und Baumphysiologie,
Fakultät für Forstwissenschaften und Waldökologie

Jun.-Prof. Dr. Kai Heimel

Abteilung Mikrobielle Zellbiologie,
Institut für Mikrobiologie und Genetik

Dr. Martin Fulda

Abteilung Biochemie der Pflanze,
Albrecht-von-Haller Institut für Pflanzenwissenschaften

Tag der mündlichen Prüfung: 9 April 2018

Promovierenden-Erklärung

1. Die Gelegenheit zum vorliegenden Promotionsvorhaben ist mir nicht kommerziell vermittelt worden. Insbesondere habe ich keine Organisation eingeschaltet, die gegen Entgelt Betreuerinnen und Betreuer für die Anfertigung von Dissertationen sucht oder die mir obliegenden Pflichten hinsichtlich der Prüfungsleistungen für mich ganz oder teilweise erledigt.

2. Hilfe Dritter wurde bis jetzt und wird auch künftig nur in wissenschaftlich vertretbarem und prüfungsrechtlich zulässigem Ausmaß in Anspruch genommen. Insbesondere werden alle Teile der Dissertation selbst angefertigt; unzulässige fremde Hilfe habe ich dazu weder unentgeltlich noch entgeltlich entgegengenommen und werde dies auch zukünftig so halten.

3. Die Richtlinien zur Sicherung der guten wissenschaftlichen Praxis an der Universität Göttingen werden von mir beachtet.

4. Eine entsprechende Promotion wurde an keiner anderen Hochschule im In- oder Ausland beantragt; die eingereichte Dissertation oder Teile von ihr wurden nicht für ein anderes Promotionsvorhaben verwendet.

Mir ist bekannt, dass unrichtige Angaben die Zulassung zur Promotion ausschließen bzw. später zum Verfahrensabbruch oder zur Rücknahme des erlangten Grades führen.



Dimitri Stepanets

Göttingen, 8 Februar 2018

Abstract

Verticillium longisporum induces developmental reprogramming of *A. thaliana* Col-0 leading to transdifferentiation of chloroplast-containing bundle sheath cells to functional xylem elements. Moreover, re-initiation of cambial activity and transdifferentiation of xylem parenchyma cells result in xylem hyperplasia within the *Arabidopsis* vascular system. The *de novo* xylem formation is accompanied by enhanced water storage capacity and enhanced drought tolerance of *V. longisporum* infected plants (Reusche *et al.*, 2012).

Induction of *de novo* xylem formation is not restricted to *V. longisporum*. In a recent study, the interaction phenotypes of *A. thaliana* Col-0 with 47 *V. dahliae* isolates were systematically analysed. Virulent *V. dahliae* isolates fall into two distinct interaction classes, eliciting clearly distinguishable disease phenotypes on *A. thaliana*. Five *V. dahliae* isolates were identified which trigger *V. longisporum*-like symptoms including *de novo* xylem formation, stunted growth, leaf chlorosis and early senescence. In marked contrast, 36 isolates showed *V. dahliae*-like wilting, stunted growth and decay of older rosette leaves (K. Thole, PhD thesis, 2016). These clearly distinguishable disease phenotypes were designated as “chlorosis” and “wilting”. It was postulated that these disease phenotypes are triggered by lineage-specific *Verticillium* effector molecules which induce distinct transcriptional and developmental reprogramming patterns in the host plant (K. Thole, PhD thesis, 2016). In the study conducted by K. Thole several putatively secreted candidate effectors that are differentially expressed *in planta* by chlorosis- and wilting-inducing *V. dahliae* isolates were identified by comparative analyses of the *Verticillium* genome and transcriptome. Using the RNA-sequencing data generated by K. Thole, in this study a plant transcriptome analysis was performed, aiming at the identification of differentially expressed host genes that may be involved in establishment of the chlorosis disease phenotype in response to putative *Verticillium* effectors.

This transcriptome analysis revealed *N. benthamiana* homologs of *Arabidopsis* G-type lectin receptor-like kinase *At5g24080*, NAC domain transcriptional factor *ANAC071* and dehydrin *RD17* as candidate genes that are highly and specifically induced by chlorosis isolate infection. Consequently, homozygous *Arabidopsis* T-DNA insertion mutants were isolated for the three chlorosis induced candidate genes and analysed in detail. Characterisation of the *rd17* mutant demonstrated that the T-DNA insertion had no effect on *RD17* transcript abundance. Disease phenotypes of the G-type lectin receptor-like kinase mutant and NAC domain transcriptional factor mutant were not altered as compared to wild-type, suggesting that corresponding genes are not involved in establishment of the chlorosis disease phenotype.

In silico analyses of publically available microarray data indicated that a number of chlorosis isolate induced candidate genes, among them the G-type lectin receptor-like kinase *At5g24080*, are responsive to abscisic acid (ABA). Quantitative PCR and immunoblot analyses demonstrated an increase in *At5g24080* transcripts as well as AT5G24080-Venus fusion protein levels after exogenous application of ABA. Furthermore, *At5g24080* expression was reduced in the *aba1-101* ABA biosynthesis mutant background during *Verticillium* chlorosis isolate infection. Together these results suggested that ABA might contribute to transcriptional reprogramming during chlorosis isolate infection.

To test this hypothesis, the *Arabidopsis* ABA biosynthesis mutant *aba1-101* was analysed with regard to symptom development established upon infection with a *Verticillium* chlorosis isolate. These experiments demonstrated wilting-like disease symptoms of *aba1-101* mutant plants at 21 days after infection and absence of leaf chlorosis as well as absence of early senescence, indicating that host plant ABA biosynthesis is required for establishment of chlorosis and early senescence symptoms. Notably, bundle sheath cell transdifferentiation was not impaired in the *aba1-101* mutant, suggesting that functional ABA biosynthesis is not required for *de novo* xylem formation. In addition, *aba1-101* mutant plants were less susceptible to *V. dahliae* chlorosis isolate c-V76. HPLC-MS/MS demonstrated that ABA levels are strongly increased in *A. thaliana* Col-0 during *Verticillium* chlorosis isolate infection as compared to mock treatment or wilting isolate challenge, supporting the concept that ABA-dependent (signalling) processes are important for *Verticillium* lineage-specific symptom development. In summary, results of this thesis suggest that ABA contributes to transcriptional reprogramming during chlorosis isolate infection, which leads to establishment of chlorosis and early senescence symptoms. Furthermore, ABA represents a susceptibility factor in *A. thaliana* - *Verticillium* chlorosis isolate interaction.

Zusammenfassung

Die Infektion mit dem phytopathogenen Pilz *Verticillium longisporum* induziert eine entwicklungsphysiologische Reprogrammierung der Wirtspflanze *A. thaliana* Col-0, welche eine Transdifferenzierung der chloroplast-haltigen Bündelscheidenzellen zu funktionsfähigen Xylemelementen zur Folge hat. Zusätzlich resultiert die Wiederaufnahme der kambialen Aktivität und Transdifferenzierung von Zellen des Xylem-Parenchyms in der sogenannten Xylem-Hyperplasie. Die Neubildung von Xylemelementen wird durch eine erhöhte Wasser Speicherkapazität und verbesserte Trockenstresstoleranz *V. longisporum* infizierter Pflanzen begleitet (Reusche *et al.*, 2012).

Die Induktion der Xylem-Neubildung ist nicht nur auf *V. longisporum* beschränkt. In einer kürzlich durchgeführten Studie wurden die Infektionsphänotypen von 47 *V. dahliae* Isolaten auf *A. thaliana* Col-0 systematisch analysiert. Virulente *V. dahliae* Isolate fielen in zwei unterschiedliche Interaktionsklassen, welche deutlich unterscheidbare Infektionsphänotypen auf *A. thaliana* auslösten. Fünf *V. dahliae* Isolate lösten *V. longisporum*-ähnliche Symptome aus, die die Xylemneubildung, Größenreduktion der Rosette (das sogenannte *stunting*), Blattchlorosen und verfrühte Seneszenz umfassen. Im Gegensatz dazu verursachten 36 Isolate *V. dahliae*-ähnliche Welke, *stunting* und das Absterben älterer Blätter (K. Thole, PhD thesis, 2016). Diese klar unterscheidbaren Infektionsphänotypen wurden „Chlorose“ und „Welke“ benannt. Es wurde postuliert, dass diese Infektionsphänotypen durch isolatspezifische *Verticillium* Effektoren ausgelöst werden, welche klar unterscheidbare transkriptionelle und entwicklungsphysiologische Reprogrammierung der Wirtspflanze induzieren (K. Thole, PhD thesis, 2016). In der durch K. Thole durchgeführten Studie wurden in vergleichenden Analysen der pilzlichen Genome und Transkriptome einige potenziell sekretierte Effektorandidaten identifiziert, die durch *V. dahliae* Chlorose- und Welke-Isolate *in planta* differenziell exprimiert werden. Unter Verwendung der durch K. Thole generierten RNA-Sequenzierungsdaten wurde in dieser Doktorarbeit eine Analyse des pflanzlichen Transkriptoms durchgeführt. Dabei sollten differenziell exprimierte Wirtsgene, welche an der Ausprägung des Chlorose Infektionsphänotyps beteiligt sind, identifiziert werden.

In dieser Transkriptomanalyse wurden *N. benthamiana* Homologe der *Arabidopsis* G-type lectin receptor-like Kinase *At5g24080*, des NAC Transkriptionsfaktors *ANAC071* und des Dehydrin *RD17* als spezifische Chlorose-Isolat induzierte Kandidatengene ausgewählt. Für die drei Chlorose-Isolat induzierten Gene wurden homozygote *Arabidopsis* T-DNA Insertionsmutanten isoliert und im Detail charakterisiert. Die Charakterisierung der *rd17* Mutante zeigte, dass die T-DNA Insertion keine Auswirkung auf die *RD17* Transkriptmenge

hatte. Der Infektionsphänotyp der G-type lectin receptor-like Kinase Mutante und NAC Transkriptionsfaktor Mutante unterschied sich nicht von dem des Wildtyps. Dies deutet darauf hin, dass die entsprechenden Gene nicht an der Ausprägung des Chlorose Infektionsphänotyps beteiligt sind.

Bioinformatische Analysen von öffentlich zugänglichen Mikroarraydaten zeigten, dass einige Chlorose-Isolat induzierte Gene, unter ihnen die G-type lectin receptor-like Kinase *At5g24080*, Abscisinsäure (ABA) responsiv sind. In quantitativen PCR bzw. Immunoblot Analysen akkumulierten *At5g24080* Transkripte sowie das AT5G24080-Venus Fusionsprotein nach exogener Gabe von ABA. In der *aba1-101* ABA Biosynthesemutante war die Expression von *At5g24080* während der Infektion mit einem *Verticillium* Chlorose-Isolat reduziert. Zusammengenommen deuten diese Ergebnisse darauf hin, dass ABA zu der transkriptionellen Reprogrammierung während der Chlorose-Isolat Infektion beiträgt.

Um diese Hypothese zu prüfen, wurde die *Arabidopsis* ABA Biosynthesemutante *aba1-101* im Hinblick auf die nach der Infektion mit einem Chlorose-Isolat entwickelten Symptome analysiert. In diesen Experimenten zeigten *aba1-101* Pflanzen Welke-ähnliche Symptome 21 Tage nach Infektion, jedoch keine Blattchlorosen und keine verfrühte Seneszenz. Dies weist darauf hin, dass die ABA Biosynthese der Wirtspflanze für die Ausprägung der Chlorose- und der verfrühten Seneszenzsymptome notwendig ist. Die Transdifferenzierung von Bündelscheidenzellen zu Xylemelementen war in der *aba1-101* Mutante nicht beeinträchtigt. Somit ist ABA vermutlich nicht an der Xylemneubildung beteiligt. Zusätzlich waren die *aba1-101* Pflanzen weniger anfällig gegenüber dem *V. dahliae* Chlorose-Isolat c-V76 im Vergleich zum Wildtyp. HPLC-MS/MS Analysen zeigten einen starken Anstieg der ABA Mengen in *Verticillium* Chlorose-Isolat infizierten *A. thaliana* Col-0 im Vergleich zur Mock-Behandlung oder Infektion mit einem Welke-Isolat und unterstützen somit das Konzept, dass ABA-abhängige (signaltransduktions-) Prozesse in der isolatspezifischen Symptomausprägung durch *Verticillium* eine Rolle spielen. Zusammengefasst implizieren diese Ergebnisse, dass ABA an der transkriptionellen Reprogrammierung während der Chlorose-Isolat Infektion beteiligt ist, welche zur Ausprägung der Chlorose- und der verfrühten Seneszenzsymptome führt. Außerdem stellt ABA einen Suszeptibilitätsfaktor in der *A. thaliana* – *Verticillium* Chlorose-Isolat Interaktion dar.

Table of contents

Abstract.....	I
Zusammenfassung	III
Table of contents.....	V
Table of abbreviations	IX
1. Introduction	1
1.1 Vascular fungal phytopathogens of the <i>Verticillium</i> genus	1
1.2 The plant immune system	3
1.3 The role of phytohormones as regulators of plant immunity.....	7
1.4 <i>V. longisporum</i> and <i>V. dahliae</i> isolates induce distinct disease symptoms and developmental reprogramming in <i>Arabidopsis</i>	11
1.5 Transcriptional and developmental reprogramming of the host plant by pathogen infection	16
1.6 Aim of the study	19
2. Materials and Methods	20
2.1 Materials	20
2.1.1 <i>Arabidopsis thaliana</i> plant material.....	20
2.1.2 <i>Nicotiana benthamiana</i> plant material.....	21
2.1.3 Pathogens.....	21
2.1.4 Vectors.....	22
2.1.5 Bacterial strains used for cloning and plant transformation	23
2.1.5.1 <i>Escherichia coli</i>	23
2.1.5.2 <i>Agrobacterium tumefaciens</i>	23
2.1.6 Antibiotics.....	24
2.1.7 Oligonucleotides (<i>Primers</i>).....	24
2.1.8 Antibodies.....	27
2.1.9 Enzymes.....	27
2.1.9.1 Restriction endonucleases	27
2.1.9.2 DNA-polymerases and nucleic acid modifying enzymes.....	27
2.1.10 Chemicals.....	28
2.1.11 Media.....	28
2.1.12 Buffers and solutions	29
2.2 Methods	34
2.2.1 Working with plant material	34
2.2.1.1 Plant growth conditions and propagation.....	34
2.2.1.2 Seed sterilisation.....	35

2.2.1.3	<i>Agrobacterium</i> -mediated stable transformation of <i>A. thaliana</i> by floral dipping	35
2.2.1.4	BASTA® selection of stably transformed <i>A. thaliana</i>	36
2.2.1.5	Infiltration of <i>A. thaliana</i> with abscisic acid	36
2.2.1.6	Confocal laser scanning microscopy.....	37
2.2.2	Working with bacteria and fungi.....	37
2.2.2.1	Glycerol stocks of <i>Verticillium</i> spore cultures.....	37
2.2.2.2	Cultivation of <i>Verticillium</i>	37
2.2.2.3	<i>Verticillium</i> infection of soil grown <i>A. thaliana</i> and <i>N. benthamiana</i>	37
2.2.2.4	<i>Verticillium</i> infection of <i>in vitro</i> grown <i>A. thaliana</i>	38
2.2.2.5	<i>Botrytis cinerea</i> drop inoculation of <i>A. thaliana</i>	38
2.2.2.6	<i>Hyaloperonospora arabidopsidis</i> maintenance and spray inoculation of <i>A. thaliana</i>	39
2.2.2.7	Quantification of <i>Hyaloperonospora arabidopsidis</i> propagation	39
2.2.2.8	<i>Pseudomonas syringae</i> vacuum infiltration of <i>A. thaliana</i>	39
2.2.2.9	Transformation of chemically competent <i>E. coli</i>	40
2.2.2.10	Transformation of electro competent <i>A. tumefaciens</i>	41
2.2.3	Biochemical methods.....	41
2.2.3.1	Total protein extraction.....	41
2.2.3.2	Receptor-like kinase optimised total protein extraction.....	41
2.2.3.3	Bradford protein assay	42
2.2.3.4	Denaturing SDS-polyacrylamide gel electrophoresis (SDS-PAGE).....	42
2.2.3.5	Immunoblot analysis.....	43
2.2.3.6	HPLC-MS/MS analysis of abscisic acid levels in <i>A. thaliana</i>	44
2.2.4	Molecular biological methods.....	44
2.2.4.1	PCR based genotyping of <i>A. thaliana</i> mutants	44
2.2.4.2	Polymerase Chain Reaction (PCR).....	45
2.2.4.3	Agarose gel-electrophoresis	45
2.2.4.4	Isolation of total RNA from <i>Arabidopsis thaliana</i>	46
2.2.4.5	Isolation of DNA from <i>Verticillium</i> infected <i>A. thaliana</i>	46
2.2.4.6	Reverse transcription	46
2.2.4.7	Semi-quantitative Reverse Transcription-PCR (RT-PCR).....	47
2.2.4.8	Quantitative PCR (qPCR)	47
2.2.4.9	Extraction of PCR products from agarose gels.....	48
2.2.4.10	Plasmid assembly	48
2.2.4.11	Isolation of bacterial Plasmid DNA.....	49
2.2.4.12	Restriction endonuclease digestion of DNA.....	49
2.2.4.13	DNA sequencing	49

2.2.5 Histochemical methods.....	50
2.2.5.1 Propidium iodide staining.....	50
2.2.5.2 Safranin-O staining.....	50
2.2.5.3 Trypan blue staining.....	50
2.2.6 Leaf area measurements.....	51
2.2.7 RNA-sequencing analysis.....	51
3. Results.....	53
3.1 Host plant genes which are differentially regulated by <i>Verticillium</i> chlorosis or wilting isolate infection were identified by RNA-Sequencing.....	53
3.2 Expression of candidate genes during <i>Verticillium</i> infection of <i>Arabidopsis</i> was analysed by reverse transcription PCR.....	57
3.3 Reverse genetic analysis of <i>rd17</i>	59
3.3.1 Characterisation of a <i>rd17</i> T-DNA insertion mutant.....	60
3.4 Reverse genetic analysis of <i>anac071</i>	62
3.4.1 Characterisation of <i>anac071</i> knockout mutants.....	62
3.4.2 Analysis of <i>anac071</i> disease phenotype during <i>Verticillium</i> chlorosis and wilting isolate infection.....	64
3.5 Reverse genetic analysis of <i>at5g24080</i>	68
3.5.1 <i>In silico</i> analyses suggest that AT5G24080 is an active G-type lectin receptor-like kinase.....	68
3.5.2 Characterisation of <i>at5g24080</i> knockout mutants.....	74
3.5.3 Analysis of <i>at5g24080</i> disease phenotype during <i>Verticillium</i> chlorosis and wilting isolate infection.....	77
3.5.4 Analysis of the role of <i>At5g24080</i> in defence against <i>Pseudomonas syringae</i> , <i>Botrytis cinerea</i> and <i>Hyaloperonospora arabidopsidis</i>	81
3.5.5 <i>At5g24080</i> is co-regulated with genes involved in cell wall modification, lignin and suberin biosynthesis as well as drought tolerance.....	84
3.5.6 <i>At5g24080</i> gene expression is inducible by abscisic acid.....	88
3.5.7 AT5G24080-Venus fusion protein accumulates after ABA treatment.....	91
3.5.8 AT5G24080-Venus fusion protein accumulates in <i>Arabidopsis</i> leaf and root tissues after ABA treatment.....	95
3.5.9 AT5G24080-Venus subcellular localisation after ABA treatment correlates with subcellular localisation after overexpression.....	98
3.5.10 <i>At5g24080</i> expression is reduced in the <i>aba1-101</i> ABA biosynthesis mutant background.....	101
3.6 The ABA biosynthesis mutant <i>aba1-101</i> shows wilting-like disease phenotype during <i>Verticillium</i> chlorosis isolate infection.....	102
3.7 Proliferation of the chlorosis-inducing <i>Verticillium</i> isolate c-V76 is reduced in the <i>aba1-101</i> ABA biosynthesis mutant compared to wild-type.....	106
3.8 ABA content is significantly increased in <i>Arabidopsis</i> wild-type plants during infection with the chlorosis-inducing <i>Verticillium</i> isolate c-V76.....	108

4. Discussion	110
4.1 Identification of candidate genes which are specifically induced by chlorosis and wilting isolates	110
4.2 Homozygous T DNA insertion lines as a tool for reverse genetic analyses	113
4.3 G-type LecRLK <i>At5g24080</i> is inducible by chlorosis isolate infection and abscisic acid.....	114
4.4 Abscisic acid is likely required for chlorosis and early senescence symptom development.....	118
4.5 Abscisic acid likely represents a susceptibility factor in the <i>A. thaliana</i> – <i>Verticillium</i> chlorosis isolate interaction	122
4.6 Outlook	123
5. References	126
6. Supplemental Material	141
7. Deposition of transcriptome data	175
Danksagung	176
Lebenslauf	178

Table of abbreviations

::	fused to (used in transgenic constructs)
°C	Degree Celsius
μ	micro
ABA	abscisic acid
<i>A. thaliana</i> / <i>At</i>	<i>Arabidopsis thaliana</i>
<i>A. tumefaciens</i>	<i>Agrobacterium tumefaciens</i>
APS	ammonium persulfate
Avr	avirulence
<i>B. cinerea</i>	<i>Botrytis cinerea</i>
bp	base pairs
c-	(prefix) chlorosis-
C-	(prefix) carboxy-
CaMV	cauliflower mosaic virus
cDNA	complementary DNA
CK	cytokinin
CLSM	confocal laser scanning microscopy
cm	centimetres
CNL	coiled-coil/nucleotide binding/leucine-rich repeat
Col-0	Columbia
d	days
DAMP	damage-associated molecular pattern
dH ₂ O	deionised water
DMSO	dimethylsulfoxide
DNA	deoxyribonucleic acid
DNAse	deoxyribonuclease
dNTP	deoxynucleosidetriphosphate
dpi	days post infection
<i>E. coli</i>	<i>Escherichia coli</i>
EDTA	Ethylenediaminetetraacetic acid
EF-Tu	ELONGATION FACTOR THERMO UNSTABLE
e.g.	<i>exempli gratia</i> , for example
EGFP	enhanced green fluorescent protein
ET	ethylene
<i>et al.</i>	<i>et alii</i> ; and others
ETI	effector-triggered immunity
ETS	effector-triggered susceptibility
EYFP	enhanced yellow fluorescent protein
Fig.	figure
fwd	forward
g	gram
gDNA	genomic DNA
GUS	β-glucuronidase
h	hours
HPLC	high performance liquid chromatography
HR	hypersensitive response

i.e.	<i>id est</i> , that is
JA	jasmonate
kb	kilobase pairs
kDa	kilodaltons
log	decadic logarithm
L2F	log2 fold
L	litre
LecRLKs	lectin receptor-like kinases
LPS	lipopolysaccharide
LRR	leucine-rich repeats
LS	lineage specific
LysM	lysine motif
m	milli
M	molar
MAMP	microbe-associated molecular pattern
MAPK/ MPK	mitogen activated protein kinase
min	minutes
ml	millilitres
mM	millimolar
mRNA	messenger ribonucleic acid
MS	Murashige and Skoog medium
MS/MS	tandem mass spectrometry
NASC	Nottingham Arabidopsis Stock Centre
N-	amino-
NB	nucleotide binding
<i>N. benthamiana</i> / <i>Nb</i>	<i>Nicotiana benthamiana</i>
NOCO2	<i>Hyaloperonospora arabidopsidis</i> isolate NOCO2
NP	native promoter
OD	optical density
OE	overexpressor
ORF	open reading frame
PAGE	polyacrylamide gel electrophoresis
PAMP	pathogen-associated molecular pattern
PCR	polymerase chain reaction
PDB	potato dextrose broth
pH	negative log of the hydrogen ion activity in a solution
PR	pathogenesis related
PRR	Pattern recognition receptor
<i>Pst</i>	<i>Pseudomonas syringae</i> pv. <i>tomato</i>
PI	propidium iodide
prom	promoter
PTI	PAMP-triggered immunity
pv.	pathovar
qPCR	quantitative polymerase chain reaction
R	resistance
rev	reverse
RNA	ribonucleic acid

RNase	ribonuclease
ROS	reactive oxygen species
rpm	rounds per minute
RT-PCR	reverse transcription polymerase chain reaction
SA	salicylic acid
SAIL	Syngenta Arabidopsis Insertion Library
SAR	systemic acquired resistance
SCF	Skp, Cullin, F-box protein
SDS	sodium dodecyl sulphate
SXM	simulated xylem sap
T-DNA	transfer DNA
TAE	tris-acetate-EDTA
<i>Taq</i>	<i>Thermus aquaticus</i>
TBS	Tris buffered saline
TEMED	N,N,N',N'-tetramethylethane-1,2-diamine
TF	Transcription factor
TNL	Toll interleukin 1 receptor/nucleotide binding/leucine-rich repeat
Tris	Tris-(hydroxymethyl)-aminomethane
v/v	volume per volume
<i>V. albo-atrum</i>	<i>Verticillium albo-atrum</i>
<i>V. dahliae</i>	<i>Verticillium dahliae</i>
<i>V. longisporum</i>	<i>Verticillium longisporum</i>
w-	(prefix) wilting-
w/v	weight per volume

1. Introduction

1.1 Vascular fungal phytopathogens of the *Verticillium* genus

Vascular wilt diseases affect several important crop plants and cause major economic losses worldwide. A major causal agent of vascular wilt diseases are fungal phytopathogens of the genus *Verticillium*. *V. dahliae*, *V. albo-atrum* and *V. longisporum* represent the most virulent and economically most important species within the *Verticillium* genus (Klosterman *et al.*, 2009). These *Verticillium* species are hemibiotrophic fungal pathogens with a biotrophic life phase within the plants vasculature and a necrotrophic phase in the areal tissues. Resting structures of these soil-borne pathogens may persist within the ground in absence of a susceptible host plant and germinate after decades, making effective disease control difficult and expensive (Wilhelm, 1955; Schnathorst, 1981; Mol and Scholte, 1995). In addition, the unusual habitat within the plant's vasculature, lack of resistant crop cultivars as well as the wide host range of some *Verticillium* species hinder adequate and efficient disease control.

V. dahliae has a wide host range and infects a large variety of dicotyledonous crop plants including tomato, potato, sunflower, cotton, flax but also fruit plants, flowers and ornamental trees (Fradin and Thomma, 2006; Klosterman *et al.*, 2009). During infection, *V. dahliae* produces large amounts of microsclerotia, resting structures composed of clusters of melanised, thick-walled cells which can remain viable for 10-15 years (Wilhelm, 1955). Upon germination of microsclerotia, fungal hyphae infect the host plant root gaining access at the root tip or at sites of lateral root formation (Fig. 1) (Bishop and Cooper, 1983; Fradin and Thomma, 2006; Reusche *et al.*, 2014). Subsequently, the fungus crosses the root cortex and enters the vessels of the plant's vasculature. *Verticillium* colonizes the whole plant by producing conidia, which are dispersed by the transpiration stream. Colonization of xylem triggers disruption of water transport within the plant and in turn causes typical wilting like symptoms as well as in some hosts chloroses, necrosis, early senescence and defoliation (Schnathorst, 1981; Fradin and Thomma, 2006; Klosterman *et al.*, 2009). In contrast to *V. dahliae*, the rather distantly related *V. albo-atrum* does not produce microsclerotia but melanised, dark resting mycelia (Isaac, 1949; Inderbitzin, Bostock, *et al.*, 2011). Furthermore *V. albo-atrum* has a narrow host range and is mainly restricted to potato, tomato, alfalfa, hop and soybean (Fradin and Thomma, 2006; Klosterman *et al.*, 2009).

V. longisporum is an allopolyploid hybrid which originated from *V. dahliae* and a species related to *V. albo-atrum* (Clewes *et al.*, 2008; Inderbitzin, Davis, *et al.*, 2011). Phylogenetic analyses performed by Inderbitzin *et al.* (2011) showed that *V. longisporum* evolved recently

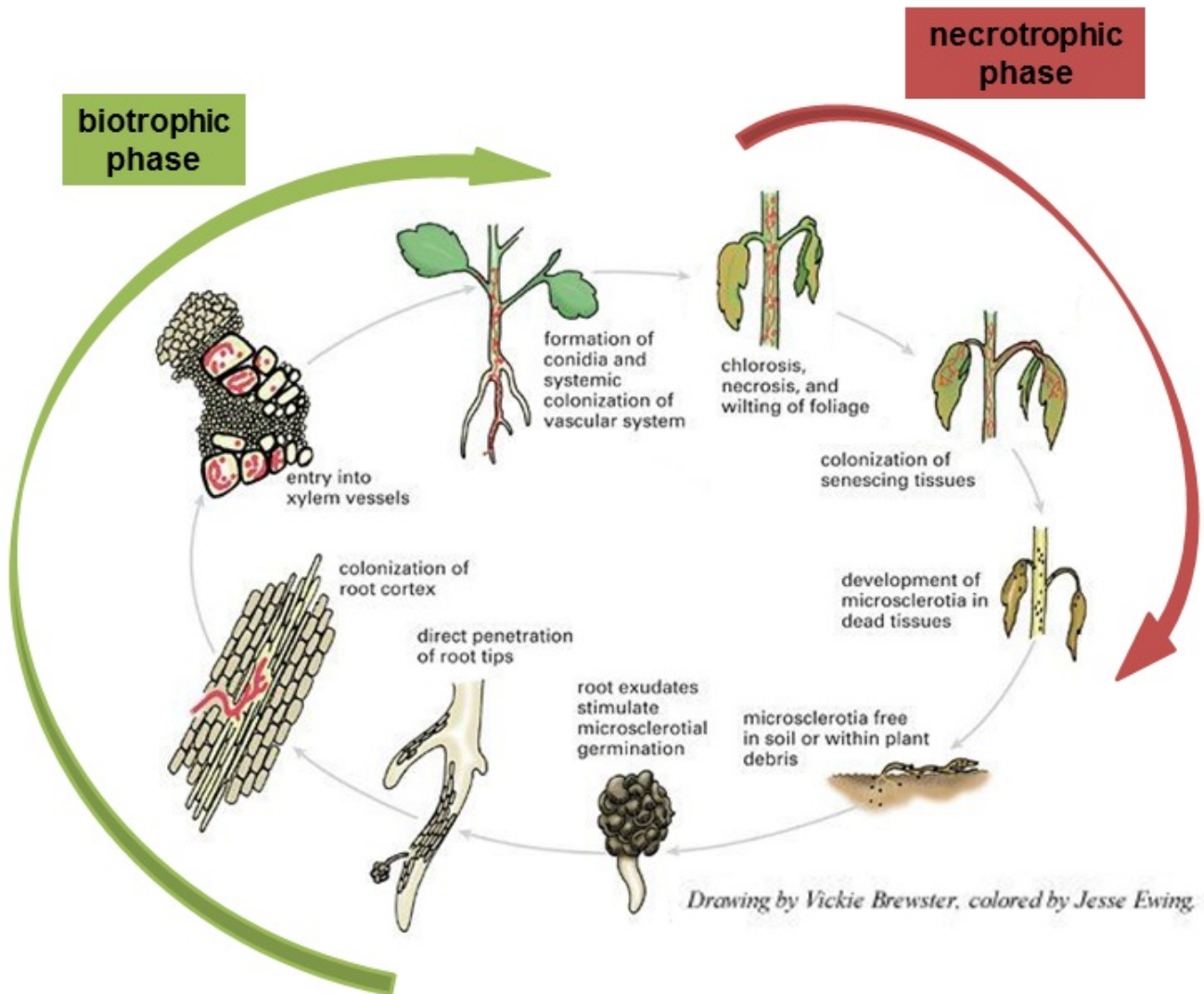


Figure 1. The *Verticillium* disease cycle. *Verticillium* species are hemibiotrophic fungal pathogens with a biotrophic life phase within the plants vasculature (green) and a necrotrophic phase in the areal tissues (red). Resting structures of the fungus, the melanised microsclerotia, germinate stimulated by root exudates. The hyphae directly penetrate root epidermis cells without development of specific infection structures and grow through the cortex towards the central cylinder where they invade the xylem vessels. *Verticillium* colonizes the whole plant by producing conidia, which are dispersed by the transpiration stream. During the necrotrophic phase the fungus exits the vasculature and feeds on senescing plant tissue. Finally, microsclerotia are deployed into the soil with the decomposing plant material and the cycle begins again, once a new host plant is present. Figure modified from (<https://www.apsnet.org/edcenter/intropp/lessons/fungi/ascomycetes/Pages/VerticilliumWilt.aspx>).

from three different hybridisation events between *V. albo-atrum* related, yet unknown species A1 with *V. dahliae* lineage D2, *V. dahliae* lineage D3 and *V. dahliae* related, but also non-described species D1 (Inderbitzin, Davis, *et al.*, 2011). The hybridisation event led to the rise of a new species with specific phenotypes. *V. longisporum* produces microsclerotia and conidia which are longer compared to those of *V. dahliae*. In addition, *V. longisporum* developed a new host range and was rendered virulent to *Brassicaceae* (Karapapa *et al.*, 1997; Eynck *et al.*, 2007). Infections with *Verticillium* usually cause wilting symptoms on the host

plant. Remarkably, *V. longisporum* infection of *Brassicaceae* hosts such as *Arabidopsis thaliana* or *Brassica napus* is not accompanied by wilting symptoms (Floerl *et al.*, 2010; Lopisso *et al.*, 2017). Instead, challenge with *V. longisporum* induces developmental reprogramming of these host plants leading to *de novo* xylem formation, which likely allows maintaining the plant's water status (Reusche *et al.*, 2012). A detailed description of the *V. longisporum* disease phenotype is given in section 1.4. The pathogen was first described in the 1960s (Stark, 1961) and has since then become a major economic threat in Europe, the main cropping area for oilseed rape (*Brassica napus* spp. *oleifera*). Adaption to *Brassicaceae* species as host plants indicates that *V. longisporum* could have evolved new strategies to overcome plant lineage-specific immune responses on molecular level.

1.2 The plant immune system

In contrast to mammals, plants do not possess an adaptive immune system but depend on the innate immunity of single cells during pathogen attack (Ausubel, 2005; Jones and Dangl, 2006). The plant immune system is composed of two branches (Fig. 2). The first branch largely depends on transmembrane receptor proteins, so called pattern recognition receptors (PRRs). Most of the characterised PRRs constitute either receptor-like kinases (RLKs) or receptor-like proteins (RLPs). RLKs are composed of a ligand-binding ectodomain, a transmembrane domain and an intracellular kinase domain, mediating downstream signal transduction. RLPs lack the intracellular kinase domain and likely depend on oligomerisation with RLKs for signalling (Zipfel, 2009; Macho and Zipfel, 2014). Cell surface localised PRRs recognize conserved microbial molecules and structural motifs summarized as pathogen-associated molecular patterns (PAMPs) or microbe-associated molecular patterns (MAMPs). In *Arabidopsis* for instance, the conserved epitope of bacterial flagellin, flg22, is perceived by the leucine-rich repeat (LRR) receptor-like kinase FLAGELLIN SENSING 2 (FLS2) (Chinchilla *et al.*, 2006). EFR (EF-Tu receptor), a further LRR receptor-like kinase, senses the conserved N-terminal peptide elf18 of the bacterial elongation factor Tu (Zipfel *et al.*, 2006). The fungal cell-wall polymer chitin is perceived by the lysin motif (LysM) CHITIN ELICITOR RECEPTOR KINASE 1 (CERK1) (Miya *et al.*, 2007; Wan *et al.*, 2008; Petutschnig *et al.*, 2010).

Recent findings suggest that lectin receptor-like kinases (LecRLKs) also function as PRRs. Lectins are a diverse family of carbohydrate binding proteins present in plant and animal kingdoms. Lectin proteins exhibit a large diversity of carbohydrate binding sites and selectively

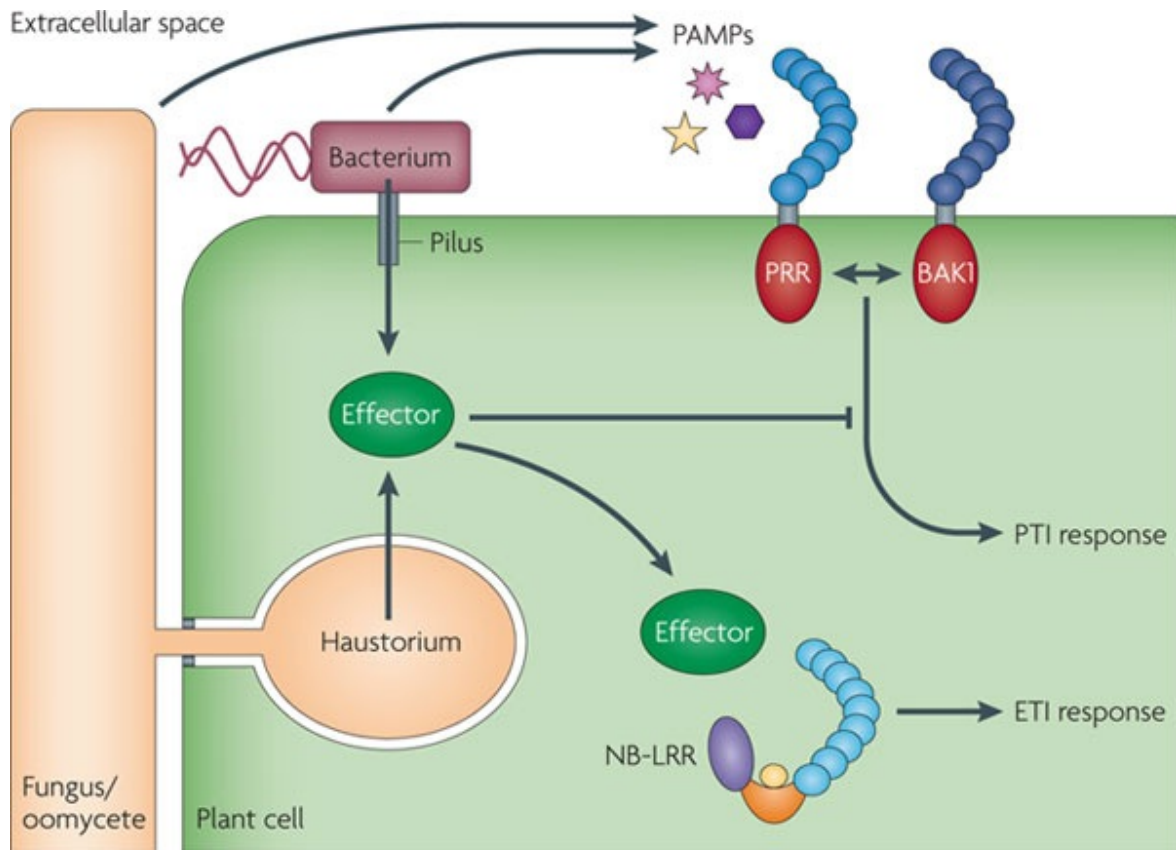


Figure 2. Model of the plant immune system. Bacterial pathogens usually enter their host plant through wounds or natural openings, e.g. stomata. Fungal pathogens and oomycetes, in addition, often directly penetrate preformed physical barriers such as cuticula and cell walls utilising specialised penetration organs (appressoria). Cell surface localised pattern recognition receptors (PRRs) perceive presence of the pathogen by sensing conserved pathogen-associated molecular patterns (PAMPs) and elicit PAMP-triggered immunity (PTI). In turn, pathogens secrete effector molecules, which suppress onset of PTI, resulting in effector-triggered susceptibility (ETS). Several bacterial effectors are translocated into the host cell via a syringe-like structure, the prokaryotic type III secretion system. Fungal and oomycete effectors are likely secreted via the eukaryotic type II secretory pathway into the apoplast and are presumably translocated into the host cell by a plant endocytic pathway (Panstruga and Dodds, 2009). Pathogen effectors are sensed by intracellular NB-LRR resistance proteins. Effector perception results in effector-triggered immunity (ETI). Figure adapted from (Dodds and Rathjen, 2010).

bind mono- as well as oligosaccharides (Loris, 2002; Van Damme *et al.*, 2008). In *A. thaliana*, these proteins are classified into C-type, L-type and G-type lectins, according to their carbohydrate binding domains. C-type lectins contain a calcium binding domain and depend on Ca^{2+} for carbohydrate binding (Bellande *et al.*, 2017). L-type lectins harbour a typical legume-type lectin domain, which folds into a β -sandwich (Bellande *et al.*, 2017). A D-mannose binding bulb-type lectin domain, an S-locus glycoprotein domain and a PAN (plasminogen-apple-nematode)-like domain are characteristic for G-type lectins. (Bellande *et al.*, 2017). Recently, the *A. thaliana* G-type lectin receptor-like kinase

LIPOOLIGOSACCHARIDE-SPECIFIC REDUCED ELICITATION (LORE) has been proposed to function as a PRR in perception of lipopolysaccharide (LPS) PAMPs from *Pseudomonas* and *Xanthomonas* bacteria (Ranf *et al.*, 2015). Lectin receptor-like kinases from other plant species were also shown to function in defence against bacterial as well as fungal pathogens and herbivorous insects, supporting the role of LecRLKs in plant immunity (Kim *et al.*, 2009; Chen *et al.*, 2006; Gilardoni *et al.*, 2011; Cheng *et al.*, 2013; Cole and Diener, 2013; Liu *et al.*, 2015). Function of FLS2 and likely also of EFR depends on interaction with the LRR receptor-like kinase BRASSINOSTEROID INSENSITIVE 1-ASSOCIATED KINASE 1 (BAK1) (Fig. 2) (Chinchilla *et al.*, 2007; Zipfel, 2009). In contrast, PAMP perception by CERK1 and LORE does not require BAK1 (Miya *et al.*, 2007; Wan *et al.*, 2008; Petutschnig *et al.*, 2010; Ranf *et al.*, 2015; Couto and Zipfel, 2016).

In addition to PAMPs, the plant immune system also responds to endogenous degradation products released upon pathogen action, such as cell wall fragments, termed danger-associated molecular patterns (DAMPs) (Boller and Felix, 2009). PAMP or DAMP perception by PRRs elicits a basal defence response which is associated with expression of *pathogenesis-related* (*PR*) genes, accumulation of reactive oxygen species (ROS) as well as callose deposition at the site of attempted pathogen ingress (Boller and Felix, 2009; Zipfel, 2009; Dodds and Rathjen, 2010). PRR activated basal defence responses halt colonisation by non-adapted pathogens and result in PAMP-triggered immunity (PTI) (Fig. 2).

In two recent studies, several cotton (*Gossypium spec.*) LysM receptor-like kinases (LyKs), a LysM-type receptor-like protein (Lyp) and an extracellular LysM protein (LysMe) were proposed to function as PRRs in defence responses to *Verticillium dahliae* (Gu *et al.*, 2017; Xu *et al.*, 2017). The cotton LysM receptor-like kinases Gh-LYK1 and Gh-LYK2 were experimentally shown to bind chitin and expression of the corresponding genes was demonstrated to be inducible by chitin treatment and *V. dahliae* infection (Gu *et al.*, 2017). Virus-induced gene silencing (VIGS) of *Gh-LYK1* and *Gh-LYK2* results in reduced defence gene expression after chitin treatment, enhanced *V. dahliae* proliferation and stronger *V. dahliae* induced disease symptoms (Gu *et al.*, 2017). Together these findings suggest a function of Gh-LYK1 and Gh-LYK2 as PRRs in chitin induced defence responses during *V. dahliae* infection. Expression of cotton *Lyp1*, *Lyk7* and *LysMe3* is also inducible by chitin and *V. dahliae* challenge (Xu *et al.*, 2017). Moreover, these three LysM proteins are required for disease resistance of cotton to *V. dahliae* and expression of several cotton defence related genes as well as *PR* genes indicating that *Lyp1*, *Lyk7* and *LysMe3* may play a role as potential PRRs in chitin perception during *Verticillium* infection (Xu *et al.*, 2017).

Besides chitin, conserved 20-23 amino acid peptides of *V. dahliae* Nep1-like proteins (NLPs) potentially function as PAMPs in *Verticillium* root infection. The nlp20 peptide motifs, which are present in bacterial, fungal and oomycete NLPs elicit typical PAMP-induced defence responses such as MAP kinase activation, *PR* gene expression, ROS production and callose deposition (Böhm *et al.*, 2014). Treatment of cotton (*Gossypium hirsutum*) roots with *V. dahliae* derived nlp20^{Vd2}, nlp23^{Vd3}, and nlp23^{Vd4} triggers expression of several *PR* genes, suggesting that these peptides represent *Verticillium* derived PAMPs (Du *et al.*, 2017). In *Arabidopsis thaliana*, nlp20 perception depends on a tripartite complex consisting of the LRR receptor protein RLP23 and the LRR receptor like kinases BAK1 and SUPPRESSOR OF BIR1-1 (SOBIR1) (Albert *et al.*, 2015).

Host adapted pathogens circumvent PTI by secreting virulence factors, so called effectors, into the host cell. Effector molecules interfere with PTI and suppress basal defence responses, resulting in effector-triggered susceptibility (ETS) of the host. Pathogen effectors can in turn be specifically recognised by intracellular receptors, collectively described as plant resistance (R)-proteins, which constitute the second branch of the plant immune system (Jones and Dangl, 2006). In addition to intracellular receptors, extracellular plasma membrane-anchored R-proteins have also been described (Stergiopoulos and de Wit, 2009; Wulff *et al.*, 2009). Recognised effectors are referred to as avirulence (Avr) proteins. R-proteins either perceive effector molecules by direct interaction (Jia *et al.*, 2000; Dodds *et al.*, 2006) or recognise effector action on host targets, such as proteolytic cleavage or phosphorylation of host proteins, allowing a relatively small R-protein repertoire to detect a large variety of pathogen effectors (Dangl and Jones, 2001; Mackey *et al.*, 2002; Axtell and Staskawicz, 2003; Mackey *et al.*, 2003). Nucleotide binding (NB) leucine-rich repeat (LRR) domain proteins constitute the largest class of plant resistance proteins (Jones and Dangl, 2006). NB-LRR resistance proteins are further subdivided according to their N-terminal domain into Toll interleukin 1 receptor/nucleotide binding/leucine-rich repeat (TNL)-type and coiled-coil/nucleotide binding/leucine-rich repeat (CNL)-type R-proteins. Downstream signal transduction of TNL-type resistance proteins depends on ENHANCED DISEASE SUSCEPTIBILITY 1 (EDS1) (Aarts *et al.*, 1998; Falk *et al.*, 1999). EDS1 along with its interaction partners PHYTOALEXIN DEFICIENT 4 (PAD4) and SENESCENCE ASSOCIATED GENE 101 (SAG101) constitutes a key positive regulator of basal defence responses and TNL-type R-protein mediated immunity (Feys *et al.*, 2005; Wiermer *et al.*, 2005). In contrast, immunity conferred by CNL-type R-proteins generally does not require EDS1 but depends on NON-RACE SPECIFIC DISEASE RESISTANCE 1 (NDR1) (Aarts *et al.*, 1998). Effector

perception by NB-LRR proteins results in a strongly amplified and accelerated PTI response - the effector-triggered immunity (ETI) (Fig. 2). ETI triggers a strong defence reaction often culminating in localized cell death (HR) at attempted site of pathogen ingress and accumulation of salicylic acid (SA) (Tao *et al.*, 2003; Pitzschke *et al.*, 2009).

The tomato (*Solanum lycopersicum*) *Ve1* receptor represents the best-characterised R-protein conferring resistance to *Verticillium*. The *Ve1* gene encodes an extracellular LRR receptor-like protein (Kawchuk *et al.*, 2001). *Ve1* perceives the avirulence protein *Ave1* (Avirulence on *Ve1* tomato). Tomato cultivars carrying the *Ve1* are resistant to *V. dahliae* and *V. albo-atrum* race 1 isolates, which carry the *Ave1* gene but not race 2 isolates lacking *Ave1* (Fradin *et al.*, 2009; de Jonge *et al.*, 2012). Interfamily transfer of tomato *Ve1* confers *Verticillium* race 1 resistance to *Arabidopsis thaliana*, tobacco (*Nicotiana tabacum*) and cotton (*Gossypium hirsutum*), suggesting that *Ve1* downstream signal transduction pathways are conserved among plant families (Fradin *et al.*, 2011; Song *et al.*, 2018). Furthermore, tomato *Ve1* was demonstrated to mediate resistance to the vascular fungal pathogen *Fusarium oxysporum* and *Ave1* homologs from *F. oxysporum* as well as the phytopathogenic fungus *Cercospora beticola* were shown to induce HR in a *Ve1* dependent manner (de Jonge *et al.*, 2012; Song *et al.*, 2017). These results imply that *Ve1* plays a role in *Ave1* triggered immunity against several fungal phytopathogens. The TNL-type R-protein *GbaNA1* was recently described to be required for resistance of cotton (*Gossypium barbadense*) to a *V. dahliae* race 2 isolate lacking *Ave1* (Li *et al.*, 2017). Consequently, *GbaNA1* likely provides resistance to cotton independently of *Ave1* recognition.

1.3 The role of phytohormones as regulators of plant immunity

Phytohormones play decisive roles in plant developmental processes, as regulators of plant growth and in responses to environmental stimuli (Gray, 2004; Santner *et al.*, 2009; Jaillais and Chory, 2010). In addition, phytohormones act as key regulators of defence responses in plant immunity (Pieterse *et al.*, 2009; Denancé *et al.*, 2013). Salicylic acid, jasmonate and ethylene constitute the classical defence related phytohormones and have been extensively studied over the past decades (Pozo *et al.*, 2004; Loake and Grant, 2007; van Loon *et al.*, 2006; Robert-Seilaniantz *et al.*, 2011). However, recent findings suggest that other hormones such as cytokinins and abscisic acid are involved in plant defence responses to pathogen ingress (Naseem *et al.*, 2014; Lievens *et al.*, 2017).

Salicylic acid (SA) regulates defence responses to biotrophic and hemi-biotrophic phytopathogens and is required for establishment of systemic-acquired resistance (SAR), a long

lasting pathogen-induced resistance of the entire plant to subsequent infection (Glazebrook, 2005; Conrath, 2006; Loake and Grant, 2007; Denancé *et al.*, 2013). Upon pathogen challenge, SA is mainly synthesised from chorismate via the isochorismate pathway by ISOCHORISMATE SYNTHASE (ICS) and ISOCHORISMATE PYRUVATE LYASE (IPL) in the chloroplast (Verberne *et al.*, 2000; Wildermuth *et al.*, 2001; Strawn *et al.*, 2007; Vlot *et al.*, 2009). SA can be converted to several SA-conjugates, such as methyl salicylate (MeSA), salicyloyl glucose ester (SGE) and SA O- β -glucoside (SAG) (Vlot *et al.*, 2009). SA dependent activation of defence gene expression, including the *pathogenesis-related* (PR) genes, is mediated by NON-EXPRESSOR OF PR GENES 1 (NPR1). In the cytoplasm, NPR1 resides as an oligomer. NPR1 oligomerisation likely results from disulfide bond formation (Mou *et al.*, 2003). Cellular accumulation of SA is suggested to change the redox potential inside the cell, thus reducing NPR1 and triggering its monomerisation (Després *et al.*, 2003). In turn, monomeric NPR1 localises to the nucleus, where it interacts with TGA transcription factors and as a co-activator drives expression of defence related genes (Fan and Dong, 2002; Johnson *et al.*, 2003; Lindermayr *et al.*, 2010). SA likely plays a role in the *Verticillium* - *A. thaliana* interaction. SAG levels are increased in *A. thaliana* during *V. longisporum* infection (Floerl *et al.*, 2012; Ralhan *et al.*, 2012). Moreover, PR gene expression is induced in *A. thaliana* during *V. longisporum* and *V. dahliae* challenge (Tjamos *et al.*, 2005; Johansson *et al.*, 2006; Ralhan *et al.*, 2012).

Jasmonate (JA) along with ethylene (ET) mediates defence responses to necrotrophic phytopathogens and herbivorous insects (Glazebrook, 2005; Bari and Jones, 2009; Denancé *et al.*, 2013). Jasmonate is a lipid-derived hormone, which is synthesised from 18:3 linolenic acid in a biosynthetic pathway localised in the chloroplast and peroxisomes (Schaller and Stintzi, 2009). JA conjugated to the amino acid isoleucine (JA-Ile) represents the bioactive form of jasmonate. JA-Ile is perceived by the CORONATINE INSENSITIVE 1 (COI1) F-box protein, which is a part of the SCF^{COI1} E3 ubiquitin-ligase protein complex (Fonseca *et al.*, 2009). SCF^{COI1} targets proteins of the JASMONATE ZIM-domain-containing (JAZ) family, which are repressors of jasmonate signalling, for proteosomal degradation (Chini *et al.*, 2007; Thines *et al.*, 2007). De-repression of JA responsive transcriptional factors, including the well characterised AtMYC2, in turn activates expression of JA responsive genes (Lorenzo *et al.*, 2004; Dombrecht *et al.*, 2007). COI1 is required for full disease susceptibility of *A. thaliana* to *V. longisporum* infection. *V. longisporum* proliferation is reduced and disease symptoms are less pronounced in the *coi1-t* mutant as compared to *A. thaliana* wild-type. Moreover, *V. longisporum* produces a lower number of microsclerotia in the *coi1-t* mutant, indicating that

the life cycle competition of *V. longisporum* is impaired in this mutant background (Ralhan *et al.*, 2012). Interestingly, COI1 promotes susceptibility to *V. longisporum* independently of JA. Although JA and JA-Ile levels are increased during *V. longisporum* infection in wild-type *A. thaliana*, disease symptoms and fungal proliferation in the JA biosynthesis mutant *dde2* are comparable to wild-type (Ralhan *et al.*, 2012).

Salicylic acid and jasmonate have been described to act as antagonists in plant defence responses. Increases in SA levels upon pathogen attack are associated with a repression of JA signalling. SA mediated repression of JA signalling requires NPR1, the major regulator of SA-dependent defence gene expression (Spoel *et al.*, 2003). Moreover, SA-inducible glutaredoxin oxidoreductases were demonstrated to repress expression of the JA marker gene *PLANT DEFENSIN 1.2 (PDF1.2)*, in a TGA transcription factor dependent manner (Ndamukong *et al.*, 2007; Zander *et al.*, 2012). In turn, MPK4, a MAP kinase implicated in JA-mediated resistance to necrotrophic pathogens, acts as a negative regulator of salicylic acid (SA)-dependent defence signalling. *mpk4* mutants show enhanced SA levels, spontaneous cell death, up-regulation of *pathogenesis-related (PR)* genes and enhanced resistance to biotrophic pathogens (Petersen *et al.*, 2000; Brodersen *et al.*, 2006). Furthermore, the JA responsive transcriptional factor AtMYC2 negatively regulates SA signalling. *myc2* mutants accumulate SA, show enhanced *PR1* expression and are less susceptible to the hemi-biotrophic bacterial phytopathogen *Pseudomonas syringae* (Laurie-Berry *et al.*, 2006).

Abscisic acid (ABA) represents one of the classical phytohormones, which has been associated with seed germination, leaf senescence, leaf abscission as well as responses to abiotic stress, such as salt, cold and drought stress (Gepstein and Thimann, 1980; Léon-Kloosterziel *et al.*, 1996; Swamy and Smith, 1999; Xiong *et al.*, 2002; He *et al.*, 2005; Tuteja, 2007; Breeze *et al.*, 2011; Lee *et al.*, 2011). Abscisic acid is an isoprenoid compound synthesised by several catalytic steps localised in the chloroplast and cytosol from isopentenyl diphosphate (IPP). ABA is produced via carotenoid precursors including zeaxanthin, which is converted by the zeaxanthin epoxidase ABA1 into antheraxanthin and subsequently violaxanthin. The 9-cis-epoxycarotenoid dioxygenase NCED3 converts violaxanthin into xanthoxin, which represents the first cytoplasmic precursor of ABA (Wasilewska *et al.*, 2008). ABA is perceived by PYRABACTIN RESISTANCE LIKE (PYL) family cytosolic receptors (Ma *et al.*, 2009; Park *et al.*, 2009). PYLs bind PP2C protein serine/threonine phosphatases. PP2Cs are negative regulators of SnRK2 (SNF1-related protein kinase 2) family protein kinases, which mediate ABA signalling, including phosphorylation of transcriptional factors and expression of ABA responsive genes. Upon ABA perception, PYLs interact with PP2C protein phosphatases. This

leads to de-repression of SnRK2 protein kinases and in turn activation of ABA signalling (Vlad *et al.*, 2009; Umezawa *et al.*, 2009; Fujii *et al.*, 2009; Umezawa *et al.*, 2010; Kulik *et al.*, 2011). ABA levels are increased in *A. thaliana* during *V. longisporum* infection, suggesting that ABA signalling is likely involved in *A. thaliana* – *Verticillium* interaction (Ralhan *et al.*, 2012). Moreover, ABA amounts were shown to increase by two fold in cotton during infection with *V. albo-atrum* isolate T9, which causes severe defoliation symptoms. In contrast, ABA was not induced by the non-defoliating isolate SS4. Most interestingly, ABA levels were increased at 5 to 7 days post inoculation, when symptoms were most pronounced, suggesting that ABA plays a role in disease symptom development in cotton (Wiese and Devay, 1970).

Cytokinins (CKs) are a group of phytohormones, which represent derivatives of the nucleoside adenine substituted at the N⁶ position. Cytokinins are implicated in various plant developmental processes, e.g. cell division, lateral root formation, suppression of leaf senescence as well as development of the vascular system, gametophyte and shoot apical meristem (Hwang *et al.*, 2012; Kieber and Schaller, 2014). However, in the recent past, cytokinins have been shown to play a role in defence responses against phytopathogens, such as *Pseudomonas syringae* and *Hyaloperonospora arabidopsidis* (Choi *et al.*, 2010; Argueso *et al.*, 2012). Cytokinins also play a role in the *A. thaliana* – *V. longisporum* interaction. *V. longisporum* has been proposed to influence cytokinin levels during *A. thaliana* infection, in order to promote disease symptom establishment and fungal proliferation. Levels of the adenine-type cytokinin trans-zeatin are significantly reduced in *V. longisporum* infected plants as compared to the mock control. *Verticillium* induced reduction in trans-zeatin levels is accompanied by enhanced expression of cytokinin oxidase/dehydrogenase (CKX) genes *CKX1*, *CKX2* and *CKX3*, suggesting that cytokinin is degraded. Pharmacological treatments with CKX inhibitors or expression of the cytokinin biosynthesis gene *IPT* (*ISOPENTENYL TRANSFERASE*) from *Agrobacterium tumefaciens* under the control of a senescence responsive promoter lead to a reduction of chlorosis and early senescence symptoms as well as a decrease in fungal proliferation (Reusche *et al.*, 2013).

ABA has been reported to cross talk with cytokinin signalling in plant immunity. ABA was shown to impair cytokinin-induced resistance of tobacco to *Pseudomonas syringae*. Cytokinin treatment reduces ABA levels in tobacco and enhances cytokinin-induced resistance, whereas exogenous application of ABA or inhibition of ABA degradation leads to enhanced *P. syringae* proliferation (Großkinsky *et al.*, 2014).

1.4 *V. longisporum* and *V. dahliae* isolates induce distinct disease symptoms and developmental reprogramming in *Arabidopsis*

As described in section 1.1, *V. dahliae* infection is typically associated with wilting symptoms. It has been proposed, that *Verticillium* Nep1-like proteins (NLPs) act as wilt-inducing elicitors. NLPs are mostly secreted proteins and carry the characteristic conserved NPP1 domain, which was defined based on the *Phytophthora parasitica* Nep1-like protein NPP1 (Fellbrich *et al.*, 2002; Gijzen and Nürnberger, 2006). NLP family proteins are widespread among phytopathogenic bacteria, fungi and oomycetes and commonly elicit cell death and necrosis when expressed *in planta* (Oome and Van den Ackerveken, 2014; Lenarčič *et al.*, 2017). However, besides cell death, several *V. dahliae* Nep1-like proteins (NLPs) have been demonstrated to induce dehydration as well as wilting symptoms in cotton (Wang *et al.*, 2004; Palmer *et al.*, 2005; B.,-J., Zhou *et al.*, 2012).

Proliferation of vascular pathogens often results in clogging of water conducting xylem vessels and leads to reduction in turgor pressure. *Xylella fastidiosa*, a phytopathogenic bacterium, which proliferates in xylem vessels of grapevine (*Vitis vinifera*), was shown to aggregate to large colonies and block host plant's xylem vessels resulting in water stress symptoms (Newman *et al.*, 2003). Vessel elements are separated by the pit membrane of bordered pits. The pit membrane prevents the spread of embolisms and thus obstruction of the transpiration stream but additionally limits pathogen movement (Choat *et al.*, 2008). *X. fastidiosa* secretes cell wall degrading enzymes, which act on the pit membrane in order to allow pathogen spread. Interestingly, degradation products, which are potentially released into the xylem vessels were demonstrated to reduce or abolish water flow in grapevine stems (Pérez-Donoso *et al.*, 2010). Vascular clogging has also been reported to occur during *Fusarium oxysporum* f. sp. *cubense* infection of castor bean (*Ricinus communis*) and banana (*Musa acuminata*) (VanderMolen *et al.*, 1983; VanderMolen *et al.*, 1986). *Fusarium oxysporum* f. sp. *cubense* is a vascular fungal phytopathogen and the causal agent of banana wilt disease (Mostert *et al.*, 2017). Secreted cell wall degrading enzyme preparations from *Fusarium oxysporum* f. sp. *cubense* were shown to induce formation of vascular system-obstructing gels (VanderMolen *et al.*, 1983).

In addition to clogging of xylem vessels due to proliferation of vascular pathogens and pathogen induced vascular gels, colonised host plants actively block pathogen growth by tyloses. Tyloses are invaginations of surrounding parenchyma cells into the lumen of vessel elements through bordered pits (Yadeta and Thomma, 2013). Tylosis formation has been observed in several plant species in response to infection with *V. dahliae* and *V. albo-atrum* (Talboys, 1958; Dixon and Pegg, 1969; Robb *et al.*, 1979; Benhamou, 1995). Intriguingly, infection of tomato plants

with hop *V. albo-atrum* isolates triggered tylosis formation, whereas infection with a tomato isolate did not, suggesting that tyloses represent an isolate specific defence response of the host plant (Dixon and Pegg, 1969). Already in the late 1950, Talboys observed that intensive tylosis formation in hop plants infected with *V. albo-atrum* is associated with re-initiated cambial activity resulting in *de novo* xylem formation – the so called xylem hyperplasia (Talboys, 1958). Xylem hyperplasia likely compensates for reduced water transport capacity of clogged xylem vessels and thus ensures water transport in the infected plant (Talboys, 1958; Baayen, 1986). In summary, infection with vascular pathogens often results in wilting symptoms, which are likely caused by NLP family proteins as well as clogging of water conducting xylem vessels due to pathogen proliferation, formation of vascular gels and tyloses. *De novo* xylem formation likely compensates for reduced water transport capacity of clogged xylem vessels.

Infection of the model plant *Arabidopsis thaliana* with *Verticillium dahliae* results in wilting, stunted growth and decay of older rosette leaves (Fig. 3A, right) (Reusche *et al.*, 2014). *Verticillium longisporum* infection of *A. thaliana* results in a similar degree of stunting. In contrast to *V. dahliae* however, *V. longisporum* does not induce wilting symptoms, but a distinct disease phenotype including leaf chlorosis and early senescence (Fig. 3A, middle) (Reusche *et al.*, 2012; Reusche *et al.*, 2014).

In addition to differences in macroscopic disease symptoms, *V. longisporum* induces vast developmental reprogramming of *A. thaliana*. On the one hand, chloroplast-containing bundle sheath cells transdifferentiate to functional xylem elements. Macroscopically, bundle sheath cell transdifferentiation becomes apparent as yellowing of leaf veins – the so called vein clearing (Fradin and Thomma, 2006; Reusche *et al.*, 2012). On the cellular level, cells of the bundle sheath cell layer surrounding the vascular bundle (Fig. 3B and E) disappear in favour of protoxylem, showing characteristic annular and helical secondary cell wall fortifications (Fig. 3C and F) or metaxylem with reticulate secondary cell walls. At the molecular level, bundle sheath cell transdifferentiation during *V. longisporum* infection of *A. thaliana* requires the VASCULAR RELATED NAC DOMAIN transcriptional factor VND7. Kubo *et al.* (2005) described VND7 as a transcriptional regulator of protoxylem formation in *A. thaliana* and poplar, since its overexpression promotes and its repression inhibits protoxylem development (Kubo *et al.*, 2005). VND7 expression is induced during *V. longisporum* infection of *A. thaliana*. Furthermore, VND7 repression significantly decreased the number of transdifferentiated bundle sheath cells in transgenic *A. thaliana* during *V. longisporum* challenge (Reusche *et al.*, 2012).

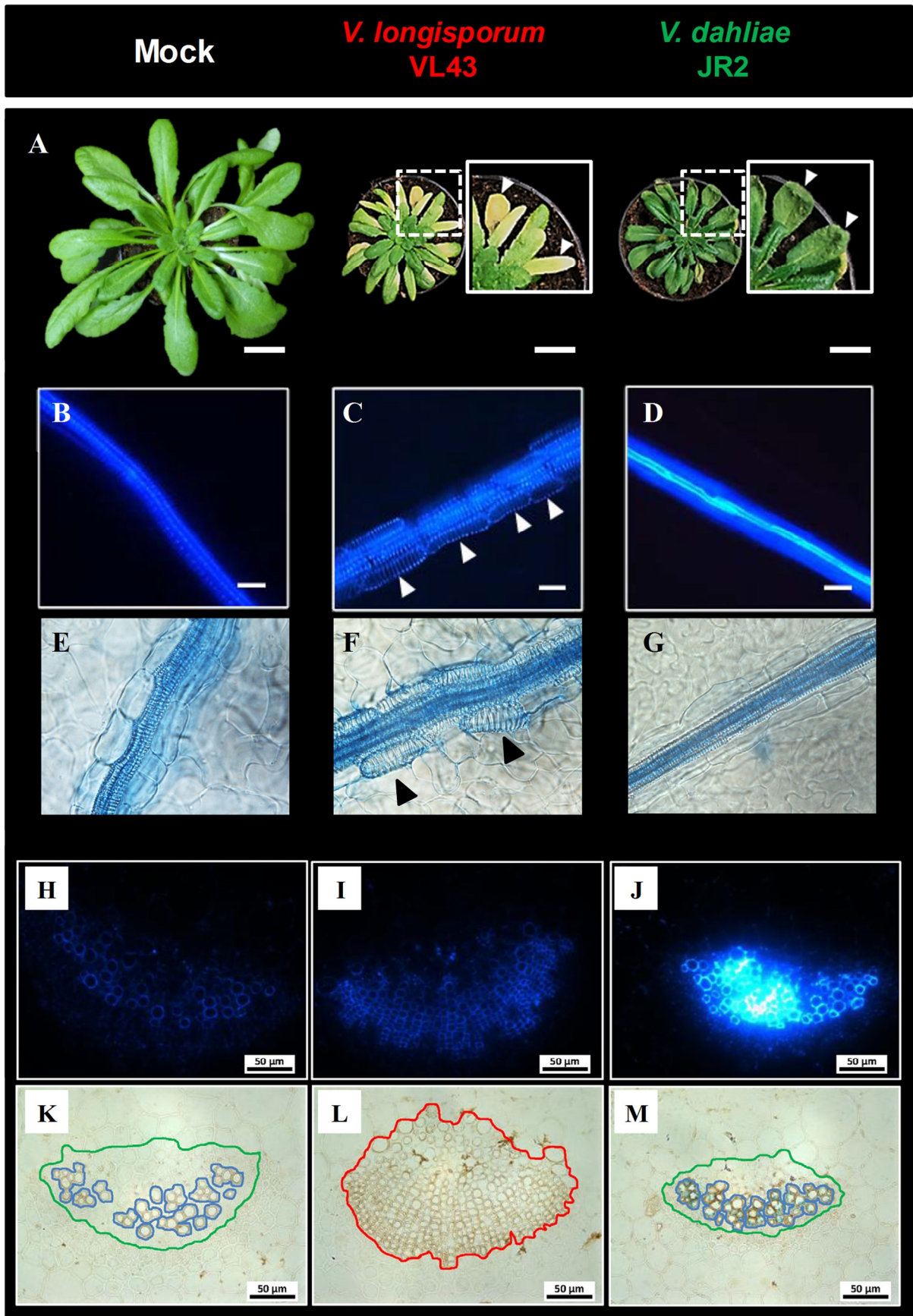


Figure 3. Disease symptoms and vascular developmental changes of *A. thaliana* during *V. longisporum* isolate VL43 and *V. dahliae* isolate JR2 infection. (A) Macroscopic disease symptoms at 21 days post infection (dpi). Insets represent magnifications of areas marked with dotted boxes. Arrowheads indicate chlorotic and

necrotic leaf of *V. longisporum* VL43 infected plant and wilting leaves of a *V. dahliae* JR2 infected plant. Scale bar = 2 cm. **(B-D)** Epifluorescence images of bundle sheath cells in leaf vascular bundles of *A. thaliana* at 21 dpi after infection with the respective *Verticillium* isolate. Scale bar = 25 μ m. **(E-G)** Bright field images of bundle sheath cell transdifferentiation at 21 dpi. Plant leaves were stained with trypan blue. Arrowheads in **(B-G)** point at *de novo* formed tracheary elements. Note that bright field and epifluorescence images in figures **B-G** do not show the same vascular bundle. **(H-J)** Epifluorescence images of leaf midrib cross-sections of *A. thaliana* at 28 dpi after infection with the respective *Verticillium* isolate. **(K-M)** Bright field images of leaf midrib cross-sections. Tissues were stained with potassium permanganate to visualize lignin as brown stain. Xylem vessels are encircled in blue, xylem parenchyma cells in green and hyperplastic xylem in red. Note that bright field and epifluorescence images in figures **H-M** do not show the same cross section. Figure modified from Reusche *et al.* (2014) and K. Thole, PhD Thesis (2016).

Additionally to bundle sheath cell transdifferentiation, *V. longisporum* triggers xylem hyperplasia in *A. thaliana* leaf vascular bundles, hypocotyl xylem and central cylinder of the root (Reusche *et al.*, 2012). As described by Talboys for the *V. albo-atrum* – hop interaction, vast amounts of *de novo* formed lignified xylem cells are present in vascular bundles of *V. longisporum* inoculated *A. thaliana* (Fig. 3I and L). Xylem hyperplasia likely results from transdifferentiation of xylem parenchyma cells and renewed cambial activity (Fig. 3H, I, K and L) (Reusche *et al.*, 2012). This assumption is supported by an increase in expression of the *ARABIDOPSIS THALIANA HOMEBOX-8 (ATHB-8)* gene during *V. longisporum* infection of *A. thaliana*, which represents a marker for cambial activity (Scarpella *et al.*, 2004; Reusche *et al.*, 2012). Xylem hyperplasia is suggested to compensate for reduced water transport capacity of clogged xylem vessels and thus ensure water transport in the infected plant (Talboys, 1958; Baayen, 1986). Intriguingly, in *V. longisporum* infected *A. thaliana*, *de novo* formed xylem not only compensates for clogged xylem vessels but leads to enhanced drought stress tolerance as compared to mock treated plants, which likely results from increased water storage capacity of the *de novo* formed xylem (Reusche *et al.*, 2012). Roos *et al.* (2014) proposed that the enhanced drought stress tolerance of *V. longisporum* challenged *A. thaliana* may also be a consequence of reduced stomatal aperture, since it is decreased by 75 % in infected plants compared to mock treatment (Roos *et al.*, 2014).

In contrast to *V. longisporum*, *V. dahliae* typically induces neither bundle sheath cell transdifferentiation, nor xylem hyperplasia during *A. thaliana* infection (Fig. 3D, G, J and M) (Reusche *et al.*, 2014). Moreover, drought stress tolerance of *V. dahliae* infected plants does not differ as compared to *A. thaliana* wild-type (Reusche *et al.*, 2014). However, *V. dahliae* triggers enhanced lignification of existing vessel elements, which is visualised by strong autofluorescence (Fig. 3J) and the strong staining with the lignin specific stain potassium permanganate (Fig. 3M) (Reusche *et al.*, 2014). In conclusion, *Verticillium longisporum* and

Verticillium dahliae trigger clearly distinguishable disease phenotypes and distinct developmental reprogramming of the model plant *Arabidopsis thaliana*. In the following, these clearly distinguishable disease phenotypes will be referred to as “chlorosis” and “wilting”. Chlorosis-inducing *Verticillium* isolates will be marked with the prefix “c” and wilting isolates with the prefix “w”.

Recently, interaction phenotypes of *A. thaliana* with 22 *V. longisporum* and 47 *V. dahliae* isolates were systematically analysed. This collection comprised isolates from various host plants and distinct geographical locations in Europe and North America (K. Thole, PhD thesis, 2016). The chlorosis-inducing *V. longisporum* reference isolate c-VL43 as well as the wilting-inducing *V. dahliae* reference isolate w-JR2, used by Reusche *et al.* (2014) for the initial characterisation of the chlorosis and wilting phenotypes, were included. The analysed isolates were classified into the three interaction classes “asymptomatic”, “wilting” and “chlorosis”. In asymptomatic interactions, isolates do not trigger disease symptoms during infection of *A. thaliana*. Among the asymptomatic interaction group, 10 *V. longisporum* and 6 *V. dahliae* isolates were identified. On the one hand, these asymptomatic isolates could represent endophytes. Endophytes are defined as microorganisms, which proliferate in plant tissues usually without triggering disease symptoms (Hardoim *et al.*, 2015). On the other hand, *A. thaliana* could be resistant to isolates of the asymptomatic interaction class and thus restrict fungal growth. Resistance could either result from PAMP-triggered defence responses, which are sufficient to restrict proliferation of asymptomatic isolates or effector perception by *A. thaliana* R-proteins and thus resulting ETI. Proliferation analyses in *A. thaliana* ecotype Col-0 showed that all 6 asymptomatic *V. dahliae* isolates are able to colonise the hypocotyl and some of the isolates also colonise the leaf vasculature. However, these isolates accumulate low amounts of fungal biomass in *A. thaliana* and only few fungal hyphae are detectable in the plant’s xylem vessels, indicating that asymptomatic interaction rather results from effective disease resistance than from endophytic growth (I. Sjuts, MSc Thesis, 2014).

Among compatible interactions, 36 *V. dahliae* isolates induced w-JR2-like wilting, stunted growth and decay of older rosette leaves. None of the analysed *V. longisporum* isolates triggered w-JR2-like wilting disease symptoms, indicating that the wilting disease phenotype is most likely restricted to isolates of *V. dahliae* species. All of the 12 symptomatic *V. longisporum* isolates triggered c-VL43-like chlorosis disease symptoms including *de novo* xylem formation stunted growth, leaf chlorosis and early senescence. Most importantly, 5 *V. dahliae* isolates induced c-VL43-like chlorosis disease symptoms on *A. thaliana*. In conclusion, the chlorosis disease phenotype is not restricted to *V. longisporum* isolates and distinct *V. dahliae* isolates

are capable of triggering either chlorosis or wilting disease symptoms. Consequently, chlorosis and wilting disease phenotypes represent *Verticillium* isolate specific and not species specific disease responses of *A. thaliana*.

In a comparative genome analysis of 10 *V. dahliae* isolates, de Jonge *et al.* (2013) identified lineage-specific (LS) genomic regions, which are enriched in putative *in planta* expressed effector genes. Reverse genetic analyses experimentally supported the presence of effector genes in LS regions. Deletion of two effector genes present in the isolate w-JR2 LS region and one effector gene present in a w-VdLs17 LS region resulted in reduced pathogenicity of these isolates during infection of tomato (de Jonge *et al.*, 2013). In addition, the previously described avirulence factor Ave1 (Avirulence on Ve1 tomato), which triggers resistance mediated by the Ve1 receptor-like protein, is encoded by a LS region (de Jonge *et al.*, 2012; de Jonge *et al.*, 2013). It is conceivable, that putative lineage-specific effector molecules, encoded by LS regions of *V. longisporum* and *V. dahliae* induce distinct transcriptional and developmental reprogramming of the host *A. thaliana* leading to the establishment of the clearly distinguishable chlorosis or wilting disease phenotype. Identification of putatively secreted candidate effectors that are differentially expressed *in planta* by chlorosis- and wilting-inducing *V. dahliae* isolates supports this assumption (K. Thole, PhD thesis, 2016).

1.5 Transcriptional and developmental reprogramming of the host plant by pathogen infection

Perception of phytopathogens, e.g. by PRRs or R-genes, results in a vast transcriptional reprogramming of the attacked plant leading to induction of defence mechanisms (Doehlemann *et al.*, 2008; Iven *et al.*, 2012; Lyons *et al.*, 2015; Lewis *et al.*, 2015). Pathogens, on the other hand, employ effectors in order to modify host gene expression and development thus promoting disease (Barash and Manulis-Sasson, 2007; Gheysen and Mitchum, 2011; Doehlemann *et al.*, 2014; Toruño *et al.*, 2016).

A transcriptome analysis conducted by Iven *et al.* (2012) demonstrated that *V. longisporum* infection leads to a rapid transcriptional reprogramming of *A. thaliana* roots. Two key enzymes of the tryptophan-derived secondary metabolism, *CYP79B2* and *CYP79B3*, were identified among genes specifically induced by *V. longisporum* (Hull *et al.*, 2000; Iven *et al.*, 2012). Disruption of *CYP79B2* and *CYP79B3* function in the corresponding double mutant results in enhanced *V. longisporum* proliferation, stronger chlorosis symptoms and stunting, implying that tryptophan-derived secondary metabolism is required for defence against this vascular

pathogen (Iven *et al.*, 2012). Among others, tryptophan-derived secondary metabolites include antifungal glucosinolates and the phytoalexin camalexin (Mithen *et al.*, 2010; Bednarek, 2012a; Bednarek, 2012b). Yet, Iven *et al.* (2012) could not conclusively show, which tryptophan-derived compound restricts *V. longisporum* colonisation *in planta*. In areal tissues of *A. thaliana*, metabolites derived from the phenylpropanoid pathway contribute to *V. longisporum* resistance. Biosynthesis genes within the phenylpropanoid pathway are up-regulated after *V. longisporum* infection, which coincides with an accumulation of phenylpropanoids in *Arabidopsis* leaves. Genetic disruption or overexpression of biosynthesis genes as well as *in vitro* growth inhibition studies revealed sinapate and coniferin as phenylpropanoids involved in *V. longisporum* resistance (König *et al.*, 2014). Roos *et al.* (2015) demonstrated the role of monoterpene secondary metabolites produced by the monoterpene synthase TPS23/27 as susceptibility factors in *V. longisporum* infection of *A. thaliana* (Roos *et al.*, 2015).

As *Verticillium*, *Fusarium oxysporum* is a soil-borne hemi-biotrophic pathogen, that colonises the plant vascular system (Gordon, 2017). *F. oxysporum* infection of *A. thaliana* was shown to trigger substantial tissue-specific transcriptional reprogramming (Lyons *et al.*, 2015). Whereas expression of auxin and ABA signalling components, mannose binding lectins and peroxidases is strongly regulated in the root, plant defensins and genes involved in cold stress and senescence are transcriptionally responsive to *Fusarium* in leaf tissues. JA biosynthesis and signalling genes are up-regulated in root and leaf tissues during *F. oxysporum* infection (Lyons *et al.*, 2015). JA signalling components promote susceptibility of *Arabidopsis* to *Fusarium* (Anderson *et al.*, 2004; Thatcher *et al.*, 2009; Thatcher, Powell, *et al.*, 2012). The *F. oxysporum* effector SECRETED IN XYLEM 4 (*SIX4*) has been suggested to play a role in transcriptional activation of host JA responses. *SIX4* is highly expressed during *A. thaliana* infection by a *F. oxysporum* isolate, which induces severe chlorosis and necrosis symptoms. Plants challenged with *F. oxysporum* *SIX4* deletion mutants exhibit less chlorosis and necrosis symptoms as well as a decreased fungal proliferation in leaf tissues (Thatcher, Gardiner, *et al.*, 2012). Interestingly, impaired virulence of *SIX4* deletion mutants correlates with a reduction in the expression of JA signalling, biosynthesis, and defence related genes, indicating that *SIX4* activates *Arabidopsis* JA responses to promote disease (Thatcher, Gardiner, *et al.*, 2012). Besides *SIX4*, further pathogen effectors manipulate expression of host hormone dependent genes. The HopX1 and HopZ1 effectors of the bacterial leaf pathogen *Pseudomonas syringae*, for instance, contribute to virulence by mediating degradation of JAZ repressors of JA signalling (Jiang *et al.*, 2013; Gimenez-Ibanez *et al.*, 2014). *V. dahliae* interferes with the SA

metabolism of its host plant by secreting the isochorismatase effector VdIcs1, which is required for full pathogenicity on cotton. VdIcs1 hydrolyses the SA precursor isochorismate thus suppressing SA mediated immunity and expression of the SA marker gene *PR1* (T., Liu *et al.*, 2014). Pathogen effectors can directly activate transcription of host genes. A prominent example are the transcriptional activator-like effectors (TALEs), which directly and specifically bind promoter sequences of target genes through a domain of tandem repeats (Boch *et al.*, 2009). The PthXo1, PthXo3 and AvrXa7 TALEs secreted by *Xanthomonas oryzae* bacteria during rice (*Oryza sativa*) infection induce expression of host sucrose transporter genes, likely to provide nutrients for the pathogen (Yang *et al.*, 2006; Antony *et al.*, 2010). A recent report suggests that pathogen effectors also interfere with host gene transcription by regulating histone acetylation. The *Phytophthora sojae* effector PsAvh23 disrupts assembly of the plant histone acetyltransferase complex SAGA, thus suppressing activation of defence related genes (Kong *et al.*, 2017).

Several pathogens induce developmental reprogramming of their host plant. Phytopathogenic *Agrobacterium tumefaciens* bacteria cause development of crown galls, tumorous outgrowths on roots and stems of a large variety of plants (Ikeuchi *et al.*, 2013). Along with several effectors, *A. tumefaciens* transfers a T-DNA into the plant cell, which is randomly integrated into the host genome. The T-DNA encodes hormone biosynthesis genes. Accumulation of auxin and cytokinin leads to tumorous cell proliferation and formation of crown galls (Ikeuchi *et al.*, 2013; Gohlke and Deeken, 2014). In contrast to *A. tumefaciens*, gall formation by the bacterial pathogen *Pantoea agglomerans* primarily depends on secreted effector molecules (Barash and Manulis-Sasson, 2007). Induction of leaf tumours by the biotrophic fungus *Ustilago maydis*, the causal agent of smut disease on maize (*Zea mays*), also relies on fungal effector molecules (Redkar *et al.*, 2017; Matei *et al.*, 2018). During tumour development maize mesophyll cells become hypertrophic, i.e. enlarged in size, whereas bundle sheath cells undergo a hyperplastic cell division. A comparative transcriptome analysis identified putative cell-type specific *U. maydis* effector genes, which may play a role in developmental reprogramming of maize mesophyll and bundle sheath cell during leaf tumour formation (Matei *et al.*, 2018). Intriguingly, Matei *et al.* (2018) demonstrated that hyperplastic division of bundle sheath cells is dependent on the *U. maydis* effector See1, which was previously described to be required for leaf tumour induction (Redkar *et al.*, 2015). Leaf tumours of plants infected with the *U. maydis* *see1* deletion mutant lacked hyperplastic bundle sheath cells, but contained hypertrophic mesophyll cells (Matei *et al.*, 2018).

1.6 Aim of the study

Verticillium chlorosis- and wilting-inducing isolates cause clearly distinguishable disease phenotypes on *Arabidopsis thaliana* Col-0. *V. longisporum* and *V. dahliae* chlorosis-inducing isolates trigger *V. longisporum*-like symptoms including *de novo* xylem formation, stunted growth, leaf chlorosis and early senescence. In marked contrast, infection with *V. dahliae* wilting-inducing isolates leads to wilting, stunted growth and decay of older rosette leaves. It was postulated that these disease phenotypes are triggered by lineage-specific *Verticillium* effector molecules which induce distinct transcriptional and developmental reprogramming patterns of the host plant (K. Thole, PhD thesis, 2016). In her PhD Thesis, K. Thole identified several putatively secreted candidate effectors that are differentially expressed *in planta* by chlorosis- and wilting-inducing *V. dahliae* isolates and may possibly be causal for the respective disease phenotype.

The aim of this study was to identify differentially expressed host genes that may be involved in establishment of the chlorosis disease phenotype in response to putative effectors. To this end, same RNA-sequencing data as analysed by K. Thole for the identification of chlorosis isolate specific fungal effectors was used. A comparative transcriptome analysis of *A. thaliana* and *Nicotiana benthamiana* plants infected with five chlorosis-inducing *V. dahliae* isolates as well as five wilting-inducing isolates was conducted. As *A. thaliana*, *N. benthamiana* also demonstrates *de novo* xylem formation in response to chlorosis isolate infection but not during wilting isolate challenge, suggesting that chlorosis isolates trigger similar transcriptional reprogramming of this solanaceous host (K. Thole, PhD thesis, 2016). On the one hand, *A. thaliana* root transcriptome was analysed, in order to assess early host responses to *Verticillium* infection, i.e. during penetration and establishment of plant-pathogen interaction in the root. On the other hand, *N. benthamiana* shoot transcriptome was analysed in a time course at advanced time points of infection. With this approach, late responses to *Verticillium* challenge, i.e. during colonization of the xylem and the necrotrophic phase, should be evaluated. In order to confirm results of the transcriptome analysis, expression of host candidate genes was analysed in independent infection experiments. Finally, reverse genetic analyses were performed, to assess the role of candidate genes in *de novo* xylem formation, establishment of chlorosis, early senescence and wilting disease symptoms as well as in disease resistance or susceptibility to *Verticillium*.

2. Materials and Methods

2.1 Materials

2.1.1 *Arabidopsis thaliana* plant material

Table M1. Wild-type *Arabidopsis thaliana* accessions used in this study.

Accession	Abbreviation	Reference
Columbia-0	Col-0	N1092; NASC ¹

¹ Nottingham Arabidopsis Stock Centre (NASC), University of Nottingham, Loughborough, United Kingdom

Table M2. *Arabidopsis thaliana* mutant lines used in this study.

Genotype	Mutation	Reference/ Source
<i>at5g24080-1</i>	SALK_086625, T-DNA insertion in <i>At5g24080</i>	N586625, NASC ¹
<i>at5g24080-2</i>	SALK_147104, T-DNA insertion in <i>At5g24080</i>	N647104, NASC ¹
<i>at5g24080-3</i>	SAIL_551_D12, T-DNA insertion in <i>At5g24080</i>	N823334, NASC ¹
<i>anac071-1</i>	SALK_012841, T-DNA insertion in <i>At4g17980</i>	N512841, NASC ¹
<i>anac071-2</i>	SALK_105147, T-DNA insertion in <i>At4g17980</i>	N605147, NASC ¹
<i>rd17</i>	SAIL_1295_D06, T-DNA insertion in <i>At1g20440</i>	N848473, NASC ¹
<i>aba1-101 (sre3)</i>	T-DNA insertion in <i>At5g67030</i>	Barrero <i>et al.</i> , 2005
<i>mpk3</i>	MPK3-DG, produced by Deleteagene method (Li <i>et al.</i> , 2002)	Miles <i>et al.</i> , 2005
<i>eds1-2</i>	mutation in <i>At3g48090</i> , produced by fast neutron-bombardment	Bartsch <i>et al.</i> , 2006
<i>snc1</i>	mutation in <i>At4g16890</i> , produced by EMS mutagenesis	Li <i>et al.</i> , 2001
<i>mos7-1</i>	mutation in <i>At5g05680</i> , produced by fast neutron bombardment	Cheng <i>et al.</i> , 2009
<i>sgn3-3</i>	SALK_043282, T-DNA insertion in <i>At4g20140</i>	Pfister <i>et al.</i> , 2014

¹ Nottingham Arabidopsis Stock Centre (NASC), University of Nottingham, Loughborough, United Kingdom

Table M3. Transgenic *Arabidopsis* lines. All transgenic lines were generated in this study.

Name	Introduced construct	Genetic background
DS21	pC3-promAt5g25080::At5g24080::Venus	at5g24080-1
DS22	pC3-promAt5g25080::At5g24080::Venus	at5g24080-2
DS25	pHG152-35S::At5g24080::Venus	at5g24080-1
DS26	pHG152-35S::At5g24080::Venus	at5g24080-2

2.1.2 *Nicotiana benthamiana* plant material

Nicotiana benthamiana seeds were received from the Max-Planck-Institute for Plant Breeding Research in Cologne, Germany. *Nicotiana benthamiana* plants were used in RNA-sequencing analyses (2.2.7).

2.1.3 Pathogens

Table M4. *Verticillium* isolates used in this study.

Isolate	Species	Geographical origin	Isolated from	Reference
Vl43	<i>V. longisporum</i>	Germany	<i>B. napus</i> (<i>Brassicaceae</i>)	G. Braus ¹
V76	<i>V. dahliae</i>	Mexico	<i>Gossypium spec.</i> (<i>Malvaceae</i>)	A. v. Tiedemann ²
T9	<i>V. dahliae</i>	California (USA)	<i>Gossypium spec.</i> (<i>Malvaceae</i>)	A. v. Tiedemann ²
ST100	<i>V. dahliae</i>	Belgium	Soil	B. Thomma ³
V781I	<i>V. dahliae</i>	Cordoba (Spain)	<i>Olea europaea</i> (<i>Oleaceae</i>)	R. Jiménez-Díaz ⁴
V138I	<i>V. dahliae</i>	Cordoba (Spain)	<i>Gossypium spec.</i> (<i>Malvaceae</i>)	R. Jiménez-Díaz ⁴
V192I	<i>V. dahliae</i>	Sevilla (Spain)	<i>Gossypium spec.</i> (<i>Malvaceae</i>)	R. Jiménez-Díaz ⁴
JR2	<i>V. dahliae</i>	Ontario (Canada)	<i>S. lycopersicum</i> (<i>Solanaceae</i>)	B. Thomma ³
VdLs17	<i>V. dahliae</i>	California (USA)	<i>Lactuca sativa</i> (<i>Asteraceae</i>)	B. Thomma ³
DVD-31	<i>V. dahliae</i>	Essex Co.(Canada)	<i>S. lycopersicum</i> (<i>Solanaceae</i>)	B. Thomma ³
DVD-S29	<i>V. dahliae</i>	Essex Co.(Canada)	Soil	B. Thomma ³

¹ Department of Molecular Microbiology & Genetics, University of Göttingen, Germany;

² Division of Plant Pathology and Crop Protection, University of Göttingen, Germany;

³ Laboratory of Phytopathology, University of Wageningen, The Netherlands;

⁴ Department of Plant Pathology, University of Córdoba and Institute of Sustainable Agriculture, Cordoba, Spain.

Table M5. Genetically modified *Verticillium* isolates used in this study.

Isolate	Species	Description	Reference
VI43-GFP	<i>V. longisporum</i>	GFP-tagged line used in CLSM analyses of <i>A. thaliana</i> root infection	Reusche <i>et al.</i> , 2014
JR2-GFP	<i>V. dahliae</i>	used in CLSM analyses as control of root infection for RNA sequencing	K. Thole, PhD thesis, 2016

Table M6. Pathogens used in this study, which do not belong to *Verticillium* spp.

Species	Pathovar/ isolate	Reference
<i>Hyaloperonospora arabidopsisdis</i>	NOCO2	Parker <i>et al.</i> , 1993
<i>Pseudomonas syringae</i>	pv. <i>tomato</i> DC3000 (Δ AvrPto/AvrPtoB)	Lin and Martin, 2005
<i>Botrytis cinerea</i>	B05.10	A. Sharon ¹

¹ The George S. Wise Faculty of Life Sciences, Tel Aviv University, Tel Aviv-Jaffa, Israel.

2.1.4 Vectors

Table M7. Vectors used in this study. Vectors were assembled using Gibson Assembly[®] protocol (New England Biolabs). Vector maps are shown in Fig. M1.

Name	Description	Selection marker
pC3-promAt5g25080:: At5g24080::Venus	Binary <i>Agrobacterium</i> and plant transformation vector expressing At5g24080 with a C terminal Venus fluorescent protein tag under the control of its native promoter in the pC3 vector backbone (Ghareeb <i>et al.</i> , 2016).	Bacteria: Kanamycin Plants: BASTA [®]
pHG152-35S:: At5g24080::Venus	Binary <i>Agrobacterium</i> and plant transformation vector expressing At5g24080 with a C terminal Venus fluorescent protein tag under the control of the constitutive 35S promoter in the pHG152 vector backbone (H. Ghareeb ¹).	Bacteria: Kanamycin Plants: BASTA [®]

¹ Department of Plant Cell Biology, Georg August University Göttingen, Göttingen, Germany

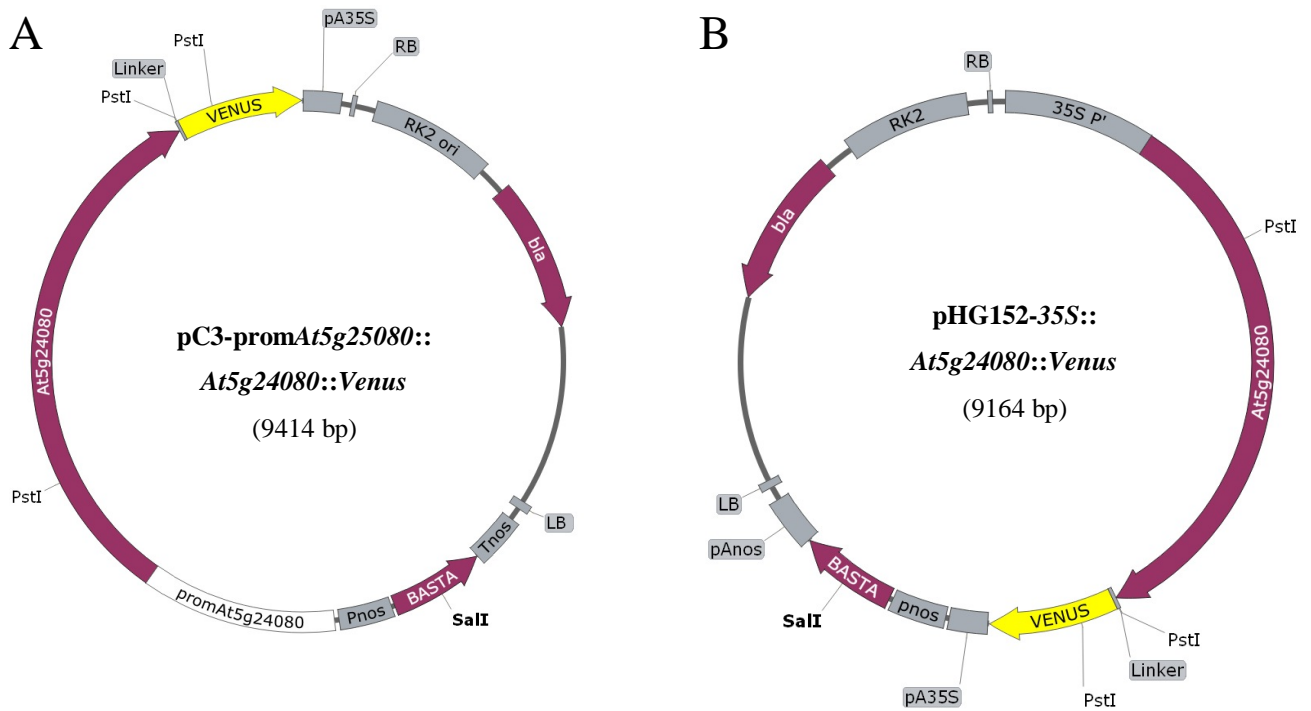


Figure M1. The vectors used in this study. bla (beta-lactamase), LB (left border), RB (right border), 35S P' (35S promoter), pA35S (terminator of the 35S promoter), RK2 ori (origin of replication in gram-negative bacteria), pnos (nopaline synthase promoter), pAnos (nopaline synthase terminator). **(A)** The binary vector pC3-promAt5g25080::At5g24080::Venus. **(B)** The binary vector pHG152-35S::At5g24080::Venus.

2.1.5 Bacterial strains used for cloning and plant transformation

2.1.5.1 *Escherichia coli*

Escherichia coli strain TOP10 (genotype: F⁻ mcrA Δ(mrr-hsdRMS-mcrBC) Φ80lacZΔM15 ΔlacX74 deoR recA1 araD139 Δ(ara-leu)7697 galU galK rpsL (StrR) endA1 nupG) was used for vector amplification. *E. coli* TOP10 were ordered from Invitrogen™ (Karlsruhe, Germany).

2.1.5.2 *Agrobacterium tumefaciens*

Agrobacterium tumefaciens strain GV3101 pMP90RK was used for transformation of *A. thaliana* (2.2.1.3). This strain carries the helper plasmid pMP90RK and is Gentamycin, Kanamycin and Rifampicin resistant (Koncz and Schell, 1986).

2.1.6 Antibiotics

Kanamycin (Kan)	50 mg/ml in H ₂ O
Carbenicillin (Carb)	50 mg/ml in H ₂ O
Rifampicin (Rif)	50 mg/ml in DMSO
Gentamycin (Gent)	15 mg/ml in H ₂ O
Ampicillin (Amp)	100 mg/ml in H ₂ O
Cefotaxime (Cef)	250 mg/ml in H ₂ O

Aqueous solutions were sterile filtrated. 1000x stock solutions were stored -20 °C

2.1.7 Oligonucleotides (*Primers*)

Oligonucleotides were ordered from Invitrogen™ (Karlsruhe, Germany). Lyophilised oligonucleotides were resuspended in H₂O to 100 µM stock solutions and kept at -20 °C, which in turn were diluted to 10 µM working stocks. Sequences highlighted in **green** represent overhangs used for Gibson assembly of pC3-promAt5g25080::At5g24080::Venus or pHG152-35S::At5g24080::Venus respectively. Sequences highlighted **blue** show an introduced *RsrII* restriction site. Sequences marked in **red** represent linker between At5g24080 and Venus.

Table M8. Oligonucleotides used in this study.

Primer	Sequence (5' to 3')	Description
DS12	TAGCATCTGAATTTTCATAACCAATCTCG ATACAC	Left T-DNA border primer for SAIL-lines
DS33	ATGACGCACAATCCCACTATCCTTCGCA	35S fwd.; for sequencing and colony-PCR
DS64	GACGCTTCATCTCGTCC	<i>AtUBQ5</i> mRNA fwd.; qPCR
DS65	GTAAACGTAGGTGAGTCCA	<i>AtUBQ5</i> mRNA rev.; qPCR
DS66	CGATGAAGCTCAATCCAAACGA	<i>AtUBQ5</i> mRNA fwd.; RT-PCR
DS67	CAGAGTCGAGCACAATACCG	<i>AtUBQ5</i> mRNA rev.; RT-PCR
DS70	ATTTTGCCGATTCGGAAC	Left T-DNA border primer for SALK-lines
DS83	GCCTCATTCTCTTTTGTTAC	<i>At5g24080</i> sequencing fwd. 1 as well as 5'-mRNA fwd.; RT-PCR
DS84	CCTAGGAGACATTGAAGAATAAC	<i>At5g24080</i> sequencing rev. 3

Primer	Sequence (5' to 3')	Description
DS85	TTTGGGAGGAGAGTGTCGG	<i>At5g24080</i> sequencing rev. 1 as well as 5'-mRNA rev.; RT-PCR
DS86	CGATTCTTACTGAGCATTTGG	<i>At5g24080</i> sequencing fwd. 2
DS87	TAGTTGTGGGGATGCTTGTG	<i>At5g24080</i> sequencing fwd. 3 as well as 3'-mRNA fwd.; RT-PCR
DS88	CTGGAGATCGCGGTAAGTG	<i>At5g24080</i> sequencing rev. 2 as well as 3'-mRNA rev.; RT-PCR
DS95	TTTTTTTTTTTTTTTTTTTTV (V = dA, dC or dG)	dT18V (oligo dT), for cDNA synthesis
DS98	AGAGCATTCGCATGTGGTTAC	Left primer for genotyping of SALK_147104 (<i>at5g24080-2</i>)
DS99	GAAACGCTCTCATGGAAGTTG	Right primer for genotyping of SALK_147104 (<i>at5g24080-2</i>)
DS100	GCGGTAAGTGAACTCACAGG	Left primer for genotyping of SALK_086625 (<i>at5g24080-1</i>)
DS101	GAAACCTCGTACTCTCCGACC	Right primer for genotyping of SALK_086625 (<i>at5g24080-1</i>)
DS102	CAAGGTCATGTGATGCATTG	Left primer for genotyping of SAIL_551_D12 (<i>at5g24080-3</i>)
DS103	ACATCAATCTTGACCCTCACG	Right primer for genotyping of SAIL_551_D12 (<i>at5g24080-3</i>)
DS104	AACGGTTCTCGAACCAATAGG	Left primer for genotyping of SALK_012841 (<i>anac071-1</i>)
DS105	TTGGTCCAATTAATGATTGAGAAG	Right primer for genotyping of SALK_012841 (<i>anac071-1</i>)
DS106	AATTACCTGGCAACTCCCAAG	Left primer for genotyping of SALK_105147 (<i>anac071-2</i>)
DS107	ACGCCCAAAGTGAGTTACATG	Right primer for genotyping of SALK_105147 (<i>anac071-2</i>)
DS108	TTTAGCCGACGTGTCTAATGG	Left primer for genotyping of SAIL_1295_D06 (<i>rd17</i>)
DS109	GTGTCAAGAGAAGGGTCCAGG	Right primer for genotyping of SAIL_1295_D06 (<i>rd17</i>)
DS121	ACGAATTCGGCCGCTGCAGCCCTAGGAGACA TTGAAGAATAAC	Rev. for <i>At5g24080</i> (including native promoter) assembly into pC3-prom <i>At5g25080</i> :: <i>At5g24080</i> :: <i>Venus</i>
DS122	GGGCTGCAGCGGCCGAATTCGTGAGCAAGGGC GAGGAG	Fwd. for <i>Venus</i> assembly into pC3-prom <i>At5g25080</i> :: <i>At5g24080</i> :: <i>Venus</i> as well as pHG152-35S:: <i>At5g24080</i> :: <i>Venus</i>
DS123	GTGATTTTTGCGGACTCTAGACTAGTTTAGTA CAGCTCGTCCATGCC	Rev. for <i>Venus</i> assembly into pC3-prom <i>At5g25080</i> :: <i>At5g24080</i> :: <i>Venus</i> as well as pHG152-35S:: <i>At5g24080</i> :: <i>Venus</i>

Primer	Sequence (5' to 3')	Description
DS124	GCGCCGGCCTCAGAGGCCCGGTCCG GAAGCG CAAAGAAACGAG	Fwd. for <i>At5g24080</i> (including native promoter) assembly into pC3-prom <i>At5g25080</i> :: <i>At5g24080</i> :: <i>Venus</i>
DS125	GCATGCATGTAAACCGTTC	prom <i>At5g24080</i> sequencing rev
DS126	CCACTACCTGAGCTACCAG	<i>Venus</i> sequencing fwd.
DS127	TCGTGCTGCTTCATGTGGTC	<i>Venus</i> sequencing rev.
DS128	GAGCGAAACCCTATAAGAACC	35S terminator sequencing rev.
DS129	TGTAGTGGTTGACGATGGTG	<i>BASTA^r</i> sequencing fwd.
DS130	GGAGAGGACCGCGGTCCGGGATCC ATGTCTT CATTTCATTTTTATTTTCC	Fwd. for <i>At5g24080</i> assembly into pHG152-35S:: <i>At5g24080</i> :: <i>Venus</i>
DS131	ACGAATTCGGCCGCTGCAGC CCTAGGAGACAT TGAAGAATAAC	Rev. for <i>At5g24080</i> assembly into pHG152-35S:: <i>At5g24080</i> :: <i>Venus</i>
DS134	CCGAGACAGAGAGGAAAAGC	<i>TSPO</i> mRNA fwd.; RT-PCR
DS135	TACCAGCGACCGGACTTATC	<i>TSPO</i> mRNA rev.; RT-PCR
DS136	GGGGAGTTCATGTTTGCCTC	5'-primer <i>ANAC071</i> mRNA fwd.; RT-PCR
DS137	TCGGTATCCAGCTATAACATGC	5'-primer <i>ANAC071</i> mRNA rev.; RT-PCR
DS138	TGTCGCGTAGTTAAGAAGAATG	3'-primer <i>ANAC071</i> mRNA fwd.; RT-PCR
DS139	CGTGGTGACCGGAAAATG	3'-primer <i>ANAC071</i> mRNA rev.; RT-PCR
DS140	TCTCCCAACTTCTTGGATCAGGTG	<i>At5g24080</i> mRNA fwd.; qPCR
DS141	TTCACCGCGACTAGCGTTTCAC	<i>At5g24080</i> mRNA rev.; qPCR
DS142	AGGTTGCTTCTGAGTGCTTTCCC	<i>ANAC071</i> mRNA fwd.; qPCR
DS143	AAATTCCACGTGGTGGTTTGCC	<i>ANAC071</i> mRNA rev.; qPCR
DS144	TGTGGCTCCTACACACAACGTG	<i>TSPO</i> mRNA fwd.; qPCR
DS145	CATACAAGCCACGCAGCCAAAC	<i>TSPO</i> mRNA rev.; qPCR
DS146	TCCAACAGCTCTTCTTCTCTTCG	<i>RD17</i> mRNA fwd.; qPCR
DS147	GAGCTTCTCCTTGATCTTCTCCAC	<i>RD17</i> mRNA rev.; qPCR
DS166	CCCAGTCACGAAACCCTACG	<i>Verticillium beta-Tubulin</i> mRNA fwd.; qPCR for fungal biomass
DS167	CCAGAGGCCTGCAAAGAAAG	<i>Verticillium beta-Tubulin</i> mRNA rev.; qPCR for fungal biomass
DS179	GAAGAGTCTCCACAATCACTTGG	<i>RD29B</i> mRNA fwd.; qPCR and RT-PCR
DS180	CAACTCACTTCCACCGGAAT	<i>RD29B</i> mRNA rev.; qPCR and RT-PCR
EP23	CTTCAACGTTGCGGTTCTGTCAAGT	Right T-DNA border primer for SALK-lines

2.1.8 Antibodies

Table M9. Primary and Secondary antibodies used in this study. Antibodies were stored at 4 °C.

Primary antibody	Source (organism)	Dilution	Obtained from
α -GFP	Rat, monoclonal	1:3000	ChromoTek GmbH (Planegg-Martinsried, Germany)
Secondary antibody	Source (organism)	Dilution	Obtained from
α -rat IgG AP conjugate	Rabbit, polyclonal	1:5000	Sigma-Aldrich (Deisenhofen, Germany)

2.1.9 Enzymes

2.1.9.1 Restriction endonucleases

Restriction endonucleases were obtained from Thermo Scientific (Waltham, USA). Restriction digest reactions were set up according to manufacturer's instruction using the supplied 10x reaction buffer.

2.1.9.2 DNA-polymerases and nucleic acid modifying enzymes

Standard PCR reactions were performed with the home-made *Taq* DNA-polymerase. The proofreading high-fidelity Phusion[®] DNA-polymerase (Thermo Fisher Scientific, Waltham, USA) was used, in order to generate PCR products for cloning. The Gibson Assembly[®] Master Mix (New England Biolabs, Frankfurt, Germany) was used in order to assemble PCR products into vectors. DNaseI (Thermo Scientific, Waltham, USA) was used to reduce DNA contamination during RNA extraction. cDNA synthesis was carried out with the RevertAid[™] H Minus Reverse Transcriptase (Thermo Fisher Scientific, Waltham, USA). qPCR analyses were performed using the SsoFast[™] EvaGreen[®] supermix (Bio-Rad, Hercules, CA, USA). All reactions were set up according to manufacturer's instructions, if not further specified in the Methods section.

2.1.10 Chemicals

All chemicals were purchased from Analytic Jena (Jena, Germany), Roth (Karlsruhe, Germany), VWR (Darmstadt, Germany), Merck (Darmstadt, Germany), Sigma-Aldrich (Deisenhofen, Germany), Serva (Heidelberg, Germany), Invitrogen (Karlsruhe, Germany), New England Biolabs (Frankfurt, Germany), Difco (Heidelberg, Germany), Duchefa Biochemie (Haarlem, the Netherlands), Qiagen (Venlo, the Netherlands), Becton Dickinson (Franklin Lakes, NJ, USA), Thermo Fisher Scientific (Waltham, USA) or Bio-Rad (Hercules, CA, USA).

2.1.11 Media

All media were autoclaved at 121 °C for 20 min. Upon storage media were boiled in a microwave until no solid agar was visible. Media were cooled down to ca. 60 °C before adding antibiotics and other heat labile compounds.

Agrobacterium tumefaciens medium

DYT

Peptone	16	g/L
Yeast extract	10	g/L
NaCl	5	g/L
pH 7,2		

For agar plates 1.5 % (w/v) agar were added to the liquid DYT-Medium.

Arabidopsis thaliana medium

½ MS (Murashige-Skoog)

MS/vitamins	2.2	g/l
MES	0.6	g/l
Saccharose	10	g/l
pH 5.7 (KOH)		

For agar plates 1.5 % (w/v) plant agar were added to the liquid MS-Medium

Escherichia coli medium

LB (Luria-Bertani)

Peptone	10	g/L
Yeast extract	5	g/L
NaCl	5	g/L
pH 7,0		

For agar plates 1.5 % (w/v) agar were added to the liquid DYT-Medium.

Pseudomonas syringae medium

NYG

Peptone	5	g/L
Yeast extract	3	g/L
Glycerol	20	ml/L
pH 7,0		

For agar plates 1.5 % (w/v) agar were added to the liquid DYT-Medium.

Verticillium spp. Medium

SXM (Simulated Xylem Sap)

Casein	4	g/L
Pectin (Apple)	2	g/L
1 M MgSO ₄	2	ml/L
Trace element solution (1000x)	1	ml/L
AspA (50x)	20	ml/L

For agar plates 1.5 % (w/v) agar were added to the liquid DYT-Medium.

2.1.12 Buffers and solutions

All Buffers and solutions were autoclaved or subjected to filter sterilisation. Heat labile compounds were added upon autoclaving. General buffers and solutions are listed below. For buffers used in particular experiments the reader is referred to the respective method.

<u>AspA (50x):</u>	NaNO ₃	3.5	M
	KCl	350	mM
	KH ₂ PO ₄	350	mM
	pH 5.5 (KOH)		
<u>CERK1 extraction buffer</u>	Sucrose	250	mM
	HEPES-KOH, pH 7.5	100	mM
	Glycerol	5	% (v/v)
	Na ₄ P ₂ O ₇	50	mM
	Na ₂ MoO ₄	1	mM
	NaF	25	mM
	EDTA	10	mM
	DTT	1	mM
	Triton X-100	0.5	% (w/v)
	Add 1:100 PIC before use		
<u>Chloral hydrate solution</u>	Chloral hydrate	2500	g/L
<u>DNA gel loading dye (6x):</u>	Sucrose	4	g
	EDTA (0.5 M)	2	ml
	Bromphenol blue	25	mg
	H ₂ O to 10 ml		
<u>FTA Super Soft Puffer</u>	Tris	10	mM
	EDTA	2	mM
	Tween [®] 20	0.1	% (v/v)
<u>High salt precipitation buffer:</u>	NaCl	7.01	g
	Trisodium citrate dehydrate	23.53	g
	H ₂ O to 100 ml		
<u>KCl/ MES buffer:</u>	KCl	1	mM
	MES	5	mM
	pH 5.8		

<u>PCR reaction buffer (10x):</u>	Tris	100 mM
	KCl	500 mM
	MgCl ₂	15 mM
	Triton X-100	1 % (w/v)
	pH 9.0	

This buffer was used for homemade *Taq* DNA polymerase.

<u>Propidium iodide solution</u>	Propidium iodide	10 µg/ml
----------------------------------	------------------	----------

<u><i>Pseudomonas</i> infiltration medium:</u>	MgCl ₂	5 mM
	Sylvet	0.002 % (v/v)

<u>Safranin O solution</u>	Safranin O	1 % (w/v)
----------------------------	------------	-----------

SDS-PAGE:

SDS-loading buffer (4x)	Tris-HCl, pH 6.8	200 mM
	DTT	400 mM
	SDS	8 % (w/v)
	Glycerol	40 % (v/v)
	Bromphenol blue	0.1 (w/v)

Laemli-loading buffer (2x)	Tris	125 mM
	SDS	4 % (w/v)
	Glycerol	20 % (v/v)
	Bromphenol blue	0.02 % (w/v)
	DTT	0.2 M
	pH 6.8 (HCl)	

SDS running buffer (10x)	Tris	30.28 g/L
	Glycine	144.13 g/L
	SDS	10 g/L

Transfer buffer (20x)	Tris-base	1 M
	Boric acid	1 M
	pH 8.3	

TBS-T (20x)	NaCl	3	M
	Tris-HCl, pH 8.0	200	mM
	Tween-20	1	% (v/v)
Stacking gel buffer (4x)	Tris pH 6.8 (HCl)	0.5	M
Resolving gel buffer (4x)	Tris pH 8.8 (HCl)	1.5	M
Alkaline phosphatase buffer	Tris, pH 9.5	100	mM
	NaCl	100	mM
	MgCl ₂	50	mM
<u>TAE buffer (50x):</u>	Tris	242	g
	EDTA	18.6	g
	Glacial acetic acid	57.1	ml
	H ₂ O to 1000 ml		
	pH 8.5		
<u>TE buffer:</u>	Tris	10	mM
	EDTA	1	mM
	pH 8.0 (HCl)		
<u>TE-1 buffer:</u>	Tris	10	mM
	EDTA	0.1	mM
	pH 8.0 (HCl)		
<u>Trace elements solution (1000x):</u>			
Solution A:	FeSO ₄ · 7 H ₂ O	5	g/L
	EDTA	50	g/L
Solution B:	ZnSO ₄ · 7 H ₂ O	22	g/L
	H ₃ BO ₃	11	g/L
	MnCl ₂ · 4 H ₂ O	5	g/L
	CoCl ₂ · 6 H ₂ O	1.6	g/L
	CuSO ₄ · 5 H ₂ O	1.6	g/L
	(NH ₄) ₆ Mo ₇ O ₂₄ · 4 H ₂ O	1.1	g/L

Ingredients of Solution B have to be dissolved in H₂O in the given order. Solution A and B are mixed 1:1. Subsequently pH is adjusted to 6.5 with KOH and the Trace elements solution is sterile filtered.

<u>TRIzol buffer:</u>	Guanidine thiocyanate	47.264	g
	Ammonium thiocyanate	15.224	g
	Glycerol	25	ml
	Sodium acetate, pH 5.0 (from 3 M stock)	16.7	ml
	Phenol in saturated citrate-solution (pH 4.3)	190	ml
	H ₂ O to 1000 ml		

<u>Trypan blue staining solution:</u>	Lactic acid	10	ml
	Phenol	10	ml
	Glycerol	10	ml
	H ₂ O	10	ml
	Trypan blue	10	mg
	Ethanol (96 %)	40	ml

<u>Vogel-buffer:</u>	Sucrose	15	g
	Trisodium citrate · 2 H ₂ O	2.5	g
	K ₂ HPO ₄	5	g
	MgSO ₄ · 7 H ₂ O	0.2	g
	CaCl ₂ · 2 H ₂ O	0.1	g
	NH ₄ NO ₃	2	g
	H ₂ O to 1000 ml		
	pH 6.0		

2.2 Methods

2.2.1 Working with plant material

2.2.1.1 Plant growth conditions and propagation

For infection experiments *Arabidopsis thaliana* or *Nicotiana benthamiana* plants were grown in perforated plastic pots (17.5 cm · 13 cm · 5.5 cm). In order to ensure optimal aeration a perforated plastic pot was placed into a second perforated plastic pot containing empty 2 ml eppendorf tubes as spacer. The upper pot was filled with 200 ml clay granules (Seramis GmbH, Mogendorf, Germany) and 800 ml of a sand-soil mixture in a ratio of 1:1. Subsequently, the sand-soil mixture was watered with 250 ml H₂O supplemented with 0.1 % (v/v) Wuxal[®] liquid fertilizer (Manna, Ammerbuch-Pfäffingen, Germany) and ca. 60 single seeds were placed with a toothpick on the surface at a steady distance. Finally, seeds were stored for 2 days at 4 °C for vernalisation and cultivated in a short day growth chamber (8 h light at 22 °C; 16 h dark at 18 °C; 65 % relative humidity).

For seed setting plants were grown in square plastic pots (8 cm) filled with soil in a long day growth chamber (16 h light at 22 °C; 8 h dark at 18 °C; 65 % relative humidity) and seeds collected 12-16 week after germination. In order to collect seed, inflorescence stems were covered with a paper bag before silique maturation and opening. Soil grown plants were watered every 2-3 days with tap water.

In vitro *A. thaliana* seedlings were grown on angled agar plates, in order to allow root growth on the agar surface. For this purpose one side of a square petri dish (10 cm · 10 cm) was placed on its lid and filled with ½ MS-agar. *A. thaliana* seeds were surface sterilised as described in 2.2.1.2. After the agar solidified, 10 seeds per plate were placed in a row on the upper, thin side of the agar plate. Agar plates were sealed with Millipore tape (Merck, Darmstadt, Germany), stored for 2 days at 4 °C for vernalisation and cultivated in a Percival[®] growth chamber (CLF Plant Climatics, Wertingen, Germany) under short day conditions (10 h light at 22° C, 14 h dark at 20° C, 65 % relative humidity). If used for *Verticillium* root infection, *in vitro* seedlings were cultivated in a short day growth chamber (8 h light at 22 °C; 16 h dark at 18 °C; 65 % relative humidity).

2.2.1.2 Seed sterilisation

In order to avoid contamination of growth chambers by insect of the *Thysanoptera* genus, seeds of soil grown plants were cold sterilised. Seeds were sealed in airtight plastic bags and stored for 48 h at -20 °C. Afterwards, seeds were kept in the sealed plastic bags at room temperature until they warmed up.

In vitro grown *A. thaliana* seedlings were surface sterilised with ethanol under a sterile bench. Seeds were transferred into 1.5 ml microcentrifuge tubes, covered with 1 ml 70 % ethanol and incubated at room temperature for 10 min under vigorous shaking. Thereafter, 70 % ethanol was exchanged with 96 % ethanol. Subsequently, seeds were shaken for additional 5 min. Finally, ethanol was removed and seeds washed briefly with H₂O by pipetting up and down. Seeds were then transferred onto a sterile filter paper and allowed to dry.

2.2.1.3 *Agrobacterium*-mediated stable transformation of *A. thaliana* by floral dipping

40 ml DYT-medium containing selective antibiotics were inoculated with *Agrobacterium tumefaciens*. Bacterial cultures were grown over night in a shaker at 28° C and 190 rpm. The 40 ml over night culture was used to inoculate a 400 ml DYT-medium containing selective antibiotics. This culture was incubated over night under aforementioned conditions. Next morning, cultures were spun at 4000 rpm for 15 min and the pellet resuspended in in 5 % (w/v) sucrose. Before floral dipping, 0.05 % (v/v) Sylvet-77 was added to *Agrobacterium* cell suspension, to reduce the surface tension. *A. thaliana* plants were grown in trays under long day conditions until bolting. The first inflorescence stems were removed in order to induce development of additional inflorescence stems. Inflorescences were submerged and gently shaken in the *Agrobacterium* cell suspension. After dipping, residual *Agrobacterium* cell suspension was removed with a paper towel, trays were covered with plastic lids and stored in the dark overnight. Finally, plants were transferred into a long day growth chamber to allow development of seeds.

2.2.1.4 BASTA® selection of stably transformed *A. thaliana*

T₁ seeds of stably transformed *A. thaliana* were sown in square pots (8 cm) and grown for 1 week under short day conditions. Subsequently, seedlings were sprayed with the herbicide BASTA® (200 g/L glufosinate ammonium solution, Bayer CropScience AG, Monheim, Germany) diluted 1:1000 in H₂O. Afterwards, BASTA® was applied every 2 days for 2-3 times, until non-transformed seedlings became senescent. Finally, non-transformed, senescent seedlings were removed with forceps and stably transformed *A. thaliana* T₁ kept for further analyses and seed setting.

2.2.1.5 Infiltration of *A. thaliana* with abscisic acid

Abscisic acid (ABA) was dissolved in methanol and stored as a 10 mM stock at -20° C. 50 µM ABA was prepared fresh for each experiment by diluting the ABA stock in 5 mM KCl/MES buffer. For mock treatment, the same amount of methanol without ABA was added to 5 mM KCl/MES buffer. For vacuum infiltration, 8 leaf discs (Ø 0.55 cm) were collected from fully expanded leaves of 10-11 week old *A. thaliana* plants. Leaf discs were transferred into a 10 ml disposable syringe (Servoprax GmbH, Wesel, Germany) filled with 2 ml of 50 µM ABA or KCl/MES buffer containing methanol. Air was released and syringe sealed with a closing cone (B. Braun Melsungen AG, Melsungen, Germany). The syringe was compressed for several times and thus vacuum applied until all leaf discs became entirely translucent. Infiltrated leaf discs were incubated over night. Next morning, leaf discs were dried with a paper towel, subsequently transferred into microcentrifuge tubes, frozen in liquid nitrogen and stored at -80 °C.

A. thaliana seedlings were incubated in 50 µM ABA. For this purpose, wells of a 24-well plate were filled with 2 ml of 50 µM ABA or KCl/MES buffer containing methanol. 5-6 *in vitro* grown seedlings per well were submerged in the respective solution. If used for RNA extraction, after 3 or 24 h of incubation, seedlings were briefly washed in H₂O, dried with a paper towel and transferred into 2 ml microcentrifuge tubes containing 2 stainless steel beads (Ø 0.4 cm). Seedlings were frozen in liquid nitrogen and stored at -80 °C. Seedlings, which were used in confocal microscopy, were briefly washed in H₂O and directly mounted on microscopy slides.

2.2.1.6 Confocal laser scanning microscopy

Confocal laser scanning microscopy (CLSM) was performed using a Leica SP5-DM6000 microscope (Leica, Wetzlar, Germany), an argon ion laser as excitation source and the Leica LAS AF software (v.2.6.7266.0). Excitation wavelength of 514 nm was used for Venus and emission detected at 518 to 570 nm. For GFP an excitation wavelength of 488 nm was used and emission detected at 489 to 510 nm. Detection of autofluorescence was performed at 699 to 751 nm.

2.2.2 Working with bacteria and fungi

2.2.2.1 Glycerol stocks of *Verticillium* spore cultures

Spores were harvested as described in 2.2.2.2 from a *Verticillium* liquid culture under sterile conditions. Spore suspension was not adjusted to a specific concentration. 750 µl of *Verticillium* spore suspension were mixed with 250 µl of 60 % (v/v) glycerol and mixed by pipetting up and down. Immediately, spore suspension was frozen in liquid nitrogen and stored at -80 °C.

2.2.2.2 Cultivation of *Verticillium*

180 ml Simulated Xylem Sap (SXM) supplemented with 250 mg/ml cefotaxime and 100 mg/ml ampicillin were inoculated with *Verticillium* spore suspension from a glycerol stock (a frozen piece of Ø 0.5 cm). The culture was grown in the dark in Baffled Erlenmeyer flasks for 1 week at 22 °C and 90 rpm on a rotary shaker. Subsequently, spores were harvested by filtering the culture through a filter paper. The filtrate was spun down for 15 min at 4 °C and 4000 rpm. Afterwards, the supernatant was discarded and the pellet was washed with 30 ml sterile H₂O. Finally, the pellet was resuspended in 5 ml sterile H₂O and spore concentration was determined with a Thoma counting chamber, if spores were used for infection experiments.

2.2.2.3 *Verticillium* infection of soil grown *A. thaliana* and *N. benthamiana*

3 ½-week-old *Arabidopsis thaliana* and 2 ½-week-old *Nicotiana benthamiana* plants were used. Plants were carefully removed from the sand soil mixture and roots were mechanically

injured by twirling in order to facilitate fungal penetration. Plant roots were incubated for 45 min in *Verticillium* spore suspension (titer of $1 \cdot 10^6$ spores/ml) or mock treated with H₂O. Finally, infected plants were transferred into single round pots (Ø 80 mm, steam-sterilized soil) and further cultivated under short day conditions.

2.2.2.4 *Verticillium* infection of *in vitro* grown *A. thaliana*

A. thaliana were grown *in vitro* on ½ MS agar as described in section 2.2.1.1 for 2 ½ weeks. Subsequently, plants were transferred to angled 1 % (w/v) agarose plates and incubated for 1 day in a short day growth chamber. During and after infection, *A. thaliana* plants remained on 1 % agarose plates. Due to a lack of nutrients, 1 % agarose avoids saprophytic growth of *Verticillium* on plates and supports infection of the *A. thaliana* root system. Root system of *in vitro* grown plants was spray inoculated with *Verticillium* spore suspension at a titer of $1 \cdot 10^5$ spores/ml or mock treated with H₂O. After infection, agarose plates were sealed with Millipore tape and lower part of plates was covered with aluminium foil, leaving photosynthetically active plant tissues accessible to light. Plants were transferred into a short day growth chamber. Finally, *A. thaliana* root system was either subjected to confocal laser scanning microscopy 2 days post infection (dpi) or harvested at 4 dpi and subjected to RNA extraction.

2.2.2.5 *Botrytis cinerea* drop inoculation of *A. thaliana*

For infection experiments a spore stock of the *B. cinerea* strain B05.10, provided by M. Wiermer (University of Göttingen, Germany), was used. Spore stocks containing a titer of $2.5 \cdot 10^6$ spores/ml were stored at -80° C and thawed on ice before use. Spore stocks were diluted in ¼ Potato Dextrose Broth (PDB, Sigma-Aldrich, St. Louis, USA) to a titer of $5 \cdot 10^4$ spores/ml. In order to allow germination, spore suspension was incubated for 4 h at room temperature. Fully expanded leaves of 5-week-old *A. thaliana* were inoculated with 6 µl droplets of *B. cinerea* spore suspension. Plants were propagated in a Percival® growth chamber under short day conditions in fully sealed table top greenhouses, in order to ensure high humidity. After 3 days, necrotic lesion diameter was measured using a digital caliper MarCal 16ER (Mahr, Göttingen, Germany).

2.2.2.6 *Hyaloperonospora arabidopsidis* maintenance and spray inoculation of *A. thaliana*

A culture of *H. arabidopsidis* isolate NOCO2 was maintained on soil grown seedlings of its compatible host *A. thaliana* Col-0. For maintenance, culture was transferred every 7 days onto new seedlings. For spray inoculation, infected seedlings were harvested at 7 dpi into 50 ml Falcon tubes and vortexed in H₂O. Subsequently, plant material was separated from the spore suspension by filtering. Concentration of the spore suspension was determined using a Thoma counting chamber and adjusted to $5 \cdot 10^4$ spores/ml. 2-week-old seedlings grown under short day conditions were spray inoculated with *H. arabidopsidis* spore suspension. Finally, plants were transferred into a Percival[®] growth chamber (CLF Plant Climatics, Wertingen, Germany) under short day conditions (10 h light at 18° C, 14 h dark at 18° C, 65 % relative humidity) and propagated in tightly sealed table top greenhouses to ensure high humidity.

2.2.2.7 Quantification of *Hyaloperonospora arabidopsidis* propagation

35-45 seedlings of the analysed *A. thaliana* genotype were inoculated in 4 biological replicates and propagation of *H. arabidopsidis* was quantified at 6 dpi. For this purpose spores were harvested from spray inoculated seedlings as described in section 2.2.2.6. In order to obtain the number of spores per g plant tissue the weight of harvested plant material was determined before addition of H₂O. Thereafter, 10 µl H₂O were added per mg plant tissue. The number of spores was determined using a Thoma counting chamber. Counting was performed 4 times per biological replicate and mean value used for calculation of spore concentration.

2.2.2.8 *Pseudomonas syringae* vacuum infiltration of *A. thaliana*

Pseudomonas syringae pv. *tomato* (*Pst*) DC3000 Δ AvrPto/AvrPtoB was maintained on selective NYG agar plates containing 50 µg/ml Rifampicin and Kanamycin. Agar plates were incubated for 2 days at 28° C and stored at 4° C. *Pst* DC3000 Δ AvrPto/AvrPtoB was transferred onto new selective NYG agar plates every 3-4 weeks. Plants for vacuum infiltration were grown in square plastic pots (8 cm) covered with a polyester mesh, which prevents soil from getting out of the pot when turned over. 50 ml NYG-medium containing selective antibiotics were inoculated with *Pst* DC3000 Δ AvrPto/AvrPtoB. Bacterial cultures were grown over night in a

shaker at 28° C and 190 rpm. Next morning, 4 ml of this culture were used for inoculation of 50 ml of fresh NYG-medium containing selective antibiotics. This culture was incubated under same conditions for 3 h, in order to ensure that bacteria used for vacuum infiltration of *A. thaliana* were in the log growth phase. Afterwards, bacterial culture was spun down at 4000 rpm for 20 min and resuspended in 50 ml 10 mM MgCl₂. OD of the culture was measured and adjusted to an OD₆₀₀ = 0.0002 (1 · 10⁵ c.f.u/ml). One square plastic pot containing 5- to 6-week-old *A. thaliana* was inverted and placed into a desiccator filled with 600 ml bacterial suspension. Vacuum was applied for 1 min 45 sec and maintained for further 15 sec. The desiccator was shaken gently during application of vacuum in order to release air bubbles from plant leaves. Thereafter, plants were washed in a water bath containing tap water. Non-infiltrated leaves were removed using forceps.

Day 0 (d0) samples were harvested in duplicates from 4 leaves of independent plants. 4 leaf discs (Ø 0.55 cm) were macerated in a 1.5 ml microcentrifuge tube containing 100 µl 10 mM MgCl₂, subsequently diluted 1:10 and 50 µl of macerated plant tissue were plated on selective NYG agar plates. Vacuum infiltrated plants were transferred into a short day Percival® growth chamber. Day 3 (d3) samples were taken in triplicates. 4 leaf discs (Ø 0.55 cm) were macerated in a 1.5 ml microcentrifuge tube containing 100 µl 10 mM MgCl₂. A 10⁻¹ to 10⁻⁷ dilution series was prepared and 10 µl of each dilution pipetted on a selective NYG agar plate using a multichannel pipette. Finally, agar plates were incubated for 2 days at 28° C and *Pst* DC3000 ΔAvrPto/AvrPtoB c.f.u. were counted.

2.2.2.9 Transformation of chemically competent *E. coli*

50 µl aliquots One Shot® TOP 10 chemically competent *E. coli* cells (Invitrogen™, Karlsruhe, Germany) were used. Aliquots were stored at -80° C and thawed on ice before use. 10 to 25 ng plasmid DNA were added to the *E. coli* aliquot and incubated on ice for 30 min. Subsequently, the reaction mix was transferred into a preheated 42° C thermomixer for 45 sec and immediately cooled down on ice for 5 min. Afterwards 800 µl LB medium were added and cells incubated for 1 h at 37° C on a rotary shaker. The suspension was spun down at 2500 g, the supernatant removed and pellet resuspended in 50 µl LB medium. Finally, *E. coli* cells were plated on selective LB agar plates and incubated over night at 37° C.

2.2.2.10 Transformation of electro competent *A. tumefaciens*

40 μ l aliquots of electro competent *A. tumefaciens* cells were diluted 1:3 with dH₂O and mixed with 50 ng of plasmid DNA. Subsequently, cells were transferred into a precooled electroporation cuvette. The BioRad Micro Pulser™ electroporation apparatus was set to 25 μ F, 2.5 kV and 400 Ω . Immediately after electroporation, cells were transferred on ice and cuvettes filled with 1 ml precooled DYT medium. Cells were resuspended, pipetted into 2 ml microcentrifuge tubes and incubated in a thermomixer for ca. 3 h at 28° C and 600 rpm. Finally, 5 μ l and 50 μ l aliquots of the transformed cells were plated on selective DYT- agar plates and incubated for 2 days at 28° C.

2.2.3 Biochemical methods

2.2.3.1 Total protein extraction

Arabidopsis thaliana leaf material (leaf discs, \varnothing 0.55 cm) was collected into 2 ml microcentrifuge tubes and frozen in liquid nitrogen. 2 stainless steel beads (\varnothing 0.4 cm) were added before freezing. Frozen samples were homogenized into a fine powder in a bead mill (TissueLyser LT, Qiagen). The homogenization process was carried out 6 · 1 min and samples cooled down in liquid nitrogen in between. Subsequently, 150 μ l 2x SDS-PAGE sample buffer were added per 50 mg homogenized *A. thaliana* leaf material. Samples were vortexed briefly, boiled at 96° C for 8 min and centrifuged at 17000 g for 20 min. Finally, the supernatant was either transferred into a new microcentrifuge tube and stored at -20° C or loaded directly onto SDS PAGE gels.

2.2.3.2 Receptor-like kinase optimised total protein extraction

Leaf discs were collected into 1.5 ml microcentrifuge tubes, frozen in liquid nitrogen and stored at -80° C. 200 μ l CERK1 extraction buffer and a small spatula of sea sand were added to the frozen leaf discs. Subsequently, leaf discs were homogenised using a glass pistil and the IKA® RW 20 digital drill (IKA Werke, Staufen, Germany). After plant tissue was homogenised, the pistil was rinsed with 200 μ l CERK1 extraction buffer, to recover all plant material. Finally, the microcentrifuge tube was filled up to 1 ml with CERK1 extraction buffer. Samples were spun down at 17000 g and 4° C for 10 min in a tabletop centrifuge and the supernatant was

transferred into new microcentrifuge tubes and stored on ice. Protein concentration was determined as described in section 2.2.3.3. Thereafter, protein concentration was adjusted to that of the sample with lowest concentration. 60-120 μ l of the protein extract were mixed with 4x SDS loading dye and stored at -20° C or used in SDS PAGE. Before loading onto SDS PAGE gels protein extracts were boiled for 3-5 min at 95° C.

2.2.3.3 Bradford protein assay

The Bradford protein assay was used in order to determine protein concentration. Known concentrations of bovine serum albumin (BSA) were measured for a calibration curve. For this purpose 0, 3, 5, 10 and 15 μ l of 1 mg/ml BSA were pipetted into a cuvette and 1 ml of Roti[®]-Quant solution (Roth) were added. The cuvettes were vortexed and incubated at room temperature for 10 min. Afterwards, absorption was measured at 595 nm using a WPA Biowave II photometer (Biochrom, Berlin, Germany). Protein samples of unknown concentration were measured in duplicates and the mean was used for calculation of protein concentration. 3 μ l of protein sample were mixed with Roti[®]-Quant solution and absorption measured as described above. The calibration curve was generated by plotting absorption of the BSA standard against its concentration and concentration of protein samples determined using the calibration curve.

2.2.3.4 Denaturing SDS-polyacrylamide gel electrophoresis (SDS-PAGE)

SDS-gel electrophoresis was used for separation of proteins according to their molecular weight. Mini-PROREAN[®] Tetra Systems (BioRad) as well as polyacrylamide (PAA) gels were used for denaturing SDS-polyacrylamide gel electrophoresis. Resolving gels (Table M10) were poured between clean glass plates and overlaid with 500 μ l 50 % isopropanol. After polymerisation of resolving gels the isopropanol was removed by rinsing the gel with water. Residual water was removed using filter paper. Afterwards, the stacking gel (Table M11) was poured on top of the resolving gel. A comb was inserted into the stacking gel. 1.5 mm thick gels were used. The combs were removed under running water after polymerisation of the polyacrylamide gels. Gels were submerged into an electrophoresis chamber filled with 1 x SDS running buffer. The gels were loaded with protein samples as well as protein molecular weight marker and run at 80 V (stacking gel) or 100 V (resolving gel) respectively.

Table M10. Resolving polyacrylamide gel components.

Compound	10 % resolving gel
H ₂ O	4,1 ml
4x resolving gel buffer	2,5 ml
2,2,2-Trichlorethanol	25 µl
10 % SDS	0,1 ml
30 % Acrylamide/bis solution, 29:1 (Roth)	3,3 ml
TEMED (Roth)	5,0 µl
10 % APS	75 µl

Table M11. Stacking polyacrylamide gel components.

Compound	4 % stacking gel
H ₂ O	6,1 ml
4x stacking gel buffer	2,5 ml
10 % SDS	0,1 ml
30 % Acrylamide/bis solution, 29:1 (Roth)	1,3 ml
TEMED (Roth)	10 µl
10 % APS	100 µl

2.2.3.5 Immunoblot analysis

Protein samples separated by denaturing SDS-PAGE were transferred to a polyvinylidene difluoride (PVDF) membrane with a pore size of 0.45 µm. PVDF membranes were dipped in methanol before use. Stacking gels were removed with a scalpel and UV-illuminated using the ChemiDoc™ Imaging System (Bio-Rad). UV-illumination induces a reaction of tryptophans in proteins with 2,2,2-Trichlorethanol (TCE) and allows visualisation of total protein on a 300 nm transilluminator (Ladner *et al.*, 2004). Subsequently, PAA gels and PVDF membranes were pre-incubated in 1x transfer buffer on a rotary shaker for 10 min and blotting apparatus (Mini Trans-Blot® Cell, BioRad) assembled according to manufacturer's instructions. Transfer was carried out at 100 V for 2 h. Thereafter, blots were disassembled and membranes washed 3 x 2 min with ultrapure H₂O at room temperature (RT) on a rotary shaker. All further steps were carried out at RT and a rotary shaker if not stated otherwise. Membranes were then incubated for 10 min in SuperSignal™ Western blot Enhancer Antigen Pretreatment Solution (Thermo Fisher Scientific) and washed 5 x 2 min with ultrapure H₂O. Afterwards, membranes were blocked for 1 h with TBS-T containing 3 % milk powder (Roth). Membranes were rinsed briefly 3 x with TBS-T and washed for additional 5 min with TBS-T. Incubation with primary

antibody was carried out over night at 4° C on a slowly moving shaker. The primary antibody (Table M9) was diluted in SuperSignal™ Western blot Enhancer Antibody Diluent (Thermo Scientific). Upon incubation, primary antibody was removed and membranes washed 6 x 10 min with TBS-T containing 3 % milk powder. This step was followed by incubation for 2 h with the secondary antibody (Table M9) diluted in TBS-T containing 3 % milk powder. Afterwards, secondary antibody was removed and membranes washed 4 x 15 min with TBS-T. This step was followed by equilibration of the membranes in AP buffer for 10 min. Finally, 500 µl Immun-Star™ AP substrate (BioRad, Munich, Germany) were placed on membranes. Chemoluminescence and afterwards TCE-UV modified total protein was visualized using the ChemiDoc™ Imaging System.

2.2.3.6 HPLC-MS/MS analysis of abscisic acid levels in *A. thaliana*

High performance liquid chromatography-tandem mass spectrometry (HPLC-MS/MS) analysis was performed by Dr. Krzysztof Zienkiewicz (Department for Plant Biochemistry, University of Göttingen, Germany) as described in Bruckhoff *et al.*, 2016. For this purpose an Agilent 1100 HPLC system (Agilent Technologies, USA) coupled to an Applied Biosystems 3200 hybrid triple quadruple/linear ion trap mass spectrometer was used.

2.2.4 Molecular biological methods

2.2.4.1 PCR based genotyping of *A. thaliana* mutants

Single *Arabidopsis thaliana* plants were numbered and labelled. Subsequently, one leaf was harvested from each plant. Harvested leaflets were pressed through Parafilm on Whatman® FTA® classic cards using a glass tube. Usually, eight leaves were printed in a row and prints labelled according to the plants' numbering. The prints were dried at room temperature for 1 h. Afterwards, one punch (Ø = 1 mm) from each print was transferred into a PCR tube filled with 50 µl FTA Super Soft buffer. The samples were incubated for 5 min. Subsequently, FTA buffer was removed and samples incubated in 140 µl TE-1 buffer for 5 min. Again, buffer was removed and PCR mix added to the samples. Finally PCR reaction was carried out and amplified DNA separated by agarose gel electrophoresis.

2.2.4.2 Polymerase Chain Reaction (PCR)

Table M12. Typical PCR mix (20 µl final volume).

Component	Volume
Template DNA	1 µl
10x PCR reaction buffer	2 µl
DMSO	0.5 µl
dNTP Mix (10 mM dATP, dCTP, dGTP, dTTP each)	0.5 µl
Forward primer (10 µM)	1 µl
Reverse primer (10 µM)	1 µl
<i>Taq</i> DNA polymerase (4U/µl)	0.5 µl
Nuclease free water	filled up to 20 µl

Table M13. Typical PCR-conditions.

Step	Temperature	Time	Number of Cycles
Initial denaturing	94° C	5 min	1x
Denaturing	94° C	30 sec	25-50x
Annealing	50-60° C	30 sec	
Elongation	72° C	1 min per 1 kb	
Final elongation	72° C	7 min	1x

Homemade *Taq* polymerase was used for standard PCR-reactions (e.g. genotyping). All PCR reactions were carried out in a MyCycler Thermocycler (Biorad, Germany). Typical PCR conditions and mixes are listed in Table M12 and M13.

2.2.4.3 Agarose gel-electrophoresis

DNA fragments were separated by agarose gel-electrophoresis in a 0.8-1 % agarose gel. Biozym® LE Agarose (Hessisch Oldendorf, Germany) was dissolved in 1x TAE buffer by boiling in a microwave. Afterwards, agarose was cooled to approx. 60° C and a drop ethidium bromide (10 mg/ml) per 50 ml was added. Subsequently, agarose was poured into a gel carrier and upon polymerization submerged in a TAE-filled electrophoresis tank. DNA samples were mixed with 10x DNA loading dye and loaded on the polymerized agarose gel. Separated DNA fragments were visualized using an UV-transilluminator.

2.2.4.4 Isolation of total RNA from *Arabidopsis thaliana*

Liquid nitrogen frozen plant material was ground to a fine powder either using a mortar and pestle or a bead mill (TissueLyser LT, Quiagen). Subsequently, 1.3 ml TRIzol buffer were added to the frozen plant material, samples were shaken briefly and vortexed for 10 min. After vortexing the samples were mixed with 250 μ l chloroform, vortexed for 10 min and spun at 4° C and 13000 rpm for 45 min. 800 μ l of the upper aqueous phase were transferred into a new 2 ml microcentrifuge tube, containing 320 μ l isopropanol and 320 μ l high salt precipitation buffer. In order to precipitate RNA the samples were inverted 5-6 times, incubated for 10 min at room temperature and subsequently spun at 4° C and 13000 rpm for 30 min. The supernatant was removed by pipetting and pelleted RNA was washed with 800 μ l -20° C cold 75 % Ethanol by inverting the tube. Afterwards, samples were spun at 4° C for 15 min and the ethanol was removed by pipetting. Residual ethanol was removed by pipetting upon additional 1 min of centrifugation. Finally, the RNA pellet was air dried and resuspended in 50 μ l nuclease free water. For quality control 1 μ g of total RNA was loaded on a 0.8 % agarose gel. All extracted RNA samples were adjusted to the same concentration with nuclease free water and stored at 80° C.

2.2.4.5 Isolation of DNA from *Verticillium* infected *A. thaliana*

Whole *Arabidopsis thaliana* rosettes of *Verticillium* infected plants were used for DNA isolation. DNA was extracted using the DNeasy Plant Mini Kit (Qiagen, Hilden, Germany) according to the manufacturer's instructions. DNA was adjusted to 20 ng/ μ l and stored at -4° C.

2.2.4.6 Reverse transcription

Reverse transcription was carried out using Reverd Aid H Minus Reverse Transcriptase (Thermo Scientific). 1-3 μ g of total RNA were mixed with 1 μ l 100 μ M oligo d(T)₁₈ primer. Nuclease free water was added to a volume of 13 μ l and incubated at 65° C for 5 min. Subsequently, samples were cooled on ice for 2 min and mixed with 4 μ l 5x RT-buffer, 2 μ l 10 mM dNTPs as well as 1 μ l reverse transcriptase. Finally, reverse transcription was carried out at 42° C for 70 min and the enzyme was heat inactivated at 75° C for 5 min.

2.2.4.7 Semi-quantitative Reverse Transcription-PCR (RT-PCR)

Table M14. Typical semi-quantitative RT-PCR mix (20 μ l final volume).

Component	Volume
cDNA (250 ng/ μ l)	1 μ l
5x Phusion HF buffer	4 μ l
DMSO	0.5 μ l
dNTP Mix (10 mM dATP, dCTP, dGTP, dTTP each)	0.5 μ l
Forward primer (10 μ M)	0.75 μ l
Reverse primer (10 μ M)	0.75 μ l
Phusion DNA polymerase	0.2 μ l
Nuclease free water	filled up to 20 μ l

Table M15. Typical semi-quantitative RT-PCR conditions.

Step	Temperature	Time	Number of Cycles
Initial denaturing	98° C	30 sec	1x
Denaturing	98° C	30 sec	
Annealing	50-60° C	30 sec	25-32x
Elongation	72° C	30 sec per 1 kb	
Final elongation	72° C	10 min	1x

Semi-quantitative RT-PCR was performed in order to evaluate transcript abundance in RNA preparations. Complementary DNA (cDNA) was generated as described in 2.2.4.6, amplified by PCR and transcript abundance analysed by agarose gel-electrophoresis as described in 2.2.4.3. Homemade *Taq* or Phusion polymerases were used. Homemade 10x PCR reaction buffer was applied in reactions performed with the *Taq* polymerase, whereas 5x Phusion HF Buffer (Thermo Scientific) was used in case of the Phusion polymerase. PCR reactions were carried out in a MyCycler Thermocycler (Biorad, Germany). Typical PCR conditions and mixes used for the Phusion polymerase are listed in Tables M14 and M15.

2.2.4.8 Quantitative PCR (qPCR)

qPCR reactions were carried out using the CFX96 Touch™ Real-Time PCR Detection System and the SsoFast™ EvaGreen® Supermix (Biorad, Germany). Relative transcript levels were calculated employing the Biorad CFX Manager software (version 3.0) and the cycle threshold method (Pfaffl, 2001). PCR conditions and mixes are listed in Tables M16 and M17.

Table M16. Typical qPCR mix (20 µl final volume).

Component	Volume
cDNA (1:7.5 or 1:10 dilution of 250 ng/µl)	1 µl
2x SsoFast™ EvaGreen® Supermix	10 µl
Forward and reverse primer mix (4 µM each)	2 µl
Nuclease free water	to 20 µl

Table M17. Typical qPCR conditions.

Step	Temperature	Time	Number of Cycles
Initial denaturing	95° C	30 sec	1x
Denaturing	95° C	5 sec	
Annealing/Elongation	58° C	10 sec	44x
Melt curve	60° C - 95° C 0.5 °C per step	5 sec	71x

2.2.4.9 Extraction of PCR products from agarose gels

Ethidium bromide stained DNA was visualized by UV light. DNA fragments of expected size were excised from agarose gels with a scalpel. The NucleoSpin® Extract II kit (Macherey-Nagel, Düren, Germany) was used for extraction. DNA extraction was carried out according to the provided protocol.

2.2.4.10 Plasmid assembly

Plasmid vectors were assembled using Gibson Assembly® protocol (New England Biolabs, Frankfurt, Germany) according to the manufacturer's instructions. 5'- and 3'-overhangs were introduced to inserts by PCR via primer design. Vector backbones were digested with restriction endonucleases as described in section 2.2.4.12. A 3:1 molar ratio of insert to vector backbone was used. To calculate the amount of insert and vector backbone for optimal plasmid assembly, following formula was employed:

$$pmols = mass [ng] \cdot 1000 / base\ pairs \cdot 650\ daltons$$

Typical insert and vector amounts used for plasmid assembly are shown in Table M18.

Table M18. Typical Gibson Assembly[®] reaction mix.

Component	Amount
Insert (2)	0.06 pmol
Vector backbone	0.02 pmol
Gibson Assembly [®] master mix	5 μ l
Nuclease free water	filled up to 10 μ l

2.2.4.11 Isolation of bacterial Plasmid DNA

Plasmid DNA was isolated using the GeneJET[™] Plasmid Miniprep kit (Thermo Scientific, Waltham, USA) proceeding according to the provided protocol.

2.2.4.12 Restriction endonuclease digestion of DNA

Restriction digestion of DNA was carried out according to endonuclease manufacturer's instructions. Restriction reactions were carried out in 0.5 ml PCR tubes. Reaction mixes were incubated for at least 30 min at 37° C. A typical reaction mix is listed in Table M19.

Table M19. Typical restriction endonuclease reaction mix.

Component	Volume
10x Fast Digest buffer	1 μ l
Plasmid DNA	1 μ l
Enzyme	0.4 μ l
Nuclease free water	filled up to 10 μ l

2.2.4.13 DNA sequencing

DNA sequencing was performed using the Barcode Economy Run service of SEQLAB Sequence Laboratories (Göttingen, Germany). For this purpose, 1-12 μ l DNA were mixed with 3 μ l 10 μ M primer and the sequencing mix filled up to 15 μ l with dH₂O. Obtained DNA sequencing data was analysed with Geneious version 8.1.8 (Kearse *et al.*, 2012).

2.2.5 Histochemical methods

2.2.5.1 Propidium iodide staining

Arabidopsis thaliana seedlings were grown for 5 days on angled agar plates under short day conditions (see section 2.2.1.1). Whole seedlings were incubated for 30 sec in 10 µg/ml propidium iodide (PI) solution the dark and afterwards rinsed twice with H₂O. In order to prevent PI from entering xylem vessels, damage of *A. thaliana* roots hat do be avoided. Therefore, featherweight forceps were used and seedlings held by the cotyledons. Seedlings were mounted on microscopy slides with a sufficient amount of H₂O and cover slip laid gently on the microscopy slide to avoid squeezing of the root. PI staining of the root was analysed by confocal laser scanning microscopy. Excitation was performed with an argon laser at 513 nm and fluorescence detected at 580-630 nm.

2.2.5.2 Safranin-O staining

Arabidopsis thaliana leaves were detached from the rosette with a scalpel at the petiole base. The petiole base was immediately placed into a 1 % (w/v) safranin-O solution and incubated for 2 h. After incubation, petioles were washed in H₂O. Subsequently, epidermis and mesophyll layers were removed from leaves with a razor blade. Leaves were mounted on microscopy slides with H₂O and xylem vessels analysed with a bright field microscope.

2.2.5.3 Trypan blue staining

Leaves were harvested into 50 ml Falcon tubes and covered with 10-15 ml trypan blue staining solution. Subsequently, the Falcon tubes were boiled in a water bath for 5 min. The trypan blue solution was thoroughly removed and leaves incubated in 10-15 ml chloral hydrate solution at room temperature for destaining. Next day the chloral hydrate solution was exchanged and leaves were destained for at least additional three days. Finally, the chlorate hydrate solution was removed. The leaves were stored in 60 % glycerol. For microscopy, leaves were mounted on microscopy slides with 60 % glycerol. Trypan blue stained leaves were analysed with a Leica DM 5000B fluorescence microscope (Leica, Wetzlar, Germany) using an ATL filter cube for epifluorescence images.

2.2.6 Leaf area measurements

Leaf area was determined using the BlattFlaeche image processing software (Datinf[®] GmbH, Tübingen, Germany). For this purpose photographs of single plants were taken from above with a Panasonic Lumix FZ150 digital camera (Panasonic, Hamburg, Germany). The diameter of plastic plant pots was used as size standard.

2.2.7 RNA-sequencing analysis

Infection of *Arabidopsis thaliana* and *Nicotiana benthamiana* plants for RNA-sequencing as well as RNA extraction was carried out by Dr. Karin Thole (Department of Plant Cell Biology, University of Göttingen, Germany) as described in sections 2.2.2.4, 2.2.2.3 and 2.2.4.4 respectively. In order to control for successful penetration of *A. thaliana* seedling roots, *Arabidopsis* seedlings were infected in parallel with a GFP-tagged *V. dahliae* JR2 line. In case of *A. thaliana*, 40 roots were pooled per sample, whereas in case of *N. benthamiana*, 3 plant shoots were pooled per sample.

Preparation of RNA-samples, quality control, RNA-sequencing and RNA-read mapping were performed by the Transcriptome and Genome Analysis Laboratory (TAL, Department of Developmental Biochemistry, University of Göttingen, Germany). mRNA libraries were generated from total RNA using the TruSeq RNA Library Prep Kit v2 (Illumina, San Diego, CA, USA). In order to ensure cluster amplification on singleread flow cells, fixation of RNA samples to complementary adapter oligos was performed with the TruSeq SR Cluster Kit v3-cBot-HS (Illumina, San Diego, CA, USA). The Bioanalyser 2100 software (Agilent technologies, Santa Clara, CA, USA) was used for quality control of the RNA samples. RNA-sequencing was carried out using the Illumina HiSeq2000 system. For each sample ~30-35 million single-end 50 bp reads were obtained. RNA-sequencing reads were demultiplexed and transformed into fastq files with the CASAVA software v1.8.2 (Illumina, San Diego, CA, USA). Reads were mapped to the *A. thaliana* TAIR10 genome release (Berardini *et al.*, 2015) and to the *N. benthamiana* draft genome version 0.4.4 (Bombarely *et al.*, 2012) using the Bowtie2 software v2.1.0 (Langmead *et al.*, 2009).

Subsequently, raw RNA-read counts were received from TAL and subjected to differential gene expression analysis using RobiNA v1.2.4 (Lohse *et al.*, 2012) and the DESeq analysis method (Anders and Huber, 2010). Raw P-values were adjusted using the False Discovery Rate algorithm (Benjamini and Hochberg, 1995). Chlorosis isolate regulated candidates were

defined as being up- or down regulated with a False Discovery Rate (FDR) of ≤ 0.05 and a log₂ fold (L2F) change in expression of $\geq +1$ and ≤ -1 in the chlorosis group but not the wilting and mock group. Wilting isolate regulated candidates were defined as being up- or down regulated with the abovementioned FDR and L2F cut-offs in the wilting group but not the chlorosis and mock group. In order to control differential gene expression analysis and further reduce the number of false discoveries, expression of obtained candidate genes was manually analysed in every sample. For this purpose raw RNA-read counts were manually converted into reads per million (RPM) and compared to L2F values of differential gene expression analysis. Outliers were removed from candidate lists.

3. Results

3.1 Host plant genes which are differentially regulated by *Verticillium* chlorosis or wilting isolate infection were identified by RNA-Sequencing

Verticillium longisporum induces substantial developmental reprogramming of its host plant *Arabidopsis thaliana* leading to transdifferentiation of chloroplast-containing bundle sheath cells to functional xylem elements. Furthermore, re-initiation of cambial activity and transdifferentiation of xylem parenchyma cells result in xylem hyperplasia within the *Arabidopsis* vascular system. The *de novo* xylem formation is associated with enhanced water storage capacity and enhanced drought tolerance of *V. longisporum* infected plants (Reusche *et al.*, 2012).

Induction of *de novo* xylem formation is not restricted to *V. longisporum*. In a recent study, the interaction phenotypes of *A. thaliana* Col-0 with 47 *V. dahliae* isolates were systematically analysed. Among compatible interactions five *V. dahliae* isolates were described which trigger *V. longisporum*-like symptoms including *de novo* xylem formation, stunted growth, leaf chlorosis and early senescence. In marked contrast, 36 isolates caused wilting, stunted growth and decay of older rosette leaves (K. Thole, PhD thesis, 2016). In the following, these clearly distinguishable disease phenotypes will be referred to as “chlorosis” and “wilting”. Chlorosis-inducing *Verticillium* isolates will be marked with the prefix “c” and wilting isolates with the prefix “w”. It was postulated that these disease phenotypes are triggered by lineage-specific *Verticillium* effector molecules, which induce distinct transcriptional and developmental reprogramming patterns of the host plant. Several *V. dahliae* chlorosis isolate specific, putatively secreted candidate effectors are transcriptionally induced *in planta* and may possibly trigger the chlorosis disease phenotype (K. Thole, PhD thesis, 2016).

This study aimed at the identification of differentially expressed plant host genes that in response to putative effectors may be involved in establishment of the chlorosis disease phenotype. Therefore, same RNA-sequencing data as employed by K. Thole for the identification of chlorosis isolate specific fungal effectors was used. In her RNA-Sequencing experiment, K. Thole spray inoculated two-week-old *A. thaliana* Col-0 *in vitro* seedlings with *Verticillium* spore suspension and analysed the root transcriptome at 4 days post infection (dpi). This approach was chosen in order to assess early host responses to *Verticillium* infection, i.e. during penetration and establishment of plant-pathogen interaction in the root. In addition, K. Thole inoculated 2 ½-week-old *N. benthamiana* soil grown seedlings with *Verticillium* and analysed the shoot transcriptome in a time course at 8, 12 and 16 dpi. With this approach, late

responses to *Verticillium* infection, i.e. during colonization of the xylem and the necrotrophic phase, were assessed. *N. benthamiana* was chosen as host plant for the analysis of late time points of infection, since it accumulates higher amounts of *Verticillium* biomass compared to *A. thaliana* (Faino *et al.*, 2012). Sufficient amounts of fungal biomass were essential, in order to obtain high quality RNA-sequencing data of the fungal transcriptome. As in *A. thaliana* Col-0, chlorosis-inducing *Verticillium* isolates trigger bundle sheath cell transdifferentiation in *N. benthamiana*, whereas wilting isolates do not (K. Thole, PhD thesis, 2016), suggesting that chlorosis isolate infection leads to similar transcriptional and developmental reprogramming of this solanaceous host. Plants were infected with five chlorosis-inducing as well as five wilting-inducing *V. dahliae* isolates (Table 1), genome sequence of which was either published in previous studies or *de novo* assembled by K. Thole (Klosterman *et al.*, 2011; de Jonge *et al.*, 2012; de Jonge *et al.*, 2013; K. Thole, PhD Thesis, 2016). For each time point, three mock treated controls were analysed.

Table 1. *Verticillium* isolates used in *A. thaliana* and *N. benthamiana* infection for RNA-sequencing analysis.

<i>Verticillium</i> species	Isolate	Symptoms on <i>A. thaliana</i> Col-0	Symptom intensity*
<i>V. dahliae</i>	c-V76	chlorosis	++
<i>V. dahliae</i>	c-V138I	chlorosis	++
<i>V. dahliae</i>	c-T9	chlorosis	++
<i>V. dahliae</i>	c-V781I	chlorosis	+++
<i>V. dahliae</i>	c-ST100	chlorosis	+++
<i>V. dahliae</i>	w-V192I	wilting	-/+
<i>V. dahliae</i>	w-VdLs17	wilting	+
<i>V. dahliae</i>	w-JR2	wilting	+++
<i>V. dahliae</i>	w-DVD-S29	wilting	+++
<i>V. dahliae</i>	w-DVD-31	wilting	+++

* macroscopically determined intensity of disease symptom development as described in K. Thole, PhD thesis, 2016: mild symptoms (-/+), moderate symptoms (+), strong symptoms (++) , very strong symptoms (+++).

Preparation of RNA-samples, quality control, RNA-sequencing and RNA-read mapping were performed by the Transcriptome and Genome Analysis Laboratory (TAL, Department of Developmental Biochemistry, Georg August University Göttingen, Göttingen, Germany) using the Illumina HiSeq 2000 system. RNA-sequencing reads obtained from the *A. thaliana* 4 dpi root samples were mapped to the *A. thaliana* TAIR10 genome release (Berardini *et al.*, 2015), whereas reads obtained from the *N. benthamiana* 8, 12 and 16 dpi shoot samples were mapped to the *N. benthamiana* draft genome version 0.4.4 (Bombarely *et al.*, 2012). Subsequently, raw

RNA-read counts were received from TAL and subjected to differential gene expression analysis using *RobiNA* v1.2.4 (Lohse *et al.*, 2012) and the DESeq analysis method (Anders and Huber, 2010).

Differential gene expression analysis performed in my PhD thesis aimed at the identification of plant genes, which are specifically up- or down-regulated during infection with the chlorosis- or wilting-inducing *V. dahliae* isolates, since these genes may be implicated in establishment of the respective disease phenotype. In order to find host genes, which are significantly regulated during infection with chlorosis-inducing isolates, raw RNA-read counts of the chlorosis group samples were compared to the read counts of the wilting and mock group. Genes which were up- or down-regulated with a False Discovery Rate (FDR) of ≤ 0.05 and a log₂ fold (L2F) change in expression of $\geq +1$ and ≤ -1 in the chlorosis group but not the wilting and mock group were considered as significantly regulated. Host genes, which are significantly regulated during infection with wilting-inducing isolates were identified with the same approach. Here, the wilting group was compared to the chlorosis and mock group. A complete list of significantly regulated genes at 4 days post infection of *A. thaliana* roots and 8, 12 and 16 days post infection of *N. benthamiana* shoots with *V. dahliae* chlorosis-inducing or wilting-inducing isolates is shown in Supplementary Tables S1-S7.

Disease symptom intensities and infection kinetics often vary between single infection experiments. It is conceivable that a gene appears to be regulated at different time points due to variabilities in kinetics between infection experiments. In order to avoid loss of differentially regulated genes due to variabilities in infection kinetics, raw RNA-read counts of 8, 12 and 16 dpi *N. benthamiana* shoot samples were added and collectively subjected to differential gene expression analysis as described above. A complete list of significantly regulated genes during infection with chlorosis- or wilting-inducing *V. dahliae* isolates generated in the collective analysis of 8, 12 and 16 dpi *N. benthamiana* shoot samples is shown in Supplementary Tables S8 and S9.

In order to select candidates for further analyses, differentially expressed genes were grouped into functional categories based on MapMan (Thimm *et al.*, 2004) BIN names and published literature if available (Table S1-S9, right column). *A. thaliana* homologs were assigned to *N. benthamiana* genes using the *N. benthamiana* transcripts annotation file (version 0.4.4) and further analyses carried out using *A. thaliana* gene identifiers (IDs), since a much larger amount of bioinformatics resources, tools as well as published literature is available for the model plant *A. thaliana* than for *N. benthamiana*. *N. benthamiana* gene IDs, which did not have an *A. thaliana* homolog were discarded. Genes assigned to the functional categories cell wall

modification, transdifferentiation, signalling, water transport and drought response were of special interest, since they may play a potential role in the induction of the chlorosis phenotype characterised by *de novo* xylem formation and enhanced drought tolerance.

Table 2. List of selected candidate genes differentially regulated during infection with chlorosis-inducing *Verticillium* isolates. Differential gene expression was analysed using RobiNA v1.2.4 (Lohse *et al.*, 2012) and the DESeq analysis method (Anders and Huber, 2010) between samples of the chlorosis group versus wilting group and mock treatment. Raw P-values were adjusted using the False Discovery Rate algorithm (Benjamini and Hochberg, 1995). Positive L2F change in expression, representing gene induction, is highlighted in shades of red, whereas negative L2F change in expression, representing gene repression, is highlighted in shades of blue. Gene function is colour-coded.

<i>Nb</i> gene ID	<i>At</i> homolog	4 dpi (<i>At</i>)	8 dpi (<i>Nb</i>)	12 dpi (<i>Nb</i>)	16 dpi (<i>Nb</i>)	Description of <i>At</i> homolog	Functions in
<i>NbS00002660g0010</i>	<i>AT5G24080</i>	1.6	4.0	4.8	5.4	Protein Kinase Family Protein	signalling
<i>NbS00034147g0011</i>	<i>AT4G17980</i>	0.2	2.7	3.8	2.3	ANAC071 (<i>Arabidopsis</i> NAC domain containing protein 71)	transdifferentiation (tissue reunion)
<i>NbC25873455g0003</i>	<i>AT1G20440</i>	-0.3	5.5	5.6	5.5	RD17; COR47 (COLD-REGULATED 47)	drought response

Three candidate genes, which are differentially regulated during infection with chlorosis-inducing *Verticillium* isolates, were chosen for further analyses (Table 2). Firstly, *NbS00002660g0010*, a *N. benthamiana* gene which is homologous to *A. thaliana* protein kinase gene *At5g24080* was chosen. *NbS00002660g0010* was selected, because it was the only protein kinase gene significantly regulated and highly induced by chlorosis isolate infection at 8 and 12 dpi as well as in the collective analysis of 8, 12 and 16 dpi (Table S3, S4 and S8). Moreover, its *A. thaliana* homolog *At5g24080* was 1.6 log₂ fold, yet not significantly, induced in *A. thaliana* chlorosis isolate root infection at 4 dpi (Table 2). No molecular analyses of *At5g24080* were published so far (November 2017). As a protein kinase, it may be implicated in signal transduction required for the establishment of the chlorosis phenotype. Secondly, *NbS00034147g0011*, a *N. benthamiana* gene which is homologous to the *A. thaliana* transcriptional factor *ANAC071* (*Arabidopsis* NAC domain containing protein 71). *NbS00034147g0011* was selected, since expression of another NAC domain transcription factor, *VND7* (*Vascular Related NAC-Domain Protein 7*) is known to be required for *de novo* xylem formation during infection with the chlorosis-inducing *V. longisporum* isolate c-VL43 (Reusche *et al.*, 2012). Additionally, *ANAC071* was shown to be required for vascular tissue proliferation during graft reunion in hypocotyl of *Arabidopsis* seedlings (Matsuoka *et al.*, 2016). As a consequence, it is conceivable that *ANAC071* may be involved in vascular tissue proliferation during *de novo* xylem formation in chlorosis isolate infected plants. Finally,

NbC25873455g0003, a *N. benthamiana* gene which is homologous to *A. thaliana RD17* (*Responsive to Desiccation 17*) was chosen. *NbC25873455g0003* was selected, because it was the only drought responsive gene significantly regulated and highly induced by chlorosis isolate infection at 8 and 16 dpi as well as in the collective analysis of 8, 12 and 16 dpi (Table S3, S6 and S8). Its *A. thaliana* homolog *RD17* belongs to the dehydrin protein family, which is generally assumed to play a pivotal role in protection of the plant cell during dehydration (Hanin *et al.*, 2011). For this reason, this gene may be involved in enhanced drought tolerance during chlorosis isolate infection.

3.2 Expression of candidate genes during *Verticillium* infection of *Arabidopsis* was analysed by reverse transcription PCR

Three candidate genes were selected for further studies based on their induction during *V. dahliae* chlorosis isolate infection of *N. benthamiana* as shown in the RNA-sequencing analysis. Since this study focuses on the *Verticillium* - *A. thaliana* Col-0 pathosystem, expression of *Arabidopsis* homologs of the three selected *N. benthamiana* candidate genes was analysed during *Verticillium* chlorosis or wilting isolate infection of *A. thaliana* by reverse transcription PCR.

For this purpose 3 ½ -week-old *A. thaliana* Col-0 soil grown seedlings were inoculated with the *V. longisporum* chlorosis-inducing reference isolate c-VL43, as well as the *V. dahliae* chlorosis-inducing reference isolate c-V76 and the wilting-inducing reference isolate w-JR2. Isolate c-V76 is being used as a reference chlorosis *V. dahliae* isolate in our laboratory, since it induces robust and strong chlorosis disease symptoms on *A. thaliana* (K. Thole, PhD thesis, 2016). Isolate w-JR2 represents our reference wilting *V. dahliae* isolate, which was used by Reusche *et al.* (2014) for the initial dissection of the wilting disease phenotype. A mock treated control was included. Thereafter, total RNA was extracted from whole rosettes at 19 dpi. This time point was selected, since chlorosis and wilting symptoms are well detectable at 19-21 dpi. Finally, cDNA synthesis was carried out and *At5g24080*, *ANAC071* as well as *RD17* transcript abundance was analysed by semi-quantitative RT-PCR. Transcript abundance of the chlorosis induced candidate genes *At5g24080*, *ANAC071* and *RD17* increased during chlorosis isolate c-VL43 and c-V76 infection of *A. thaliana* as compared to mock treatment or wilting isolate infection (Fig. 4). *ANAC071* transcript levels were slightly higher during wilting isolate w-JR2 infection as compared to mock. *At5g24080* and *RD17* transcript amounts during w-JR2 infection were comparable to mock.

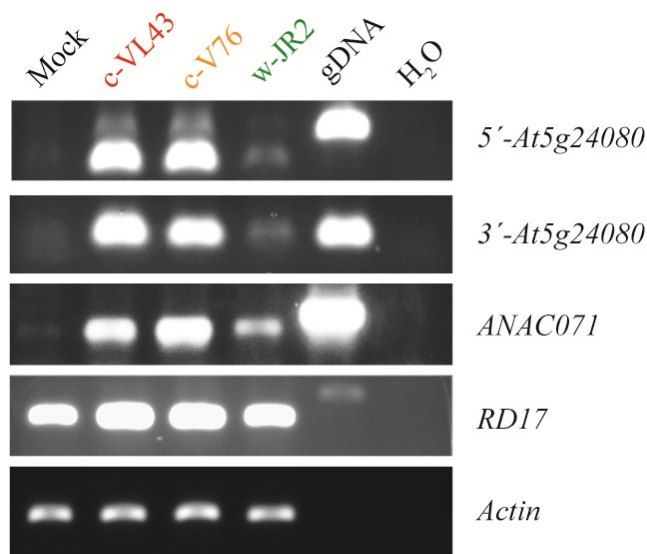


Figure 4. Semi-quantitative RT-PCR analysis of *At5g24080*, *ANAC071* and *RD17* expression during *V. longisporum* isolate c-VL43 as well as *V. dahliae* c-V76 and w-JR2 infection. Pools of 4 rosettes per sample were harvested at 19 days post infection (dpi) and subjected to RNA extraction. The housekeeping gene *Actin* was co-amplified as control. A genomic DNA (gDNA) control was included to monitor potential contamination by gDNA. A reverse primer, which binds two exon borders and spans an intron sequence was used in case of the *Actin* gene to exclude gDNA amplification. Note that 2 primer combinations

were used to test *At5g24080* expression. The 3'-*At5g24080* primer combination does not span an intron. Consequently, the 3'-*At5g24080* gDNA PCR product size corresponds to the size of the cDNA product. The experiment was performed once.

In addition to the semi-quantitative RT-PCR analysis, candidate gene expression in *A. thaliana* was independently assessed in a time course experiment during *Verticillium* chlorosis or wilting isolate infection. 3 ½ -week old *A. thaliana* Col-0 soil grown seedlings were inoculated with the *V. longisporum* chlorosis-inducing reference isolate c-VL43, as well as the *V. dahliae* chlorosis-inducing reference isolate c-V76 and the wilting-inducing reference isolate w-JR2. Subsequently, RNA was extracted from whole rosettes at 7, 14, 21 as well as 28 dpi and *At5g24080*, *ANAC071* as well as *RD17* expression analysed by quantitative PCR (qPCR).

Consistent with the results of the RT-PCR, qPCR analyses revealed a specific up-regulation of the candidate genes *At5g24080*, *ANAC071* and *RD17* by chlorosis isolate c-VL43 and c-V76 infection of *A. thaliana* as compared to mock or wilting isolate treatment (Fig. 5). *At5g24080* and *RD17* transcript levels started to increase at early time points of chlorosis isolate c-VL43 as well as c-V76 infection and peaked at 21 as well as 28 dpi (Fig. 5A and B). *At5g24080* showed the strongest induction among the three candidate genes with a ca. 300-fold higher expression in chlorosis isolate c-VL43 and ca. 460-fold higher expression in c-V76 inoculated plants compared to mock at 28 dpi (Fig. 5A). In contrast, *RD17* expression was only 27-fold induced at 28 dpi by chlorosis isolate c-V76 (Fig. 5B). *ANAC071* was up-regulated by chlorosis

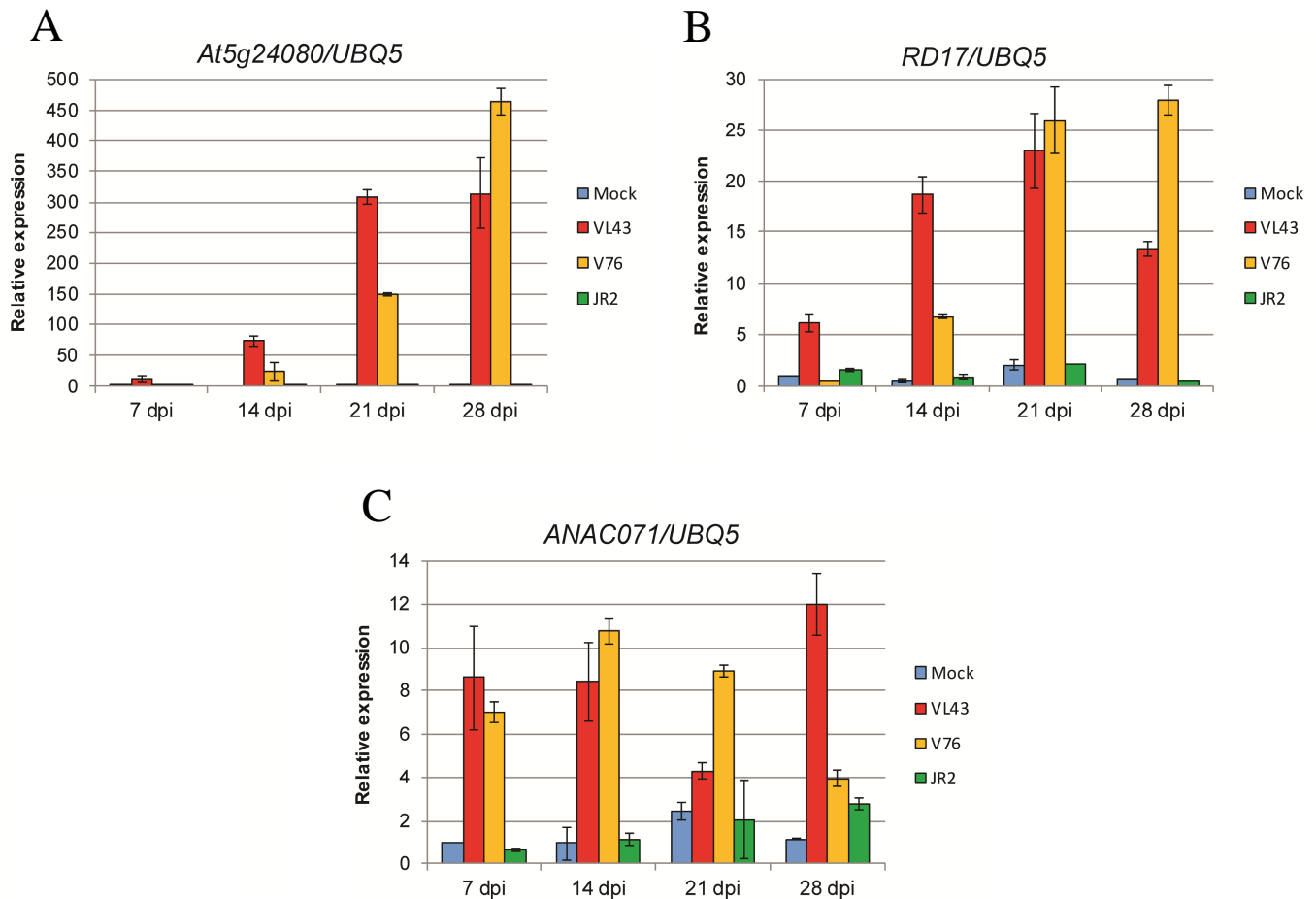


Figure 5. Quantitative PCR (qPCR) analysis of *At5g24080*, *ANAC071* and *RD17* expression in the course of *V. longisporum* isolate c-VL43 as well as *V. dahliae* c-V76 and w-JR2 infection. Pools of 4 rosettes per sample were harvested at 7, 14, 21 and 28 days post infection (dpi) and subjected to RNA extraction. Bars represent means of gene expression \pm standard deviation in arbitrary units from 2 technical replicates, normalized to the expression of *UBQ5*. **(A)** qPCR analysis of *At5g24080* expression. **(B)** *ANAC071* expression. **(C)** *RD17* expression. Experiments were repeated twice with similar results.

isolate c-VL43 and c-V76 at early and late time points of infection as compared to mock treatment (Fig. 5C). During wilting isolate w-JR2 infection, transcript levels of *At5g24080*, *ANAC071* and *RD17* were comparable to mock (Fig. 5). In summary, expression analyses demonstrated that *Arabidopsis* homologs of the three selected *N. benthamiana* candidate genes are specifically induced in *A. thaliana* Col-0 by chlorosis isolate infection.

3.3 Reverse genetic analysis of *rd17*

A *Nicotiana benthamiana* homolog of *A. thaliana* *RD17* was identified as a *V. dahliae* chlorosis isolate induced gene in the RNA-sequencing analysis performed in this study. Independent semi-quantitative RT-PCR and qPCR analyses demonstrated that *A. thaliana* *RD17* gene

expression was specifically up-regulated during infection with the *V. longisporum* chlorosis-inducing reference isolate c-VL43, as well as the *V. dahliae* chlorosis-inducing reference isolate c-V76 but not the wilting-inducing reference isolate w-JR2 (Fig. 4 and 5). *V. longisporum* chlorosis isolate c-VL43 challenge of *A. thaliana* is known to result in enhanced drought tolerance of infected plants (Reusche *et al.*, 2012). As a dehydrin, *RD17* may play a potential role in this process. In order to identify the role of *RD17* during chlorosis isolate infection an *rd17* T-DNA insertion mutant was analysed.

3.3.1 Characterisation of a *rd17* T-DNA insertion mutant

The SAIL_1295_D06 line, which carries a T-DNA insertion in the 1 kb promoter region of the *RD17* gene (Fig. 6A), was ordered from the Nottingham Arabidopsis Stock Centre (NASC, University of Nottingham, Loughborough, United Kingdom). Lines carrying a T-DNA insertion in an exon or intron of the *RD17* gene were not available. Homozygous T-DNA insertion lines were analysed using PCR based genotyping in two steps. Genotyping primers were designed with the T-DNA Express iSect tool (O'Malley *et al.*, 2015) and respective primer sequences are shown in Section 2.1.7. SAIL_1295_D06 plants were firstly analysed for homozygous T-DNA integration, using primers that flank the T-DNA insertion site. Due to its large size, the T-DNA insertion prevents amplification of the DNA-sequence encompassed by the primers. Thus, plants carrying homozygous T-DNA insertions do not show a PCR-product in this approach. Line #12 and #21 carrying homozygous T-DNA insertions in *RD17* were identified (Fig. S1, upper panel). However, it cannot be excluded that products are missing due to technical problems in the PCR. For this reason, a control PCR-based genotyping for T-DNA insertion in line #12 and #21 was performed. Here primers binding within the T DNA as well as in a flanking region were used, only yielding a PCR-product when the analysed plant carried an integrated T-DNA. In case of line #12 and #21, PCR-products were obtained in the control genotyping, confirming T-DNA insertion in *RD17* (Fig. S1, lower panel).

F₂ progeny was generated by selfing *rd17* homozygous T-DNA insertion lines and analysed for loss of functional *RD17* transcripts by semi-quantitative RT-PCR. RNA for this analysis was extracted from plants inoculated with the *Verticillium* chlorosis-inducing isolate c-VL43 and c-V76 and the wilting-inducing isolate w-JR2 at 21 dpi or mock treated plants. *RD17* transcript abundance was analysed in *Verticillium* challenged *rd17* mutant, in order to assess whether T-DNA insertion in the *RD17* promoter region had an effect on gene induction during *Verticillium* infection.

RD17 transcript abundance increased during chlorosis-inducing isolate c-VL43 and c-V76 infection of *A. thaliana* Col-0 wild-type as compared to mock treatment or wilting isolate w-JR2 infection (Fig. 6B). In the homozygous *rd17* T-DNA insertion mutant, *RD17* transcripts were detectable (Fig. 6B). Furthermore, their amounts were comparable to wild-type levels in mock treated plants as well as during chlorosis-inducing isolate c-VL43 and c-V76 as well as wilting isolate w-JR2 infection (Fig. 6B). In conclusion, T-DNA insertion in *RD17* promoter region of the homozygous *rd17* (SAIL_1295_D06) T-DNA insertion line resulted neither in a gene knock-out, nor in an abolished induction of *RD17* gene expression during chlorosis isolate infection. As a consequence, no further reverse genetic analysis were performed with the *rd17* T-DNA insertion mutant.

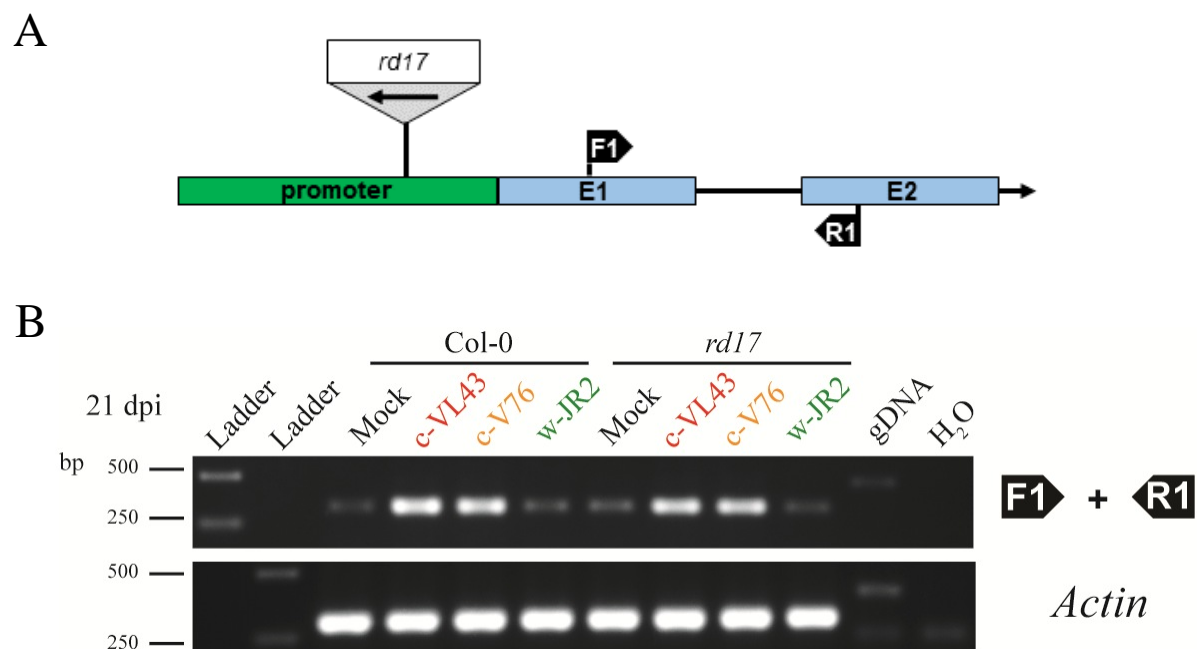


Figure 6. Characterisation of the *rd17* T-DNA insertion mutant. (A) Schematic representation of *RD17* gene structure. Exons are represented as blue boxes, whereas introns are shown as black lines. The promoter region is depicted in green. Position of the T-DNA insertion is shown as a triangle. Arrow shows the orientation of the T-DNA (left border → right border). Forward (F) and reverse (R) primer used in **B** are represented as black boxes. (B) Semi-quantitative RT-PCR analysis of *RD17* transcript abundance in *A. thaliana* Col-0 wild-type and *rd17* T-DNA insertion mutant during *V. longisporum* isolate c-VL43 as well as *V. dahliae* c-V76 and w-JR2 infection. The housekeeping gene *Actin* was amplified as control. A genomic DNA (gDNA) control was included to monitor potential contamination by gDNA. A reverse primer which binds two exon borders and spans an intron sequence was used in case of the *Actin* gene to exclude gDNA amplification. Nevertheless, a weak band is present in the *Actin* gDNA control. The *Actin* cDNA PCR product corresponds to 302 bp. Expected sizes of *RD17* F1+R1 PCR products are 332 bp cDNA and 477 bp gDNA. The experiment was performed once.

3.4 Reverse genetic analysis of *anac071*

ANAC071 represents the second *V. dahliae* chlorosis isolate induced candidate gene, which was chosen for detailed analyses. Semi-quantitative RT-PCR and qPCR experiments demonstrated that expression of *A. thaliana ANAC071* was specifically up-regulated during infection with the *V. longisporum* chlorosis-inducing reference isolate c-VL43 as well as the *V. dahliae* chlorosis-inducing reference isolate c-V76 but not the wilting-inducing reference isolate w-JR2 (Fig. 4 and 5). Chlorosis isolate infection triggers *de novo* xylem formation within the *Arabidopsis* vascular system (Reusche *et al.*, 2012; K. Thole, PhD thesis, 2016) and *ANAC071* was shown to be required for vascular tissue proliferation during graft reunion in hypocotyl of *Arabidopsis* seedlings (Matsuoka *et al.*, 2016). Therefore, I reasoned that *ANAC071* may be required for proper vascular tissue proliferation during *de novo* xylem formation in chlorosis isolate challenged plants. In order to identify the role of *ANAC071* during chlorosis isolate infection, an *anac071* knock-out mutant had to be isolated.

3.4.1 Characterisation of *anac071* knockout mutants

In order to obtain an *anac071* knock-out mutant, two T-DNA insertion lines were ordered from NASC. Firstly, SALK_012841 which was published as *anac071* in Pitaksaringkarn *et al.* (2014) and is designated *anac071-1* in this study. This line carries a T-DNA insertion in the fourth exon of the *ANAC071* gene (Fig. 7A). Additionally, the line SALK_105147, which carries a T-DNA insertion in the 1 kb promoter region of the *ANAC071* gene, was obtained. This line is designated *anac071-2* (Fig. 7A).

Homozygous *anac071-1* and *anac071-2* T-DNA insertion lines were isolated by PCR based genotyping as described for the *rd17* mutants in section 3.3.1 using genotyping-specific primers designed with the T-DNA Express iSect tool (O'Malley *et al.*, 2015). The respective primer sequences are shown in Section 2.1.7. *anac071-1* line #21 and #22 as well as *anac071-2* line #8 and #27 were identified as homozygous T-DNA insertion lines and kept for further analyses (Fig. S2 and S3). F₂ progeny was generated by selfing *anac071-1* and *anac071-2* homozygous T-DNA insertion lines and analysed for loss of functional *ANAC071* transcripts by semi-quantitative RT-PCR. RNA was extracted from plants infected with the *Verticillium* chlorosis-inducing isolate c-VL43 and c-V76 and the wilting-inducing isolate w-JR2 at 21 dpi or mock treated plants. *Verticillium* challenged *anac071* mutants were tested, in order to be able to assess whether T-DNA insertion had an effect on gene induction during *Verticillium*

infection. In the RT-PCR analysis, *ANAC071* transcript abundance was tested using a RT-PCR-specific primer combination flanking the *anac071-1* T-DNA insertion (F1 and R1 primer in Fig. 7A). Furthermore, in order to test for residual 5'-transcripts, a primer combination was used that binds in the first and second exon of the gene (F2 and R2 primer in Fig. 7A).

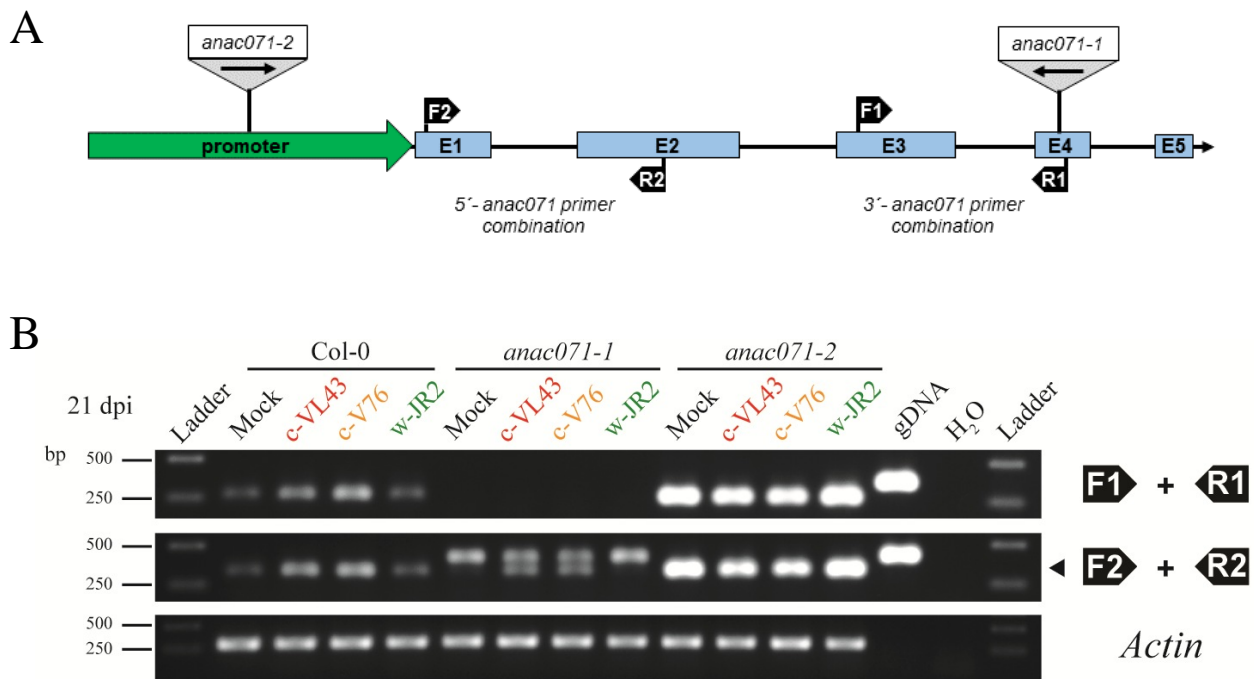


Figure 7. Characterisation of *anac071-1* and *anac071-2* T-DNA insertion mutants. (A) Schematic representation of *ANAC071* gene structure. Exons are represented as blue boxes, whereas introns are shown as black lines. The promoter region is depicted in green. Positions of T-DNA insertions are shown as triangles. Arrow shows the orientation of the T-DNA (left border → right border). Forward (F) and reverse (R) primers used in **B** are represented as black boxes. (B) Semi-quantitative RT-PCR analysis of *ANAC071* transcript abundance in *A. thaliana* Col-0 wild-type and *anac071* T-DNA insertion mutants during *V. longisporum* isolate c-VL43 as well as *V. dahliae* c-V76 and w-JR2 infection. The housekeeping gene *Actin* was amplified as a control. A genomic DNA (gDNA) control was included to monitor potential contamination by gDNA. A reverse primer which binds two exon borders and spans an intron sequence was used in case of the *Actin* gene to exclude gDNA amplification. The *Actin* cDNA PCR product corresponds to 302 bp. First panel shows 3'-*Anac071* transcript part amplified with primers F1 and R1. Expected sizes of F1+R1 PCR products are 277 bp cDNA and 366 bp gDNA. Second panel shows 5'-*Anac071* transcript part amplified with primers F2 and R2. Expected sizes of F2+R2 PCR products are 328 bp cDNA and 418 bp gDNA. The experiment was performed once.

Consistent with initial expression analyses, *ANAC071* transcript abundance increased during chlorosis-inducing isolate c-VL43 and c-V76 infection of *A. thaliana* Col-0 wild-type as

compared to mock control or wilting isolate w-JR2 infection (Fig. 7B). No *ANAC071* transcripts were detected in the *anac071-1* mutant using the F1 and R1 primer combination (Fig. 7B, upper panel). However, when using the F2 and R2 primer combination residual 5'-transcripts were detected in the *anac071-1* mutant. Yet, their amounts were reduced as compared to Col-0 wild-type (Fig. 7B, middle panel, note that upper bands represent gDNA contamination). In the *anac071-2* mutant *ANAC071* transcripts were detectable using the F1 and R1 as well as F2 and R2 primer combinations. However, transcript levels were strongly increased as compared to Col-0 wild-type (Fig. 7B). In addition, no further gene induction was visible after *Verticillium* chlorosis isolate c-VL43 and c-V76 infection (Fig. 7B). Consequently, T-DNA insertion likely lead to a constitutive overexpression of the *ANAC071* gene in the *anac071-2* mutant. Taken together, in the *anac071-1* mutant a truncated version of *ANAC071* is transcribed, whereas the *anac071-2* mutant likely represents a constitutive overexpression line.

3.4.2 Analysis of *anac071* disease phenotype during *Verticillium* chlorosis and wilting isolate infection

In order to analyse the potential role of *ANAC071* in the *A. thaliana* – *Verticillium* chlorosis isolate interaction, macroscopic disease symptoms of *anac071-1* and *anac071-2* mutants were analysed during *Verticillium* challenge. Macroscopic disease symptoms of the *anac071-1* and *anac071-2* mutant were not altered during *Verticillium* chlorosis-inducing isolate c-VL43 and c-V76 as well as wilting isolate w-JR2 infection as compared to wild-type (Fig. 8). As Col-0 wild-type, both tested *anac071* mutants showed chlorosis and early senescence of older rosette leaves during infection with the *V. longisporum* chlorosis isolate c-VL43 and *V. dahliae* chlorosis isolate c-V76 (Fig. 8A, middle panels). In addition, comparable with Col-0 wild-type, both *anac071* mutants demonstrated wilting symptoms on older rosette leaves during *V. dahliae* wilting isolate w-JR2 infection (Fig. 8A, right panel).

Stunting of the rosette was quantified as an indicator for severity of disease symptoms. Leaf area of mock treated controls was set to 100 % and leaf area of infected plants calculated as percentage of mock control. A pairwise comparison of wild-type and mutant was carried out using t-test, to analyse statistical significance. Leaf area of *anac071-1* and *anac071-2* mutants did not significantly differ from Col-0 wild-type during *Verticillium* chlorosis isolate c-VL43, c-V76 and wilting isolate w-JR2 infection (Fig. 8B), implying that mutation of the *ANAC071* gene does not affect severity of *Verticillium* induced disease symptoms.

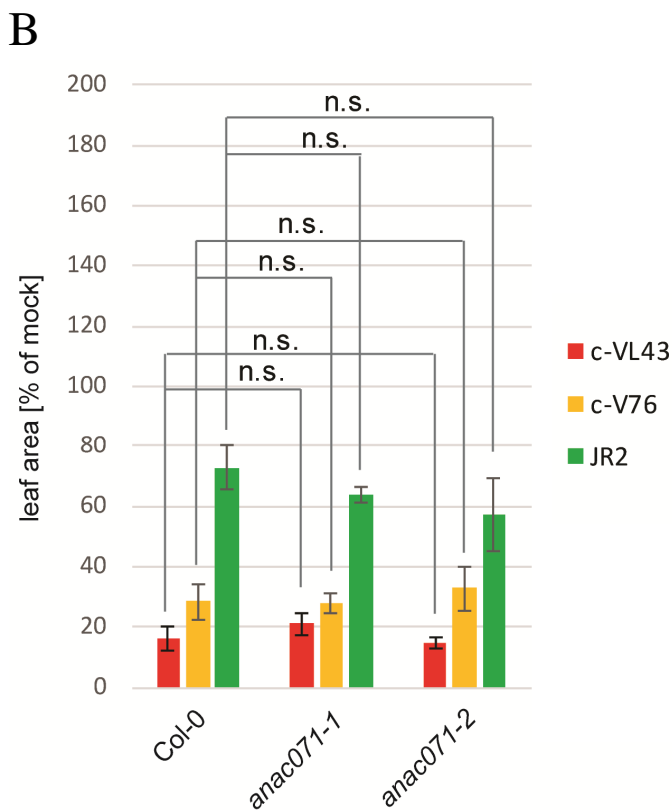
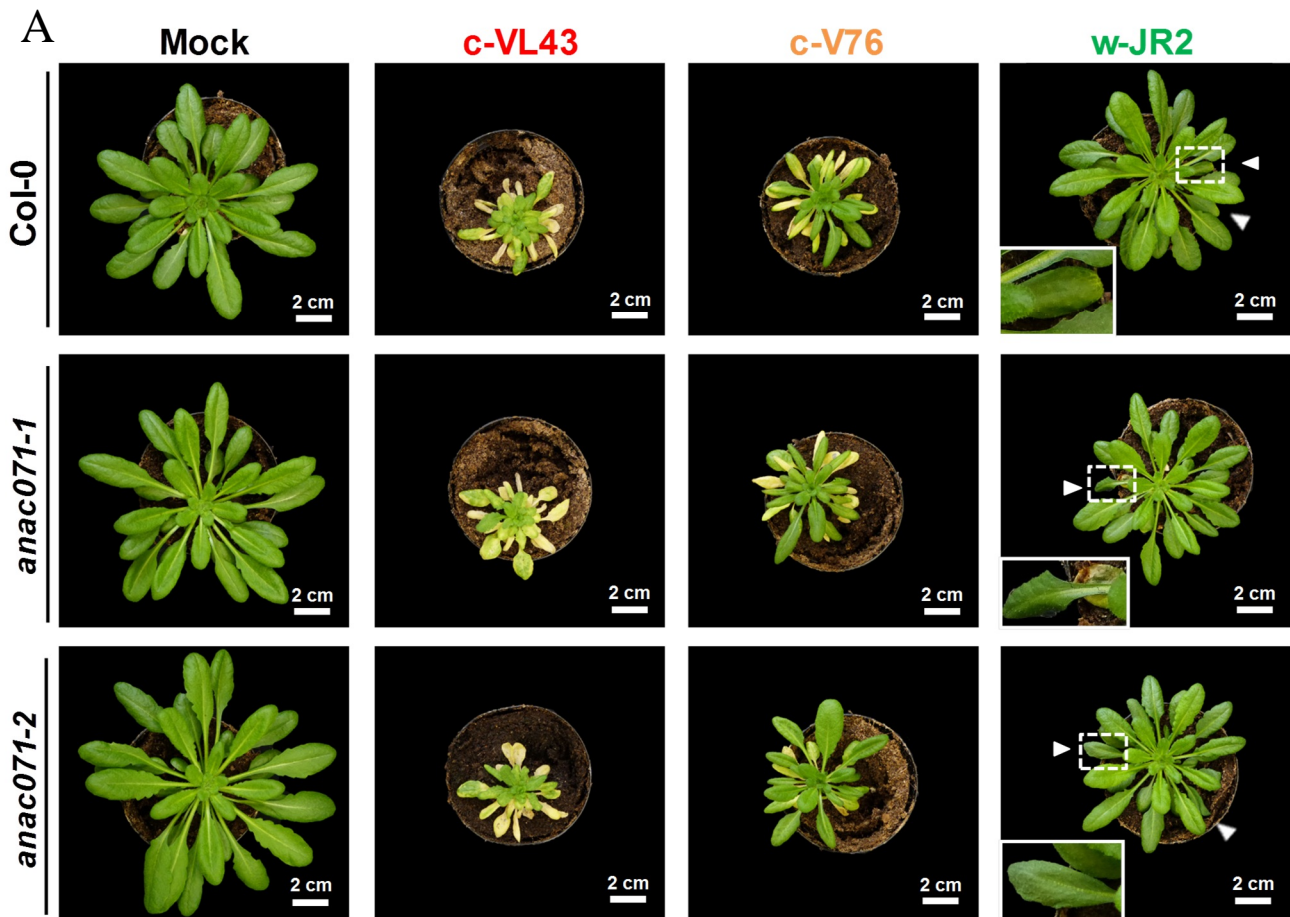


Figure 8. Disease phenotypes of *A. thaliana* Col-0 wild-type, *anac071-1* and *anac071-2* during infection with *V. longisporium* isolate c-VL43 as well as *V. dahliae* isolates c-V76 and w-JR2 (A) Disease symptoms at 21 days post infection (dpi). Insets represent magnifications of areas marked with dotted boxes. Arrowheads indicate wilting leaves. (B) Leaf area measurement at 21 days post infection. Leaf area of mock treated controls was set to 100 % and leaf area of infected plants calculated as percentage of mock control. Error bars represent standard deviation between $n = 4$ replicates. Statistical significance was tested using Student's t-test for pairwise comparison of wild-type and mutant. (n.s.) not significant. The experiment was performed once.

Subsequently, the role of *ANAC071* during *de novo* xylem formation within the *Arabidopsis* vascular system was assessed. Therefore, microscopic analyses of bundle sheath cell

transdifferentiation in *A. thaliana* Col-0 wild-type and *anac071-1* as well as *anac071-2* leaf vascular bundles were performed during *Verticillium* chlorosis isolate infection. Detached leaves were fed with the water soluble dye safranin-O, in order to visualise vascular tissue. In the mock treated Col-0 wild-type, vascular bundles are surrounded by chloroplast containing bundle sheath cells (Fig. 9A). During chlorosis isolate c-VL43 and c-V76 infection bundle sheath cells transdifferentiate to xylem elements, showing characteristic annular, helical and reticulate secondary cell wall fortifications (Fig. 9B and C). In contrast, during wilting isolate w-JR2 infection bundle sheath cell layer does not transdifferentiate (Fig. 9D). Like Col-0 wild-type, leaf vascular bundles of mock treated and wilting isolate w-JR2 infected *anac071-1* and *anac071-2* did not exhibit developmental changes (Fig. 9E, H, I and L). Furthermore, both tested *anac071* mutants showed wild-type like bundle sheath cell transdifferentiation into xylem elements during chlorosis isolate c-VL43 and c-V76 infection (Fig. 9F, G, J and K), indicating that *ANA071* does not play a role in bundle sheath cell transdifferentiation.

ANAC071 is involved in tissue reunion of incised *Arabidopsis* inflorescence stems. Tissue reunion is incomplete in the *anac071-1* mutant and *ANAC071* gene-suppressing transformants (Asahina *et al.*, 2011; Pitaksaringkarn *et al.*, 2014). For this reason, it is conceivable to postulate that defects in *ANAC071* may have an effect on connectivity of *de novo* formed xylem elements. The water soluble safranin-O dye is transported with the transpiration stream within the leaf vessel elements (Freeman and Beattie, 2009). Thus, safranin-O staining allows to test connectivity and functionality of the *de novo* formed xylem elements in water transport. Safranin-O was detectable in the lumen of newly formed xylem cells in Col-0 wild-type but also in *anac071* mutants (Fig. 9B, C, F, G, J and K), indicating that *de novo* formed xylem elements were connected to the vascular system and functional in water transport.

Taken together, neither the *anac071-1* nor the *anac071-2* mutant showed altered macroscopic disease symptoms or significant differences in disease symptom severity during infection with the *V. longisporum* chlorosis isolate c-VL43 and *V. dahliae* chlorosis isolate c-V76 as well as *V. dahliae* wilting isolate w-JR2 as compared to Col-0 wild-type. Moreover, both tested *anac071* mutants showed wild-type like bundle sheath cell transdifferentiation into connected, functional xylem elements during chlorosis isolate c-VL43 and c-V76 infection. In conclusion, these results suggest that *ANAC071* does not play a role in establishment of chlorosis disease symptoms and bundle sheath cell transdifferentiation during *Verticillium* chlorosis isolate infection.

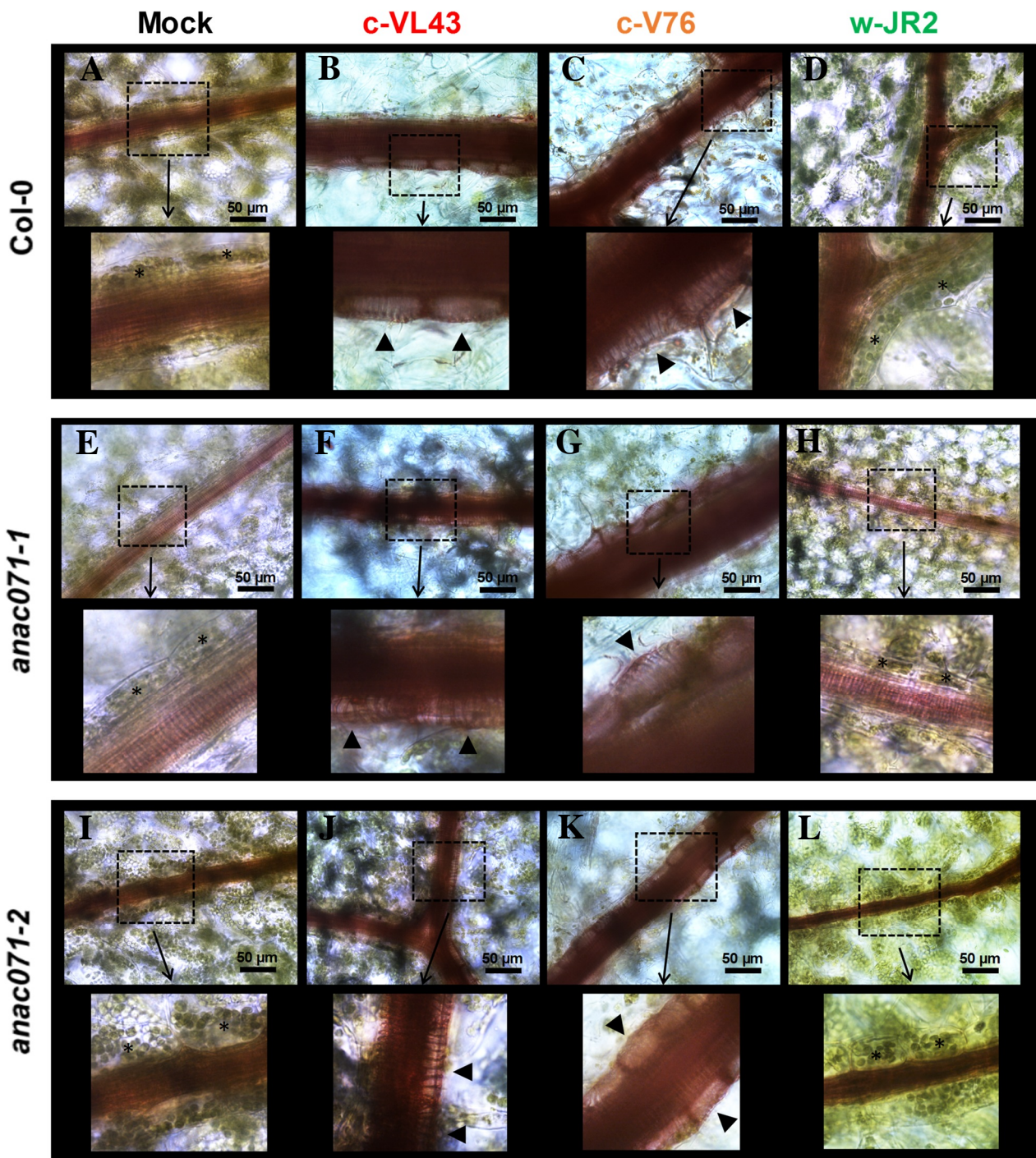


Figure 9. Analysis of bundle sheath cell transdifferentiation into functional tracheary elements in leaf vascular bundles of *A. thaliana* Col-0 wild-type and *anac071* mutants 21 days post infection (dpi) with *V. longisporum* isolate c-VL43 as well as *V. dahliae* isolates c-V76 and w-JR2. Detached leaves were fed with the water-soluble dye safranin-O. Figures (A-L) show bright field images of leaf vascular bundles with the focal plane set to the xylem cell lumen to demonstrate staining of xylem sap. Insets represent magnifications of areas marked with dotted boxes. Asterisks indicate chloroplast containing bundle sheath cells, whereas arrowheads point at *de novo* formed tracheary elements containing safranin-O stained xylem sap. The experiment was performed once.

3.5 Reverse genetic analysis of *at5g24080*

RNA-sequencing analysis performed in this study identified a *Nicotiana benthamiana* homolog of *A. thaliana* protein kinase *At5g24080* as a *V. dahliae* chlorosis isolate induced gene. *At5g24080* was selected as a candidate gene for detailed analyses, because it is significantly as well as highly induced by chlorosis isolate infection and no molecular analyses of *At5g24080* were published so far (November 2017). Semi-quantitative RT-PCR and qPCR revealed that *A. thaliana At5g24080* was specifically up-regulated during infection with the *V. longisporum* chlorosis-inducing reference isolate c-VL43, as well as the *V. dahliae* chlorosis-inducing reference isolate c-V76 but not the wilting-inducing reference isolate w-JR2 (Fig. 4 and 5). As a protein kinase, it may play a potential role in signal transduction required for the establishment of the chlorosis phenotype.

3.5.1 *In silico* analyses suggest that AT5G24080 is an active G-type lectin receptor-like kinase

At5g24080 is annotated in the *A. thaliana* TAIR10 genome release as a 1681 bp gene consisting of four exons (Berardini *et al.*, 2015). Yet, in the RNA-sequencing analysis, a vast number of reads mapped up to 1350 bp upstream of the annotated transcriptional start (Fig. S4), indicating that the transcription start site annotated in the TAIR10 genome release was incorrect. In order to identify the actual transcriptional start, the upstream sequence was analysed for presence of a start codon, which was in frame with the TAIR10 annotated open reading frame (ORF). For this purpose splice site prediction was carried out using the NetGene2 Server (Hebsgaard *et al.*, 1996) and ORF prediction of putative coding sequences performed in Geneious version 8.1.8 (Kearse *et al.*, 2012). Indeed, a 3058 bp ORF which was in frame with the TAIR10 annotation and was covered by the RNA-sequencing reads was identified. The amino acid sequence corresponding to the obtained ORF is shown in Fig. 10.

In the *A. thaliana* TAIR10 genome release, AT5G24080 is annotated as a protein-kinase family protein, containing a transmembrane domain and a serine/threonine protein kinase domain (Fig. 10, sequence underlined green). The ORF, which was predicted in this study and is covered by the RNA-sequencing reads, harbours an N-terminal signal peptide (Fig. 10). N-terminal peptides mediate targeting of secretory and membrane proteins to the endoplasmic reticulum (Nothwehr and Gordon, 1990; Kapp *et al.*, 2013), suggesting that AT5G24080 likely represents a secretory or membrane localised protein. In addition, this ORF contains a bulb-type

lectin domain, an S-locus glycoprotein domain and a PAN-like domain (Fig. 10). Bulb-type lectin domains are known to be involved in carbohydrate binding and are mainly specific for D-mannose monosaccharides but also oligomannosides and N-linked high mannose glycans (Van Damme *et al.*, 2008; Bellande *et al.*, 2017). S-locus glycoprotein domains are characteristic for kinases of self-incompatibility locus in flowering plants (Hinata *et al.*, 1995; Sakamoto *et al.*, 1998). PAN domains mediate protein-protein and protein-carbohydrate interaction (Tordai *et al.*, 1999). A domain architecture consisting of a bulb-type lectin domain followed by S-locus glycoprotein domain and a PAN-like domain is typical for G-type lectin proteins (Bellande *et al.*, 2017). As AT5G24080 also contains a transmembrane domain and a serine/threonine protein kinase domain, it can be classified as a putative G-type lectin receptor-like kinase (G-type LecRLK).

MSSFHFYFPSVGLFSFFCFLLVSLA^{TEPH}I^{GLGSKLKASEPNRAWVSANGTFAIGFTRFKPTDRFLLSIWFAQLPGDPTIVWSPNRSNRPVTKEA}
VLELEATGNLVLSDQNTVVWTSNTSNHGVESAVMSESGN^{FLLLGTEVTAGPTIWQ}SFSQPSDTLLPNQPLTVSLELTSNPSRHRGHYSLKMLQ
QHTSLSLGLTYNINLDPHANYSYWSGPDISNVTGDVTAVLDDTGSFKIVYGESSIG^{AVVYVYKNPVDNRRNYNNSNLGLTKNPVLRRLVLENNC}
NLRLYRWDNDMNGSSQVWPEAAVSNP^{CDIAGICGNGVCNLDRTKKNADCLCLPG}SVKLPDQENAKLCSDNSSLV^{QECESNINRNGSFKISTVQ}
ETNYFYSERSV^{IENISDISNVRKCGE}^{CLSDCKCVASVYGLDDEKPYCWLKSLNFGGFRDPGSTLFVKTRANESYPSNSNNNDKSRKSHGLR}
QKV^{LVIPIVVGMVLVLLGMLLY}YNLDRKRTLKRAAKNSL^{LICDSPVSFTYRDLQNC}T^{NNFSQLLGSGGFGTVYKGTVAGETLVAVKRLDRAL}
SHGEREFITEVNTIGSMH^{HMNLVRLCGYCE}SDSHRLLVY^{EYMINGSLDKWIF}SSEQTANLLDWRTRFEIAVATAOGIAYFHEQCRNRIIHCDIK
PENILLDDNFCPKVSD^{DFGLAKMMGREHSHVVTMIRGTRGYLAPEWVSNRPITVKADVYSYGMLLLEIVGGRNLDMSYDAEDFFYPGWAYKELT}
NGTSLKA^{VDKRLQGVAAEEEEVVKALKVAFWCIODEVSMRPSMGEVVKLE}EGTSD^{EINL}PPMPOTILELIEEGLEDVYRAMRREFNNOLSS^{SLTVN}
TITTSQSYR^{SSSRSHATCSYSSMSPR}

Figure 10. AT5G24080 amino acid sequence and domain structure. The N-terminal signal peptide is marked in purple, the bulb-type lectin domain is shown in turquoise, S-locus glycoprotein domain in dark green, the PAN-like domain in grey, the transmembrane domain is depicted in orange and the serine/threonine protein kinase domain in yellow. The sequence underlined in green represents the Open Reading Frame (ORF) resulting from the TAIR10 *At5g24080* genomic DNA sequence. N-terminal signal peptide prediction was carried out using SignalP 4.1 (Petersen *et al.*, 2011). The bulb-type lectin domain, S-locus glycoprotein domain, PAN-like domain as well as the serine/threonine protein kinase domain were predicted by PROSITE release 20.16 (Sigrist *et al.*, 2013). Prediction of the transmembrane domain was carried out using DAS-TMfilter (Cserző *et al.*, 2002).

In order to assess whether the AT5G24080 kinase domain is catalytically active, its primary structure was analysed for conserved features. AT5G24080 kinase domain amino acid sequence was aligned to the kinase domain sequence of *Bos taurus* Cyclic AMP dependent protein kinase catalytic subunit, alpha form (PKA-C α) and *A. thaliana* EF-Tu receptor (EFR), CHITIN ELICITOR RECEPTOR KINASE 1 (CERK1) as well as the G-type LecRLK LIPOOLIGOSACCHARIDE-SPECIFIC REDUCED ELICITATION (LORE). PKA-C α

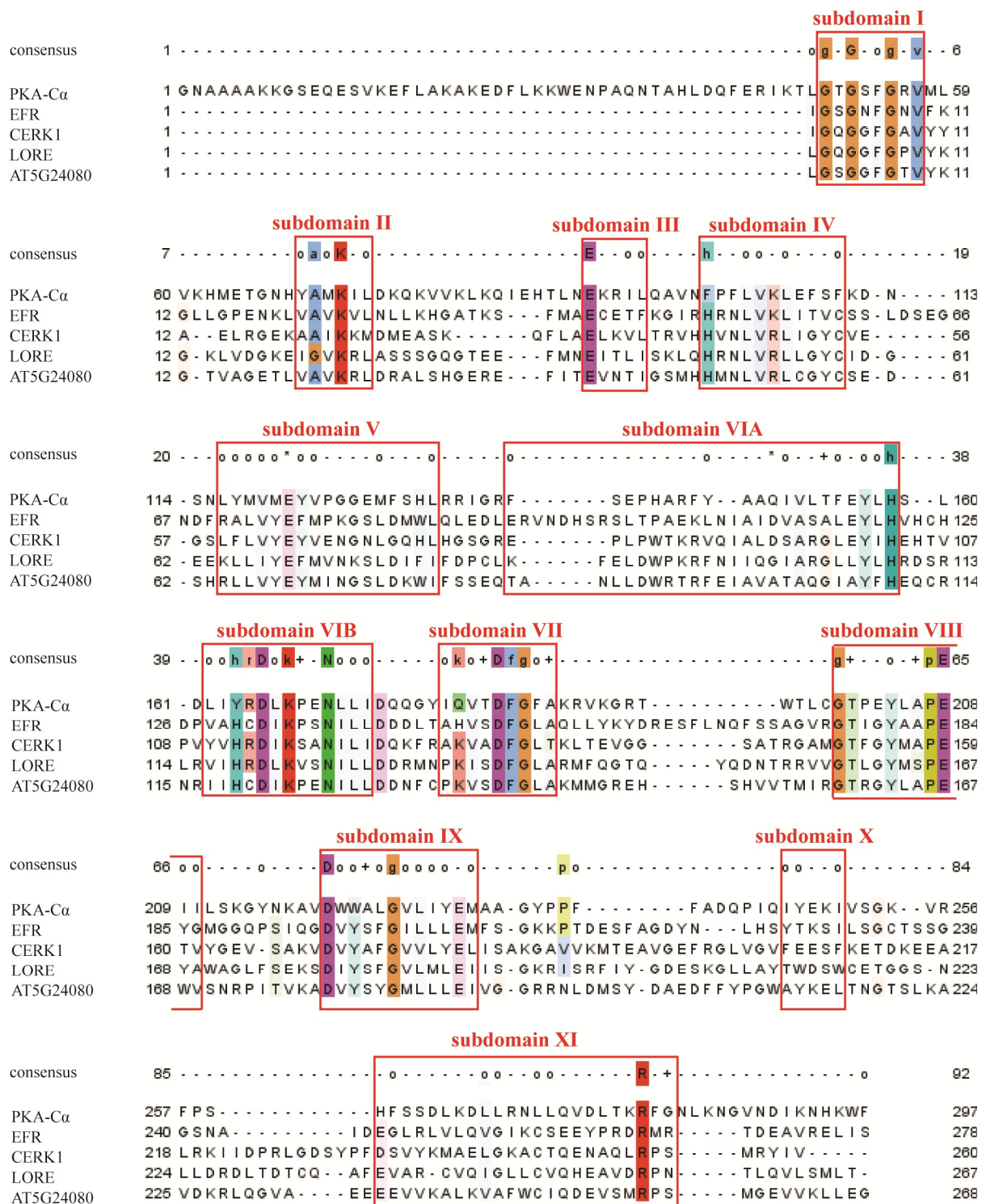


Figure 11. Amino acid sequence alignment of AT5G24080 with the *Bos taurus* Cyclic AMP-dependent protein kinase catalytic subunit, alpha form (PKA-C α) and members of the *Arabidopsis* receptor-like protein kinase (RLK) superfamily with active kinase domains. Amino acid sequences of the kinase domains only are shown. Conserved subdomains are indicated by red boxes. Capital letters in the consensus sequence indicate invariant amino acid residues, whereas lowercase letters indicate nearly invariant residues. o represents conserved nonpolar residues, * polar residues, + small nearly neutral residues. PKA-C α sequence was obtained from www.uniprot.org, *Arabidopsis* RLK sequences from www.arabidopsis.org and the consensus sequence from Hanks and Hunter, 1995. The alignment was produced in MEGA7 (Kumar *et al.*, 2016) using the MUSCLE algorithm (Edgar, 2004).

serves as catalytically active reference kinases, since crystal structure of its kinase domain is well characterised (Bramson *et al.*, 1982; Engh *et al.*, 1996; Prade *et al.*, 1997; Davies *et al.*, 2007). EFR and CERK1 represent typical immune related *A. thaliana* receptor-like kinases with experimentally proven phosphorylation activity (Schwessinger *et al.*, 2011; Suzuki *et al.*, 2016). LORE was included as an *A. thaliana* G-type LecRLK, playing a role in PAMP perception (Ranf *et al.*, 2015). The obtained amino acid alignment is shown in Fig. 11.

Active protein kinase domains harbour twelve subdomains which are not interrupted by long insertions and contain several invariant or nearly invariant residues (Hanks and Hunter, 1995). All twelve kinase subdomains were found in the AT5G24080 amino acid sequence, containing all invariantly conserved amino acid residues (Fig. 11). Subdomains I, II, III and V are involved in adenosine triphosphate (ATP) binding and contain the conserved glycine (G) in subdomain I, lysine (K) in subdomain II, glutamate (E) in subdomain III. Subdomain VIB contains the catalytic loop with the invariant aspartate (D) and asparagine (N) residue. Subdomain VII contains the highly conserved DFG motif (aspartate-phenylalanine-glycine) and is implicated in magnesium (II) ion binding. Subdomain VIII is involved in kinase activation and harbours the conserved glutamate (E). Furthermore, conserved aspartate (D) and arginine (R) residues are present in subdomains IX and XI respectively. Moreover, none of the subdomains harbours large amino acid insertions (Fig. 11). As a consequence, AT5G24080 is most likely an active protein kinase.

Lectin receptor kinases from various plant species were shown to function in defence against bacterial as well as fungal pathogens and herbivorous insects (Kim *et al.*, 2009; Chen *et al.*, 2006; Gilardoni *et al.*, 2011; Cheng *et al.*, 2013; Cole and Diener, 2013; Liu *et al.*, 2015). Most important, the *A. thaliana* G-type LecRLK LORE has recently been proposed to function as a pattern recognition receptor (PRR) for perception of lipopolysaccharide (LPS) pathogen associated molecular patterns (PAMPs) from *Pseudomonas* and *Xanthomonas* bacteria (Ranf *et al.*, 2015). These results may also suggest a potential role of AT5G24080 in plant immunity. In order to test whether AT5G24080 is phylogenetically related to the putative immune receptor LORE, an amino acid sequence-based phylogenetic analysis of all 39 known *A. thaliana* G-type lectin receptor-like kinases (Bellande *et al.*, 2017) was carried out.

In the phylogenetic analysis *A. thaliana* G-type RLKs clustered into 2 major groups which were reproduced in 100 % of bootstrap replicates (Fig. 12, red and blue branches) and several smaller groups consisting of 2-4 members (Fig. 12, black branches). LORE and AT5G24080 clustered into 2 clearly separated groups, suggesting that AT5G24080 is not closely phylogenetically related to the putative immune receptor LORE. The group which harboured AT5G24080 was

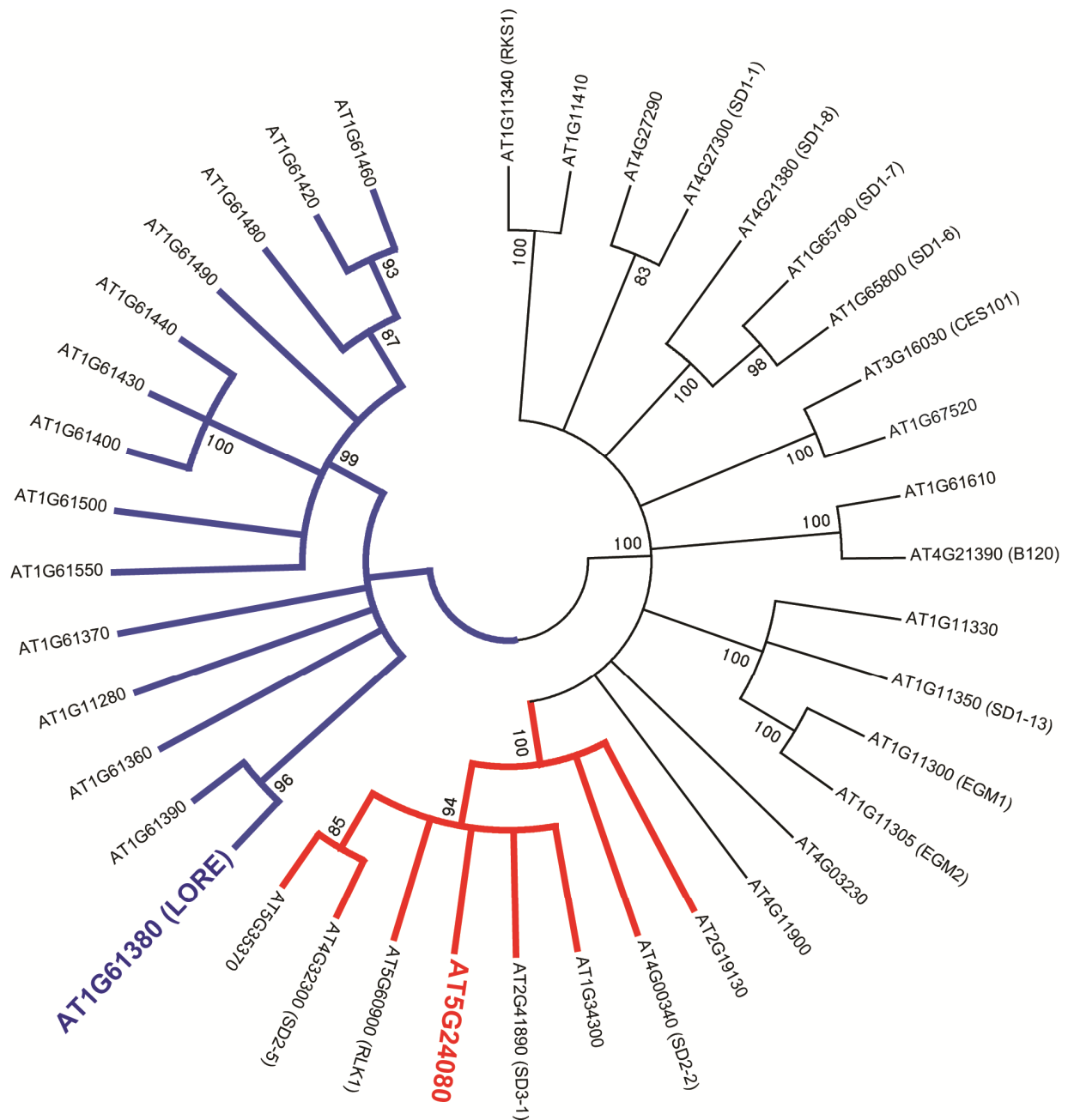


Figure 12. Phylogenetic analysis of *Arabidopsis* G-type lectin receptor-like kinases (LecRLK). Amino acid sequences of 39 *Arabidopsis* G-type LecRLKs (Bellande *et al.*, 2017) were obtained from www.uniprot.org and www.arabidopsis.org. The sequences were aligned in MEGA7 (Kumar *et al.*, 2016) using the MUSCLE algorithm (Edgar, 2004). Regions with high degree of length polymorphisms were excluded from the alignment as described in Olsson *et al.*, 2009. The consensus tree was inferred from 1000 bootstrap replicates using the maximum likelihood method and the Jones-Taylor-Thornton (JTT) model (Jones *et al.*, 1992). Branches corresponding to partitions reproduced in less than 80 % bootstrap replicates are collapsed. Bootstrap values of supported taxa are shown in [%]. The group containing AT5G24080 (designated group 1) is highlighted red, whereas the group containing LORE (designated group 2) is highlighted blue.

designated group 1 (Fig. 12, red branches), whereas the group containing LORE was designated group 2 (Fig. 12, blue branches). Members of a phylogenetic group often share a common

ancestor and their function may be conserved. However, no molecular analyses of G-type RLK group 1 members were published so far (November 2017). Thus, phylogenetic analysis did not allow to draw any conclusions about AT5G24080s putative function.

Functional redundancy among the phylogenetically related G-type RLK group 1 members may pose a problem in reverse genetic analyses. In order to assess whether AT5G24080 may function redundantly with other G-type RLK group 1 members, a co-expression analysis was performed. Co-regulation of expression was determined across tissues and developmental stages, after hormone treatment, during abiotic stress and during pathogen stress using the Botany Array Resource (BAR) Expression Browser (Toufighi et al., 2005) and the respective AtGenExpress expression dataset. The transcription factor gene *MYB102* (*At4g21440*) showing high degree of co-regulation with *At5g24080* in all four expression datasets represented by Pearson's correlation coefficient of ca. 0.7-0.9 (Fig. 13, highlighted green) was used as a positive control. In the tissue and development as well as hormone expression datasets, *At5g24080* together with *MYB102* fell into a separate cluster as compared to other G-type RLK group 1 members (Fig. 13A and B). *At5g24080* and *MYB102* clustered together with *At5g35570* in the abiotic stress dataset (Fig. 13C). However, co-expression of *At5g24080* and *At5g35570* was rather low, represented by a Pearson's correlation coefficient of ca. 0.4 as compared to 0.8 of *At5g24080* and *MYB102*. In the pathogen stress dataset, *At5g24080* and *MYB102* clustered together with *SD2-5* (*At4g32300*) (Fig. 13D). Again, *At5g24080* and *SD2-5* showed a low co-expression represented by a Pearson's correlation coefficient of ca. 0.2 as compared to 0.7 of *At5g24080* and *MYB102*. Taken together, expression of *At5g24080* through distinct tissues and developmental stages, after hormone treatment, during abiotic stress and during pathogen stress does not strongly correlate with other G-type RLK group 1 members, suggesting that they are not likely to function redundantly with *At5g24080*.

In summary, *in silico* analyses of RNA-sequencing reads demonstrated that AT5G24080 represents a putative G-type lectin receptor-like kinase. *In silico* analysis of the AT5G24080 kinase domain suggests that it is catalytically active. In the phylogenetic analysis of *A. thaliana* G-type RLKs, AT5G24080 clustered into a group consisting of eight members of unknown function but not with the defence related G-type RLK LORE. Finally, *At5g24080* expression in distinct tissues and developmental stages as well as in response to hormone, abiotic and biotic stress stimuli did not correlate with expression of the other seven phylogenetic group members.

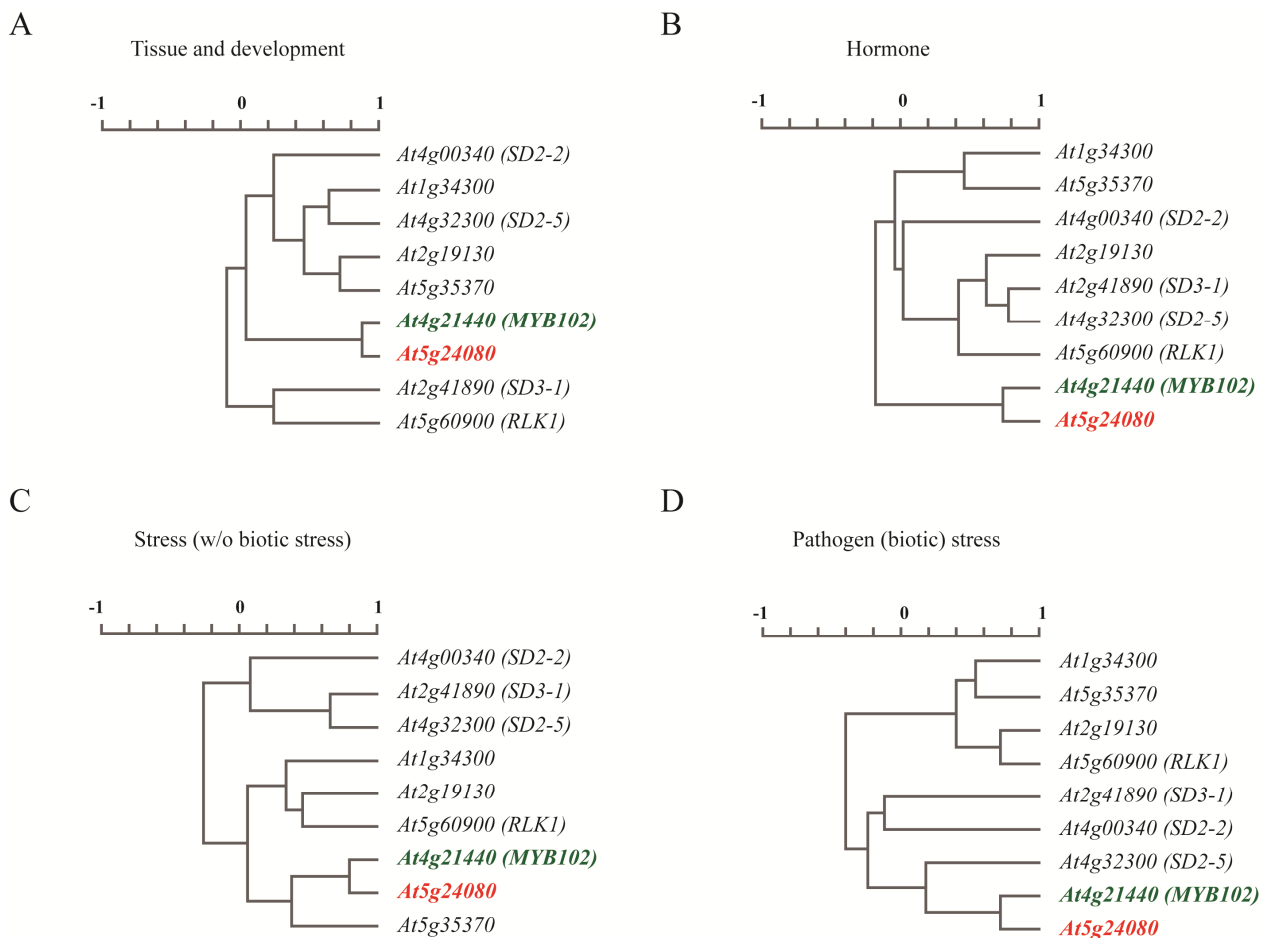


Figure 13. Co-expression analysis of *At5g24080* and seven group 1 *Arabidopsis* G-type lectin receptor-like kinases. Co-regulation of expression was determined using the Botany Array Resource (BAR) Expression Browser (Toufighi *et al.*, 2005) in which genes were clustered according to their expression profiles. Scale bar shows degree of co-regulation represented by Pearson's correlation coefficient where 1 is maximum positive correlation, 0 is no correlation and -1 is maximum negative correlation. *At4g21440* (*MYB102*) was used as a positive control showing high degree of co-regulation with *At5g24080*. (A) Co-expression analysis of group 1 G-type LecRLKs across tissues and developmental stages using the AtGenExpress Plus Extended Tissue dataset. (B) Analysis of co-expression after hormone treatment using the AtGenExpress Hormone dataset. (C) Co-expression analysis during abiotic stress treatment using the AtGenExpress Stress dataset excluding the biotic stress samples. (D) Analysis of co-expression during pathogen stress using the AtGenExpress Pathogen dataset.

3.5.2 Characterisation of *at5g24080* knockout mutants

In order to obtain an *at5g24080* knock-out mutant, three T-DNA insertion lines were ordered from NASC. Lines SALK_086625 and SAIL_551_D12, which both carry a T-DNA insertion in the second exon of the *At5g24080* gene were designated *at5g24080-1* and *at5g24080-3* respectively (Fig. 14A). In addition, the line SALK_147104, which is annotated to carry a T-DNA insertion in the 3'-untranslated region (UTR) of *At5g24080* according to the T-DNA

Express Arabidopsis Gene Mapping Tool (O'Malley *et al.*, 2015) was designated *at5g24080-2*. However, Sanger sequencing of homozygous mutants demonstrated that the T-DNA insertion in the *at5g24080-2* line was located in the fifth exon of the *At5g24080* gene (Fig. 14A and Fig. S8). The amino acid sequences, which correspond to ORFs resulting from the T-DNA insertions in *at5g24080* mutants, are shown in Fig. S9.

Homozygous T-DNA insertion lines were isolated by PCR based genotyping in two steps as described for the *rd17* mutants in section 3.3.1 using genotyping-specific primers designed with the T-DNA Express iSect tool (O'Malley *et al.*, 2015). The respective primer sequences are shown in Section 2.1.7. *at5g24080-1* line #7, #8, #13 and #27, *at5g24080-2* line #2, #9, #17 and #28 as well as *at5g24080-3* line #1, #3 and #26 were kept as homozygous T-DNA insertion lines for further analyses (Fig. S5, S6 and S7). F₂ progeny was generated by selfing of *at5g24080-1*, *at5g24080-2* and *at5g24080-3* homozygous T-DNA insertion lines and analysed for loss of functional *At5g24080* transcripts by semi-quantitative RT-PCR. RNA was extracted from plants infected with the *Verticillium* chlorosis-inducing isolate c-VL43 and c-V76 and the wilting-inducing isolate w-JR2 at 21 dpi or mock treated plants. *Verticillium* challenged *at5g24080* mutants were tested, since *At5g24080* transcripts were hardly detectable in mock treated samples in initial RT-PCR analyses (Fig. 4). Furthermore, analysis of *Verticillium* challenged *at5g24080* mutants allowed to assess whether T-DNA insertion had an effect on gene induction during *Verticillium* infection. *At5g24080* transcript abundance was tested using a RT-PCR-specific primer combination binding at the transcriptional start and stop, thus flanking all three T-DNA insertion sites (F1 and R2 primer in Fig. 14A). Moreover, in order to test for residual 5'- as well as 3'-transcripts, primer combinations were used that bind in the first and second exon of the gene (F1 and R1 primer in Fig. 14A) and in the fourth and fifth exon of the gene (F4 and R2 primer in Fig. 14A).

Consistent with initial expression analyses, *At5g24080* transcript abundance increased during chlorosis-inducing isolate c-VL43 and c-V76 infection of *A. thaliana* Col-0 wild-type as compared to mock treatment or wilting isolate w-JR2 infection (Fig. 14B). No *At5g24080* transcripts were present in all three tested *at5g24080* mutants using the F1 and R2 primer combination (Fig. 14B, upper panel). Yet, when using the F1 and R1 primer combination residual 5'-transcripts were detected in the *at5g24080-1*, *at5g24080-2* and *at5g24080-3* mutants (Fig. 14B, second panel). When using the F4 and R2 primer combination, transcripts were detected in the *at5g24080-1* and *at5g24080-3*, suggesting that these mutants in addition produce residual 3'-transcripts (Fig. 14B, third panel). Note that in the RT-PCR with primer F1 and R1 as well as F4 and R2 two bands of different size are present. The lower band represents

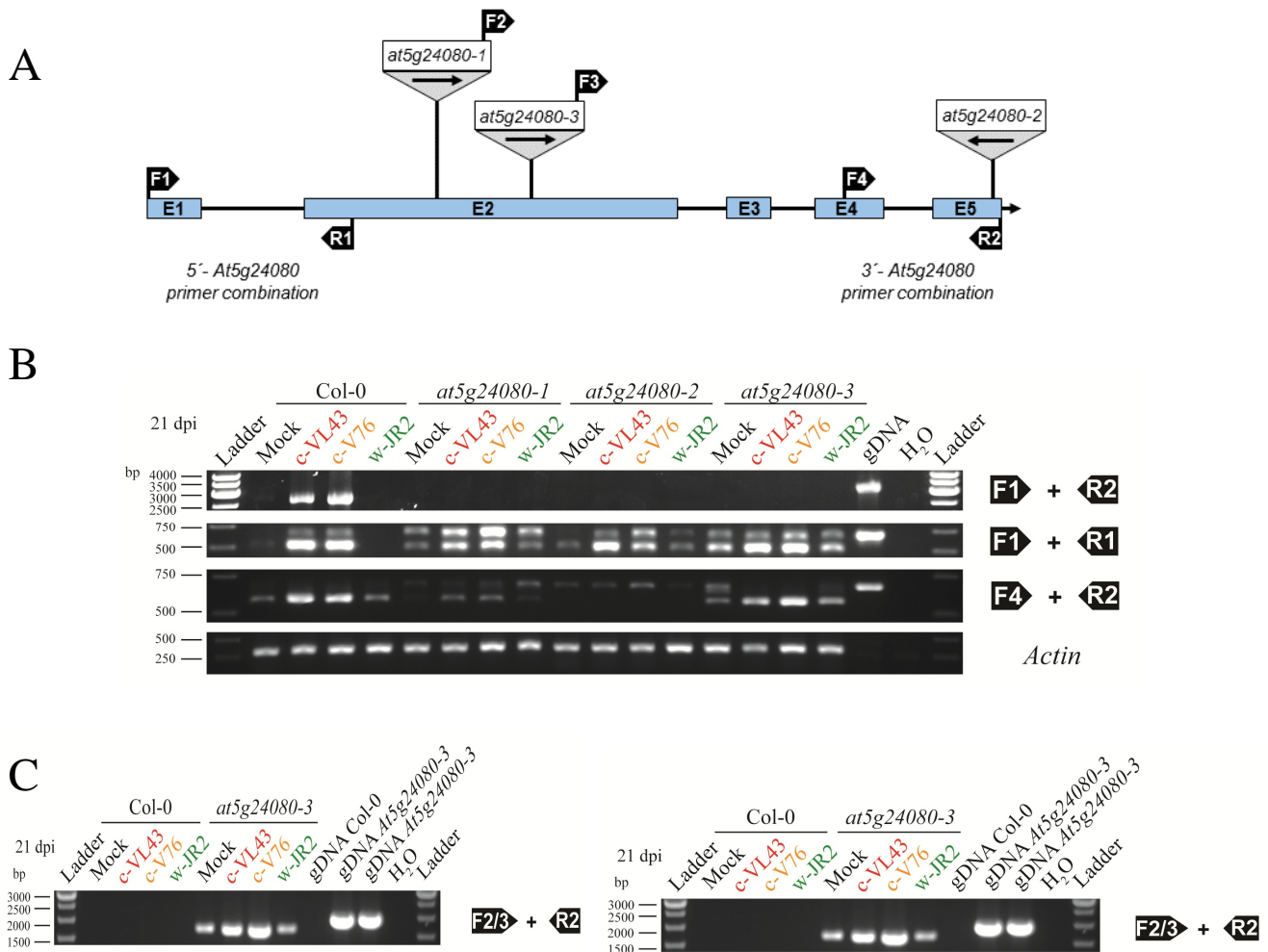


Figure 14. Characterisation of *at5g24080-1*, *at5g24080-2* and *at5g24080-3* T-DNA insertion mutants.

(A) Schematic representation of *At5g24080* gene structure. Exons are represented as blue boxes, whereas introns are shown as black lines. Positions of T-DNA insertions determined experimentally by Sanger sequencing of homozygous mutants (Figure S8) are shown as triangles. Arrow shows the orientation of the T-DNA (left border → right border). Forward (F) and reverse (R) primers used in B and C are represented as black boxes.

(B) Semi-quantitative RT-PCR analysis of *At5g24080* transcript abundance in *A. thaliana* Col-0 wild-type and *at5g24080* T-DNA insertion mutants during *V. longisporum* isolate c-VL43 as well as *V. dahliae* c-V76 and w-JR2 infection. The housekeeping gene *Actin* was amplified as a control. A genomic DNA (gDNA) control was included to monitor potential contamination by gDNA. A reverse primer which binds two exon borders and spans an intron sequence was used in case of the *Actin* gene to exclude gDNA amplification. The *Actin* cDNA PCR product corresponds to 302 bp. First panel shows full length *At5g24080* transcript amplified with primers F1 and R2. Expected sizes of F1+R2 PCR products are 2619 bp cDNA and 3058 bp gDNA. Second panel shows 5'-*At5g24080* transcript part amplified with primers F1 and R1. Expected sizes of F1+R1 PCR products are 514 bp cDNA and 684 bp gDNA. Third panel shows 3'-*At5g24080* transcript part amplified with primers F4 and R2. Expected sizes of F4+R2 PCR products are 580 bp cDNA and 681 bp gDNA.

(C) Semi-quantitative RT-PCR analysis for 3'-*At5g24080* transcript in *at5g24080-1* and *at5g24080-3* arising due to transcriptional activation by the SAIL or SALK T-DNA. PCR was performed as described in B using same cDNA. Left panel shows T-DNA activated 3'-*At5g24080* transcript in *at5g24080-1* amplified with primers F2 and R2. Expected sizes of F2+R2 PCR products are 2110 bp cDNA and 2378 bp gDNA. Right panel shows T-DNA activated 3'-*At5g24080* transcript in *at5g24080-3* amplified with primers F3 and R2. Expected sizes of F3+R2 PCR products are 1662 bp cDNA and 1930 bp gDNA. The experiment was performed once.

the cDNA band whereas the upper band represents gDNA contamination. In order to assess, whether residual 3'-transcripts in *at5g24080-1* and *at5g24080-3* mutants may arise due to transcriptional activation by the SAIL or SALK T-DNA construct, a RT-PCR using the T-DNA binding F2 or F3 forward primer respectively and the *At5g24080* binding R2 reverse primer was performed. Indeed, transcripts were obtained with the F2 and R2 primer combination in *at5g24080-1* as well as the F3 and R2 primer combination in *at5g24080-3* (Fig. 14C).

Taken together, RT-PCR analyses demonstrated that *at5g24080-1*, *at5g24080-2* and *at5g24080-3* mutants lack full-length *At5g24080* transcripts. Moreover, 5'-transcripts were present in all tested *at5g24080* mutants, indicating that a truncated version of *At5g24080* mRNA is produced. Furthermore, 3'-transcripts were detected in *at5g24080-1* and *at5g24080-3*, suggesting transcriptional activation by the SAIL or SALK T-DNA construct.

3.5.3 Analysis of *at5g24080* disease phenotype during *Verticillium* chlorosis and wilting isolate infection

In order to analyse the potential role of *At5g24080* in the *A. thaliana* – *Verticillium* chlorosis isolate interaction, macroscopic disease symptoms of *at5g24080-1*, *at5g24080-2* and *at5g24080-3* mutants were analysed during *Verticillium* infection. Macroscopic disease symptoms of all tested *at5g24080* mutants were not altered during *V. longisporum* chlorosis-inducing isolate c-VL43 as well as *V. dahliae* chlorosis-inducing isolate c-V76 and wilting isolate w-JR2 infection as compared to wild-type (Fig. 15 and Fig. S10 to S13). As on Col-0 wild-type, chlorosis and early senescence symptoms were visible on older *at5g24080-1*, *at5g24080-2* and *at5g24080-3* rosette leaves during infection with the chlorosis-inducing isolate c-VL43 and c-V76 (Fig. 15A, middle panels). Moreover, like Col-0 wild-type, all tested *at5g24080* mutants showed wilting symptoms on older rosette leaves during *V. dahliae* wilting isolate w-JR2 infection (Fig. 15A, right panel).

Stunting of *at5g24080* mutant plants during *Verticillium* infection was analysed as an indicator for severity of disease symptoms. None of the tested *at5g24080* mutants showed significant quantitative differences in disease symptoms during *Verticillium* chlorosis isolate c-VL43, c-V76 and wilting isolate w-JR2 infection as compared to Col-0 wild-type (Fig. 15B). Together, these results suggest that disruption of the *At5g24080* gene affects neither development of macroscopic disease symptoms during *Verticillium* challenge nor severity of *Verticillium* induced disease symptoms.

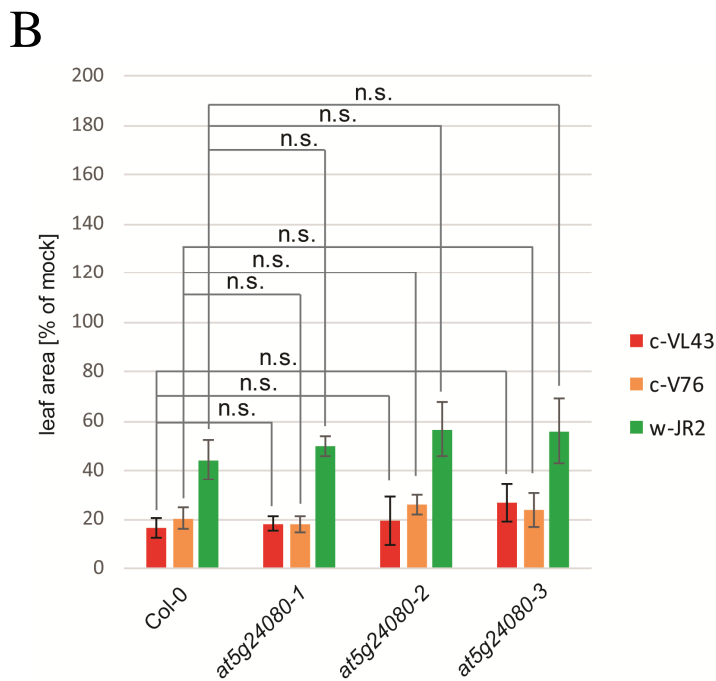
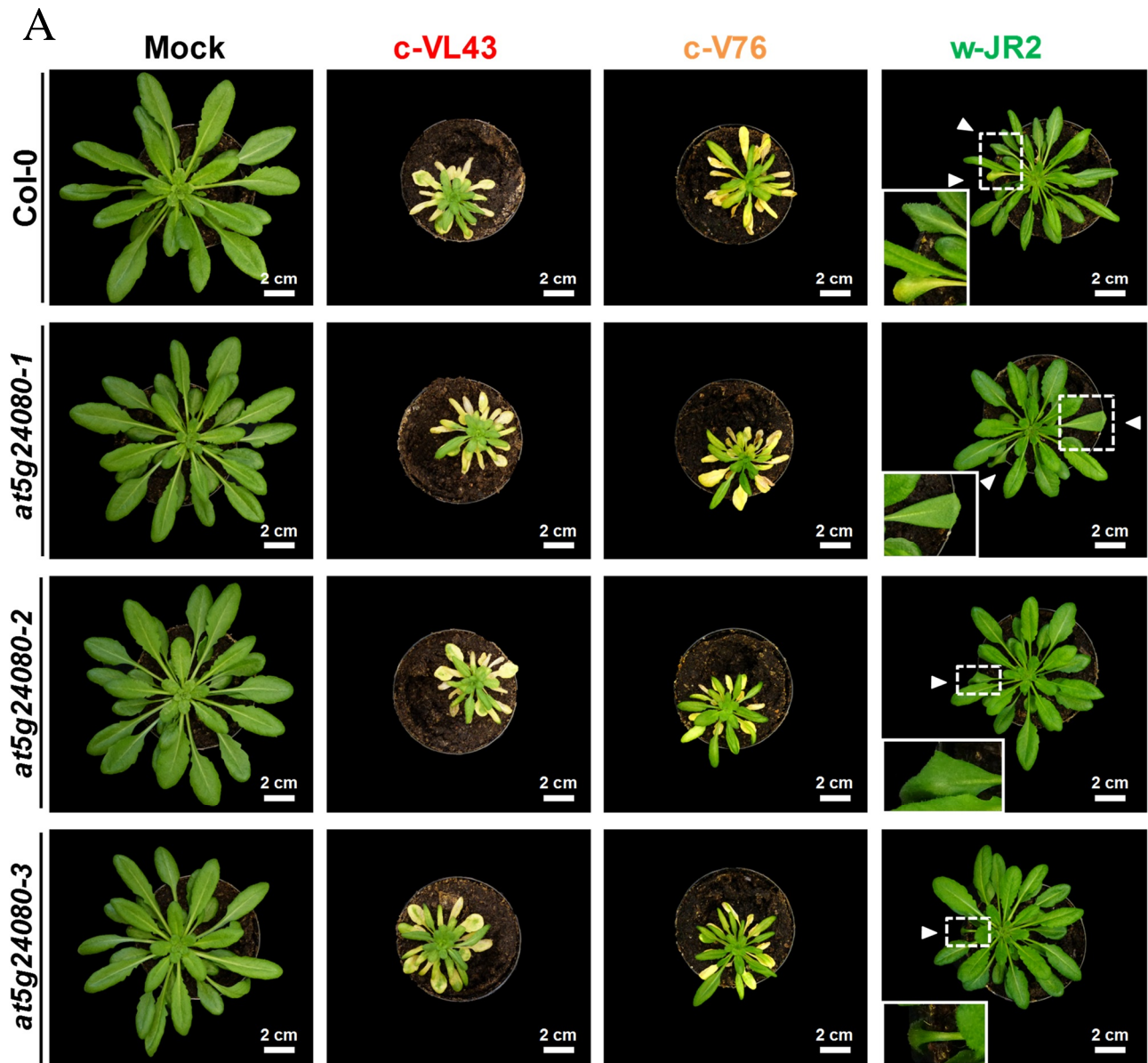


Figure 15. Disease phenotypes of *A. thaliana* Col-0 wild-type and *at5g24080* mutants during infection with *V. longisporum* isolate c-VL43 as well as *V. dahliae* isolates c-V76 and w-JR2. (A) Disease symptoms at 21 days post infection (dpi). Insets represent magnifications of areas marked with dotted boxes. Arrowheads indicate wilting leaves. (B) Leaf area measurement at 21 days post infection. Leaf area of mock treated controls was set to 100 % and leaf area of infected plants calculated as percentage of mock control. Error bars represent standard deviation between $n = 4$ replicates. Statistical significance was tested using Student's t-test for pairwise comparison of wild-type and mutant. (n.s.) not significant. The experiment was performed once.

Thereafter, the role of *At5g24080* in *de novo* xylem formation within the *Arabidopsis* vascular system was assessed. For this purpose, microscopic analyses of bundle sheath cell transdifferentiation in *A. thaliana* Col-0 wild-type and *at5g24080-1*, *at5g24080-2* as well as *at5g24080-3* leaf vascular bundles was performed during *Verticillium* chlorosis isolate infection. In order to visualise vascular tissue, detached leaves were stained with trypan blue. This dye is excluded by living cells with an intact plasma membrane, such as bundle sheath cells or mesophyll cells, and thus only stains dead tissue such as xylem elements. In the mock treated Col-0 wild-type, vascular bundles are surrounded by living bundle sheath cells, which are not stained by trypan blue (Fig. 16A). During chlorosis isolate c-VL43 and c-V76 infection bundle sheath cells transdifferentiate to xylem elements, showing characteristic annular, helical and reticulate secondary cell wall fortifications (Fig. 16B and C). Since xylem elements represent dead tissue, they are stained by trypan blue. During wilting isolate w-JR2 infection, the bundle sheath cell layer does not transdifferentiate (Fig. 16D). As in Col-0 wild-type, bundle sheath cells of mock treated and wilting isolate w-JR2 infected *at5g24080-1*, *at5g24080-2* as well as *at5g24080-3* did not show developmental changes (Fig. 16E, H, I, L, M and P). Moreover, *at5g24080-1*, *at5g24080-2* and *at5g24080-3* showed wild-type like bundle sheath cell transdifferentiation into xylem elements during chlorosis isolate c-VL43 and c-V76 infection (Fig. 16F, G, J, K, N and O), indicating that *At5g24080* does not play a role in bundle sheath cell transdifferentiation.

In summary, none of the tested *at5g24080* mutants demonstrated altered macroscopic disease symptoms or significant differences in disease symptom severity during infection with the *V. longisporum* chlorosis isolate c-VL43 and *V. dahliae* chlorosis isolate c-V76 as well as *V. dahliae* wilting isolate w-JR2 as compared to Col-0 wild-type. Furthermore, all tested *at5g24080* mutants showed wild-type like bundle sheath cell transdifferentiation to xylem elements during chlorosis isolate c-VL43 and c-V76 infection. In conclusion, these results suggest that *At5g24080* does not play a role in establishment of chlorosis disease symptoms and bundle sheath cell transdifferentiation during *Verticillium* chlorosis isolate infection.

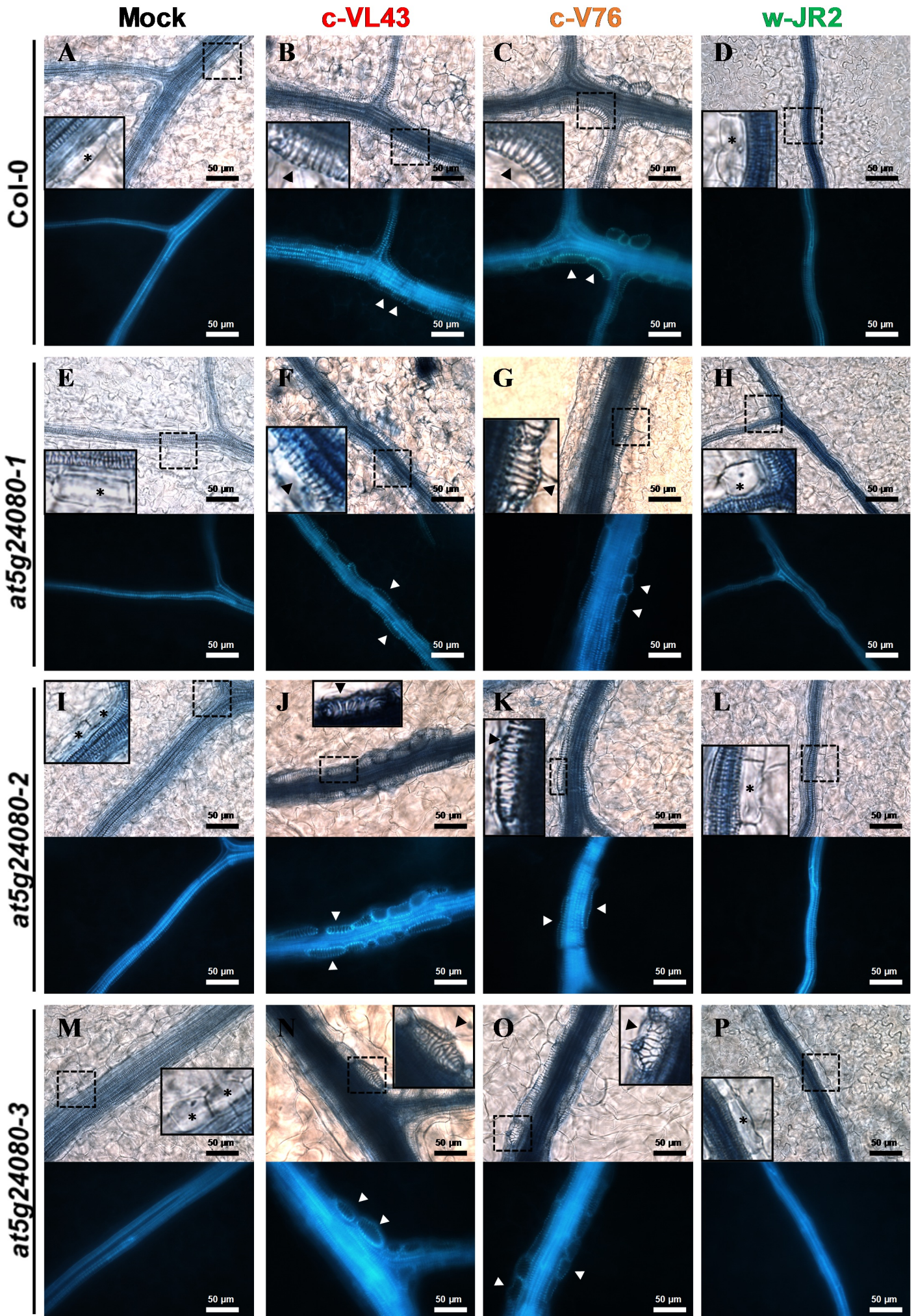


Figure 16. Analysis of bundle sheath cell transdifferentiation in leaf vascular bundles of *A. thaliana* Col-0 wild-type and *at5g24080* mutants 28 days post infection (dpi) with *V. longisporum* isolate c-VL43 as well as *V. dahliae* isolates c-V76 and w-JR2. Plant leaves were stained with trypan blue. Figures (A-P) show bright field (upper panel) and epifluorescence (lower panel) images of leaf vascular bundles. Insets represent magnifications of areas marked with dotted boxes. Asterisks indicate bundle sheath cells, whereas arrowheads point at *de novo* formed tracheary elements. The experiment was performed once.

3.5.4 Analysis of the role of *At5g24080* in defence against *Pseudomonas syringae*, *Botrytis cinerea* and *Hyaloperonospora arabidopsidis*

Expression of the G-type LecRLK gene *At5g24080* is strongly up-regulated during infection with chlorosis-inducing isolates of the vascular plant pathogen *Verticillium*. In addition, *Arabidopsis* G-type LecRLK LORE and lectin receptor kinases from various plant species were shown to function in defence against bacterial as well as fungal pathogens and herbivorous insects (Kim *et al.*, 2009; Chen *et al.*, 2006; Gilardoni *et al.*, 2011; Cheng *et al.*, 2013; Cole and Diener, 2013; Liu *et al.*, 2015; Ranf *et al.*, 2015), suggesting that AT5G24080 as a LecRLK may be involved in plant immunity. Since *at5g24080* mutants did not show any altered disease phenotypes in response to *Verticillium*, next susceptibility of *at5g24080-1*, *at5g24080-2* and *at5g24080-3* mutants to a biotrophic, necrotrophic and a hemi-biotrophic phytopathogen was analysed. The set of tested pathogens included the hemibiotrophic bacterium *Pseudomonas syringae*, the necrotrophic fungus *Botrytis cinerea* and the obligate biotrophic oomycete *Hyaloperonospora arabidopsidis*.

Publically available expression data indicate, that *At5g24080* is induced 2, 6 and 24 h after infection of 5-week-old *A. thaliana* Col-0 with the virulent *Pseudomonas syringae* pv. tomato DC3000 (*Pst* DC3000) as well as 6 and 24 h after infection with the avirulent *Pseudomonas syringae* pv. tomato avrRpm1 as compared to mock treatment (*Arabidopsis* eFP Browser, Winter *et al.*, 2007). In addition, expression of the *At5g24080* gene is up-regulated 4 h after infiltration with the epitope of bacterial flagellin, flg22 and bacterial hairpin protein HrpZ, which both represent well known elicitors of plant defence. For these reasons, *at5g24080* mutant susceptibility to the hemibiotrophic bacterium *Pseudomonas syringae* was assessed.

In order to assess susceptibility of the *at5g24080-1*, *at5g24080-2* and *at5g24080-3* mutant, 5- to 6-week-old plants were vacuum infiltrated with mildly virulent *Pst* DC3000 Δ AvrPto/AvrPtoB bacteria. Use of the mildly virulent *Pst* DC3000 Δ AvrPto/AvrPtoB strain allows visualising subtle differences in disease susceptibility. Leaf samples were taken at day 0 as a control for equal infiltration and at day 3 to quantify bacterial proliferation. *A. thaliana* Col-0 was used as

a wild-type control and *eds1-2* as a susceptible control. EDS1 represents a positive regulator of basal and TNL-type R-protein mediated resistance (Wiermer *et al.*, 2005). Bacterial titre at day 0 did not significantly differ in all tested genotypes, indicating a uniform infiltration (Fig. 17). At day 3 *Pst* DC3000 Δ AvrPto/AvrPtoB proliferation was not significantly altered in *at5g24080* mutants as compared to Col-0 wild-type (Fig. 17), suggesting that *at5g24080* is not implicated in disease resistance to this bacterial pathogen.

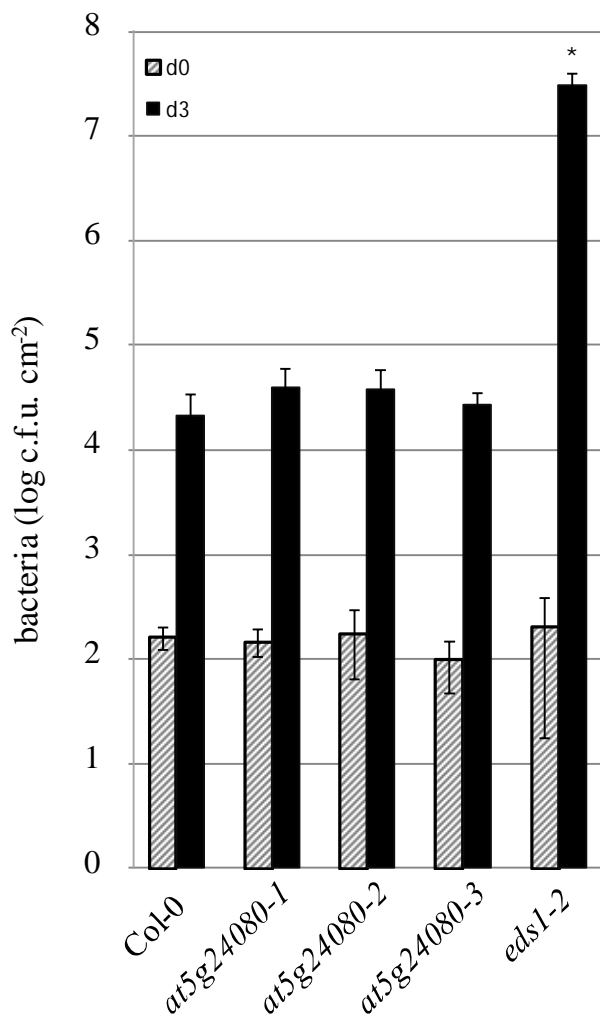


Figure 17. Quantification of *Pseudomonas syringae* pv. *tomato* (*Pst*) strain DC3000 (Δ AvrPto/AvrPtoB) growth in *Arabidopsis* Col-0 wild-type, *at5g24080* and *eds1-2* leaves. *eds1-2* represents a susceptible control. 5- to 6-week-old plants were vacuum infiltrated with a bacterial suspension of $1 \cdot 10^5$ colony forming units (c.f.u.) per ml. Leaf samples were taken in duplicates at day 0 as a control for equal infiltration (grey bars). Day 3 leaf samples were taken in triplicates (black bars). Error bars represent standard deviation between replicates. * $P < 0.05$ using Student's t-test for pairwise comparison of wild-type and mutant. The experiment was repeated twice with similar results.

Next, susceptibility of *at5g24080* to the necrotrophic fungal pathogen *Botrytis cinerea* was analysed. Leaves of 5-week-old *at5g24080-1* mutants were drop inoculated with *B. cinerea* isolate B05.10 spore suspension and the diameter of necrotic lesion measured at 3 dpi. *A. thaliana* Col-0 was used as a wild-type control and *mpk3* DG as well as *mos7-1* as susceptible controls. MPK3 is a component of a MAP kinase cascade which leads to induction of pathogenesis related genes, whereas MOS7 represents a nucleoporin protein which is required for selective nuclear retention of immune regulatory proteins (Cheng *et al.*, 2009; Wiermer *et*

al., 2010; Mao *et al.*, 2011). Both proteins were shown to be required for defence responses to *B. cinerea* (Ren *et al.*, 2008; Genencher *et al.*, 2017). The mean diameter of necrotic lesions on *at5g24080-1* leaves was not significantly altered as compared to Col-0 wild-type (Fig. 18), suggesting that *at5g24080-1* does not show enhanced susceptibility to *B. cinerea*. As a consequence, AT5G24080 is not likely involved in disease resistance to this fungal phytopathogen.

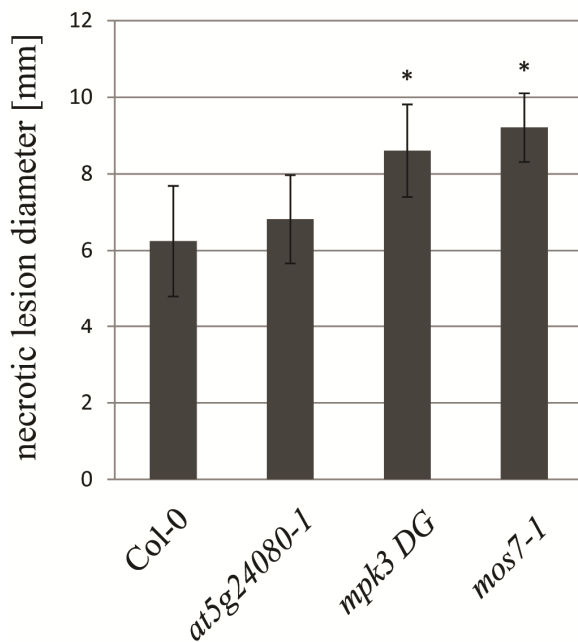


Figure 18. Disease susceptibility of *Arabidopsis* Col-0 wild-type, *at5g24080-1*, *mpk3 DG* and *mos7-1* to *Botrytis cinerea* B05.10. *mpk3 DG* and *mos7-1* represent susceptible controls. Leaves of 5-week-old plants were inoculated with 6 μ l droplets of *B. cinerea* spore suspension at a concentration of $5 \cdot 10^4$ spores per ml. Necrotic lesion diameter was measured 3 days post inoculation (dpi) with a digital calliper. Error bars represent standard deviation between 30-45 measurements. * $P < 0.05$ using Student's t-test for pairwise comparison of wild-type and mutant. The experiment was repeated twice with similar results.

Subsequently, susceptibility of *at5g24080* to the obligate biotroph *Hyaloperonospora arabidopsidis* was assessed. 2-week-old *at5g24080-1*, *at5g24080-2* and *at5g24080-3* were spray inoculated with a spore suspension of the *H. arabidopsidis* isolate NOCO2 and oomycete proliferation was quantified at 6 dpi. NOCO2 represents an *A. thaliana* Col-0 adapted isolate of *H. arabidopsidis*. For this reason *A. thaliana* Col-0 was used as a wild-type control. Furthermore, *snc1* was used as a resistant control whereas *eds1-2* represented a susceptible control. The *snc1* mutant carries a gain of function mutation in a TNL-type R-protein resulting in a constitutive immune response (Li *et al.*, 2001; Zhang *et al.*, 2003).

At 6 dpi ca. $15 \cdot 10^5$ NOCO2 spores per ml were recovered from Col-0 wild-type plants (Fig. 19). NOCO2 proliferation was significantly increased with ca. $22 \cdot 10^5$ spores per ml in *at5g24080-1* and ca. $20 \cdot 10^5$ spores per ml in *at5g24080-3* as compared to Col-0 wild-type (Fig. 19). In *at5g24080-2*, NOCO2 proliferation increased to ca. $19 \cdot 10^5$ spores per ml as compared to Col-0 wild-type. However, this result was not significant (Fig. 19). All *at5g24080* mutants were less

susceptible to NOCO2 infection as compared to the susceptible *eds1-2* control, from which $30 \cdot 10^5$ NOCO2 spores per ml were recovered at 6 dpi (Fig. 19). In addition to the experiment presented in this thesis, two further NOCO2 infection experiments were performed. In one of the two repetitions, all tested *at5g24080* mutants were more susceptible to NOCO2 as compared to Col-0 wild-type, whereas susceptibility of *at5g24080* mutants was comparable to wild-type in the second repetition.

As a conclusion, it can be stated that *at5g24080-1*, *at5g24080-2* and *at5g24080-3* mutations did not result in enhanced susceptibility to the hemibiotrophic bacterial pathogen *Pseudomonas syringae* and necrotrophic fungus *B. cinerea*. However, *at5g24080* mutants showed a trend to enhanced susceptibility to *H. arabidopsidis* isolate NOCO2. Yet, infection experiments have to be repeated in the future.

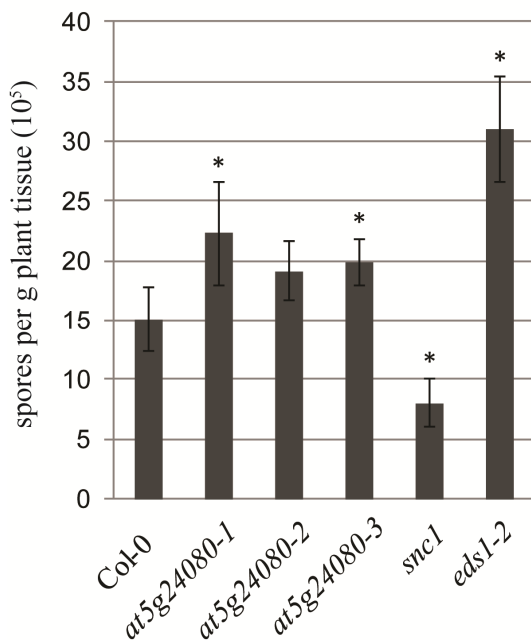


Figure 19. *Hyaloperonospora arabidopsidis* isolate NOCO2 proliferation 6 days post infection of *Arabidopsis* Col-0 wild-type, *at5g24080*, *snc1* and *eds1-2* mutant. *snc1* represents a resistant control, whereas *eds1-2* is a susceptible control. 35-45 2-week-old seedlings were spray inoculated with a suspension of $5 \cdot 10^4$ spores per ml. Error bars represent standard error between $n = 4$ replicates. * $P < 0.05$ using Student's t-test for pairwise comparison of wild-type and mutant. The experiment was performed three times. Similar results were observed in 2 out of 3 experiments.

3.5.5 *At5g24080* is co-regulated with genes involved in cell wall modification, lignin and suberin biosynthesis as well as drought tolerance

To further deduce the putative function of the G-type LecRLK AT5G24080 during *Verticillium* chlorosis isolate infection, analysis of its co-regulated genes was performed. *At5g24080* co-regulon analysis was carried out using the ATTED II *Arabidopsis thaliana* microarray database Ath-m version c6.0 and RNAseq database Ath-r version c2.0 with the ATTED II web interface version 8.0 (<http://atted.jp>, Aoki *et al.*, 2016). In contrast to the co-expression analysis shown in section 3.5.1, co-regulation of *At5g24080* with all genes included in the ATTED II

databases was analysed. Firstly, the top 50 *At5g24080* co-regulated genes were extracted from each database (Table. S10 and S11). Thereafter, top 50 candidates were analysed for genes, which were significantly regulated by *Verticillium* chlorosis isolate infection of *A. thaliana* or *N. benthamiana* in the RNA-sequencing analysis performed in this study. *N. benthamiana* homologs of four of the *At5g24080* co-regulated genes were significantly induced by *Verticillium* chlorosis isolate infection in the RNA-sequencing analysis (Table 3).

Table 3. List of *At5g24080* co-regulated genes which are significantly up-regulated during infection with chlorosis-inducing *Verticillium* isolates. Gene function is colour-coded.

<i>Nb</i> gene ID	<i>At</i> homolog	Description of <i>At</i> homolog	Putative function
<i>NbS00036208g0008</i>	<i>At4g21440</i>	MYB102 (MYB-Like 102)	Controls expression of genes required for cell wall modification (De Vos <i>et al.</i> , 2006)
<i>NbS00012878g0008</i>	<i>At2g20880</i>	ERF53, AP2 Domain-Containing Transcription Factor	Implicated in tolerance to drought stress (Cheng <i>et al.</i> , 2012)
<i>NbS00030442g0004</i>	<i>At4g28110</i>	AtMYB41 (MYB Domain Protein 41)	Affects lignin and suberin synthesis (Kosma <i>et al.</i> , 2014)
<i>NbS00058524g0002</i>	<i>At5g41040</i>	RWP1 (REDUCED LEVELS OF WALL-BOUND PHENOLICS 1)	Suberin biosynthesis in root (Gou <i>et al.</i> , 2009)

NbS00036208g0008, a *N. benthamiana* gene which is homologous to the *A. thaliana* MYB domain transcriptional factor *MYB102* was up-regulated by chlorosis isolates as shown in the collective analysis of 8, 12 and 16 dpi *N. benthamiana* shoot samples (Table. S8). Expression of this MYB transcription factor is induced by dehydration, osmotic stress, the abiotic stress related phytohormone abscisic acid (ABA) and to a higher extent by combined osmotic stress and wounding (Denekamp and Smeekens, 2003). In addition, MYB102 was shown to contribute to resistance against an herbivorous insect. Microarray analyses of *MYB102* overexpressing lines suggest that MYB102 controls expression of defence related genes and genes required for cell wall modifications (De Vos *et al.*, 2006). *NbS00012878g0008*, a *N. benthamiana* homolog of another *A. thaliana* drought related gene *ERF53*, which was induced at 8 dpi by chlorosis isolate infection (Table. S3) was found among *At5g24080* co-regulated genes. ERF53 is an AP2/ERF transcription factor. Its expression is induced by drought and more important *ERF53* overexpression was demonstrated to result in enhanced drought tolerance of *Arabidopsis* (Cheng *et al.*, 2012).

Since *Verticillium* chlorosis isolate infection induces enhanced drought tolerance of infected *A. thaliana* plants and drought related transcription factors are co-regulated with *At5g24080*, this G-type LecRLK may be involved in establishment of drought tolerance during chlorosis isolate infection. In order to address this question, *At5g24080* expression during combined drought stress and *Verticillium* chlorosis isolate infection was analysed by semi-quantitative

RT-PCR in *A. thaliana* Col-0 wild-type plants. However, *At5g24080* expression did not differ during combined drought stress and chlorosis isolate challenge from gene expression in the watered control (Fig. S14). In the mock treated plants, only a slight induction was visible during drought stress as compared to the watered control (Fig. S14). Moreover, *at5g24080* mutants did not show an altered drought tolerance phenotype under combined drought stress and chlorosis isolate challenge (data not shown). Consequently, *at5g24080* is most likely not involved in drought tolerance of chlorosis isolate infected *A. thaliana* plants.

Two of the *At5g24080* co-regulated and chlorosis isolate induced genes play a role in suberin biosynthesis (Table 3). Firstly, *NbS00030442g0004*, a *N. benthamiana* gene that is homologous to the *A. thaliana* MYB domain transcription factor *MYB41* was up-regulated by chlorosis isolates in the collective analysis of 8, 12 and 16 dpi *N. benthamiana* shoot samples (Table. S8). Studies of *MYB41promoter::GUS* fusions demonstrated that this transcriptional factor is expressed in endodermal and cortical cells of *A. thaliana* roots after ABA treatment and salt stress but not in unchallenged plants. Overexpression of *MYB41* led to accumulation of lignin and suberin biosynthetic gene transcripts as well as high amounts of monolignols and suberin-type aliphatic monomers in *Arabidopsis* leaves (Kosma *et al.*, 2014). Secondly, *NbS00058524g0002*, a *N. benthamiana* gene which is homologous to the *A. thaliana* *RWP1* (*REDUCED LEVELS OF WALL-BOUND PHENOLICS 1*) was up-regulated by chlorosis isolates at 16 dpi (Table. S6). This regulation was confirmed in the collective analysis of 8, 12 and 16 dpi *N. benthamiana* shoot samples (Table. S8). *RWP1* encodes an acyl-CoA dependent acyltransferase which is implicated in formation of aromatic suberin in *Arabidopsis* seeds and roots (Gou *et al.*, 2009).

Lignin and suberin constitute major components of the root endodermis. *V. longisporum* isolate c-VL43 and *V. dahliae* isolate w-JR2 were shown to enter the vascular cylinder via endodermis free zones during the initial steps of root infection (Reusche *et al.*, 2014). *At5g24080* is strongly expressed in the procambium of unchallenged *Arabidopsis* roots according to publically available microarray data (*Arabidopsis* eFP Browser, Winter *et al.*, 2007) and was 1.6 log₂ fold, yet not significantly, induced in *A. thaliana* chlorosis isolate root infection (Table 2). Co-regulation with the lignin and suberin biosynthesis related genes *MYB41* and *RWP1* indicate a potential role of *At5g24080* in endodermal barrier formation. In order to test this hypothesis the endodermal barrier in *at5g24080* mutants was analysed in a propidium iodide staining assay. Propidium iodide (PI) is used to visualise functional endodermal barriers, since its diffusion into the root stele is blocked by the lignin and suberin containing Casparian strip. A non-functional Casparian strip will result in propidium iodide staining of the stele.

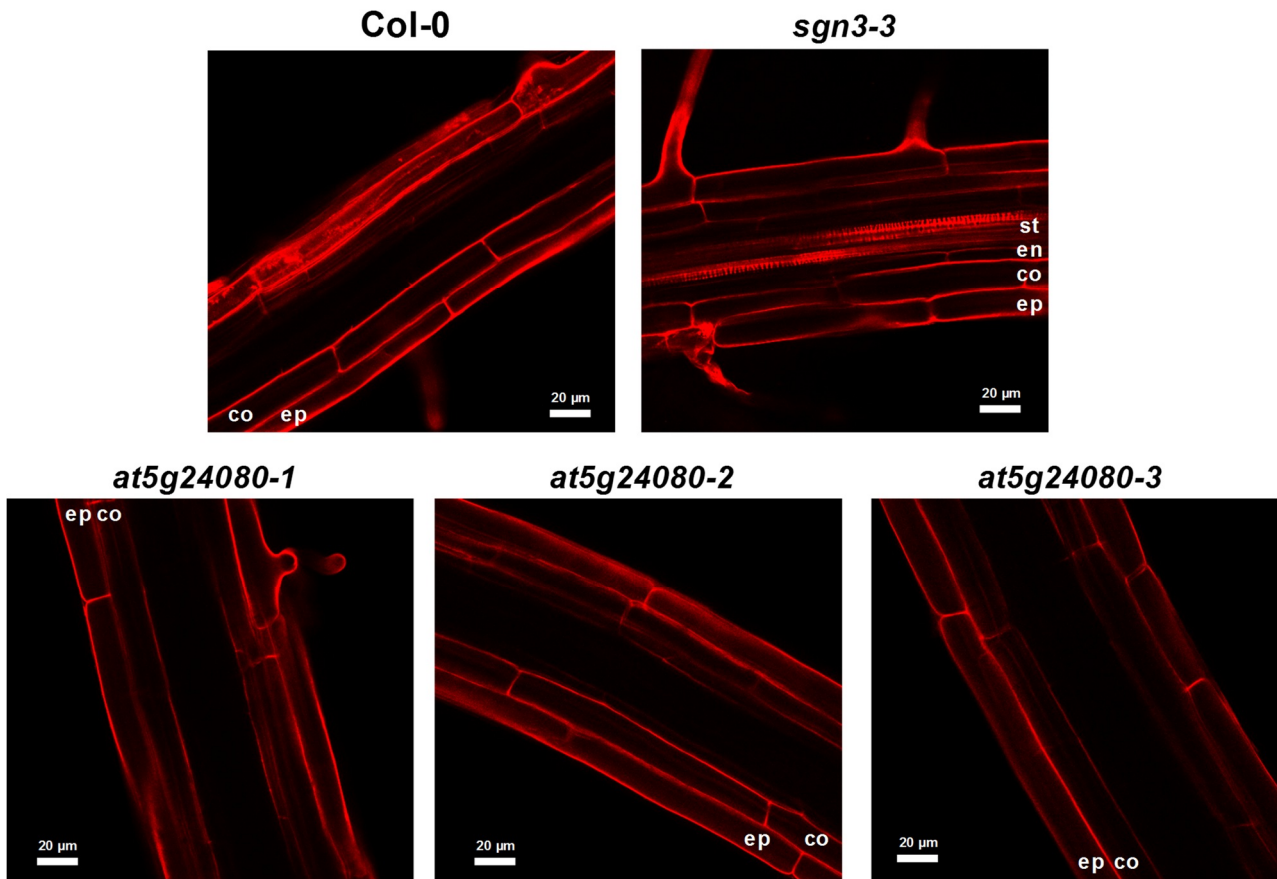


Figure 20. Microscopic analysis of root endodermal barrier in *A. thaliana* Col-0 wild-type, *at5g24080* and *sgn3-3* mutants. Whole 5-days-old *in vitro* seedlings were incubated in the dark in a 15 μ M propidium iodide (PI) solution for 10 min and analysed for presence of PI in stele of the mature root. Ep: epidermis, co: cortex, en: endodermis, st: stele. Three seedlings per genotype were analysed. Representative image is shown. The experiment was performed once.

In the propidium iodide assay 5-days-old *at5g2408-1*, *at5g24080-2* and *at5g24080-3* *in vitro* seedlings were incubated in a PI solution and subsequently analysed for propidium iodide presence in the stele of the mature root where the endodermal barrier is fully differentiated. *A. thaliana* Col-0 was used as a wild-type control, whereas *sgn3-3* represented a positive control. SGN3 is a receptor-like kinase, which is required for proper localisation of the CASPARIAN STRIP DOMAIN PROTEIN (CASP) scaffold and thus proper endodermal barrier formation (Pfister *et al.*, 2014). PI diffusion into the stele was blocked in Col-0 wild-type but also all analysed *at5g24080* mutants (Fig. 20), indicating an intact endodermal barrier. In contrast, endodermis and stele of the positive control *sgn3-3* were stained by propidium iodide (Fig. 20). In summary, *in silico* co-regulon analyses revealed that *At5g24080* is co-regulated with genes implicated in cell wall modification, lignin and suberin biosynthesis as well as

drought stress tolerance, suggesting that *At5g24080* may play a potential role in these processes. However, *At5g24080* expression was not altered during combined drought stress and *Verticillium* chlorosis isolate infection. Moreover, formation of the lignin and suberin containing endodermal barrier was not compromised in *at5g24080* mutants. As a consequence, implication of *At5g24080* in these processes could not be proven.

3.5.6 *At5g24080* gene expression is inducible by abscisic acid

Expression of the *At5g24080* co-regulated MYB domain transcriptional factor genes *MYB102* and *MYB41* is known to be inducible by the phytohormone abscisic acid (ABA) (Denekamp and Smeekens, 2003; Kosma *et al.*, 2014). In order to check whether *At5g24080* and further genes from its co-regulon are ABA inducible, expression of the top 50 *At5g24080* co-regulated genes after ABA treatment was analysed in an *in silico* approach using publically available microarray data. Expression data after 10 μ M ABA treatment was retrieved using the TRABAS web interface (Choudhury and Lahiri, 2008) as log₂ fold change in expression. Indeed, 36 out of the top 50 ATTED II microarray database co-regulated genes and 28 out of the top 50 ATTED II RNAseq database co-regulated genes were more than 2.0 log₂ fold induced at 3 h after 10 μ M ABA (Table. S10 and S11). *At5g24080* itself showed a log₂ fold induction of 3.3 at 3 h after 10 μ M ABA treatment (Table. S10 and S11, top row).

Next, the *At5g24080* promoter region was analysed for presence of ABA responsive cis-acting elements. For this purpose the 1.1 kb genomic DNA-sequence upstream of the *At5g24080* start-codon was analysed using PlantCARE World Wide Web interface (Lescot *et al.*, 2002). In the 1.1 kb promoter region of *At5g24080*, several TATA-box core promoter elements, CAAT-box cis-acting elements as well as light responsive elements were identified (Fig. 21 and Table 4). Most important, an ABA response element (ABRE) was found 151 bp upstream of the *At5g24080* start-codon (Fig. 21 and Table 4). Molecular analyses of ABA responsive promoters demonstrated that the ABRE sequence alone is not sufficient for induction of gene expression. Instead, two or more ABRE or a combination of an ABRE with a coupling element (CE) is required for ABA responsiveness of a plant promoter (Shen and Ho, 1995; Shen *et al.*, 1996; Hobo *et al.*, 1999; Narusaka *et al.*, 2003; Shen *et al.*, 2004). In a microarray analysis, *At5g24080* was identified among genes regulated by the ABA responsive transcription factor ABI4 (ABA INSENSITIVE 4) (Reeves *et al.*, 2011). ABI4 binds the CE1 coupling element (Niu *et al.*, 2002). Therefore, the *At5g24080* promoter was analysed for presence of a CE1 element. The core sequence of CE1 is defined as CCACC (Shen and Ho, 1995; Shen *et al.*,

Taken together *in silico* analyses suggest that the G-type LecRLK *At5g24080* represents an ABA inducible gene and is co-regulated with a set of other ABA responsive genes. Furthermore, *At5g24080* promoter region contains an ABRE as well as a CE1 cis-acting element, which are sufficient for ABA dependent gene induction.

In order to test the results of the *in silico* analysis experimentally, *At5g24080* expression after ABA treatment was analysed by semi-quantitative RT-PCR. In this analysis, 12-days-old *Arabidopsis* Col-0 seedlings were incubated for 3 h and 24 h in 50 μ M ABA and *At5g24080* transcript abundance analysed by semi-quantitative RT-PCR. Expression of the known ABA inducible gene *RD29B* (Yamaguchi-Shinozaki and Shinozaki, 1993) was monitored as a control for successful ABA treatment. Transcript levels of the positive control *RD29B* were increased after 3 h and 24 h in 50 μ M ABA treated samples as compared to mock (Fig. 22, middle panel), suggesting that ABA was taken up by *A. thaliana* Col-0 seedlings. *At5g24080* transcript abundance was strongly increased in ABA treated samples as compared to mock after 3 h and 24 h of 50 μ M ABA application. *At5g24080* transcript levels were higher after 24 h of 50 μ M ABA application as compared to 3 h (Fig. 22, upper panel).

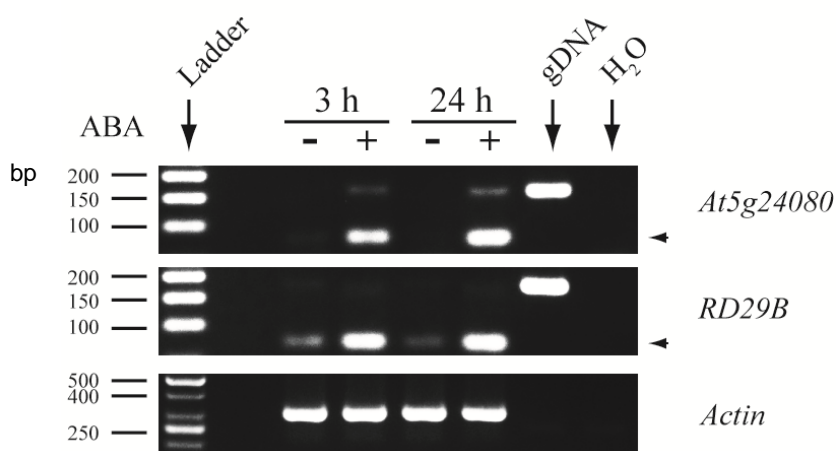


Figure 22. Semi-quantitative RT-PCR analysis of *At5g24080* and *RD29B* expression in 12-days-old *Arabidopsis* Col-0 seedlings treated with 50 μ M ABA. Pools of 20 seedlings per sample were used for RNA extraction. “+” indicates samples collected from ABA treated plants, whereas “-” represents the mock treated control. The housekeeping gene *Actin* was amplified as a control. A genomic DNA (gDNA) control was included

to monitor potential contamination by gDNA. A reverse primer which binds two exon borders and spans an intron sequence was used in case of the *Actin* gene to exclude gDNA amplification. The *Actin* cDNA PCR product corresponds to 302 bp. Expected sizes of *At5g24080* PCR products are 79 bp cDNA and 161 bp gDNA. Sizes of *RD29B* PCR products are 72 bp cDNA and 170 bp gDNA. The arrowhead indicates *At5g24080* or *RD29* cDNA bands respectively. The experiment was repeated twice with similar results.

Additionally to the semi-quantitative RT-PCR analysis, *At5g24080* expression after ABA treatment was analysed by qPCR. Again, expression of *RD29B* was monitored as a positive control. *At5g24080* transcript levels were increased ca. 530 fold after 3 h and ca. 930 fold after 24 h of 50 μ M ABA application as compared to mock treatment (Fig. 23A). Transcript

abundance of the positive control *RD29B* was ca. 1000 fold increased after 3 h and ca. 2360 fold after 24 h of 50 μ M ABA application as compared to mock (Fig. 23B).

In summary, *in silico* analyses of publically available microarray data indicated that *At5g24080* represents an ABA inducible gene and that the majority of its co-regulated genes is also ABA responsive. Moreover, *in silico* promoter analysis demonstrated that *At5g24080* contains an ABRE cis-acting element as well as a CE1 coupling element in its promoter sequence. A combination of ABRE and a coupling element is known to be sufficient for transcriptional induction of ABA dependent genes (Shen and Ho, 1995; Shen *et al.*, 1996; Hobo *et al.*, 1999; Narusaka *et al.*, 2003; Shen *et al.*, 2004). Semi quantitative RT-PCR and qPCR analyses of *At5g24080* expression after ABA treatment confirmed inducibility of this G-type LecRLK gene by abscisic acid. The results corroborate that *At5g24080* gene expression is ABA inducible.

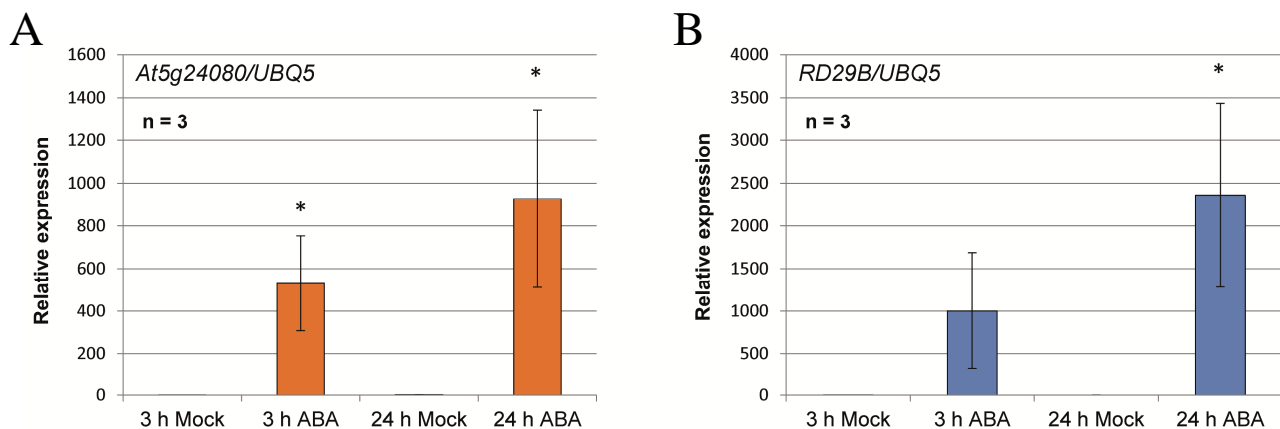


Figure 23. qPCR analysis of *At5g24080* and *RD29B* expression in 12-days-old *Arabidopsis* Col-0 seedlings treated with 50 μ M ABA. Bars represent means of gene expression \pm standard deviation in arbitrary units from $n = 3$ biological replicates (1 replicate = pool of 20 seedlings), normalized to the expression of *UBQ5*. 3 h mock was set to 1 and relative expression was normalised to this sample. Three technical replicates for each biological replicate were analysed by qPCR. * $P < 0.05$ using Student's t-test for pairwise comparison of mock and ABA treatment. The experiment was performed once (A) *At5g24080* transcript abundance in mock and ABA treated Col-0 seedlings. (B) *RD29B* transcript abundance in mock and ABA treated Col-0 seedlings.

3.5.7 AT5G24080-Venus fusion protein accumulates after ABA treatment

In order to test whether AT5G24080 protein accumulates after ABA treatment and to determine subcellular localization of the protein, constructs for expression of AT5G24080 fusion with a fluorescent protein tag under control of the native promoter were generated. For this purpose the *At5g24080* genomic sequence was amplified with 1.1 kb of its promoter sequence and

without the stop-codon for C-terminal tagging (promAt5g24080::At5g24080- Δ stop) by PCR. The *Venus* fluorescent protein gene was amplified without start-codon (Δ start-*Venus*) using the binary vector pC3 as template (Ghareeb *et al.*, 2016). Both PCR products were then assembled into the pC3 expression vector backbone using the Gibson Assembly[®] protocol (New England Biolabs). Therefore, 5' and 3' overlapping overhangs were introduced into promAt5g24080::At5g24080- Δ stop and Δ start-*Venus* by PCR primer design. A linker sequence between the *At5g24080* gene and *Venus* fluorescent protein was introduced as well. The generated vectors were transformed into *E. coli* TOP 10 cells (Invitrogen). Subsequently, transformants were plated on selective LB Agar plates and successful transformation verified by colony-PCR. Here, primer pairs binding in the pC3 backbone and *At5g24080* or *Venus* and pC3 backbone were used, only yielding a PCR product when promAt5g24080::At5g24080- Δ stop and Δ start-*Venus* were inserted into pC3 backbone in the correct orientation. Vectors were verified by digestion as well as Sanger sequencing and subsequently transformed into *Agrobacterium tumefaciens* strain GV3101 pMP90RK. Transformants were plated on selective LB Agar plates and successful transformation verified by colony-PCR.

The promAt5g24080::At5g24080::*Venus* construct was introduced into the *at5g24080-1* and *at5g24080-2* mutant using the floral dip protocol for *Agrobacterium* mediated transformation of *A. thaliana*. T₁ transgenic plants were selected with glufosinate ammonium, as they carried a resistance to this herbicide. To test expression of the transgene, 12 independent T₁ transgenic lines of each genotype were screened for expression of the AT5G24080-*Venus* fusion protein by confocal laser scanning microscopy (CLSM). Yet, *Venus* fluorescence was not detectable in either of the lines (data not shown). Since *in silico* and expression analyses demonstrated inducibility of *At5g24080* by ABA, AT5G24080-*Venus* accumulation was analysed by CLSM in leaf discs of the stable transgenic *A. thaliana* T₁ plants infiltrated with 50 μ M ABA. Line #1, #2, #3, #4, #5 and #6 of *at5g24080-1* transformed with promAt5g24080::At5g24080::*Venus* were selected for subsequent analyses, as *Venus* fluorescence was detectable in these lines (data not shown). In case of *at5g24080-2* transformed with promAt5g24080::At5g24080::*Venus*, line #1, #2, #4 and #12 were chosen for subsequent analyses.

In order to confirm inducibility of the promAt5g24080::At5g24080::*Venus* construct by ABA, leaf discs of stable transgenic *A. thaliana* T₁ plants were infiltrated with 50 μ M ABA and *At5g24080* as well as *At5g24080*::*Venus* transcript abundance analysed by semi-quantitative RT-PCR. *At5g24080* transcript levels were increased in Col-0 wild-type and all tested independent stable transgenic lines after treatment with 50 μ M ABA overnight as compared to mock treatment (Fig. S15A and S16A, upper panel). Interestingly, *At5g24080* transcript

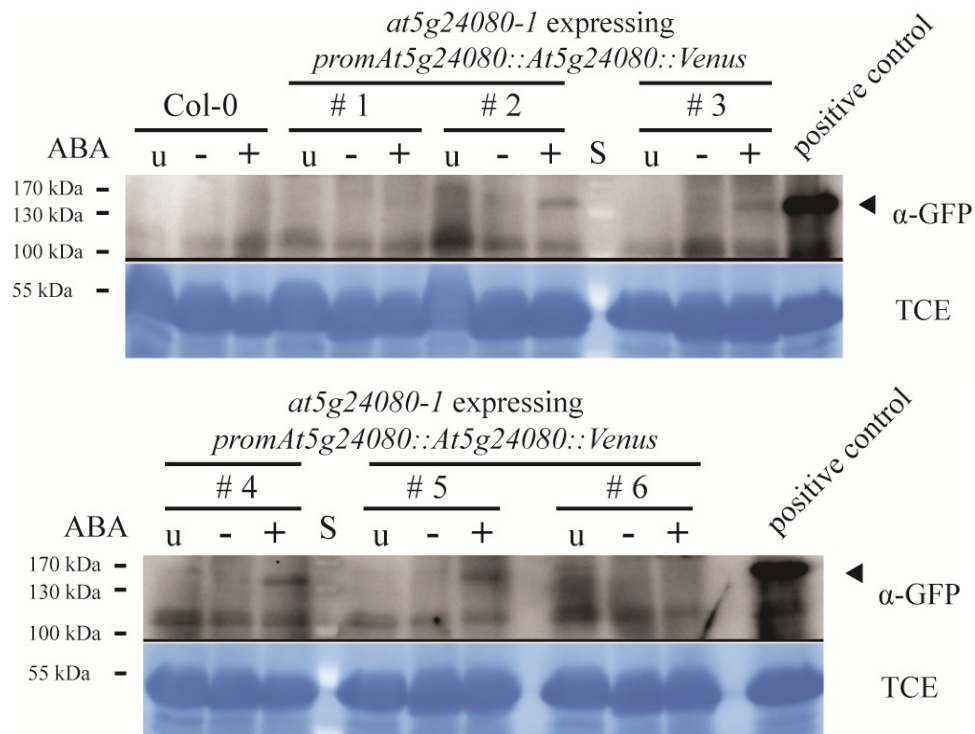
abundance was higher in several mock treated stable transgenic lines transformed with *promAt5g24080::At5g24080::Venus* as compared to mock treated Col-0 wild-type (Fig. S15A and S16A, upper panel), indicating that the transgene was inserted at a transcriptionally more active locus. When using *At5g24080::Venus* specific primer pair, which binds in the *At5g24080* and *Venus* gene, an increase in transcript abundance was observed after 50 μ M ABA treatment as compared to mock, suggesting that the introduced *promAt5g24080::At5g24080::Venus* construct is inducible by abscisic acid (Fig. S15A and S16A, middle panel). In addition to semi-quantitative RT-PCR, *At5g24080* transcript levels in stable transgenic T₁ lines were assessed by qPCR. Results of the qPCR analyses corresponded to the results obtained in semi-quantitative RT-PCR (Fig. S15B and S16B).

Thereafter, immunoblot analyses were performed in order to test whether full length AT5G24080-Venus protein accumulates after ABA treatment. For this purpose leaf discs of stable transgenic *A. thaliana* T₁ plants were infiltrated with 50 μ M ABA and total protein extraction was carried out. In immunoblot analyses *A. thaliana* Col-0 wild-type was used as a negative control. In the experiment shown in Fig. 24A a transgenic line overexpressing AT5G24080-Venus was included as a positive control. The calculated molecular weight of AT5G24080-Venus fusion protein corresponds to ca. 125 kDa.

Interestingly, AT5G24080-Venus protein band corresponded to a size of ca. 140 kDa (Fig. 24), suggesting posttranslational modification of the protein. In case of *at5g24080-1* transformed with *promAt5g24080::At5g24080::Venus*, AT5G24080-Venus fusion protein accumulated in the independent stable transgenic T₁ lines #2, #3, #4 and #5 after 50 μ M ABA treatment as compared to the mock and untreated controls (Fig. 24A). The strongest AT5G24080-Venus protein accumulation was observed in line #2 and #4. In *at5g24080-2* transformed with *promAt5g24080::At5g24080::Venus*, AT5G24080-Venus fusion protein accumulated after 50 μ M ABA treatment in independent stable transgenic T₁ line #1, #2, #4 and #12 as compared to mock (Fig. 24B). The strongest AT5G24080-Venus accumulation was observed in line #4. An AT5G24080-Venus protein band was not detectable in the Col-0 wild-type.

In summary, semi-quantitative RT-PCR analyses demonstrated inducibility of the *promAt5g24080::At5g24080::Venus* construct by ABA in in stable transgenic T₁ *at5g24080-1* and *at5g24080-2* lines. Subsequent qPCR analyses supported results of the semi-quantitative RT-PCR. AT5G24080-Venus fusion protein accumulated after ABA treatment in independent stable transgenic T₁ *at5g24080-1* and *at5g24080-2* lines expressing the AT5G24080-Venus fusion protein under control of the native promoter, indicating that AT5G24080 is ABA inducible.

A



B

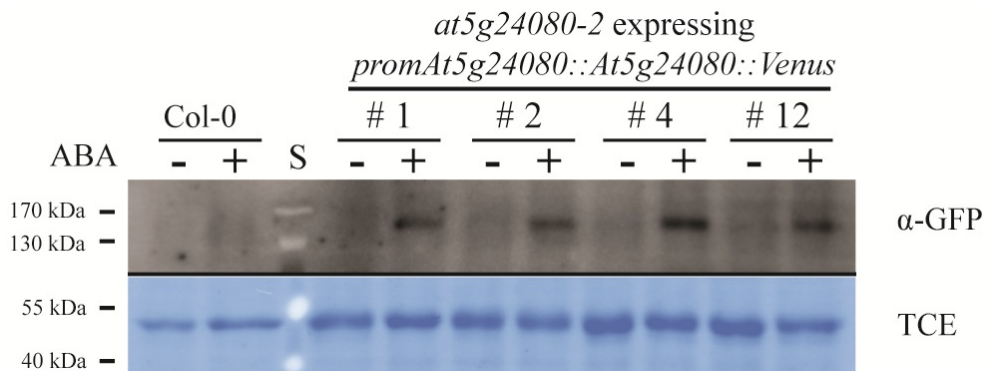


Figure 24. Immunoblot analysis of independent transgenic *Arabidopsis thaliana* T₁ lines stably expressing *At5g24080::Venus* under the control of its native promoter after ABA treatment. Upper panels show α-GFP immunoblot detecting Venus, whereas lower panels represent 2,2,2-Trichloroethanol (TCE) in-gel total protein visualisation as control for equal loading. Eight leaf discs (Ø 0.55 cm) from 10-week-old plants were pressure infiltrated with 50 μM ABA (+) or mock (-) treated overnight. “S” represents the size standard. The experiments were repeated with similar results. **(A)** AT5G24080 protein levels in *A. thaliana at5g24080-1* expressing *promAt5g24080::At5g24080::Venus*. The upper panel displays *A. thaliana* Col-0 and transgenic lines #1 to #3. The lower panel displays transgenic lines #4 to #6. 35S::AT5G24080::Venus was used as positive control. “u” represents untreated control. Protein extraction was performed using the total protein extraction protocol. **(B)** AT5G24080 protein levels in *A. thaliana at5g24080-2* expressing *promAt5g24080::At5g24080::Venus* line #1, #2, #4 and #12. Since unspecific bands and strong background signal was observed in the experiment shown in (A), protein extraction was performed using the receptor-like kinase optimised protocol.

3.5.8 AT5G24080-Venus fusion protein accumulates in *Arabidopsis* leaf and root tissues after ABA treatment

Next, subcellular localisation of AT5G24080-Venus fusion protein was analysed. Since AT5G24080-Venus was hardly detectable in untreated or mock treated plants by immunoblotting, subcellular localisation studies were performed with ABA treated plants. For this purpose 12-day-old *in vitro* grown seedlings of independent transgenic T₂ *at5g24080-1* and *at5g24080-2* lines stably expressing *promAt5g24080::At5g24080::Venus* were either mock treated or incubated in 50 µM ABA for 4 h and subsequently analysed by Confocal Laser Scanning Microscopy (CLSM). For analysis of *at5g24080-1* expressing *promAt5g24080::At5g24080::Venus*, lines #2, #3 and #4 were chosen. However, line #3 showed hardly any Venus fluorescence and results are not included in this thesis. Lines #1, #2 and #4 of *at5g24080-2* transgenics expressing *promAt5g24080::At5g24080::Venus* were analysed. Weak Venus fluorescence was detectable in line #1 or #2 respectively. Therefore, these lines are not shown in this thesis. The low Venus fluorescence in T₂ *at5g24080-1* line #3 and T₂ *at5g24080-2* lines #1 and #2 is in accordance with the weakest induction of the transgene (Fig. S15 and S16) as well as lowest AT5G24080-Venus fusion protein levels (Fig. 24) in the T₁ generation among the six lines chosen for CLSM analysis. Venus fluorescence was not detectable in leaf epidermis of mock treated transgenic T₂ *at5g24080-1* and *at5g24080-2* lines stably expressing *promAt5g24080::At5g24080::Venus*. In mock treated plants, chloroplast autofluorescence was observed in the Venus fluorescence channel (Fig. 25, left panel). In addition, strong fluorescence at the periphery of the stomatal opening was observed (Fig. 25, left panel), which likely represented autofluorescence, because this signal was also detectable in the *A. thaliana* Col-0 wild-type control (Fig. S17, upper panel). After 50 µM ABA treatment of *at5g24080-1* lines #2 and #4 stably expressing *promAt5g24080::At5g24080::Venus*, Venus fluorescence was observed at the cell periphery of pavement cells as well as in guard cells (Fig. 25, right panel). No nuclear signal or fluorescence of cytoplasmic strands was detected. In case of *at5g24080-2* line #4 stably expressing *promAt5g24080::At5g24080::Venus*, strong Venus fluorescence was detectable in guard cells but not in pavement cells (Fig. 25, right panel).

Publically available microarray data suggest that *At5g24080* is strongly expressed in the procambium of unchallenged *Arabidopsis* roots (*Arabidopsis* eFP Browser, Winter *et al.*, 2007). For this reason, AT5G24080-Venus subcellular localisation was analysed in roots of mock or 50 µM ABA treated 12-day-old *in vitro* grown seedlings of independent transgenic T₂ *at5g24080-1* and *at5g24080-2* lines stably expressing *promAt5g24080::At5g24080::Venus*.

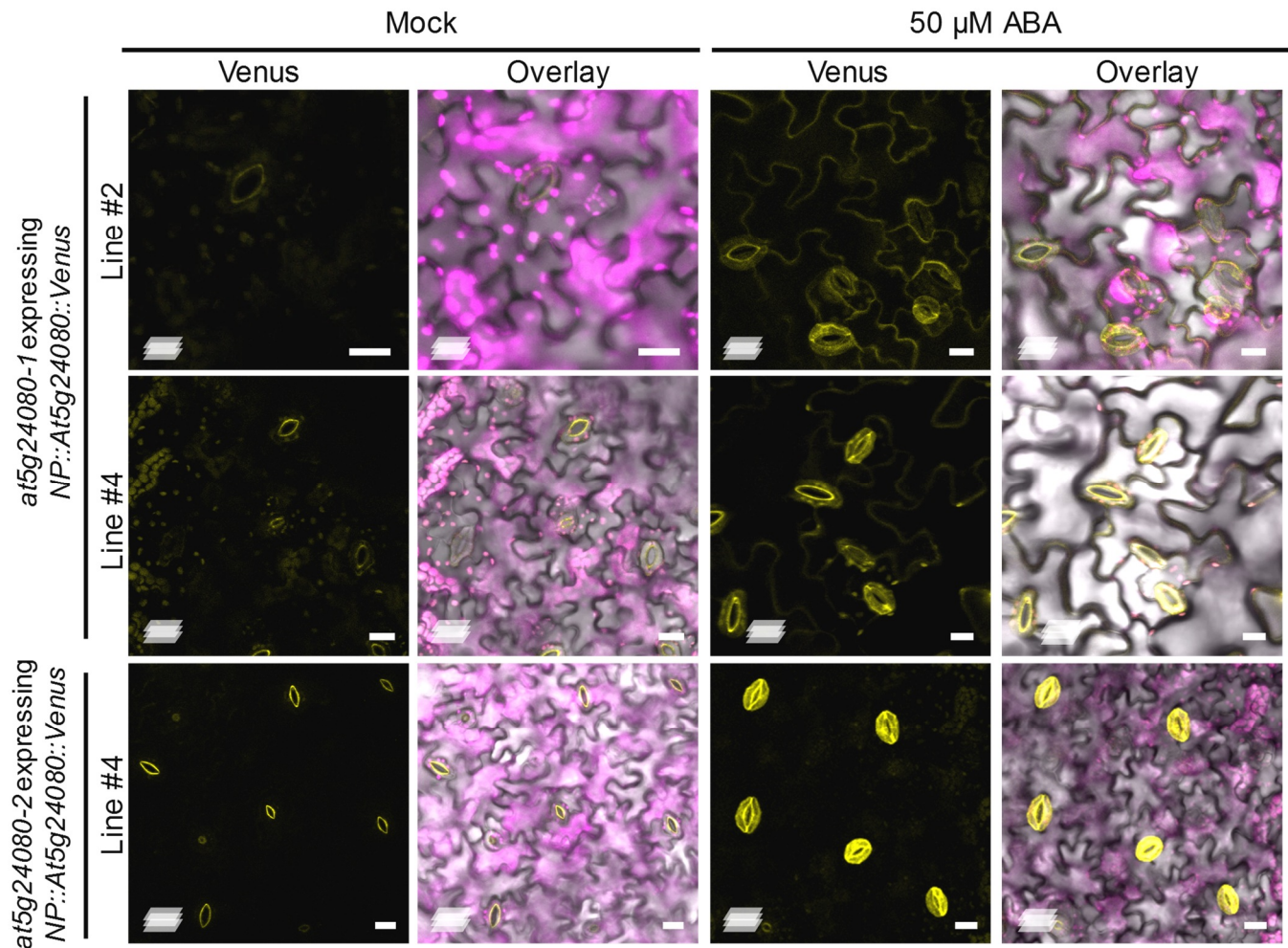


Figure 25. AT5G24080-Venus localisation after ABA treatment in leaves of independent transgenic *A. thaliana* T₂ lines stably expressing *promAt5g24080*::*At5g24080*::*Venus*. 12-day-old *in vitro* grown seedlings were either mock treated or incubated in 50 μ M ABA for 4 h and subsequently subjected to Confocal Laser Scanning Microscopy (CLSM). Figure shows maximum projection images of Venus fluorescence (yellow) as well as overlays of the Venus fluorescence with the chloroplast autofluorescence (magenta) and the bright field channel (grey). Scale bar = 15 μ m. NP: *promAt5g24080*. The experiment was performed once, however, similar results were observed in the T₁ generation.

Venus fluorescence was not detectable in roots of mock treated stable transgenic T₂ lines. In the Venus fluorescence channel of mock treated plants a signal was observed, which likely represented autofluorescence, as it was also detectable in the root of *A. thaliana* Col-0 wild-type control (Fig. 26, left panel and S17). After 50 μ M ABA treatment of *at5g24080-1* line #2 and *at5g24080-2* line #4 stably expressing *promAt5g24080*::*At5g24080*::*Venus*, strong Venus fluorescence was observed in epidermal cells of newly emerged lateral roots (Fig. 26, right panel). At higher magnification, Venus fluorescence was detectable at the periphery of root epidermis cells, but also at the nuclear envelope (Fig. 26, right panel). Since *At5g24080*

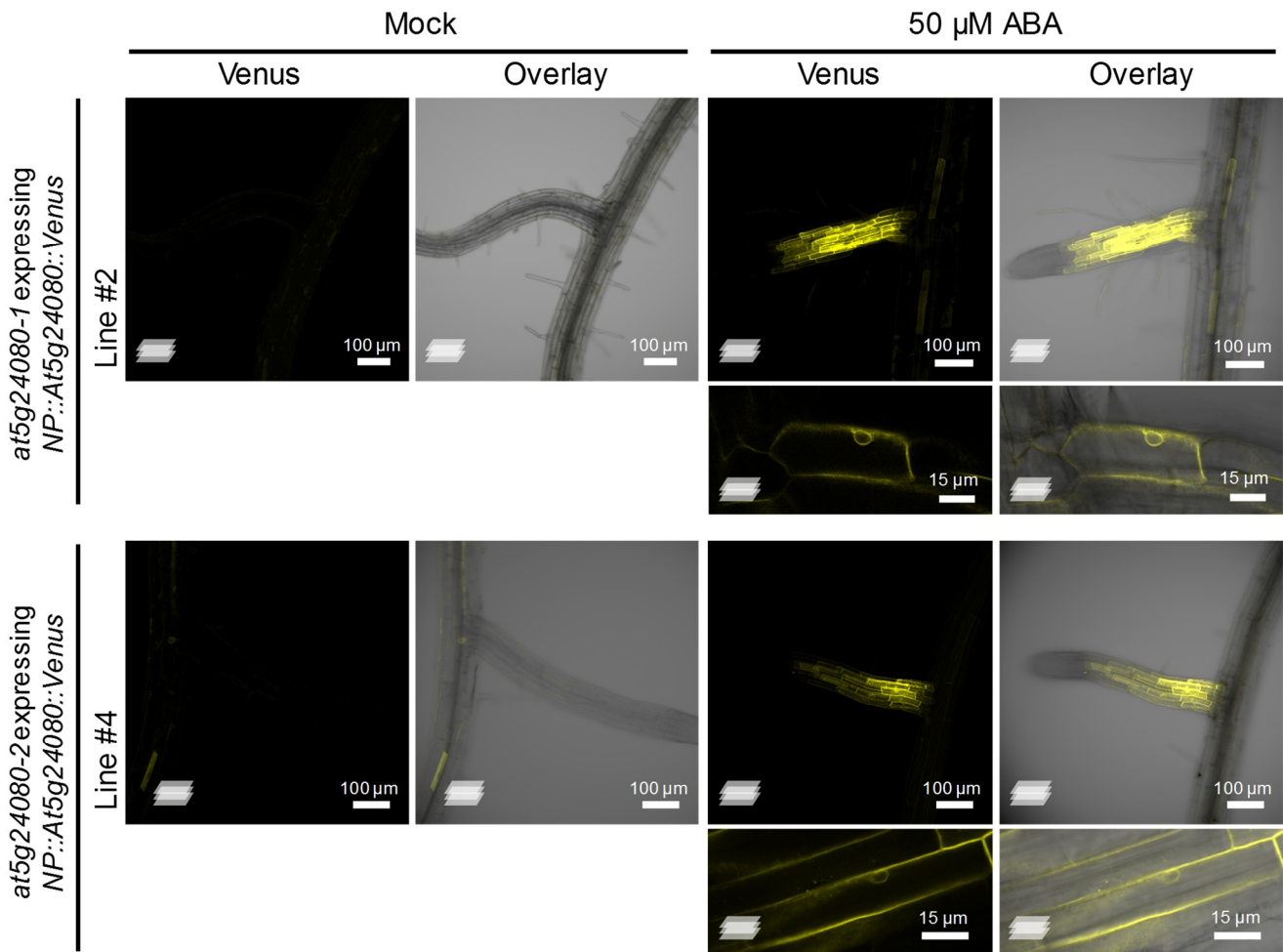


Figure 26. AT5G24080::Venus localisation after ABA treatment in roots of independent transgenic *A. thaliana* T₂ lines stably expressing *promAt5g24080*::*At5g24080*::*Venus*. 12-day-old *in vitro* grown seedlings were either mock treated or incubated in 50 μ M ABA for 4 h and subsequently subjected to Confocal Laser Scanning Microscopy (CLSM). Figure shows maximum projection images of Venus fluorescence (yellow) as well as an overlay of the Venus fluorescence with the bright field channel (grey). NP: *promAt5g24080*. The experiment was performed once.

represents a *Verticillium* chlorosis isolate induced gene, AT5G24080-Venus subcellular localisation was analysed during *A. thaliana* root infection with *V. longisporum* chlorosis isolate c-VL43. However, no Venus fluorescence was observed. Autofluorescence was visible in the Col-0 wild-type control and the transgenics (Fig. S18).

In summary, results of the CLSM analysis suggest that AT5G24080-Venus fusion protein accumulates 4 h after 50 μ M ABA treatment of independent stable transgenic *Arabidopsis* T₂ lines but is not detectable in mock treated plants. In leaf epidermis of *at5g24080-1* lines #2 and #4, AT5G24080-Venus localised to the cell periphery of pavement cells as well as to the guard cells. However, Venus fluorescence was observed only in guard cells but not in pavement cells of *at5g24080-2* line #4. In the root of stable transgenic *Arabidopsis* T₂ plants, AT5G24080-Venus strongly accumulated in epidermal cells of newly emerged lateral roots. In

addition to the periphery of root epidermis cells, Venus fluorescence was also detectable at the nuclear envelope.

3.5.9 AT5G24080-Venus subcellular localisation after ABA treatment correlates with subcellular localisation after overexpression

No AT5G24080-Venus fluorescence was detectable in independent transgenic T₂ *at5g24080-1* and *at5g24080-2* lines stably expressing *promAt5g24080::At5g24080::Venus* without induction of transgene expression by ABA. Consequently, lines overexpressing *At5g24080::Venus*, which would allow to monitor AT5G24080-Venus subcellular localisation without ABA treatment, were generated. For this purpose, the binary expression vector pHG152, which contains the constitutive Cauliflower Mosaic Virus 35S promoter (H. Ghareeb, personal communication) was used. Genomic *At5g24080* was amplified without its promoter sequence and without the stop-codon for C-terminal tagging (*At5g24080-Δstop*) by PCR. The *Venus* fluorescent protein gene was amplified without start-codon (*Δstart-Venus*) using the binary vector pC3 as template (Ghareeb *et al.*, 2016). Both PCR products were then assembled into the backbone of the binary expression vector pHG152 using the Gibson Assembly[®] protocol (New England Biolabs). Therefore, 5' and 3' overlapping overhangs were introduced into *At5g24080-Δstop* and *Δstart-Venus* by PCR primer design. A linker sequence between the *At5g24080* gene and *Venus* fluorescent protein was introduced as well. The generated vectors were amplified and verified as described in section 3.5.7. Finally, the *35S::At5g24080::Venus* construct was introduced into the *at5g24080-1* and *at5g24080-2* mutant using the floral dip protocol for *Agrobacterium* mediated transformation of *A. thaliana*. Subsequently, stable transgenic T₁ *at5g24080-1* and *at5g24080-2* lines expressing *35S::At5g24080::Venus* were selected by immunoblotting. In case of *at5g24080-1* transformed with *35S::At5g24080::Venus*, a AT5G24080-Venus band corresponding to a size of ca. 140 kDa was detected in independent stable transgenic T₁ line #7, #9 and #12 (Fig. 27A). In *at5g24080-2* transformed with *35S::At5g24080::Venus*, AT5G24080-Venus was detected in independent stable transgenic T₁ line #1, #9, #12 and #15 (Fig. 27B).

Next, subcellular localisation of AT5G24080-Venus fusion protein was analysed by Confocal Laser Scanning Microscopy (CLSM) in 12-day-old *in vitro* grown seedlings of independent transgenic T₂ *at5g24080-1* and *at5g24080-2* lines stably expressing *35S::At5g24080::Venus*.

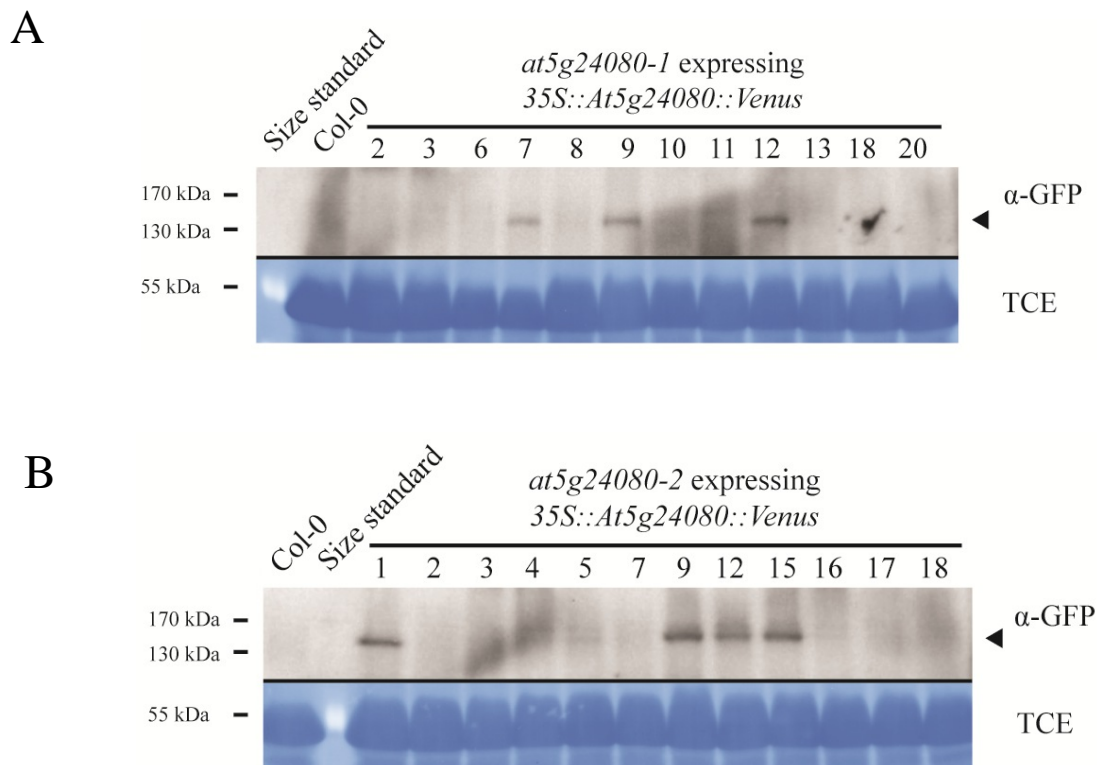


Figure 27. Immunoblot analysis of independent transgenic *Arabidopsis thaliana* T₁ lines stably expressing 35S::At5g24080::Venus. Upper panels show α -GFP immunoblot detecting Venus, whereas lower panels represent 2,2,2-Trichloroethanol (TCE) in-gel total protein visualisation as control for equal loading. Eight leaf discs (\varnothing 0.55 cm) from 10-week-old plants were used for protein extraction according to the total protein extraction protocol. The experiment was performed once. **(A)** AT5G24080 protein levels in *A. thaliana at5g24080-1* expressing 35S::At5g24080::Venus. **(B)** AT5G24080 protein levels in *A. thaliana at5g24080-2* expressing 35S::At5g24080::Venus.

In case of *at5g24080-1* expressing 35S::At5g24080::Venus, lines #7 and #12 were analysed. Lines #1 and #9 of *at5g24080-2* expressing 35S::At5g24080::Venus were chosen for characterization by CLSM. In all tested independent stable transgenic T₂ lines Venus fluorescence was observed at the cell periphery of epidermis pavement cells as well as in guard cells (Fig. 28A and B). No nuclear signal or fluorescence of cytoplasmic strands was detected. AT5G24080 contains a predicted transmembrane domain (Fig. 10). The observed Venus fluorescence at the cell periphery of pavement cells and presence of a transmembrane domain in AT5G24080 suggests that it localises to the plasma membrane. In order to test this hypothesis, AT5G24080-Venus subcellular localisation during plasmolysis was analysed. During plasmolysis AT5G24080-Venus localised to the cell membrane and to Hechtian strands, indicating plasma membrane localisation (Fig. 28C).

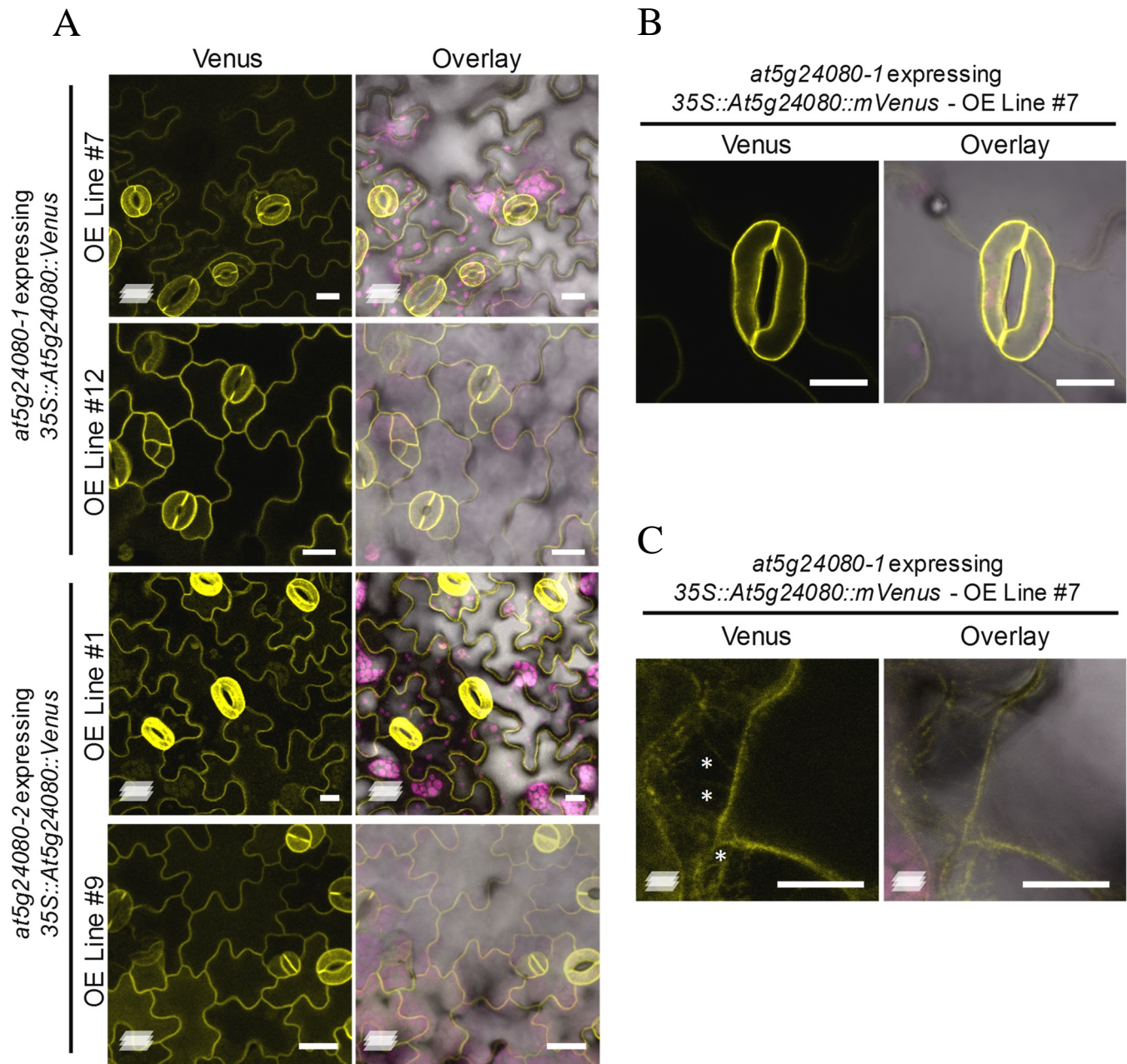


Figure 28. AT5G24080::*Venus* localisation in leaves of independent transgenic *A. thaliana* T₂ lines stably expressing 35S::*At5g24080*::*Venus*. 12-day-old *in vitro* grown seedlings were subjected to Confocal Laser Scanning Microscopy (CLSM). Images show Venus fluorescence (yellow) as well as overlays of the Venus fluorescence with the chloroplast autofluorescence (magenta) and the bright field channel (grey). Maximum projection images are indicated by a stack symbol in the left lower corner. Scale bar = 15 μ m. The experiment was performed once, however, similar results were observed in the T₁ generation. **(A-B)** AT5G24080-*Venus* localises to cell periphery of pavement cells and stomatal guard cells. **(C)** AT5G24080-*Venus* localises to Hechtian strands during plasmolysis. Plasmolysis was induced by 1M NaCl. Hechtian strands are marked by asterisks.

Taken together, AT5g24080-*Venus* localised to the cell periphery of epidermal pavement cells and guard cells of independent transgenic T₂ *at5g24080-1* and *at5g24080-2* lines stably expressing 35S::*At5g24080*::*Venus*. This subcellular localisation corresponds to

AT5G24080-Venus localisation during ABA treatment in leaf epidermis of stable transgenic T₂ plants expressing *At5g24080::Venus* under the control of its native promoter (Fig. 25). Moreover, absence of a nuclear or cytoplasmic signal as well as localisation to cell membrane and Hechtian strands during plasmolysis suggest, that AT5G24080 represents a plasma membrane localised protein.

3.5.10 *At5g24080* expression is reduced in the *aba1-101* ABA biosynthesis mutant background

In silico analyses showed that the G-type LecRLK gene *At5g24080* contains an ABA response element and a CE1 coupling element in its promoter region. Furthermore, *At5g24080* transcript as well as protein levels increase after ABA treatment, suggesting that it is inducible by abscisic acid. *At5g24080* expression is strongly up-regulated during *Verticillium* chlorosis isolate infection (Table 2, Fig. 4 and 5). To test whether *At5g24080* gene induction by chlorosis isolates is dependent on ABA, next, *At5g24080* expression was analysed in the background of the ABA biosynthesis mutant *aba1-101* (Barrero *et al.*, 2005) during *Verticillium* challenge.

For this purpose 3 ½ -week-old *A. thaliana* Col-0 wild-type and *aba1-101* soil grown seedlings were inoculated with the *V. dahliae* chlorosis-inducing reference isolate c-V76 and the wilting-inducing reference isolate w-JR2. A mock treated control was included as well. Thereafter, total RNA was extracted from whole rosettes at 21 dpi. Subsequently, cDNA synthesis was carried out and *At5g24080* transcript abundance was analysed by semi-quantitative RT-PCR. *At5g24080* expression was strongly induced in *A. thaliana* Col-0 wild-type challenged with chlorosis isolate c-V76 as compared to mock treatment or wilting isolate infection (Fig. 29A). In the chlorosis isolate c-V76 infected *aba1-101* mutant, *At5g24080* induction was diminished as compared to c-V76 challenged Col-0 wild-type control (Fig. 29A). In addition to the semi-quantitative RT-PCR analysis, *At5g24080* gene induction in the *aba1-101* mutant background was analysed by qPCR at 21 and 28 days after *Verticillium* challenge. As in semi-quantitative RT-PCR analysis, *At5g24080* transcript amounts were reduced in the chlorosis isolate c-V76 infected *aba1-101* mutant as compared to c-V76 challenged Col-0 wild-type control at 21 and 28 dpi (Fig. 29B). In both, semi-quantitative PCR and qPCR analyses *At5g24080* gene induction by chlorosis isolate infection was not completely abolished (Fig. 29). These results suggest that, *At5g24080* gene induction during chlorosis isolate infection is partially but not exclusively dependent on ABA.

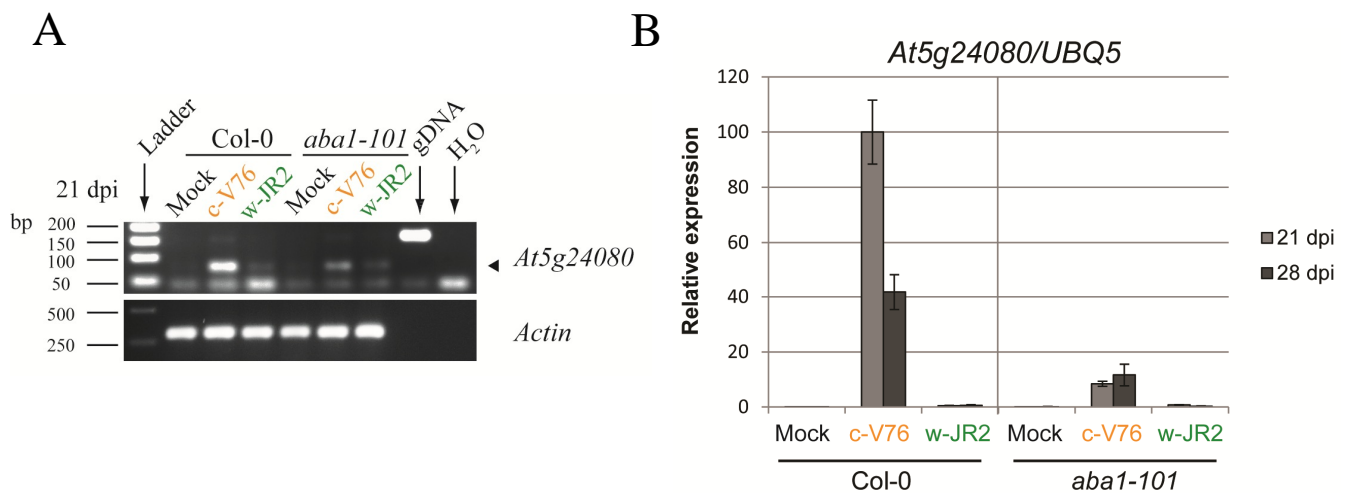


Figure 29. Analysis of *At5g24080* expression in *A. thaliana* Col-0 and *aba1-101* ABA biosynthesis mutant during *V. dahliae* c-V76 and w-JR2 infection. Pools of 4 rosettes per sample were used for RNA extraction. The experiment was repeated with similar results. **(A)** Semi-quantitative RT-PCR analysis of *At5g24080* expression. The housekeeping gene *Actin* was co-amplified as a control. A genomic DNA (gDNA) control was included to monitor potential contamination by gDNA. A reverse primer which binds two exon borders and spans an intron sequence was used in case of the *Actin* gene to exclude gDNA amplification. The *Actin* cDNA PCR product corresponds to 302 bp. Expected sizes of *At5g24080* PCR products are 79 bp cDNA and 161 bp gDNA. The arrowhead indicates *At5g24080* cDNA bands. **(B)** qPCR analysis of *At5g24080* expression. Bars represent mean gene expression \pm standard deviation in arbitrary units from 3 technical replicates, normalized to the expression of *UBQ5*.

3.6 The ABA biosynthesis mutant *aba1-101* shows wilting-like disease phenotype during *Verticillium* chlorosis isolate infection

Interestingly, the *aba1-101* mutant plants, which were used for *At5g24080* expression experiments, demonstrated a wilting-like disease phenotype during *Verticillium* chlorosis isolate c-V76 infection under standard growth conditions. Rosettes sizes of mock treated *aba1-101* plants are reduced compared to *A. thaliana* Col-0 wild-type (Fig. 30A, left panel). Col-0 wild-type demonstrated chlorosis and early senescence of older rosette leaves 21 days post infection with the chlorosis isolate c-V76 (Fig. 30A, middle panel). In contrast, no chlorosis symptoms were visible on *aba1-101* leaves during chlorosis isolate c-V76 infection (Fig. 30A, middle panel and Fig. S19). Instead, older *aba1-101* rosette leaves showed wilting symptoms (Fig. 30A, middle panel and Fig. 31F-H). Wilting symptoms of c-V76

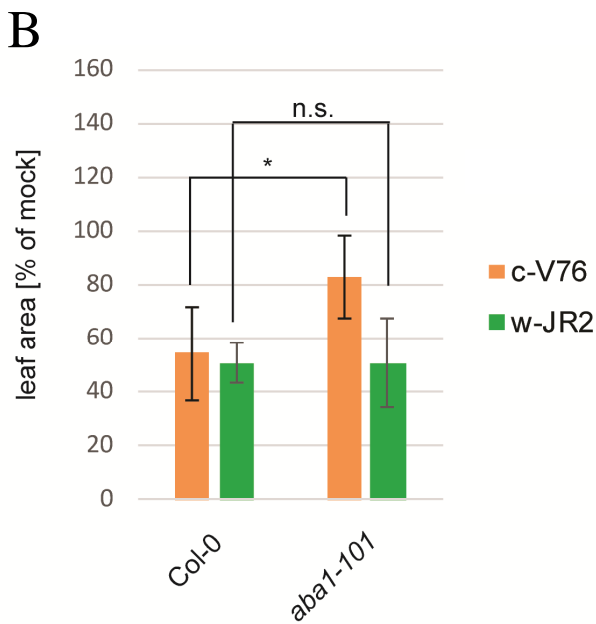
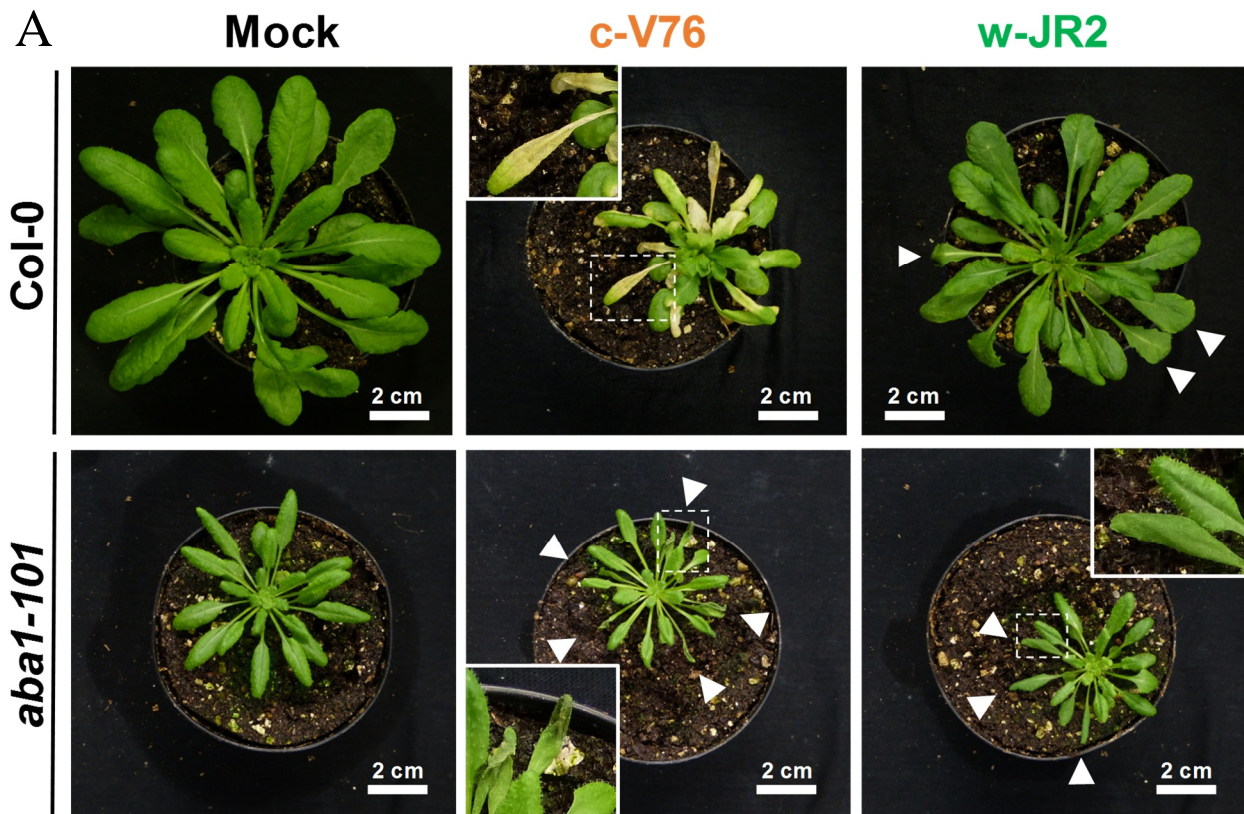


Figure 30. Disease phenotypes of *A. thaliana* Col-0 wild-type and the *aba1-101* mutant during infection with the *V. dahliae* isolates c-V76 and w-JR2. (A) Disease symptoms at 21 days post infection (dpi). Insets represent magnifications of areas marked with dotted boxes. Arrowheads indicate wilting leaves. The experiment was repeated twice with similar results. (B) Leaf area measurement at 21 days post infection. Leaf area of mock treated controls was set to 100 % and leaf area of infected plants calculated as percentage of mock control. Error bars represent standard deviation between n = 9-20 replicates. * $P < 0.05$ using Student's t-test for pairwise comparison of wild-type and mutant. (n.s.) not significant. The experiment was repeated twice with similar results.

infected *aba1-101* were more pronounced and appeared on more leaves as compared to wilting isolate w-JR2 challenged *aba1-101* as well as Col-0 wild-type (Fig. 30A, middle and right panel).

In order to quantify severity of disease symptoms, *Verticillium* triggered stunting of the *Arabidopsis* rosette was measured. Leaf area of mock treated controls was set to 100 % and leaf area of infected plants calculated as percentage of mock control. A pairwise comparison of Col-0 wild-type and the *aba1-101* mutant was carried out using t-test, to analyse statistical

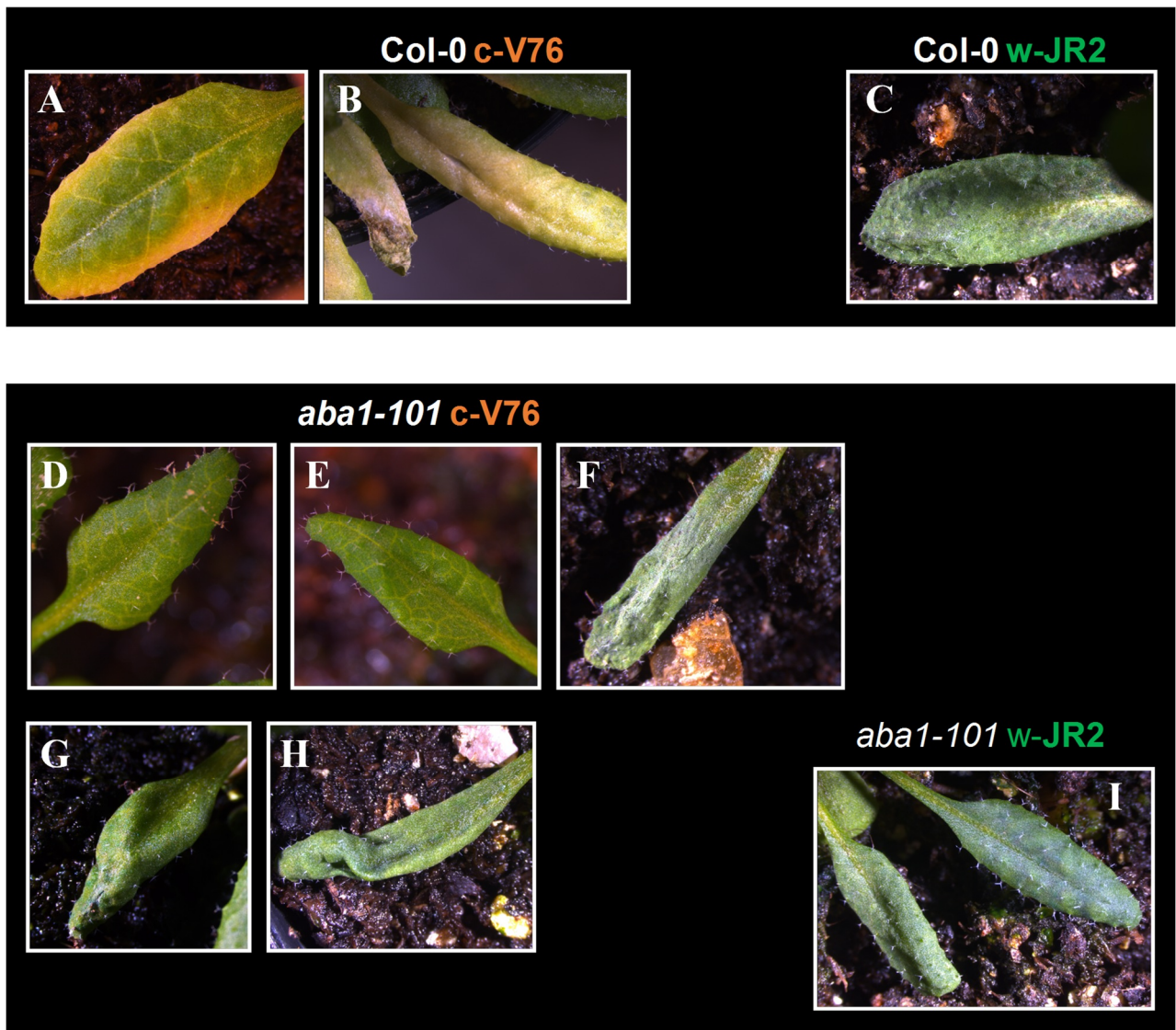


Figure 31. Disease symptoms on *A. thaliana* Col-0 wild-type (WT) and *aba1-101* mutant leaves 21 days post infection (dpi) with the *V. dahliae* isolates c-V76 and w-JR2. (A) Vein clearing and chlorosis of a Col-0 WT leaf at 21 dpi during c-V76 infection. (B) Chlorosis (right) and early senescence (left) of a Col-0 WT leaf at 21 dpi during c-V76 infection. (C) Wilting of a Col-0 WT leaf at 21 dpi during w-JR2 infection. (D and E) Vein clearing of *aba1-101* leaves at 21 dpi during c-V76 infection. (F-H) Wilting-like symptoms of *aba1-101* leaves at 21 dpi during c-V76 infection. (I) Wilting of an *aba1-101* leaf (left) at 21 dpi during w-JR2 infection. The experiment was repeated twice with similar results.

significance. Leaf area of chlorosis isolate c-V76 challenged *aba1-101* was significantly higher compared to wild-type (Fig. 30B). On the contrary, no significant differences in leaf area were observed during wilting isolate w-JR2 infection of *aba1-101* and wild-type plants (Fig. 30B). Together, these results suggest that defects in ABA biosynthesis lead to a reduction of disease symptom severity during chlorosis isolate c-V76 challenge, but not in wilting isolate w-JR2 infected plants.

The *aba1-101* mutant showed wilting-like disease symptoms and absence of leaf chlorosis as well as early senescence during *Verticillium* chlorosis isolate c-V76 infection. Besides chlorosis and early senescence symptoms, chlorosis isolate infection of *A. thaliana* is accompanied by transdifferentiation of chloroplast-containing bundle sheath cells to functional xylem elements and xylem hyperplasia within the *Arabidopsis* vascular system. In order to assess, whether *de novo* xylem formation takes place in the *aba1-101* mutant background during *Verticillium* chlorosis isolate infection, microscopic analyses of bundle sheath cell transdifferentiation in *A. thaliana* Col-0 wild-type and *aba1-101* leaf vascular bundles were performed.

Transdifferentiation of bundle sheath cells to xylem elements becomes macroscopically apparent as a phenomenon described as vein clearing (Fradin and Thomma, 2006; Reusche *et al.*, 2012). As on Col-0 wild-type, vein clearing was visible on several *aba1-101* leaves 21 days post infection with the chlorosis-inducing isolate c-V76 (Fig. 31A, D and E), indicating *de novo* xylem formation. In order to microscopically analyse bundle sheath transdifferentiation, detached leaves were stained with trypan blue as described in section 3.5.3. In the mock treated Col-0 wild-type plants vascular bundles are encompassed by living bundle sheath cells, which are not stained by trypan blue (Fig. 32A). In wild-type plants, infected with chlorosis isolate c-V76, bundle sheath cells transdifferentiate to xylem elements, showing characteristic annular, helical and reticulate secondary cell wall fortifications (Fig. 32B). During wilting isolate w-JR2 infection bundle sheath cell layer does not transdifferentiate (Fig. 32C). Wild-type like bundle sheath cell transdifferentiation into xylem elements was observed in leaves of chlorosis isolate c-V76 challenged *aba1-101* mutants (Fig. 32E). As in Col-0 wild-type, bundle sheath cell transdifferentiation was not observed in mock treated and wilting isolate w-JR2 infected *aba1-101* plants (Fig. 32D and F).

In summary, ABA biosynthesis mutant *aba1-101* demonstrated wilting-like disease symptoms and absence of leaf chlorosis as well as early senescence at 21 dpi during *Verticillium* chlorosis isolate c-V76 infection, indicating that functional ABA biosynthesis is required for establishment of chlorosis and early senescence symptoms. Moreover, bundle sheath cell transdifferentiation was not impaired in the *aba1-101* mutant, suggesting that functional ABA biosynthesis is not required for *de novo* xylem formation. In addition, *Verticillium* chlorosis isolate c-V76 induced stunting of the rosette was significantly reduced in the *aba1-101* mutant background compared to wild-type, indicating reduced susceptibility of *aba1-101* to chlorosis isolate c-V76 infection.

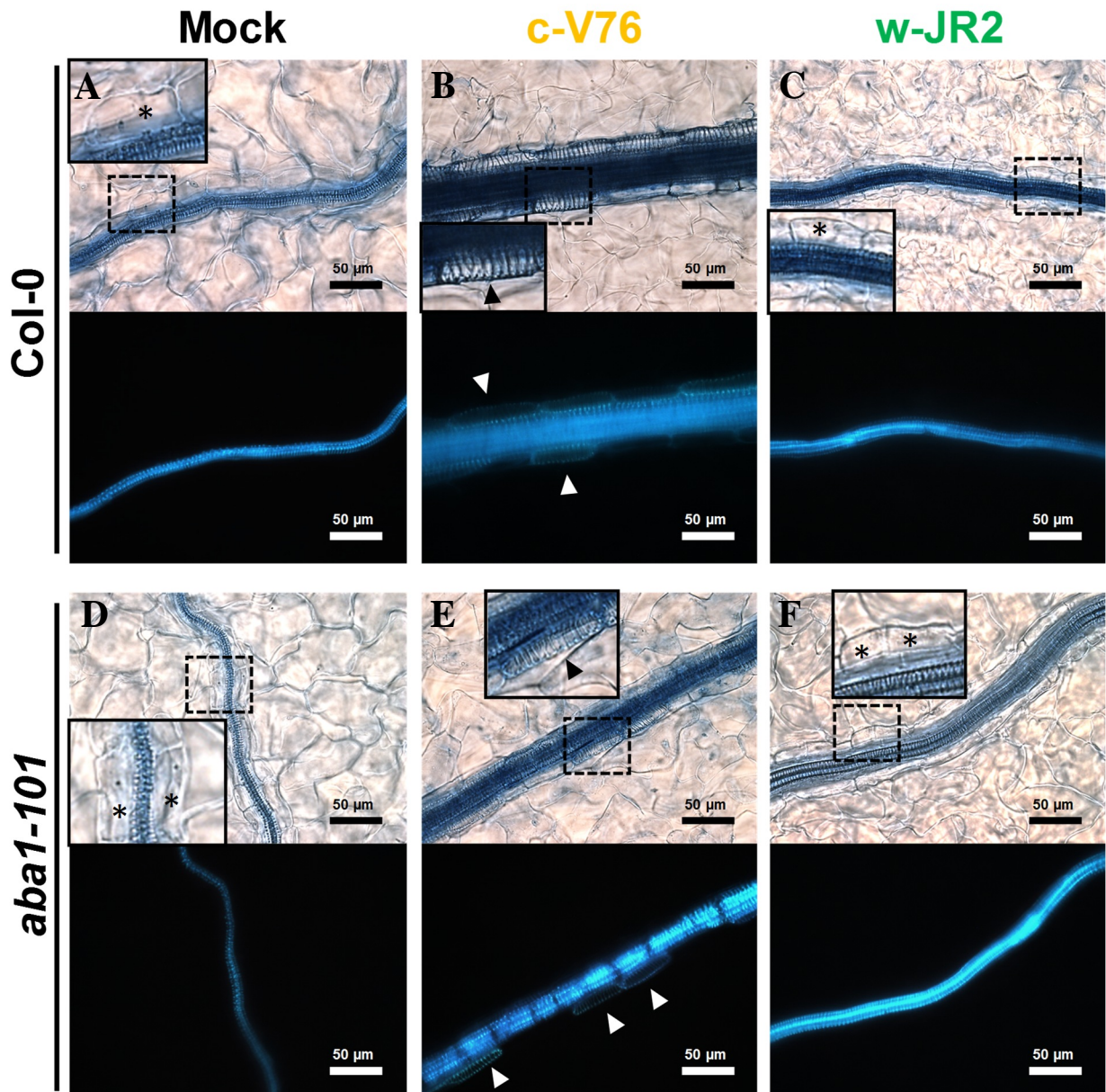


Figure 32. Analysis of bundle sheath cell transdifferentiation in leaf vascular bundles of *A. thaliana* Col-0 wild-type and the *aba1-101* mutant 28 days post infection (dpi) with *V. dahliae* isolates c-V76 and w-JR2. Plant leaves were stained with trypan blue. Figures (A-F) show bright field (upper panel) and epifluorescence (lower panel) images of leaf vascular bundles. Insets represent magnifications of areas marked with dotted boxes. Asterisks indicate bundle sheath cells, whereas arrowheads point at *de novo* formed tracheary elements. The experiment was performed once.

3.7 Proliferation of the chlorosis-inducing *Verticillium* isolate c-V76 is reduced in the *aba1-101* ABA biosynthesis mutant compared to wild-type

Leaf area measurements indicated a decrease in severity of chlorosis isolate c-V76 induced disease symptoms in *aba1-101* compared to wild-type plants. In order to analyse if reduced symptom development correlates with lower fungal proliferation, biomass of *Verticillium*

chlorosis-inducing isolate c-V76 and wilting-inducing isolate w-JR2 was analysed in *A. thaliana* Col-0 wild-type and the ABA biosynthesis mutant *aba1-101*. Relative amounts of fungal DNA in mock treated and infected plants were quantified at 21 and 28 dpi by qPCR as an indicator for fungal proliferation. Consistent with previous findings by K. Thole (K. Thole, PhD thesis, 2016), chlorosis-inducing isolate c-V76 showed higher proliferation in Col-0 wild-type plants as compared to the wilting-inducing isolate w-JR2 (Fig. 33, left panel). Proliferation of the chlorosis-inducing isolate c-V76 was diminished in the *aba1-101* mutant background at 21 as well as 28 dpi as compared to c-V76 infected Col-0 wild-type (Fig. 33). Proliferation of the wilting-inducing isolate w-JR2 was also slightly reduced in *aba1-101* at 21 as well as 28 dpi as compared to Col-0 wild-type (Fig. 33). However, w-JR2 proliferation in Col-0 wild-type and *aba1-101* were comparable in an independent repetition of the infection experiment (Fig. S20). In conclusion, consistent with the weaker *Verticillium* induced stunting symptoms, proliferation of the chlorosis-inducing isolate c-V76 was decreased in *aba1-101*. Taken together these results suggest that the ABA biosynthesis mutant *aba1-101* is less susceptible to chlorosis isolate c-V76 as compared to wild-type. Thus, plant derived ABA or ABA signalling may represent a susceptibility factor in the *A. thaliana* – *Verticillium* chlorosis isolate interaction.

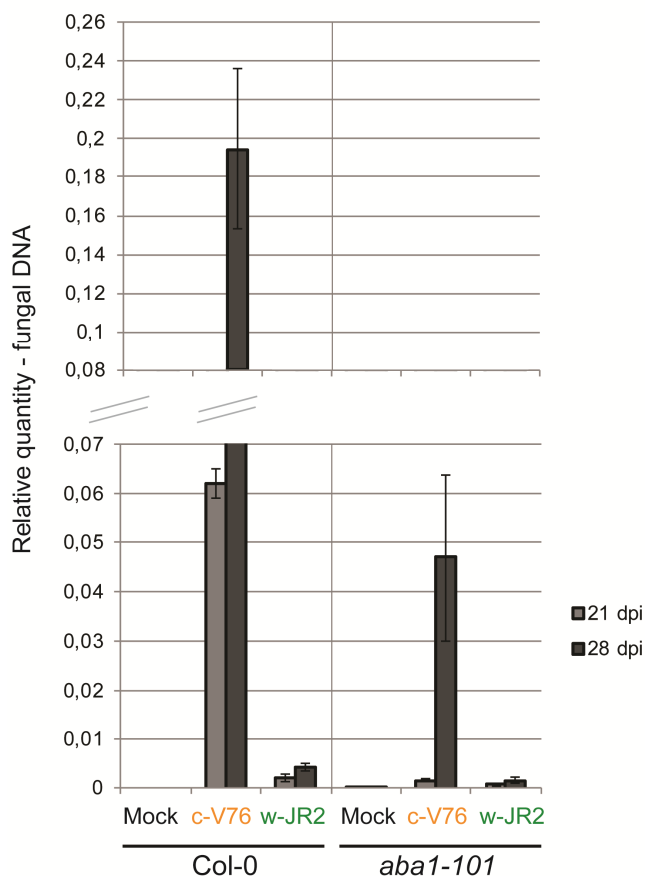


Figure 33. Proliferation of *V. dahliae* isolate c-V76 and w-JR2 in *A. thaliana* Col-0 wild-type and *aba1-101* ABA biosynthesis mutant. Pools of 4 plants per sample were used for genomic DNA (gDNA) extraction. Bars represent quantity of *Verticillium beta-Tubulin* \pm standard deviation in arbitrary units from 3 technical replicates, normalized to the expression of *A. thaliana UBQ5*. The experiment was repeated with similar results.

3.8 ABA content is significantly increased in *Arabidopsis* wild-type plants during infection with the chlorosis-inducing *Verticillium* isolate c-V76

The ABA biosynthesis mutant *aba1-101* lacks chlorosis and early senescence symptoms, which typically appear 21 days post infection with chlorosis-inducing *Verticillium* isolates, indicating that abscisic acid is required for establishment of chlorosis and early senescence symptoms. Furthermore, proliferation of chlorosis isolate c-V76 is reduced in *aba1-101* as well as the c-V76 triggered stunting of the rosette, suggesting that plant derived ABA or ABA signalling may represent a susceptibility factor in the *A. thaliana* – *Verticillium* chlorosis isolate interaction. In order to support results of the reverse genetic analyses, ABA levels in *A. thaliana* Col-0 were analysed in a time course during *Verticillium* chlorosis isolate c-V76 or wilting isolate w-JR2 infection. For this purpose, pools of 4 rosettes per sample were harvested at 7, 14, 21 and 28 dpi and subjected to HPLC-MS/MS analysis. ABA levels were strongly increased during chlorosis isolate c-V76 infection as compared to wilting isolate w-JR2 infection and mock treatment (Fig. 34). ABA levels started to increase at 7 dpi in c-V76 infected *A. thaliana* Col-0 and peaked at 21 and 28 dpi. However, a slight increase in ABA content was also observed at 14, 21 and 28 dpi in w-JR2 infected plants as compared to mock (Fig. 34).

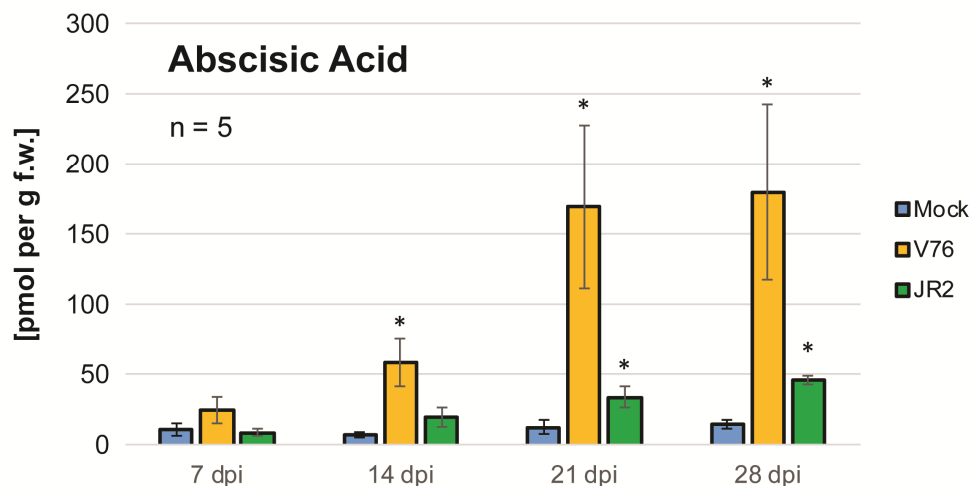


Figure 34. Abscisic Acid (ABA) content in *A. thaliana* Col-0 wild-type during the course of infection with the *V. dahliae* isolate c-V76 and w-JR2. Bars represent ABA content \pm standard error in pmol per g fresh weight (f.w.) from $n = 5$ independent experiments. In each experiment, 4 rosettes per sample were pooled and subjected to HPLC-MS/MS analysis. * $P < 0.05$ using Student's t-test for pairwise comparison of wild-type and mutant.

Analyses of fungal proliferation demonstrated that chlorosis-inducing isolate c-V76 accumulates higher amounts of fungal biomass in *A. thaliana* Col-0 compared to the wilting-inducing isolate w-JR2 (Fig. 33, left panel). Thus, it is conceivable to postulate that elevated ABA levels in c-V76 infected plants as opposed to w-JR2 infection may result from enhanced proliferation of this chlorosis-inducing isolate. In order to assess effects of fungal proliferation, ABA levels were analysed in *A. thaliana* Col-0 during *V. longisporum* chlorosis reference isolate c-VL43 infection. Isolate c-VL43 accumulates lower amounts of fungal biomass in *A. thaliana* Col-0 than isolate c-V76 (K. Thole, PhD thesis, 2016). ABA levels were increased during chlorosis isolate c-VL43 infection compared to wilting isolate w-JR2 challenge and mock treatment (Fig. S21A). Moreover, ABA content in c-VL43 infected *A. thaliana* Col-0 was equivalent to c-V76 infected plants (Fig. S21A). As before, chlorosis-inducing isolate c-V76 accumulated higher amounts of fungal biomass than wilting isolate w-JR2, whereas proliferation of the chlorosis isolate c-VL43 was comparable to w-JR2 (Fig. S21B).

In summary, ABA levels were strongly elevated in *A. thaliana* Col-0 during chlorosis-inducing isolate c-V76 infection. In contrast, only weak increases in ABA content were observed in wilting isolate w-JR2 infected plants. Higher ABA levels did not result from higher proliferation of c-V76, since same results were observed during chlorosis isolate c-VL43 infection, which accumulates comparable amounts of fungal biomass as w-JR2. As a consequence, it can be stated that chlorosis reference isolate c-V76 and c-VL43 infection of *A. thaliana* Col-0 leads to an increase in ABA content independent of fungal biomass.

4. Discussion

4.1 Identification of candidate genes which are specifically induced by chlorosis and wilting isolates

In this study an RNA-sequencing analysis of *V. dahliae* challenged plants was performed that aimed at the identification of differentially expressed host genes involved in establishment of the chlorosis disease phenotype. In an RNA-sequencing experiment, a high number of replicates leads to more robust results (Auer and Doerge, 2010; Y., Liu *et al.*, 2014; Schurch *et al.*, 2016). In this study, no biological replicates were included for *Verticillium* inoculated samples. Instead, five chlorosis- and five wilting inducing isolates were treated as biological replicates in the differential gene expression analysis. It was assumed that all isolates of one interaction class trigger differential expression of a core set of symptom-specific host genes, which are causal to chlorosis or wilting symptom development. A differential expression analysis based on a biological replicate series of a single chlorosis or wilting reference isolate would also yield isolate-specific candidate genes that are differentially regulated in response to this particular isolate. Such candidates would for example comprise host genes regulated in response to lineage-specific *Verticillium* effectors acquired solely by the reference isolate. Kombrink *et al.* (2017) recently described the *Vd2LysM* effector which is present in the *V. dahliae* isolate VdLs17 lineage-specific region but not in the genome of any other sequenced *Verticillium* isolate (Kombrink *et al.*, 2017). The use of several isolates of one interaction class in the differential expression analysis allows subtraction of isolate-specific candidates, thus yielding only a core set of symptom-specific host genes required for the establishment of the chlorosis or wilting phenotype.

In order to analyse early host responses to *Verticillium* infection, i.e. during penetration and establishment of plant-pathogen interaction, the root transcriptome of two-week-old *A. thaliana* Col-0 *in vitro* seedlings was analysed at 4 days post infection (dpi) by RNA-sequencing. Previously conducted analyses of *A. thaliana* root transcriptome in response to the reference *V. longisporum* isolate c-VL43 show that substantial host transcriptional reprogramming takes place at this early time point (Iven *et al.*, 2012; J. Schmitz, PhD Thesis, 2015). Consistent with this extensive transcriptional reprogramming, 399 *A. thaliana* genes were significantly regulated (below a cut-off of $FDR \leq 0.05$ and a \log_2 fold change in expression $\geq +1$ and ≤ -1) during root infection by all ten *V. dahliae* isolates (data not shown). However, it has to be considered that these three transcriptome analyses are not strictly comparable. Infection procedure and the quantity of *V. longisporum* spores used by Iven *et al.* (2012) differed from

the infection assay performed in this thesis. In her transcriptome analysis, J. Schmitz (2015) analysed a different *A. thaliana* genotype compared to this thesis, in particular WTAos and WT*coil-t*, two wild-types back-crossed from the respective heterozygous mutant. Nevertheless, 18.1 % of genes differentially expressed in WTAos and 19.2 % in WT*coil-t* as well as 18.8 % of differentially expressed genes from the transcriptome analysis conducted by Iven *et al.* (2012) overlap with candidates significantly regulated by *V. dahliae* isolates in this thesis (data not shown). Only few genes were differentially expressed specifically in response to chlorosis- or wilting-inducing isolates respectively at 4 dpi in *A. thaliana* roots (Table S1 and S2) indicating that transcriptional reprogramming induced by chlorosis or wilting isolates does not largely differ at this early stage of infection. This correlates to findings of Reusche *et al.* (2014) which demonstrate that the *V. longisporum* reference chlorosis isolate c-VL43 and *V. dahliae* reference wilting isolate w-JR2 exhibit similar infection strategies and growth kinetics at early stages of infection. Both isolates enter the root at endodermis free zones and by 4 dpi colonize different cell layers including the central cylinder (Reusche *et al.*, 2014).

Late responses to *Verticillium* infection, i.e. during colonization of the xylem and the necrotrophic phase, were analysed in *N. benthamiana* shoot at 8, 12 and 16 dpi. In order to select candidates, differentially expressed genes were grouped into functional categories. Genes that either were most strongly regulated by chlorosis isolate infection within a functional category, i.e. G-type LecRLK At5g24080 and RD17 or might represent putative key regulators in disease phenotype establishment, i.e. ANAC071 were chosen as candidates and further analysed in this study. However, further chlorosis isolate induced genes may play a role in establishment of the chlorosis disease phenotype. Among chlorosis-induced candidates, a number of genes encoding lipid or wax biosynthesis enzymes and lipid transfer proteins (LTPs) were present (Table S3, S4, S6 and S8). LTPs have been proposed to function in export of cuticular waxes, since LTP knock-down and knock-out lines demonstrate reduced amounts of certain wax components in the *Arabidopsis* cuticula (DeBono *et al.*, 2009; Lee *et al.*, 2009; Kim *et al.*, 2012). Interestingly, tree tobacco (*Nicotiana glauca*) was shown to increase wax deposition under drought stress and leaves from drought stressed plant were more resistant to water loss (Cameron *et al.*, 2006). Moreover, *Arabidopsis* LTP3 was demonstrated to be implicated in drought responses, since *ltp3* loss of function mutants showed reduced drought tolerance and overexpressing lines were more resistant to drought stress (Guo *et al.*, 2013). Consequently, induction of wax biosynthesis and LTP genes may contribute to enhanced drought tolerance during chlorosis isolate infection. Aquaporins constitute another group of chlorosis-induced genes, which has been reported to have beneficial effects on drought

tolerance (Guo *et al.*, 2006; S., Zhou *et al.*, 2012; Xu *et al.*, 2014; Zhuang *et al.*, 2015). Five aquaporin genes belonging to the plasma membrane- and tonoplast-intrinsic protein families were up-regulated during chlorosis isolate infection at 8, 12 and 16 dpi as well as in the collective analysis of 8, 12 and 16 dpi (Table S3, S4, S6 and S8). Five aquaporin genes belonging to these families were also induced by the *V. longisporum* chlorosis isolate c-VL43 infection of *A. thaliana* at 18 dpi in a microarray experiment conducted by H. Tappe. *PIP2;2* (*PLASMA MEMBRANE INTRINSIC PROTEIN 2;2*) and *TIP2;2* (*TONOPLAST INTRINSIC PROTEIN 2;2*) genes were up-regulated in both transcriptome analyses (H. Tappe, PhD thesis, 2008). None of the differentially expressed aquaporin genes was selected as candidate for further analysis, since members of *Arabidopsis* aquaporin subfamilies are known to be highly homologous. Members of the plasma membrane intrinsic protein subfamily share 71.8 to 97.2 % sequence homology at the amino acid level, whereas tonoplast intrinsic protein subfamily members share 44.1 to 93.1 % amino acid sequence homology (Quigley *et al.*, 2002). Thus, it is likely that aquaporins function redundantly, which makes reverse genetic analysis difficult. Furthermore, several drought responsive genes including *RD17* and *ERF53* were up-regulated by chlorosis isolate infection (Table S3, S6 and S8). Together these results suggest that drought tolerance during chlorosis isolate infection rather results from genes belonging to distinct families than from a single gene or members of one gene family.

Reusche *et al.* (2014) observed a stronger induction of the drought marker gene *RD29B* (Yamaguchi-Shinozaki and Shinozaki, 1993) in *A. thaliana* plants infected with the wilting isolate w-JR2 as compared to the chlorosis isolate c-VL43 during concomitant drought stress. Yet, *RD29B* was not expressed in the watered control *A. thaliana* plants during *Verticillium* challenge (Reusche *et al.*, 2014). Interestingly, *RD29B* as well as the drought and osmotic stress signalling components *SNRK2.9* (*SNF1-RELATED PROTEIN KINASE 2.9*) and *SNRK3.14* (*SNF1-RELATED PROTEIN KINASE 3.14*) (Tripathi *et al.*, 2009; Fujii *et al.*, 2011; Tsou *et al.*, 2012; Chen *et al.*, 2013) were up-regulated in normally watered *N. benthamiana* by wilting isolate infection (Table S2 and S9). This result implies that proliferation of wilting isolates is sufficient to trigger drought stress in *N. benthamiana* without water withdrawal. As described in section 1.4, water stress may potentially result from clogging of water conducting xylem vessels due to pathogen proliferation, formation of vascular gels and tyloses.

4.2 Homozygous T DNA insertion lines as a tool for reverse genetic analyses

Homozygous mutants carrying a T-DNA insertion in the chlorosis induced candidate genes *At5g24080*, *ANAC071* and *RD17* were isolated for analyses of their disease phenotype during *Verticillium* infection. For all three candidate genes, homozygous T-DNA insertion mutants were successfully isolated using PCR-based genotyping. The *rd17* mutant carried a homozygous T-DNA insertion in the *RD17* promoter region. According to a report, in which the effect of T-DNA insertion on transcript and protein abundance in 1084 insertion mutants was assessed, a T-DNA integration in the promoter region rather results in a knock-down than a gene knock-out (Wang, 2008). However, *RD17* transcripts were detectable in the homozygous *rd17* T-DNA insertion mutant and their abundance was not altered as compared to wild-type during *Verticillium* infection as well as in the mock treated control (Fig. 6). Consequently, T-DNA insertion in *RD17* promoter region of the homozygous *rd17* did not result in a gene knock-out or knock-down. According to the T-DNA Express Arabidopsis Gene Mapping Tool (O'Malley *et al.*, 2015), the used *rd17* insertion mutant carries a T-DNA insertion 510 bp upstream of the *RD17* start-codon. A no-effect insertion becomes more probable with increasing distance from the start-codon, from 8 % in the 1-50 bp region and 4 % in the 51-200 bp region to 17 % in the 501-1000 bp region upstream of the start-codon (Wang, 2008). Unfortunately, only promoter T-DNA insertions but no lines, which carry a T-DNA insertion in an exon or intron of the *RD17* gene are available. Considering the high probabilities of a knock-down or a no-effect mutation in promoter T-DNA insertion lines, in future experiments, other methods should be applied in order to obtain an *rd17* knock-out mutant. For instance, the Clustered Regularly Interspaced Short Palindromic Repeat (CRISPR)/CRISPR-associated protein 9 (Cas9) system. In the CRISPR/Cas9 system, a synthetic single guide RNA (sgRNA) directs the Cas9 endonuclease to the gene of interest. Cas9 introduces a double strand break in the gene of interest, which in turn is repaired by the endogenous Non-Homologous End Joining (NHEJ) pathway. Since the DNA-repair by NHEJ is error-prone, insertion or deletion mutations are introduced that may result in gene a knock-out in the gene of interest (Jinek *et al.*, 2012; Bortesi and Fischer, 2015).

Interestingly, a T-DNA insertion in the *ANAC071* promoter (*anac071-2*) resulted in overexpression of the *ANAC071* gene (Fig. 7). The pROK2 T-DNA construct, used for generation of SALK T-DNA insertion lines, contains the unidirectional constitutive Cauliflower Mosaic Virus (CaMV) 35S promoter as well as the Nopaline synthase (Nos) promoter (Baulcombe *et al.*, 1986). However, both promoters are oriented towards the left T-DNA border. In *anac071-2*, the left T-DNA border is directed to the 5' end of the *ANAC071*

promoter (Fig. 7). Thus, the *ANAC071* gene is located upstream of the unidirectional CaMV 35S and Nos promoters, which should then not drive its expression. Nevertheless, Xie *et al.* (2001) demonstrated that a unidirectional promoter can turn into a bidirectional promoter, if it is located next to a TATA-box cis-acting element (Xie *et al.*, 2001). Since the Nos promoter is located directly at the right border of the pROK2 T-DNA construct, it most likely drives the constitutive expression of the *ANAC071* gene in the *anac071-2* mutant.

In the *at5g24080-1* (SALK_086625) and *at5g24080-3* (SAIL_551_D12) T-DNA insertion mutants, residual 3' transcripts were observed (Fig. 14). The Nos promoter may also be responsible for residual 3' transcripts in *at5g24080-1*, which as *anac071-2* represents a SALK line and has the same T-DNA orientation. SAIL T-DNA insertion lines contain either the pCSA110 or pDAP101 construct (McElver *et al.*, 2001). Both constructs contain a bidirectional promoter at the left T-DNA border, which drives the expression of the BASTA[®] resistance gene *Phosphinothricin acetyltransferase (Pat)*. As in case of *anac071-2* and *at5g24080-1*, the left T-DNA border in *at5g24080-3* is directed to the 5' end of the *At5g24080* gene (Fig. 14). Thus, several genes encoded by the T-DNA are located downstream of the bidirectional promoter. However, read-through leading to transcription of T-DNA flanking genomic sequences has been reported (Ulker *et al.*, 2008). Indeed, in *at5g24080-3* transcripts consisting of the 3'-*At5g24080* region and a part of the T-DNA construct were detected, indicating potential read-through (Fig. 14C).

4.3 G-type LecRLK *At5g24080* is inducible by chlorosis isolate infection and abscisic acid

NbS00002660g0010, a *N. benthamiana* gene, which is homologous to *A. thaliana* G-type LecRLK gene *At5g24080* was identified to be highly and significantly induced by *V. dahliae* chlorosis isolate infection in the RNA-sequencing analysis at 8 and 12 dpi as well as in the collective analysis of 8, 12 and 16 dpi (Table S3, S4 and S8). Semi-quantitative RT-PCR and qPCR analyses confirmed that *At5g24080* was induced by *V. longisporum* and *V. dahliae* chlorosis isolates but not by a wilting isolate in *Arabidopsis* (Fig. 4 and Fig. 5). Despite the strong induction of its expression by chlorosis isolate infection, *At5g24080* does not appear to play a role in *A. thaliana* – *Verticillium* interaction. Neither disease symptoms nor symptom severity were altered on the three tested *at5g24080* mutants during *Verticillium* infection as compared to wild-type and all mutants showed wild-type like bundle sheath cell transdifferentiation (Fig. 15 and 16). *At5g24080* expression was inducible by abscisic acid

(ABA) (Fig. 22 and 23) and ABA levels were strongly increased in *A. thaliana* during chlorosis isolate infection as compared to mock treatment or wilting isolate challenge (Fig. 34 and S21A). These results suggest that *At5g24080* gene induction may be a side-effect of the strong increase in ABA levels and not directly be triggered by *Verticillium* chlorosis isolate infection. However, *At5g24080* induction was not completely abolished during chlorosis isolate infection in the *aba1-101* ABA biosynthesis mutant background (Fig. 29). Thus, *At5g24080* induction may not only be a side-effect of increased ABA levels, but also represent a response to chlorosis isolate infection. The trend to increased susceptibility of the *at5g24080* mutants to the compatible *H. arabidopsidis* isolate NOCO2 (Fig. 19) supports its putative role in immune responses to pathogen challenge. *Verticillium* may suppress immune responses that require *At5g24080*. This would explain the wild-type like disease phenotype of *at5g24080* mutants during *Verticillium* chlorosis isolate infection. Because of its putative role in immunity, AT5G24080 was further characterised.

In Confocal Laser Scanning Microscopy (CLSM) analyses, AT5G24080-Venus fusion protein accumulated at the cell periphery of pavement cells as well as guard cells in *A. thaliana* leaf epidermis 4 h after 50 μ M ABA treatment but was not detectable in mock treated plants (Fig. 25). A similar subcellular localisation was observed without ABA treatment in stable transgenic lines overexpressing AT5G24080-Venus under the control of the 35S promoter (Fig. 28), indicating that AT5G24080 subcellular localisation is not altered by ABA treatment. Plasmolysis experiments suggested that AT5G24080-Venus localises to the plasma membrane (Fig. 28C). The observed plasma membrane localisation is in accordance with a predicted transmembrane domain and N-terminal signal peptide in AT5G24080 (Fig. 10). A strong Venus signal was detectable in stomatal guard cells of 50 μ M ABA treated stable transgenic lines expressing AT5G24080-Venus under the control of its native promoter as well as in untreated overexpressor lines (Fig. 25 and 28). Publically available microarray data, in which gene expression in *A. thaliana* guard cells was analysed, support these findings. In the microarray experiment conducted by Yang *et al.* (2008), gene expression was assessed in guard cells as compared to mesophyll cells after 100 μ M ABA treatment as well as without treatment. *At5g24080* expression was 4 fold increased in the mesophyll cell layer after 100 μ M ABA treatment, whereas a 22 fold increase in gene expression was observed in guard cells. Moreover, *At5g24080* expression in guard cells was higher after ABA treatment as compared to the mesophyll cell layer (Yang *et al.*, 2008). A microarray analysis, in which gene expression in guard cells was compared to gene expression in the entire leaf, further supports guard cell specific expression of *At5g24080* after ABA treatment. In this microarray experiment,

At5g24080 was identified among candidates significantly regulated in guard cells by ABA treatment but not in the entire leaf (Pandey *et al.*, 2010). ABA has been proposed as a major regulator of stomatal movements by mediating ion fluxes and thus the turgor in stomatal guard cells (Schroeder and Hagiwara, 1990; Grabov *et al.*, 1997; Pei *et al.*, 1997; MacRobbie, 1998; Kim *et al.*, 2010). The strong increase in *At5g24080* transcript levels as well as AT5G24080 protein abundance in stomatal guard cells in response to ABA, as shown by publically available microarray data and this thesis, may point to a potential role of *At5g24080* in stomatal movements. In order to address this question, stomatal apertures of *at5g24080* mutants may be analysed in the future. ABA treatments of *at5g24080* mutants may be performed to investigate putative roles of the G-type RLK *At5g24080* in ABA induced stomatal closure. Eisele *et al.* (2016) recently described a rapid and simple CLSM based protocol for measurement of stomatal movements in response to various stimuli, including ABA, which can be used for this purpose (Eisele *et al.*, 2016). Stomatal apertures are reduced in *V. longisporum* inoculated *A. thaliana* as compared to mock treatment (Roos *et al.*, 2014). Stomatal apertures of *Verticillium* infected *at5g24080* mutant plants may be analysed, to assess the requirement of *At5g24080* in *Verticillium* induced stomatal closure.

In unchallenged *A. thaliana* roots, *At5g24080* is strongly expressed in the procambium but not other cell types according to publically available microarray data (Arabidopsis eFP Browser, Winter *et al.*, 2007). CLSM analyses, conducted in this study, did not support these findings. The procambium is localised to the central cylinder and steadily produces xylem and phloem tissues (Miyashima *et al.*, 2013). AT5G24080-Venus was neither detectable in the central cylinder of stable transgenic *A. thaliana* after ABA application nor in the mock treated control. Only a fluorescence signal emitting light within the wavelength of the Venus fluorophore was observed. This signal likely represented autofluorescence, as it was also detectable in the root of the wild-type control (Fig. 26, left panel and S17). The cell type specific root expression data deposited at the Arabidopsis eFP Browser is derived from a microarray study, in which 19 GFP marker lines for specific root cell types were protoplasted and GFP expressing cell types isolated by Fluorescence Activated Cell Sorting (FACS) (Brady *et al.*, 2007; Winter *et al.*, 2007; Cartwright *et al.*, 2009). However, gene expression in the procambium cell type was not analysed directly, due to lack of the respective marker line. Instead, expression data of other cell types was used to computationally infer gene expression in the procambium cell type (Brady *et al.*, 2007; Cartwright *et al.*, 2009). On the one hand, it is possible that computationally estimated *At5g24080* expression data in the procambium does not correlate with actual gene expression. On the other hand, *At5g24080* expression in this cell type and thus

AT5G24080-Venus protein levels may be below the CLSM detection limit. In order to assess, whether *At5g24080* is expressed in *A. thaliana* root procambium, *At5g24080* promoter- β -Glucuronidase fusions may be used in future experiments. β -Glucuronidase (GUS) represents an excellent reporter for low and moderately expressed genes, due to its sensitivity and long lasting activity (Jefferson *et al.*, 1987).

Interestingly, strong AT5G24080-Venus accumulation was observed in epidermal cells of newly emerged lateral roots after 50 μ M ABA application but not in mock treated plants (Fig. 26, right panel). Rapid growth of the lateral root requires expansin mediated cell wall loosening and extension of the cell by turgor pressure (Shcherban *et al.*, 1995; Vilches-Barro and Maizel, 2015; Somssich *et al.*, 2016). It is conceivable that the rapidly elongating cells of the lateral root are more permeable to ABA than cells of the differentiated root. The high ABA levels may in turn lead to the observed strong accumulation of AT5G24080. In contrast to the leaf epidermis, AT5G24080-Venus localised to the cell periphery but also to the nuclear envelope of root epidermis cells (Fig. 26, right panel). The nuclear envelope forms a continuum with the endoplasmic reticulum (ER) and fluorescent protein fusions targeted to the ER label the nuclear envelope (NE) (Nelson *et al.*, 2007; Hetzer, 2010). Partial localisation of fusion proteins to the ER often represents an overexpression artefact (Moore and Murphy, 2009). It is conceivable that the strong AT5G24080-Venus expression in root epidermal cells gave rise to an ER localisation of the fusion protein. In addition to labelling of the NE, an ER signal can be visualised in CLSM as a reticular network by setting the focal plane to the cortical cytoplasm directly under the plasma membrane (Nelson *et al.*, 2007; Liu *et al.*, 2012). However, it cannot be seen when the focal plane is set to the centre of the cell, as in Fig. 26, due to the large size of the central vacuole of fully expanded cells (Liu *et al.*, 2012). In future experiments subcellular localisation of AT5G24080-Venus in root epidermis cells after ABA treatment should be analysed in more detail, to confirm presence of the fusion protein in the ER. Moreover, the *promAt5g24080::At5g24080::Venus* construct may be transformed into an *A. thaliana* ER marker line and co-localisation studies may be performed. Treatments of *A. thaliana* seedlings with lower concentrations of ABA may lead to weaker AT5G24080-Venus expression and answer the question whether the assumed ER localisation in root epidermal cells results from overexpression of the fusion protein.

Although *At5g24080* expression was highly induced by chlorosis isolate infection, AT5G24080-Venus was not detectable in roots of stable transgenic plants during *V. longisporum* chlorosis isolate c-VL43 infection (Fig. S18). Most likely, *At5g24080* is rather induced at late stages of infection and not up-regulated during colonisation of the root. This

assumption is supported by results of the RNA-sequencing in which *At5g24080* expression was only increased by 1.6 log₂ fold at 4 days post infection of *A. thaliana* roots with chlorosis inducing *V. dahliae* isolates as compared to mock treatment (Table 2). In addition, semi-quantitative RT-PCR and qPCR demonstrated that *At5g24080* is most strongly up-regulated by chlorosis isolates in *A. thaliana* rosettes during late stages of infection at 21 and 28 dpi (Fig. 5).

For CLSM analyses AT5G24080 was fused to the Venus monomeric fluorescent protein, which provides higher fluorescence intensity as compared to other commonly used fluorescent proteins such as EGFP or EYFP (Nagai *et al.*, 2002; Chudakov *et al.*, 2010). Nevertheless, in three out of six analysed stable transgenic T₂ lines expressing *At5g24080::Venus* under the control of its native promoter, weak fluorescence was observed. qPCR and immunoblot analyses demonstrated that stable transgenic lines, which showed weak Venus fluorescence signal, also show low *At5g24080* gene induction and low AT5G24080-Venus protein levels in immunoblot analyses after ABA application (line #3 in Fig. S15B and 24A as well as lines #1 and #2 in Fig. S16B and 24B). Conversely, stable transgenic lines, which showed strong Venus fluorescence after ABA application, also demonstrated strong *At5g24080* induction and high AT5G24080-Venus protein levels in qPCR and immunoblot analyses. As a consequence, the lack or weak Venus fluorescence in line #3 as well as line #1 and #2 most likely results from weak induction of the *At5g24080::Venus* transgene and thus resulting low AT5G24080-Venus protein levels.

4.4 Abscisic acid is likely required for chlorosis and early senescence symptom development

Abscisic acid (ABA) represents one of the classical phytohormones, which has been associated with leaf senescence and leaf abscission. ABA accumulates in senescing tissues, induces expression of senescence-associated genes and promotes leaf senescence when exogenously applied (Gepstein and Thimann, 1980; Léon-Kloosterziel *et al.*, 1996; He *et al.*, 2005; Breeze *et al.*, 2011; Lee *et al.*, 2011). Results of this study suggest a pivotal role of ABA in chlorosis as well as early senescence symptom development on *A. thaliana*, because ABA levels are strongly increased during *Verticillium* chlorosis isolate infection but not during wilting isolate challenge (Fig. 34 and S21A). Additionally, chlorosis and early senescence symptoms typically detectable on Col-0 wild-type 21 days post infection with chlorosis inducing isolate c-V76 are absent on the *aba1-101* ABA biosynthesis mutant (Fig. 30, 31 and S19). Interestingly, Reusche

et al. (2013) proposed that reduced levels of the phytohormone cytokinin are responsible for induction of chlorosis and early senescence symptoms by the *V. longisporum* chlorosis isolate c-VL43. Levels of the adenine-type cytokinin trans-zeatin are significantly reduced in c-VL43 infected plants as compared to the mock control. *Verticillium* induced reduction in trans-zeatin levels is accompanied by enhanced expression of cytokinin oxidase/dehydrogenase (*CKX*) genes *CKX1*, *CKX2* and *CKX3*, suggesting that cytokinin is degraded. Pharmacological treatments with *CKX* inhibitors and expression of the cytokinin biosynthesis gene *IPT* (*ISOPENTENYL TRANSFERASE*) from *Agrobacterium tumefaciens* under the control of a senescence responsive promoter lead to a reduction of chlorosis and early senescence symptoms (Reusche *et al.*, 2013). Cytokinin signalling interacts with ABA signalling pathways (O'Brien and Benková, 2013). In several processes, cytokinins act as ABA antagonists. For instance, cytokinin counteracts ABA induced stomatal closure (Das *et al.*, 1976; Tanaka *et al.*, 2006). During drought stress, cytokinin amounts decline, whereas ABA levels increase (Hansen and Dörffling, 2003; Davies *et al.*, 2005). A further study demonstrated that the adenine-type cytokinins zeatin, 2-isopentenyladenine or adenine stimulate ABA degradation to phaseic acid, which further supports the occurrence of cytokinin-ABA crosstalk in plants (Cowan *et al.*, 1999). In plant-microbe interactions, cytokinin and ABA also counteract. ABA was shown to impair cytokinin-induced resistance of tobacco to *Pseudomonas syringae*. Cytokinin treatment reduces ABA levels in tobacco and enhances resistance, whereas exogenous application of ABA or inhibition of ABA degradation leads to enhanced *P. syringae* proliferation (Großkinsky *et al.*, 2014). Results of this thesis and findings of Reusche *et al.* (2013) indicate that cytokinin-ABA antagonism plays a role in the *A. thaliana* – *Verticillium* chlorosis isolate interaction. Degradation of cytokinin by *CKX1*, *CKX2* and *CKX3* likely leads to an increase in ABA levels and in turn triggers chlorosis and early senescence symptoms. Stabilisation of the cytokinin pool by *CKX* inhibitor treatments or *IPT* expression may lead to a decrease in endogenous ABA and thus results in milder chlorosis and early senescence symptoms.

Interestingly, in the RNA-sequencing analysis of *Verticillium* infected *N. benthamiana*, ABA responsive genes were found among chlorosis specific as well as wilting specific candidates. Among genes specifically induced by wilting isolate infection, *N. benthamiana* homologs of *Arabidopsis* ABA responsive homeodomain-leucine zipper transcriptional factor *ATHB-7* (*ARABIDOPSIS THALIANA HOMEODOMAIN-LEUCINE ZIPPER TRANSCRIPTIONAL FACTOR 7*), protein phosphatase 2C *HAI3* (*HIGHLY ABA-INDUCED PP2C GENE 3*), and dehydrin *RD29B* (*RESPONSIVE TO DESICCATION 29B*) were identified (Table S5, S7 and S9) (Yamaguchi-Shinozaki and Shinozaki, 1993; Söderman *et al.*, 1996; Fujita *et al.*, 2009). On the other hand, *N. benthamiana* homologs of

Arabidopsis At5g24080, *MYB102* and *MYB41* constituted ABA responsive genes among candidates specifically induced by chlorosis isolate infection. Considering the strong increase of ABA levels in chlorosis isolate challenged *A. thaliana* Col-0 as compared to wilting isolate infection (Fig. 34 and S21A), one would expect a larger number of ABA responsive genes to be differentially regulated by chlorosis isolate infection in the RNA-sequencing analysis. In addition, classical ABA marker genes, such as *RD29B* should not be present among wilting specific candidates. It is likely that ABA levels differ between *A. thaliana* and *N. benthamiana* during *Verticillium* infection. This assumption may be tested by measurements of ABA levels in *N. benthamiana* during *Verticillium* chlorosis and wilting isolate infection.

ABA levels were significantly increased in *A. thaliana* during wilting isolate w-JR2 infection at 21 and 28 dpi as compared to mock. However, ABA induction was minor when compared to chlorosis isolate challenged *A. thaliana* (Fig. 34 and S21A). Besides wilting, decay of older rosette leaves can be observed at late stages of *A. thaliana* infection with wilting isolates. It is possible that ABA, detected in wilting isolate infected plants, is derived from these senescing leaves.

Chlorosis and early senescence symptoms caused by *V. dahliae* on *A. thaliana* Col-0 correlate with defoliation symptoms on cotton (*Gossypium spec.*) and olive (*Olea europaea*) plants (K. Thole, PhD thesis, 2016). Originally, *V. dahliae* infection was typically associated with wilting symptoms (Fradin and Thomma, 2006; Klosterman *et al.*, 2009). The five *V. dahliae* isolates c-V76, c-V138I, c-T9, c-V781I and c-ST100, which have been shown to induce chlorosis and early senescence on *A. thaliana* trigger defoliation symptoms on cotton or olive. To the contrary, wilting inducing *V. dahliae* isolates w-V192I and w-V200I, which were initially isolated from cotton do not cause defoliation symptoms (K. Thole, PhD thesis, 2016). For a long time, ABA has been known to be implicated in petiole abscission in cotton (Ohkuma *et al.*, 1963; Cracker and Abeles, 1969). Moreover, ABA amounts were shown to increase by two fold in defoliating isolate T9 infected cotton leaves, but were not altered by non-defoliating isolate SS4 of *V. albo-atrum* (Wiese and Devay, 1970). Most interesting, ABA levels were increased at 5 to 7 days post inoculation, when symptoms were most pronounced and leaf abscission was imminent, suggesting that ABA plays a role in cotton defoliation (Wiese and Devay, 1970). The *A. thaliana* ABA biosynthesis mutant *aba1-101* did not show chlorosis or early senescence symptoms at 21 dpi during *V. dahliae* chlorosis isolate infection (Fig. 30, 31 and S19). It would be tempting to test whether defoliation is impaired in transgenic cotton defective in ABA biosynthesis during infection with chlorosis inducing/defoliating *V. dahliae* isolates c-V76, c-V138I, c-T9, c-V781I and c-ST100. This may further support the hypothesis

that chlorosis as well as early senescence in *Arabidopsis* correlates with defoliation in cotton and further support the role of ABA in these processes.

It was postulated that the chlorosis and wilting disease phenotypes are triggered by lineage-specific *Verticillium* effector molecules which induce distinct transcriptional and developmental reprogramming patterns of the host plant (K. Thole, PhD thesis, 2016). RNA-sequencing analysis performed in this study supports the assumption that transcriptional reprogramming of the host is responsible for development of chlorosis and wilting disease phenotypes. Several host genes, which can be related to the distinct disease phenotypes, were differentially regulated by *Verticillium* chlorosis or wilting isolate infection. ABA levels are also differentially regulated by *Verticillium* isolates of the distinct interaction classes. Infection with chlorosis isolates, which induce chlorosis and early senescence on *Arabidopsis* and defoliation on cotton trigger an increase in ABA levels in both plant species. In contrast, wilting/ non-defoliating isolates do not trigger ABA induction in cotton and only minor increase in ABA levels in *Arabidopsis* (Fig. 34 and S21A, Wiese and Devay, 1970). Since ABA induction is triggered by isolates of the same interaction class in these distinct plant species, it most likely represents a response to putative lineage-specific effectors encoded by *Verticillium* isolates of the distinct interaction classes. It can be excluded that the increase in ABA levels during chlorosis isolate infection results from a *Verticillium* derived ABA biosynthesis pathway. If this were the case, chlorosis isolate infection would complement the phenotype of the *aba1-101* ABA biosynthesis mutant.

Besides chlorosis and early senescence symptoms, chlorosis-inducing *Verticillium* isolates trigger *de novo* xylem formation, characterised by transdifferentiation of chloroplast containing bundle sheath cells into functional xylem elements and xylem hyperplasia in vascular bundles (Reusche *et al.*, 2012; K. Thole, PhD Thesis, 2016). Chlorosis and early senescence symptoms were absent on the *aba1-101* mutant at 21 days after chlorosis isolate c-V76 infection (Fig. 30, 31 and S19). In contrast, bundle sheath cell transdifferentiation was observed after infection with this chlorosis-inducing isolate (Fig. 32E). These results imply that development of chlorosis and early senescence symptoms depends on functional ABA biosynthesis, whereas *de novo* xylem formation is not ABA independent. Therefore, *de novo* xylem formation and development of chlorosis as well as early senescence symptoms likely represent uncoupled processes. However, amounts of *de novo* formed xylem may be reduced in the *aba1-101* mutant. In future experiments, number of transdifferentiated bundle sheath cells and hyperplastic xylem should be quantified. This may further support the hypothesis, that ABA is not implicated in *de novo* xylem formation.

4.5 Abscisic acid likely represents a susceptibility factor in the *A. thaliana* – *Verticillium* chlorosis isolate interaction

Besides its role in plant development and abiotic stress responses, ABA acts as a positive or negative regulator of defence dependent on the plant-pathogen interaction system (Ton *et al.*, 2009; Robert-Seilaniantz *et al.*, 2011; Denancé *et al.*, 2013). In the past, several reverse genetic analyses of *Arabidopsis* mutants defective in ABA signalling components or biosynthesis genes revealed the role of ABA as a susceptibility factor to bacterial, oomycete and fungal pathogens such as *Pseudomonas syringae*, *Hyaloperonospora parasitica*, *Fusarium oxysporum*, and *Plectosphaerella cucumerina* (Mohr and Cahill, 2003; Anderson *et al.*, 2004; de Torres-Zabala *et al.*, 2007; Trusov *et al.*, 2009; García-Andrade *et al.*, 2011; Sánchez-Vallet *et al.*, 2012; Denancé *et al.*, 2013). Results of this PhD thesis indicate that ABA also represents a susceptibility factor in *A. thaliana* – *Verticillium* chlorosis isolate interaction. HPLC-MS/MS analyses demonstrated that ABA levels are strongly increased in *A. thaliana* Col-0 during *Verticillium* chlorosis isolate infection compared to mock treatment or wilting isolate challenge (Fig. 34 and S21A). Furthermore, chlorosis isolate c-V76 induced stunting as well as c-V76 proliferation were diminished in the ABA biosynthesis mutant *aba1-101* compared to wild-type (Fig. 30B and 33).

A recent study conducted by Behrens *et al.* (Abstract book - Botanikertagung 2017) corroborates the role of ABA as a susceptibility factor in the *A. thaliana* - *Verticillium* interaction. Consistent with results of this PhD thesis, Behrens *et al.* (2017) observed elevated ABA amounts in *Arabidopsis* roots and leaves challenged with *Verticillium longisporum*. Moreover, a delay in symptom development and enhanced expression of the pathogenesis related gene *PR1* during *V. longisporum* infection was detected in a mutant defective in the ABA biosynthesis enzyme 9-cis-epoxycarotenoid dioxygenase (*NCED*) as compared to wild-type (Behrens *et al.*, Abstract book - Botanikertagung 2017). ABA acts as a suppressor of SA mediated defence responses (Yasuda *et al.*, 2008; de Torres Zabala *et al.*, 2009; Jiang *et al.*, 2010). Enhanced expression of the SA marker gene *PR1* in the ABA biosynthesis mutant background may be a consequence of a de-repressed SA signalling.

ABA treatment promotes disease susceptibility of *A. thaliana* to the soil-borne fungus *Fusarium oxysporum*, which similar to *Verticillium* proliferates within the plant's vasculature and induces chlorosis as well as necrosis symptoms on infected plants (Trusov *et al.*, 2009). Analysis of *A. thaliana* *aba1-6* and *aba2-1* mutants defective in the ABA biosynthesis genes ABA1 or ABA2 respectively support results of the pharmacological treatment. Both ABA biosynthesis mutants are more resistant to *F. oxysporum* infection as indicated by reduced

disease symptoms of infected plants (Anderson *et al.*, 2004; Trusov *et al.*, 2009). Anderson *et al.* (2004) proposed that enhanced resistance of ABA biosynthesis mutants to *F. oxysporum*, results from a de-repression of the JA-ethylene dependent defence responses, since expression of defence related genes within the JA-ethylene signalling pathway is elevated in the ABA biosynthesis mutant background (Anderson *et al.*, 2004). JA-ethylene signalling is likely required for defence responses against *Verticillium*, as ethylene insensitive *Arabidopsis* mutants *ein2-1*, *ein4-1* and *ein6-1* are more susceptible to *V. longisporum* infection compared to wild-type (Johansson *et al.*, 2006). In future experiments expression of defence related genes within the JA-ethylene signalling pathway should be analysed in the *aba1-101* mutant background during *Verticillium* challenge. This may answer the question, whether enhanced resistance of *aba1-101* results from up-regulation of JA-ethylene dependent defence responses. Cytokinins act as ABA antagonists in several processes (Das *et al.*, 1976; Tanaka *et al.*, 2006; Großkinsky *et al.*, 2014). In the *A. thaliana* – *Verticillium* chlorosis isolate interaction, endogenous cytokinin is degraded, whereas ABA levels increase during infection. Furthermore, stabilisation of cytokinin levels or abolishment of the ABA biosynthesis result in a reduced fungal growth of chlorosis-inducing *Verticillium* isolates (Reusche *et al.*, 2013; this thesis). These findings suggest that cytokinin-ABA antagonism also influences susceptibility of *A. thaliana* to *Verticillium* chlorosis isolate infection.

4.6 Outlook

The aim of this thesis was to identify differentially expressed host genes that in response to putative lineage-specific *Verticillium* effector molecules trigger transcriptional reprogramming leading to the establishment of the chlorosis disease phenotype. These chlorosis isolate induced host candidate genes were defined as being exclusively regulated during *Verticillium* chlorosis isolate infection but not by wilting isolate challenge and mock treatment. However, the RNA-sequencing analysis conducted in this study additionally allowed identification of *A. thaliana* and *N. benthamiana* genes, which are equally implicated in disease response to both chlorosis and wilting isolates. In the future, candidate genes, which are significantly regulated by chlorosis and wilting isolate infection as compared to mock treatment, may be isolated. These candidates may bear putative receptors and components of signalling cascades required for *Verticillium* perception as well as defence related genes and putative susceptibility factors. Moreover, genes down-regulated in response to both chlorosis and wilting isolates may represent potential targets of *Verticillium* effector activity. This approach has a major advantage

compared to microarray and RNA-sequencing experiments in which transcriptional reprogramming of the host is assessed in response to a single *Verticillium* isolate of one interaction class. Use of isolates belonging to the chlorosis and wilting interaction class allows subtraction of genes required for establishment of distinct disease symptoms and identification of a core gene set involved in disease response to isolates of both interaction classes.

Due to a limited time span of a PhD thesis, out of the large number of candidate genes significantly regulated by chlorosis or wilting isolate infection only three chlorosis isolate induced candidates were analysed in detail. In future experiments, role of further candidate genes in establishment of the chlorosis or wilting disease phenotype may be analysed by means of reverse genetics. If no T-DNA insertion lines are available, knock-out mutants will be generated using targeted mutagenesis techniques, such as CRISPR/Cas9. In the RNA-sequencing analysis, many candidate genes differentially regulated at 8, 12 and 16 dpi in *N. benthamiana* shoots were discarded, since they did not have any *A. thaliana* homologs. In the future, RNA-sequencing analysis during late stages of infection may be repeated in *A. thaliana*. Analysis of *A. thaliana* transcriptome may provide additional candidate genes and allow to compare transcriptome of the solanaceous plant *N. benthamiana* and the *Brassicaceae* *A. thaliana* in response to *Verticillium* infection.

A *N. benthamiana* homolog of the G-type LecRLK *At5g24080* was identified to be significantly induced during chlorosis isolate infection in the RNA-sequencing analysis and confirmed to be highly up-regulated by chlorosis isolates in *A. thaliana*. However, reverse genetic analyses of *at5g24080* T-DNA insertion mutants did not provide evidence for a role of *At5g24080* during *Verticillium* chlorosis isolate infection. Once T₃ stable transgenic lines expressing *At5g24080* under the control of the strong constitutive 35S promoter are available, these lines may be used to analyse the potential function of *At5g24080* in overexpression studies. Furthermore, effect of *At5g24080* overexpression may be analysed in unchallenged plants or during *Verticillium* wilting isolate infection.

The ABA biosynthesis mutant *aba1-101* demonstrated wilting-like disease symptoms at 21 dpi during *Verticillium* chlorosis isolate infection and absence of leaf chlorosis as well as early senescence, indicating that functional abscisic acid biosynthesis is required for establishment of chlorosis and early senescence symptoms. Chlorosis and early senescence symptoms caused by *V. dahliae* on *A. thaliana* correlate with defoliation symptoms on cotton and olive plants. ABA stimulates leaf abscission in cotton and ABA levels in cotton increase during infection with a defoliating *Verticillium* isolate but not a non-defoliating isolate, implying that this phytohormone plays a role in cotton defoliation (Wiese and Devay, 1970; Mishra *et al.*, 2008).

In future experiments, it may be tested whether defoliation is impaired in transgenic cotton defective in ABA biosynthesis during infection with chlorosis inducing/defoliating *V. dahliae* isolates. Knock-down or knock-out cotton mutants defective in ABA biosynthesis may be generated using RNA interference or CRISPR/Cas9 targeted mutagenesis. Both techniques were successfully applied in cotton (Abdurakhmonov *et al.*, 2016; Gao *et al.*, 2017). This may further support the role of ABA in chlorosis symptom development in *A. thaliana* and defoliation in cotton.

In *N. benthamiana*, both *V. dahliae* chlorosis and wilting isolate infection induced expression of ABA responsive genes. Thus, it is conceivable that ABA levels differ between *A. thaliana* and *N. benthamiana* during *Verticillium* infection. Measurements of ABA content in *N. benthamiana* during chlorosis and wilting isolate infection may be performed, in order to assess whether ABA marker gene induction observed in RNA-sequencing analysis of wilting isolate infected *N. benthamiana* correlate with an increase in ABA levels.

ABA content was strongly increased in *A. thaliana* during chlorosis-inducing isolate infection as compared to wilting isolate challenge or mock treatment. However, in this thesis, average ABA levels in whole *A. thaliana* rosettes were measured by HPLC-MS/MS. In the future, *Verticillium*-induced alterations in ABA levels may be analysed at the cellular level with a hormone responsive fluorescent protein reporter system. H. Ghareeb recently developed such an ABA biosensor consisting of a fluorescent protein encoding reporter gene, expression of which is driven by a hormone responsive promoter (H. Ghareeb, personal communication). Upon alteration of cellular hormone levels, amounts of the fluorescent protein change accordingly and fluorescence intensity can be quantified by confocal laser scanning microscopy. Additionally to the ABA biosensor, a salicylic acid, jasmonate/ethylene and cytokinin biosensors are available in stable transgenic *A. thaliana* lines (H. Ghareeb, personal communication). By crossing these *A. thaliana* lines, crosstalk between hormones may be analysed during *Verticillium* infection at the cellular level.

5. References

- Aarts, N., Metz, M., Holub, E., Staskawicz, B.J., Daniels, M.J. and Parker, J.E.** (1998) Different requirements for EDS1 and NDR1 by disease resistance genes define at least two R gene-mediated signaling pathways in Arabidopsis. *Proc. Natl. Acad. Sci. U. S. A.*, **95**, 10306–10311.
- Abdurakhmonov, I.Y., Ayubov, M.S., Ubaydullaeva, K.A., et al.** (2016) RNA Interference for Functional Genomics and Improvement of Cotton (*Gossypium* sp.). *Front. Plant Sci.*, **7**.
- Albert, I., Böhm, H., Albert, M., et al.** (2015) An RLP23-SOBIR1-BAK1 complex mediates NLP-triggered immunity. *Nat. Plants*, **1**, 15140.
- Anders, S. and Huber, W.** (2010) Differential expression analysis for sequence count data. *Genome Biol.*, **11**, R106.
- Anderson, J.P., Badruzaufari, E., Schenk, P.M., Manners, J.M., Desmond, O.J., Ehlert, C., Maclean, D.J., Ebert, P.R. and Kazan, K.** (2004) Antagonistic interaction between abscisic acid and jasmonate-ethylene signaling pathways modulates defense gene expression and disease resistance in Arabidopsis. *Plant Cell*, **16**, 3460–3479.
- Antony, G., Zhou, J., Huang, S., Li, T., Liu, B., White, F. and Yang, B.** (2010) Rice xa13 recessive resistance to bacterial blight is defeated by induction of the disease susceptibility gene Os-11N3. *Plant Cell*, **22**, 3864–3876.
- Aoki, Y., Okamura, Y., Tadaka, S., Kinoshita, K. and Obayashi, T.** (2016) ATTED-II in 2016: A Plant Coexpression Database Towards Lineage-Specific Coexpression. *Plant Cell Physiol.*, **57**, e5.
- Argueso, C.T., Ferreira, F.J., Epple, P., To, J.P.C., Hutchison, C.E., Schaller, G.E., Dangl, J.L. and Kieber, J.J.** (2012) Two-component elements mediate interactions between cytokinin and salicylic acid in plant immunity. *PLoS Genet.*, **8**, e1002448.
- Asahina, M., Azuma, K., Pitaksaringkarn, W., et al.** (2011) Spatially selective hormonal control of RAP2.6L and ANAC071 transcription factors involved in tissue reunion in Arabidopsis. *Proc. Natl. Acad. Sci. U. S. A.*, **108**, 16128–16132.
- Auer, P.L. and Doerge, R.W.** (2010) Statistical design and analysis of RNA sequencing data. *Genetics*, **185**, 405–416.
- Ausubel, F.M.** (2005) Are innate immune signaling pathways in plants and animals conserved? *Nat. Immunol.*, **6**, 973–979.
- Axtell, M.J. and Staskawicz, B.J.** (2003) Initiation of RPS2-specified disease resistance in Arabidopsis is coupled to the AvrRpt2-directed elimination of RIN4. *Cell*, **112**, 369–377.
- Baayen, R.P.** (1986) Regeneration of vascular tissues in relation to Fusarium wilt resistance of carnation. *Neth. J. Plant Pathol.*, **92**, 273–285.
- Barash, I. and Manulis-Sasson, S.** (2007) Virulence mechanisms and host specificity of gall-forming *Pantoea* agglomerans. *Trends Microbiol.*, **15**, 538–545.
- Bari, R. and Jones, J.D.G.** (2009) Role of plant hormones in plant defence responses. *Plant Mol. Biol.*, **69**, 473–488.
- Barrero, J.M., Piqueras, P., González-Guzmán, M., Serrano, R., Rodríguez, P.L., Ponce, M.R. and Micol, J.L.** (2005) A mutational analysis of the ABA1 gene of Arabidopsis thaliana highlights the involvement of ABA in vegetative development. *J. Exp. Bot.*, **56**, 2071–2083.
- Bartsch, M., Gobatto, E., Bednarek, P., Debey, S., Schultze, J.L., Bautor, J. and Parker, J.E.** (2006) Salicylic acid-independent ENHANCED DISEASE SUSCEPTIBILITY1 signaling in Arabidopsis immunity and cell death is regulated by the monooxygenase FMO1 and the Nudix hydrolase NUDT7. *Plant Cell*, **18**, 1038–1051.
- Baulcombe, D.C., Saunders, G.R., Bevan, M.W., Mayo, M.A. and Harrison, B.D.** (1986) Expression of biologically active viral satellite RNA from the nuclear genome of transformed plants. *Nature*, **321**, 446–449.
- Bednarek, P.** (2012a) Chemical warfare or modulators of defence responses - the function of secondary metabolites in plant immunity. *Curr. Opin. Plant Biol.*, **15**, 407–414.
- Bednarek, P.** (2012b) Sulfur-containing secondary metabolites from Arabidopsis thaliana and other Brassicaceae with function in plant immunity. *Chembiochem Eur. J. Chem. Biol.*, **13**, 1846–1859.

- Behrens, F., Schenke, D., Hossain, R., Häder, C., Zhao, Y., Zhu, W., Cai, D.** Suppression of ABA-biosynthesis at the early infection stage impairs the infection process of *Verticillium longisporum* in oilseed rape (*Brassica napus*) [abstract]. In: Abstract band Botanikertagung 2017; 2017 September 17 – 21; Kiel, Germany. Page 51.
- Bellande, K., Bono, J.-J., Savelli, B., Jamet, E. and Canut, H.** (2017) Plant Lectins and Lectin Receptor-Like Kinases: How Do They Sense the Outside? *Int. J. Mol. Sci.*, **18**.
- Benhamou, N.** (1995) Ultrastructural and cytochemical aspects of the response of eggplant parenchyma cells in direct contact with *Verticillium*-infected xylem vessels. *Physiol. Mol. Plant Pathol.*, **46**, 321–338.
- Benjamini, Y. and Hochberg, Y.** (1995) Controlling the False Discovery Rate: A Practical and Powerful Approach to Multiple Testing. *J. R. Stat. Soc. Ser. B Methodol.*, **57**, 289–300.
- Berardini, T.Z., Reiser, L., Li, D., Mezheritsky, Y., Muller, R., Strait, E. and Huala, E.** (2015) The Arabidopsis information resource: Making and mining the “gold standard” annotated reference plant genome. *Genes. N. Y. N 2000*, **53**, 474–485.
- Bishop, C.D. and Cooper, R.M.** (1983) An ultrastructural study of root invasion in three vascular wilt diseases. *Physiol. Plant Pathol.*, **22**, 15–27.
- Boch, J., Scholze, H., Schornack, S., Landgraf, A., Hahn, S., Kay, S., Lahaye, T., Nickstadt, A. and Bonas, U.** (2009) Breaking the code of DNA binding specificity of TAL-type III effectors. *Science*, **326**, 1509–1512.
- Böhm, H., Albert, I., Oome, S., Raaymakers, T.M., Van den Ackerveken, G. and Nürnberger, T.** (2014) A conserved peptide pattern from a widespread microbial virulence factor triggers pattern-induced immunity in Arabidopsis. *PLoS Pathog.*, **10**, e1004491.
- Boller, T. and Felix, G.** (2009) A renaissance of elicitors: perception of microbe-associated molecular patterns and danger signals by pattern-recognition receptors. *Annu. Rev. Plant Biol.*, **60**, 379–406.
- Bombarely, A., Rosli, H.G., Vrebalov, J., Moffett, P., Mueller, L.A. and Martin, G.B.** (2012) A draft genome sequence of *Nicotiana benthamiana* to enhance molecular plant-microbe biology research. *Mol. Plant-Microbe Interact. MPMI*, **25**, 1523–1530.
- Bortesi, L. and Fischer, R.** (2015) The CRISPR/Cas9 system for plant genome editing and beyond. *Biotechnol. Adv.*, **33**, 41–52.
- Brady, S.M., Orlando, D.A., Lee, J.-Y., Wang, J.Y., Koch, J., Dinneny, J.R., Mace, D., Ohler, U. and Benfey, P.N.** (2007) A high-resolution root spatiotemporal map reveals dominant expression patterns. *Science*, **318**, 801–806.
- Bramson, H.N., Thomas, N., Matsueda, R., Nelson, N.C., Taylor, S.S. and Kaiser, E.T.** (1982) Modification of the catalytic subunit of bovine heart cAMP-dependent protein kinase with affinity labels related to peptide substrates. *J. Biol. Chem.*, **257**, 10575–10581.
- Breeze, E., Harrison, E., McHattie, S., et al.** (2011) High-resolution temporal profiling of transcripts during Arabidopsis leaf senescence reveals a distinct chronology of processes and regulation. *Plant Cell*, **23**, 873–894.
- Brodersen, P., Petersen, M., Bjørn Nielsen, H., Zhu, S., Newman, M.-A., Shokat, K.M., Rietz, S., Parker, J. and Mundy, J.** (2006) Arabidopsis MAP kinase 4 regulates salicylic acid- and jasmonic acid/ethylene-dependent responses via EDS1 and PAD4. *Plant J. Cell Mol. Biol.*, **47**, 532–546.
- Bruckhoff, V., Haroth, S., Feussner, K., König, S., Brodhun, F. and Feussner, I.** (2016) Functional Characterization of CYP94-Genes and Identification of a Novel Jasmonate Catabolite in Flowers. *PLoS ONE*, **11**, e0159875.
- Cameron, K.D., Teece, M.A. and Smart, L.B.** (2006) Increased Accumulation of Cuticular Wax and Expression of Lipid Transfer Protein in Response to Periodic Drying Events in Leaves of Tree Tobacco. *Plant Physiol.*, **140**, 176–183.
- Cartwright, D.A., Brady, S.M., Orlando, D.A., Sturmfels, B. and Benfey, P.N.** (2009) Reconstructing spatiotemporal gene expression data from partial observations. *Bioinforma. Oxf. Engl.*, **25**, 2581–2587.
- Chen, L., Wang, Q.-Q., Zhou, L., Ren, F., Li, D.-D. and Li, X.-B.** (2013) Arabidopsis CBL-interacting protein kinase (CIPK6) is involved in plant response to salt/osmotic stress and ABA. *Mol. Biol. Rep.*, **40**, 4759–4767.
- Chen, X., Shang, J., Chen, D., et al.** (2006) A B-lectin receptor kinase gene conferring rice blast resistance. *Plant J. Cell Mol. Biol.*, **46**, 794–804.
- Cheng, M.-C., Hsieh, E.-J., Chen, J.-H., Chen, H.-Y. and Lin, T.-P.** (2012) Arabidopsis RGLG2, functioning as a RING E3 ligase, interacts with AtERF53 and negatively regulates the plant drought stress response. *Plant Physiol.*, **158**, 363–375.

- Cheng, X., Wu, Y., Guo, J., Du, B., Chen, R., Zhu, L. and He, G.** (2013) A rice lectin receptor-like kinase that is involved in innate immune responses also contributes to seed germination. *Plant J.*, **76**, 687–698.
- Cheng, Y.T., Germain, H., Wiermer, M., et al.** (2009) Nuclear pore complex component MOS7/Nup88 is required for innate immunity and nuclear accumulation of defense regulators in Arabidopsis. *Plant Cell*, **21**, 2503–2516.
- Chinchilla, D., Bauer, Z., Regenass, M., Boller, T. and Felix, G.** (2006) The Arabidopsis receptor kinase FLS2 binds flg22 and determines the specificity of flagellin perception. *Plant Cell*, **18**, 465–476.
- Chinchilla, D., Zipfel, C., Robatzek, S., Kemmerling, B., Nürnberger, T., Jones, J.D.G., Felix, G. and Boller, T.** (2007) A flagellin-induced complex of the receptor FLS2 and BAK1 initiates plant defence. *Nature*, **448**, 497–500.
- Chini, A., Fonseca, S., Fernández, G., et al.** (2007) The JAZ family of repressors is the missing link in jasmonate signalling. *Nature*, **448**, 666–671.
- Choat, B., Cobb, A.R. and Jansen, S.** (2008) Structure and function of bordered pits: new discoveries and impacts on whole-plant hydraulic function. *New Phytol.*, **177**, 608–625.
- Choi, J., Huh, S.U., Kojima, M., Sakakibara, H., Paek, K.-H. and Hwang, I.** (2010) The cytokinin-activated transcription factor ARR2 promotes plant immunity via TGA3/NPR1-dependent salicylic acid signaling in Arabidopsis. *Dev. Cell*, **19**, 284–295.
- Choudhury, A. and Lahiri, A.** (2008) TRABAS: a database for transcription regulation by ABA signaling. *In Silico Biol.*, **8**, 511–516.
- Chudakov, D.M., Matz, M.V., Lukyanov, S. and Lukyanov, K.A.** (2010) Fluorescent proteins and their applications in imaging living cells and tissues. *Physiol. Rev.*, **90**, 1103–1163.
- Clewes, E., Edwards, S.G. and Barbara, D.J.** (2008) Direct molecular evidence supports long-spored microsclerotial isolates of *Verticillium* from crucifers being interspecific hybrids. *Plant Pathol.*, **57**, 1047–1057.
- Cole, S.J. and Diener, A.C.** (2013) Diversity in receptor-like kinase genes is a major determinant of quantitative resistance to *Fusarium oxysporum* f.sp. *matthioli*. *New Phytol.*, **200**, 172–184.
- Conrath, U.** (2006) Systemic Acquired Resistance. *Plant Signal. Behav.*, **1**, 179–184.
- Couto, D. and Zipfel, C.** (2016) Regulation of pattern recognition receptor signalling in plants. *Nat. Rev. Immunol.*, **16**, 537–552.
- Cowan, A.K., Cairns, A.L.P. and Bartels-Rahm, B.** (1999) Regulation of abscisic acid metabolism: towards a metabolic basis for abscisic acid—cytokinin antagonism. *J. Exp. Bot.*, **50**, 595–603.
- Cracker, L.E. and Abeles, F.B.** (1969) Abscission: Role of Abscisic Acid. *Plant Physiol.*, **44**, 1144–1149.
- Cserző, M., Eisenhaber, F., Eisenhaber, B. and Simon, I.** (2002) On filtering false positive transmembrane protein predictions. *Protein Eng.*, **15**, 745–752.
- Dangl, J.L. and Jones, J.D.** (2001) Plant pathogens and integrated defence responses to infection. *Nature*, **411**, 826–833.
- Das, V.S.R., Rao, I.M. and Raghavendra, A.S.** (1976) Reversal of Abscisic Acid Induced Stomatal Closure by Benzyl Adenine. *New Phytol.*, **76**, 449–452.
- Davies, T.G., Verdonk, M.L., Graham, B., et al.** (2007) A structural comparison of inhibitor binding to PKB, PKA and PKA-PKB chimera. *J. Mol. Biol.*, **367**, 882–894.
- Davies, W.J., Kudoyarova, G. and Hartung, W.** (2005) Long-distance ABA Signaling and Its Relation to Other Signaling Pathways in the Detection of Soil Drying and the Mediation of the Plant's Response to Drought. *J. Plant Growth Regul.*, **24**, 285–295.
- De Vos, M., Denekamp, M., Dicke, M., Vuylsteke, M., Van Loon, L., Smeekens, S.C. and Pieterse, C.M.** (2006) The Arabidopsis thaliana Transcription Factor AtMYB102 Functions in Defense Against the Insect Herbivore *Pieris rapae*. *Plant Signal. Behav.*, **1**, 305–311.
- DeBono, A., Yeats, T.H., Rose, J.K.C., Bird, D., Jetter, R., Kunst, L. and Samuels, L.** (2009) Arabidopsis LTPG Is a Glycosylphosphatidylinositol-Anchored Lipid Transfer Protein Required for Export of Lipids to the Plant Surface. *Plant Cell*, **21**, 1230–1238.
- Denancé, N., Sánchez-Vallet, A., Goffner, D. and Molina, A.** (2013) Disease resistance or growth: the role of plant hormones in balancing immune responses and fitness costs. *Front. Plant Sci.*, **4**, 155.
- Denekamp, M. and Smeekens, S.C.** (2003) Integration of Wounding and Osmotic Stress Signals Determines the Expression of the AtMYB102 Transcription Factor Gene. *Plant Physiol.*, **132**, 1415–1423.

- Després, C., Chubak, C., Rochon, A., Clark, R., Bethune, T., Desveaux, D. and Fobert, P.R.** (2003) The Arabidopsis NPR1 disease resistance protein is a novel cofactor that confers redox regulation of DNA binding activity to the basic domain/leucine zipper transcription factor TGA1. *Plant Cell*, **15**, 2181–2191.
- Dixon, G.R. and Pegg, G.F.** (1969) Hyphal lysis and tylose formation in tomato cultivars infected by *Verticillium albo-atrum*. *Trans. Br. Mycol. Soc.*, **53**, 109–118.
- Dodds, P.N., Lawrence, G.J., Catanzariti, A.-M., Teh, T., Wang, C.-I.A., Ayliffe, M.A., Kobe, B. and Ellis, J.G.** (2006) Direct protein interaction underlies gene-for-gene specificity and coevolution of the flax resistance genes and flax rust avirulence genes. *Proc. Natl. Acad. Sci. U. S. A.*, **103**, 8888–8893.
- Dodds, P.N. and Rathjen, J.P.** (2010) Plant immunity: towards an integrated view of plant-pathogen interactions. *Nat. Rev. Genet.*, **11**, 539–548.
- Doehlemann, G., Requena, N., Schaefer, P., Brunner, F., O’Connell, R. and Parker, J.E.** (2014) Reprogramming of plant cells by filamentous plant-colonizing microbes. *New Phytol.*, **204**, 803–814.
- Doehlemann, G., Wahl, R., Horst, R.J., et al.** (2008) Reprogramming a maize plant: transcriptional and metabolic changes induced by the fungal biotroph *Ustilago maydis*. *Plant J. Cell Mol. Biol.*, **56**, 181–195.
- Dombrecht, B., Xue, G.P., Sprague, S.J., et al.** (2007) MYC2 differentially modulates diverse jasmonate-dependent functions in Arabidopsis. *Plant Cell*, **19**, 2225–2245.
- Du, X., Wang, S., Gao, F., Zhang, L., Zhao, J.-H., Guo, H.-S. and Hua, C.** (2017) Expression of pathogenesis-related genes in cotton roots in response to *Verticillium dahliae* PAMP molecules. *Sci. China Life Sci.*, **60**, 852–860.
- Edgar, R.C.** (2004) MUSCLE: multiple sequence alignment with high accuracy and high throughput. *Nucleic Acids Res.*, **32**, 1792–1797.
- Eisele, J.F., Fäßler, F., Bürgel, P.F. and Chaban, C.** (2016) A Rapid and Simple Method for Microscopy-Based Stomata Analyses. *PLoS One*, **11**, e0164576.
- Engl, R.A., Girod, A., Kinzel, V., Huber, R. and Bossemeyer, D.** (1996) Crystal structures of catalytic subunit of cAMP-dependent protein kinase in complex with isoquinolinesulfonyl protein kinase inhibitors H7, H8, and H89. Structural implications for selectivity. *J. Biol. Chem.*, **271**, 26157–26164.
- Eynck, C., Koopmann, B., Grunewaldt-Stoecker, G., Karlovsky, P. and Tiedemann, A. von** (2007) Differential interactions of *Verticillium longisporum* and *V. dahliae* with *Brassica napus* detected with molecular and histological techniques. *Eur. J. Plant Pathol.*, **118**, 259–274.
- Faino, L., Jonge, R. de and Thomma, B.P.H.J.** (2012) The transcriptome of *Verticillium dahliae*-infected *Nicotiana benthamiana* determined by deep RNA sequencing. *Plant Signal. Behav.*, **7**, 1065–1069.
- Falk, A., Feys, B.J., Frost, L.N., Jones, J.D.G., Daniels, M.J. and Parker, J.E.** (1999) EDS1, an essential component of R gene-mediated disease resistance in Arabidopsis has homology to eukaryotic lipases. *Proc. Natl. Acad. Sci. U. S. A.*, **96**, 3292–3297.
- Fan, W. and Dong, X.** (2002) In vivo interaction between NPR1 and transcription factor TGA2 leads to salicylic acid-mediated gene activation in Arabidopsis. *Plant Cell*, **14**, 1377–1389.
- Fellbrich, G., Romanski, A., Varet, A., et al.** (2002) NPP1, a Phytophthora-associated trigger of plant defense in parsley and Arabidopsis. *Plant J. Cell Mol. Biol.*, **32**, 375–390.
- Feys, B.J., Wiermer, M., Bhat, R.A., Moisan, L.J., Medina-Escobar, N., Neu, C., Cabral, A. and Parker, J.E.** (2005) Arabidopsis SENESCENCE-ASSOCIATED GENE101 stabilizes and signals within an ENHANCED DISEASE SUSCEPTIBILITY1 complex in plant innate immunity. *Plant Cell*, **17**, 2601–2613.
- Floerl, S., Druibert, C., Aroud, H.I., Karlovsky, P. and Polle, A.** (2010) Disease symptoms and mineral nutrition in Arabidopsis thaliana in response to *Verticillium longisporum* V143 infection. *J. Plant Pathol.*, **92**, 693–700.
- Floerl, S., Majcherczyk, A., Possienke, M., Feussner, K., Tappe, H., Gatz, C., Feussner, I., Kües, U. and Polle, A.** (2012) *Verticillium longisporum* infection affects the leaf apoplastic proteome, metabolome, and cell wall properties in Arabidopsis thaliana. *PLoS One*, **7**, e31435.
- Fonseca, S., Chini, A., Hamberg, M., Adie, B., Porzel, A., Kramell, R., Miersch, O., Wasternack, C. and Solano, R.** (2009) (+)-7-iso-Jasmonoyl-L-isoleucine is the endogenous bioactive jasmonate. *Nat. Chem. Biol.*, **5**, 344–350.
- Fradin, E.F., Abd-El-Haliem, A., Masini, L., Berg, G.C.M. van den, Joosten, M.H.A.J. and Thomma, B.P.H.J.** (2011) Interfamily transfer of tomato Ve1 mediates *Verticillium* resistance in Arabidopsis. *Plant Physiol.*, **156**, 2255–2265.

- Fradin, E.F. and Thomma, B.P.H.J.** (2006) Physiology and molecular aspects of Verticillium wilt diseases caused by *V. dahliae* and *V. albo-atrum*. *Mol. Plant Pathol.*, **7**, 71–86.
- Fradin, E.F., Zhang, Z., Juarez Ayala, J.C., Castroverde, C.D.M., Nazar, R.N., Robb, J., Liu, C.-M. and Thomma, B.P.H.J.** (2009) Genetic Dissection of Verticillium Wilt Resistance Mediated by Tomato Ve1. *Plant Physiol.*, **150**, 320–332.
- Freeman, B.C. and Beattie, G.A.** (2009) Bacterial growth restriction during host resistance to *Pseudomonas syringae* is associated with leaf water loss and localized cessation of vascular activity in *Arabidopsis thaliana*. *Mol. Plant-Microbe Interact. MPMI*, **22**, 857–867.
- Fujii, H., Chinnusamy, V., Rodrigues, A., et al.** (2009) In vitro reconstitution of an abscisic acid signalling pathway. *Nature*, **462**, 660–664.
- Fujii, H., Verslues, P.E. and Zhu, J.-K.** (2011) *Arabidopsis* decuple mutant reveals the importance of SnRK2 kinases in osmotic stress responses in vivo. *Proc. Natl. Acad. Sci. U. S. A.*, **108**, 1717–1722.
- Fujita, Y., Nakashima, K., Yoshida, T., et al.** (2009) Three SnRK2 protein kinases are the main positive regulators of abscisic acid signaling in response to water stress in *Arabidopsis*. *Plant Cell Physiol.*, **50**, 2123–2132.
- Gao, W., Long, L., Tian, X., Xu, F., Liu, J., Singh, P.K., Botella, J.R. and Song, C.** (2017) Genome Editing in Cotton with the CRISPR/Cas9 System. *Front. Plant Sci.*, **8**, 1364.
- García-Andrade, J., Ramírez, V., Flors, V. and Vera, P.** (2011) *Arabidopsis ocp3* mutant reveals a mechanism linking ABA and JA to pathogen-induced callose deposition. *Plant J. Cell Mol. Biol.*, **67**, 783–794.
- Genencher, B., Lipka, V., Petutschnig, E.K. and Wiermer, M.** (2017) Nucleoporin NUP88/MOS7 is required for manifestation of phenotypes associated with the *Arabidopsis* CHITIN ELICITOR RECEPTOR KINASE1 mutant *cerk1-4*. *Plant Signal. Behav.*, **12**, e1313378.
- Gepstein, S. and Thimann, K.V.** (1980) Changes in the abscisic acid content of oat leaves during senescence. *Proc. Natl. Acad. Sci. U. S. A.*, **77**, 2050–2053.
- Ghareeb, H., Laukamm, S. and Lipka, V.** (2016) COLORFUL-Circuit: A Platform for Rapid Multigene Assembly, Delivery, and Expression in Plants. *Front. Plant Sci.*, **7**, 246.
- Gheysen, G. and Mitchum, M.G.** (2011) How nematodes manipulate plant development pathways for infection. *Curr. Opin. Plant Biol.*, **14**, 415–421.
- Gijzen, M. and Nürnberger, T.** (2006) Nep1-like proteins from plant pathogens: recruitment and diversification of the NPP1 domain across taxa. *Phytochemistry*, **67**, 1800–1807.
- Gilardoni, P.A., Hettenhausen, C., Baldwin, I.T. and Bonaventure, G.** (2011) *Nicotiana attenuata* LECTIN RECEPTOR KINASE1 suppresses the insect-mediated inhibition of induced defense responses during *Manduca sexta* herbivory. *Plant Cell*, **23**, 3512–3532.
- Gimenez-Ibanez, S., Boter, M., Fernández-Barbero, G., Chini, A., Rathjen, J.P. and Solano, R.** (2014) The bacterial effector HopX1 targets JAZ transcriptional repressors to activate jasmonate signaling and promote infection in *Arabidopsis*. *PLoS Biol.*, **12**, e1001792.
- Glazebrook, J.** (2005) Contrasting mechanisms of defense against biotrophic and necrotrophic pathogens. *Annu. Rev. Phytopathol.*, **43**, 205–227.
- Gohlke, J. and Deeken, R.** (2014) Plant responses to *Agrobacterium tumefaciens* and crown gall development. *Front. Plant Sci.*, **5**, 155.
- Gordon, T.R.** (2017) *Fusarium oxysporum* and the Fusarium Wilt Syndrome. *Annu. Rev. Phytopathol.*, **55**, 23–39.
- Gou, J.-Y., Yu, X.-H. and Liu, C.-J.** (2009) A hydroxycinnamoyltransferase responsible for synthesizing suberin aromatics in *Arabidopsis*. *Proc. Natl. Acad. Sci. U. S. A.*, **106**, 18855–18860.
- Grabov, A., Leung, J., Giraudat, J. and Blatt, M.R.** (1997) Alteration of anion channel kinetics in wild-type and *abi-1* transgenic *Nicotiana benthamiana* guard cells by abscisic acid. *Plant J. Cell Mol. Biol.*, **12**, 203–213.
- Gray, W.M.** (2004) Hormonal Regulation of Plant Growth and Development. *PLoS Biol.*, **2**, e311.
- Großkinsky, D.K., Graaff, E. van der and Roitsch, T.** (2014) Abscisic Acid-Cytokinin Antagonism Modulates Resistance Against *Pseudomonas syringae* in Tobacco. *Phytopathology*, **104**, 1283–1288.
- Gu, Z., Liu, T., Ding, B., et al.** (2017) Two Lysin-Motif Receptor Kinases, Gh-LYK1 and Gh-LYK2, Contribute to Resistance against Verticillium wilt in Upland Cotton. *Front. Plant Sci.*, **8**, 2133.
- Guo, L., Wang, Z.Y., Lin, H., Cui, W.E., Chen, J., Liu, M., Chen, Z.L., Qu, L.J. and Gu, H.** (2006) Expression and functional analysis of the rice plasma-membrane intrinsic protein gene family. *Cell Res.*, **16**, 277–286.

- Guo, L., Yang, H., Zhang, X. and Yang, S.** (2013) Lipid transfer protein 3 as a target of MYB96 mediates freezing and drought stress in Arabidopsis. *J. Exp. Bot.*, **64**, 1755–1767.
- Hanin, M., Brini, F., Ebel, C., Toda, Y., Takeda, S. and Masmoudi, K.** (2011) Plant dehydrins and stress tolerance: versatile proteins for complex mechanisms. *Plant Signal. Behav.*, **6**, 1503–1509.
- Hanks, S.K. and Hunter, T.** (1995) Protein kinases 6. The eukaryotic protein kinase superfamily: kinase (catalytic) domain structure and classification. *FASEB J. Off. Publ. Fed. Am. Soc. Exp. Biol.*, **9**, 576–596.
- Hansen, H. and Dörffling, K.** (2003) Root-derived trans-zeatin riboside and abscisic acid in drought-stressed and rewatered sunflower plants: interaction in the control of leaf diffusive resistance? *Funct. Plant Biol.*, **30**, 365–375.
- Hardoim, P.R., Overbeek, L.S. van, Berg, G., Pirttilä, A.M., Compant, S., Campisano, A., Döring, M. and Sessitsch, A.** (2015) The Hidden World within Plants: Ecological and Evolutionary Considerations for Defining Functioning of Microbial Endophytes. *Microbiol. Mol. Biol. Rev. MMBR*, **79**, 293–320.
- He, P., Osaki, M., Takebe, M., Shinano, T. and Wasaki, J.** (2005) Endogenous hormones and expression of senescence-related genes in different senescent types of maize. *J. Exp. Bot.*, **56**, 1117–1128.
- Hebsgaard, S.M., Korning, P.G., Tolstrup, N., Engelbrecht, J., Rouzé, P. and Brunak, S.** (1996) Splice site prediction in Arabidopsis thaliana pre-mRNA by combining local and global sequence information. *Nucleic Acids Res.*, **24**, 3439–3452.
- Hetzer, M.W.** (2010) The Nuclear Envelope. *Cold Spring Harb. Perspect. Biol.*, **2**, a000539.
- Hinata, K., Watanabe, M., Yamakawa, S., Satta, Y. and Isogai, A.** (1995) Evolutionary aspects of the S-related genes of the Brassica self-incompatibility system: synonymous and nonsynonymous base substitutions. *Genetics*, **140**, 1099–1104.
- Hobo, T., Asada, M., Kowyama, Y. and Hattori, T.** (1999) ACGT-containing abscisic acid response element (ABRE) and coupling element 3 (CE3) are functionally equivalent. *Plant J. Cell Mol. Biol.*, **19**, 679–689.
- Hull, A.K., Vij, R. and Celenza, J.L.** (2000) Arabidopsis cytochrome P450s that catalyze the first step of tryptophan-dependent indole-3-acetic acid biosynthesis. *Proc. Natl. Acad. Sci. U. S. A.*, **97**, 2379–2384.
- Hwang, I., Sheen, J. and Müller, B.** (2012) Cytokinin signaling networks. *Annu. Rev. Plant Biol.*, **63**, 353–380.
- Ikeuchi, M., Sugimoto, K. and Iwase, A.** (2013) Plant Callus: Mechanisms of Induction and Repression. *Plant Cell*, **25**, 3159–3173.
- Inderbitzin, P., Bostock, R.M., Davis, R.M., Usami, T., Platt, H.W. and Subbarao, K.V.** (2011) Phylogenetics and taxonomy of the fungal vascular wilt pathogen *Verticillium*, with the descriptions of five new species. *PLoS One*, **6**, e28341.
- Inderbitzin, P., Davis, R.M., Bostock, R.M. and Subbarao, K.V.** (2011) The ascomycete *Verticillium longisporum* is a hybrid and a plant pathogen with an expanded host range. *PLoS One*, **6**, e18260.
- Isaac, I.** (1949) A comparative study of pathogenic isolates of *Verticillium*. *Trans. Br. Mycol. Soc.*, **32**, 137–157.
- Iven, T., König, S., Singh, S., et al.** (2012) Transcriptional activation and production of tryptophan-derived secondary metabolites in arabidopsis roots contributes to the defense against the fungal vascular pathogen *Verticillium longisporum*. *Mol. Plant*, **5**, 1389–1402.
- Jaillais, Y. and Chory, J.** (2010) Unraveling the paradoxes of plant hormone signaling integration. *Nat. Struct. Mol. Biol.*, **17**, 642–645.
- Jefferson, R.A., Kavanagh, T.A. and Bevan, M.W.** (1987) GUS fusions: beta-glucuronidase as a sensitive and versatile gene fusion marker in higher plants. *EMBO J.*, **6**, 3901–3907.
- Jia, Y., McAdams, S.A., Bryan, G.T., Hershey, H.P. and Valent, B.** (2000) Direct interaction of resistance gene and avirulence gene products confers rice blast resistance. *EMBO J.*, **19**, 4004–4014.
- Jiang, C.-J., Shimono, M., Sugano, S., et al.** (2010) Abscisic acid interacts antagonistically with salicylic acid signaling pathway in rice-Magnaporthe grisea interaction. *Mol. Plant-Microbe Interact. MPMI*, **23**, 791–798.
- Jiang, S., Yao, J., Ma, K.-W., Zhou, H., Song, J., He, S.Y. and Ma, W.** (2013) Bacterial effector activates jasmonate signaling by directly targeting JAZ transcriptional repressors. *PLoS Pathog.*, **9**, e1003715.
- Jinek, M., Chylinski, K., Fonfara, I., Hauer, M., Doudna, J.A. and Charpentier, E.** (2012) A programmable dual-RNA-guided DNA endonuclease in adaptive bacterial immunity. *Science*, **337**, 816–821.
- Johansson, A., Staal, J. and Dixelius, C.** (2006) Early responses in the Arabidopsis-*Verticillium longisporum* pathosystem are dependent on NDR1, JA- and ET-associated signals via cytosolic NPR1 and RFO1. *Mol. Plant-Microbe Interact. MPMI*, **19**, 958–969.

- Johnson, C., Boden, E. and Arias, J.** (2003) Salicylic Acid and NPR1 Induce the Recruitment of trans-Activating TGA Factors to a Defense Gene Promoter in Arabidopsis. *Plant Cell*, **15**, 1846–1858.
- Jones, D.T., Taylor, W.R. and Thornton, J.M.** (1992) The rapid generation of mutation data matrices from protein sequences. *Comput. Appl. Biosci. CABIOS*, **8**, 275–282.
- Jones, J.D.G. and Dangl, J.L.** (2006) The plant immune system. *Nature*, **444**, 323–329.
- Jonge, R. de, Bolton, M.D., Kombrink, A., Berg, G.C.M. van den, Yadeta, K.A. and Thomma, B.P.H.J.** (2013) Extensive chromosomal reshuffling drives evolution of virulence in an asexual pathogen. *Genome Res.*, **23**, 1271–1282.
- Jonge, R. de, Peter van Esse, H., Maruthachalam, K., et al.** (2012) Tomato immune receptor Ve1 recognizes effector of multiple fungal pathogens uncovered by genome and RNA sequencing. *Proc. Natl. Acad. Sci. U. S. A.*, **109**, 5110–5115.
- Kapp, K., Schrepf, S., Lemberg, M.K. and Dobberstein, B.** (2013) Post-Targeting Functions of Signal Peptides. In: Madame Curie Bioscience Database [Internet]. Austin (TX): Landes Bioscience; 2000-2013. Available from: <https://www.ncbi.nlm.nih.gov/books/NBK6322/>.
- Karapapa, V.K., Bainbridge, B.W. and Heale, J.B.** (1997) Morphological and molecular characterization of *Verticillium longisporum* comb. nov., pathogenic to oilseed rape. *Mycol. Res.*, **101**, 1281–1294.
- Kawchuk, L.M., Hachey, J., Lynch, D.R., et al.** (2001) Tomato Ve disease resistance genes encode cell surface-like receptors. *Proc. Natl. Acad. Sci. U. S. A.*, **98**, 6511–6515.
- Kearse, M., Moir, R., Wilson, A., et al.** (2012) Geneious Basic: an integrated and extendable desktop software platform for the organization and analysis of sequence data. *Bioinforma. Oxf. Engl.*, **28**, 1647–1649.
- Kieber, J.J. and Schaller, G.E.** (2014) Cytokinin. *Arab. Book Am. Soc. Plant Biol.*, **12**, e0168.
- Kim, H., Lee, S.B., Kim, H.J., Min, M.K., Hwang, I. and Suh, M.C.** (2012) Characterization of glycosylphosphatidylinositol-anchored lipid transfer protein 2 (LTPG2) and overlapping function between LTPG/LTPG1 and LTPG2 in cuticular wax export or accumulation in Arabidopsis thaliana. *Plant Cell Physiol.*, **53**, 1391–1403.
- Kim, H.S., Jung, M.S., Lee, S.M., Kim, K.E., Byun, H., Choi, M.S., Park, H.C., Cho, M.J. and Chung, W.S.** (2009) An S-locus receptor-like kinase plays a role as a negative regulator in plant defense responses. *Biochem. Biophys. Res. Commun.*, **381**, 424–428.
- Kim, T.-H., Böhmer, M., Hu, H., Nishimura, N. and Schroeder, J.I.** (2010) Guard Cell Signal Transduction Network: Advances in Understanding Abscisic Acid, CO₂, and Ca²⁺ Signaling. *Annu. Rev. Plant Biol.*, **61**, 561–591.
- Klosterman, S.J., Atallah, Z.K., Vallad, G.E. and Subbarao, K.V.** (2009) Diversity, pathogenicity, and management of verticillium species. *Annu. Rev. Phytopathol.*, **47**, 39–62.
- Klosterman, S.J., Subbarao, K.V., Kang, S., et al.** (2011) Comparative genomics yields insights into niche adaptation of plant vascular wilt pathogens. *PLoS Pathog.*, **7**, e1002137.
- Kombrink, A., Rovenich, H., Shi-Kunne, X., et al.** (2017) *Verticillium dahliae* LysM effectors differentially contribute to virulence on plant hosts. *Mol. Plant Pathol.*, **18**, 596–608.
- Koncz, C. and Schell, J.** (1986) The promoter of T₁-DNA gene 5 controls the tissue-specific expression of chimaeric genes carried by a novel type of Agrobacterium binary vector. *Mol. Gen. Genet. MGG*, **204**, 383–396.
- Kong, L., Qiu, X., Kang, J., et al.** (2017) A Phytophthora Effector Manipulates Host Histone Acetylation and Reprograms Defense Gene Expression to Promote Infection. *Curr. Biol. CB*, **27**, 981–991.
- König, S., Feussner, K., Kaefer, A., Landesfeind, M., Thurow, C., Karlovsky, P., Gatz, C., Polle, A. and Feussner, I.** (2014) Soluble phenylpropanoids are involved in the defense response of Arabidopsis against *Verticillium longisporum*. *New Phytol.*, **202**, 823–837.
- Kosma, D.K., Murmu, J., Razeq, F.M., Santos, P., Bourgault, R., Molina, I. and Rowland, O.** (2014) AtMYB41 activates ectopic suberin synthesis and assembly in multiple plant species and cell types. *Plant J. Cell Mol. Biol.*, **80**, 216–229.
- Kubo, M., Udagawa, M., Nishikubo, N., Horiguchi, G., Yamaguchi, M., Ito, J., Mimura, T., Fukuda, H. and Demura, T.** (2005) Transcription switches for protoxylem and metaxylem vessel formation. *Genes Dev.*, **19**, 1855–1860.
- Kulik, A., Wawer, I., Krzywińska, E., Bucholc, M. and Dobrowolska, G.** (2011) SnRK2 Protein Kinases - Key Regulators of Plant Response to Abiotic Stresses. *OMICS J. Integr. Biol.*, **15**, 859–872.

- Kumar, S., Stecher, G. and Tamura, K.** (2016) MEGA7: Molecular Evolutionary Genetics Analysis Version 7.0 for Bigger Datasets. *Mol. Biol. Evol.*, **33**, 1870–1874.
- Ladner, C.L., Yang, J., Turner, R.J. and Edwards, R.A.** (2004) Visible fluorescent detection of proteins in polyacrylamide gels without staining. *Anal. Biochem.*, **326**, 13–20.
- Langmead, B., Trapnell, C., Pop, M. and Salzberg, S.L.** (2009) Ultrafast and memory-efficient alignment of short DNA sequences to the human genome. *Genome Biol.*, **10**, R25.
- Laurie-Berry, N., Joardar, V., Street, I.H. and Kunkel, B.N.** (2006) The Arabidopsis thaliana JASMONATE INSENSITIVE 1 gene is required for suppression of salicylic acid-dependent defenses during infection by *Pseudomonas syringae*. *Mol. Plant-Microbe Interact. MPMI*, **19**, 789–800.
- Lee, I.C., Hong, S.W., Whang, S.S., Lim, P.O., Nam, H.G. and Koo, J.C.** (2011) Age-dependent action of an ABA-inducible receptor kinase, RPK1, as a positive regulator of senescence in Arabidopsis leaves. *Plant Cell Physiol.*, **52**, 651–662.
- Lee, S.B., Go, Y.S., Bae, H.-J., et al.** (2009) Disruption of Glycosylphosphatidylinositol-Anchored Lipid Transfer Protein Gene Altered Cuticular Lipid Composition, Increased Plastoglobules, and Enhanced Susceptibility to Infection by the Fungal Pathogen *Alternaria brassicicola*. *Plant Physiol.*, **150**, 42–54.
- Lenarčič, T., Albert, I., Böhm, H., et al.** (2017) Eudicot plant-specific sphingolipids determine host selectivity of microbial NLP cytolysins. *Science*, **358**, 1431–1434.
- Léon-Kloosterziel, K.M., Gil, M.A., Ruijs, G.J., Jacobsen, S.E., Olszewski, N.E., Schwartz, S.H., Zeevaert, J.A. and Koornneef, M.** (1996) Isolation and characterization of abscisic acid-deficient Arabidopsis mutants at two new loci. *Plant J. Cell Mol. Biol.*, **10**, 655–661.
- Lescot, M., Déhais, P., Thijs, G., Marchal, K., Moreau, Y., Van de Peer, Y., Rouzé, P. and Rombauts, S.** (2002) PlantCARE, a database of plant cis-acting regulatory elements and a portal to tools for in silico analysis of promoter sequences. *Nucleic Acids Res.*, **30**, 325–327.
- Lewis, L.A., Polanski, K., Torres-Zabala, M. de, et al.** (2015) Transcriptional Dynamics Driving MAMP-Triggered Immunity and Pathogen Effector-Mediated Immunosuppression in Arabidopsis Leaves Following Infection with *Pseudomonas syringae* pv tomato DC3000. *Plant Cell*, **27**, 3038–3064.
- Li, N.-Y., Ma, X.-F., Short, D.P.G., et al.** (2017) The Island Cotton NBS-LRR Gene *GbaNA1* Confers Resistance to the Non-race 1 *Verticillium dahliae* Isolate Vd991. *Mol. Plant Pathol.*, doi: 10.1111/mpp.12630 [Epub ahead of print].
- Li, X., Clarke, J.D., Zhang, Y. and Dong, X.** (2001) Activation of an EDS1-mediated R-gene pathway in the *snc1* mutant leads to constitutive, NPR1-independent pathogen resistance. *Mol. Plant-Microbe Interact. MPMI*, **14**, 1131–1139.
- Li, X., Lassner, M. and Zhang, Y.** (2002) Deleteagene: A Fast Neutron Deletion Mutagenesis-Based Gene Knockout System for Plants. *Comp. Funct. Genomics*, **3**, 158–160.
- Lievens, L., Pollier, J., Goossens, A., Beyaert, R. and Staal, J.** (2017) Abscisic Acid as Pathogen Effector and Immune Regulator. *Front. Plant Sci.*, **8**, 587.
- Lin, N.-C. and Martin, G.B.** (2005) An *avrPto/avrPtoB* mutant of *Pseudomonas syringae* pv. tomato DC3000 does not elicit Pto-mediated resistance and is less virulent on tomato. *Mol. Plant-Microbe Interact. MPMI*, **18**, 43–51.
- Lindermayr, C., Sell, S., Müller, B., Leister, D. and Durner, J.** (2010) Redox regulation of the NPR1-TGA1 system of Arabidopsis thaliana by nitric oxide. *Plant Cell*, **22**, 2894–2907.
- Liu, T., Song, T., Zhang, X., et al.** (2014) Unconventionally secreted effectors of two filamentous pathogens target plant salicylate biosynthesis. *Nat. Commun.*, **5**, 4686.
- Liu, Y., Burgos, J.S., Deng, Y., Srivastava, R., Howell, S.H. and Bassham, D.C.** (2012) Degradation of the endoplasmic reticulum by autophagy during endoplasmic reticulum stress in Arabidopsis. *Plant Cell*, **24**, 4635–4651.
- Liu, Y., Wu, H., Chen, H., et al.** (2015) A gene cluster encoding lectin receptor kinases confers broad-spectrum and durable insect resistance in rice. *Nat. Biotechnol.*, **33**, 301–305.
- Liu, Y., Zhou, J. and White, K.P.** (2014) RNA-seq differential expression studies: more sequence or more replication? *Bioinform. Oxf. Engl.*, **30**, 301–304.
- Loake, G. and Grant, M.** (2007) Salicylic acid in plant defence--the players and protagonists. *Curr. Opin. Plant Biol.*, **10**, 466–472.

- Lohse, M., Bolger, A.M., Nagel, A., Fernie, A.R., Lunn, J.E., Stitt, M. and Usadel, B.** (2012) RobiNA: a user-friendly, integrated software solution for RNA-Seq-based transcriptomics. *Nucleic Acids Res.*, **40**, W622-627.
- Loon, L.C. van, Geraats, B.P.J. and Linthorst, H.J.M.** (2006) Ethylene as a modulator of disease resistance in plants. *Trends Plant Sci.*, **11**, 184–191.
- Lopisso, D.T., Knüfer, J., Koopmann, B. and Tiedemann, A. von** (2017) The Vascular Pathogen *Verticillium longisporum* Does Not Affect Water Relations and Plant Responses to Drought Stress of Its Host, *Brassica napus*. *Phytopathology*, **107**, 444–454.
- Lorenzo, O., Chico, J.M., Sánchez-Serrano, J.J. and Solano, R.** (2004) JASMONATE-INSENSITIVE1 encodes a MYC transcription factor essential to discriminate between different jasmonate-regulated defense responses in *Arabidopsis*. *Plant Cell*, **16**, 1938–1950.
- Loris, R.** (2002) Principles of structures of animal and plant lectins. *Biochim. Biophys. Acta*, **1572**, 198–208.
- Lyons, R., Stiller, J., Powell, J., Rusu, A., Manners, J.M. and Kazan, K.** (2015) *Fusarium oxysporum* Triggers Tissue-Specific Transcriptional Reprogramming in *Arabidopsis thaliana*. *PLoS ONE*, **10**, e0121902.
- Ma, Y., Szostkiewicz, I., Korte, A., Moes, D., Yang, Y., Christmann, A. and Grill, E.** (2009) Regulators of PP2C phosphatase activity function as abscisic acid sensors. *Science*, **324**, 1064–1068.
- Macho, A.P. and Zipfel, C.** (2014) Plant PRRs and the activation of innate immune signaling. *Mol. Cell*, **54**, 263-272.
- Mackey, D., Belkhadir, Y., Alonso, J.M., Ecker, J.R. and Dangl, J.L.** (2003) *Arabidopsis* RIN4 is a target of the type III virulence effector AvrRpt2 and modulates RPS2-mediated resistance. *Cell*, **112**, 379–389.
- Mackey, D., Holt, B.F., Wiig, A. and Dangl, J.L.** (2002) RIN4 interacts with *Pseudomonas syringae* type III effector molecules and is required for RPM1-mediated resistance in *Arabidopsis*. *Cell*, **108**, 743–754.
- MacRobbie, E.A.** (1998) Signal transduction and ion channels in guard cells. *Philos. Trans. R. Soc. B Biol. Sci.*, **353**, 1475–1488.
- Mao, G., Meng, X., Liu, Y., Zheng, Z., Chen, Z. and Zhang, S.** (2011) Phosphorylation of a WRKY transcription factor by two pathogen-responsive MAPKs drives phytoalexin biosynthesis in *Arabidopsis*. *Plant Cell*, **23**, 1639–1653.
- Matei, A., Ernst, C., Günl, M., Thiele, B., Altmüller, J., Walbot, V., Usadel, B. and Doehlemann, G.** (2018) How to make a tumour: cell type specific dissection of *Ustilago maydis*-induced tumour development in maize leaves. *New Phytol.*, doi: 10.1111/nph.14960 [Epub ahead of print].
- Matsuoka, K., Sugawara, E., Aoki, R., Takuma, K., Terao-Morita, M., Satoh, S. and Asahina, M.** (2016) Differential Cellular Control by Cotyledon-Derived Phytohormones Involved in Graft Reunion of *Arabidopsis Hypocotyls*. *Plant Cell Physiol.*, **57**, 2620–2631.
- McElver, J., Tzafrir, I., Aux, G., et al.** (2001) Insertional mutagenesis of genes required for seed development in *Arabidopsis thaliana*. *Genetics*, **159**, 1751–1763.
- Miles, G.P., Samuel, M.A., Zhang, Y. and Ellis, B.E.** (2005) RNA interference-based (RNAi) suppression of AtMPK6, an *Arabidopsis* mitogen-activated protein kinase, results in hypersensitivity to ozone and misregulation of AtMPK3. *Environ. Pollut. Barking Essex 1987*, **138**, 230–237.
- Mishra, A., Khare, S., Trivedi, P.K. and Nath, P.** (2008) Effect of ethylene, 1-MCP, ABA and IAA on break strength, cellulase and polygalacturonase activities during cotton leaf abscission. *South Afr. J. Bot.*, **74**, 282-287.
- Mithen, R., Bennett, R. and Marquez, J.** (2010) Glucosinolate biochemical diversity and innovation in the Brassicales. *Phytochemistry*, **71**, 2074–2086.
- Miya, A., Albert, P., Shinya, T., et al.** (2007) CERK1, a LysM receptor kinase, is essential for chitin elicitor signaling in *Arabidopsis*. *Proc. Natl. Acad. Sci. U. S. A.*, **104**, 19613–19618.
- Miyashima, S., Sebastian, J., Lee, J.-Y. and Helariutta, Y.** (2013) Stem cell function during plant vascular development. *EMBO J.*, **32**, 178–193.
- Mohr, P. and Cahill, D.** (2003) Abscisic acid influences the susceptibility of *Arabidopsis thaliana* to *Pseudomonas syringae* pv. tomato and *Peronospora parasitica*. *Funct. Plant Biol.*, **30**, 461–469
- Mol, L. and Scholte, K.** (1995) Formation of microsclerotia of *Verticillium dahliae* Kleb. on various plant parts of two potato cultivars. *Potato Res.*, **38**, 143–150.
- Moore, I. and Murphy, A.** (2009) Validating the Location of Fluorescent Protein Fusions in the Endomembrane System. *Plant Cell*, **21**, 1632–1636.

- Mostert, D., Molina, A.B., Daniells, J., et al.** (2017) The distribution and host range of the banana Fusarium wilt fungus, *Fusarium oxysporum* f. sp. *cubense*, in Asia. *PLoS One*, **12**, e0181630.
- Mou, Z., Fan, W. and Dong, X.** (2003) Inducers of plant systemic acquired resistance regulate NPR1 function through redox changes. *Cell*, **113**, 935–944.
- Nagai, T., Iбата, K., Park, E.S., Kubota, M., Mikoshiba, K. and Miyawaki, A.** (2002) A variant of yellow fluorescent protein with fast and efficient maturation for cell-biological applications. *Nat. Biotechnol.*, **20**, 87–90.
- Narusaka, Y., Nakashima, K., Shinwari, Z.K., Sakuma, Y., Furihata, T., Abe, H., Narusaka, M., Shinozaki, K. and Yamaguchi-Shinozaki, K.** (2003) Interaction between two cis-acting elements, ABRE and DRE, in ABA-dependent expression of Arabidopsis rd29A gene in response to dehydration and high-salinity stresses. *Plant J. Cell Mol. Biol.*, **34**, 137–148.
- Naseem, M., Wölfling, M. and Dandekar, T.** (2014) Cytokinins for immunity beyond growth, galls and green islands. *Trends Plant Sci.*, **19**, 481–484.
- Ndamukong, I., Abdallat, A.A., Thurow, C., Fode, B., Zander, M., Weigel, R. and Gatz, C.** (2007) SA-inducible Arabidopsis glutaredoxin interacts with TGA factors and suppresses JA-responsive PDF1.2 transcription. *Plant J. Cell Mol. Biol.*, **50**, 128–139.
- Nelson, B.K., Cai, X. and Nebenführ, A.** (2007) A multicolored set of in vivo organelle markers for co-localization studies in Arabidopsis and other plants. *Plant J. Cell Mol. Biol.*, **51**, 1126–1136.
- Newman, K.L., Almeida, R.P.P., Purcell, A.H. and Lindow, S.E.** (2003) Use of a green fluorescent strain for analysis of *Xylella fastidiosa* colonization of *Vitis vinifera*. *Appl. Environ. Microbiol.*, **69**, 7319–7327.
- Niu, X., Helentjaris, T. and Bate, N.J.** (2002) Maize ABI4 Binds Coupling Element1 in Abscisic Acid and Sugar Response Genes. *Plant Cell*, **14**, 2565–2575.
- Nothwehr, S.F. and Gordon, J.I.** (1990) Targeting of proteins into the eukaryotic secretory pathway: signal peptide structure/function relationships. *BioEssays News Rev. Mol. Cell. Dev. Biol.*, **12**, 479–484.
- O'Brien, J.A. and Benková, E.** (2013) Cytokinin cross-talking during biotic and abiotic stress responses. *Front. Plant Sci.*, **4**, 451.
- Ohkuma, K., Lyon, J.L., Addicott, F.T. and Smith, O.E.** (1963) Abscisin II, an Abscission-Accelerating Substance from Young Cotton Fruit. *Science*, **142**, 1592–1593.
- Olsson, S., Buchbender, V., Enroth, J., Hedenäs, L., Huttunen, S. and Quandt, D.** (2009) Phylogenetic analyses reveal high levels of polyphyly among pleurocarpous lineages as well as novel clades. *The Bryologist*, **112**, 447–466.
- O'Malley, R.C., Barragan, C.C. and Ecker, J.R.** (2015) A User's Guide to the Arabidopsis T-DNA Insertional Mutant Collections. *Methods Mol. Biol. Clifton NJ*, **1284**, 323–342.
- Oome, S. and Van den Ackerveken, G.** (2014) Comparative and functional analysis of the widely occurring family of Nep1-like proteins. *Mol. Plant-Microbe Interact. MPMI*, **27**, 1081–1094.
- Palmer, C.S., Saleeba, J.A. and Lyon, B.R.** (2005) Phytotoxicity on cotton ex-plants of an 18.5kDa protein from culture filtrates of *Verticillium dahliae*. *Physiol. Mol. Plant Pathol.*, **67**, 308–318.
- Pandey, S., Wang, R.-S., Wilson, L., Li, S., Zhao, Z., Gookin, T.E., Assmann, S.M. and Albert, R.** (2010) Boolean modeling of transcriptome data reveals novel modes of heterotrimeric G-protein action. *Mol. Syst. Biol.*, **6**, 372.
- Panstruga, R. and Dodds, P.N.** (2009) Terrific protein traffic: the mystery of effector protein delivery by filamentous plant pathogens. *Science*, **324**, 748–750.
- Park, S.-Y., Fung, P., Nishimura, N., et al.** (2009) Abscisic acid inhibits type 2C protein phosphatases via the PYR/PYL family of START proteins. *Science*, **324**, 1068–1071.
- Parker, J.E., Szabó, V., Staskawicz, B.J., Lister, C., Dean, C., Daniels, M.J. and Jones, J.D.G.** (1993) Phenotypic characterization and molecular mapping of the Arabidopsis thaliana locus RPP5, determining disease resistance to *Peronospora parasitica*. *Plant J.*, **4**, 821–831.
- Pei, Z.M., Kuchitsu, K., Ward, J.M., Schwarz, M. and Schroeder, J.I.** (1997) Differential abscisic acid regulation of guard cell slow anion channels in Arabidopsis wild-type and *abi1* and *abi2* mutants. *Plant Cell*, **9**, 409–423.
- Pérez-Donoso, A.G., Sun, Q., Roper, M.C., Greve, L.C., Kirkpatrick, B. and Labavitch, J.M.** (2010) Cell wall-degrading enzymes enlarge the pore size of intervessel pit membranes in healthy and *Xylella fastidiosa*-infected grapevines. *Plant Physiol.*, **152**, 1748–1759.

- Petersen, M., Brodersen, P., Naested, H., et al.** (2000) Arabidopsis map kinase 4 negatively regulates systemic acquired resistance. *Cell*, **103**, 1111–1120.
- Petersen, T.N., Brunak, S., Heijne, G. von and Nielsen, H.** (2011) SignalP 4.0: discriminating signal peptides from transmembrane regions. *Nat. Methods*, **8**, 785–786.
- Petutschnig, E.K., Jones, A.M.E., Serazetdinova, L., Lipka, U. and Lipka, V.** (2010) The lysin motif receptor-like kinase (LysM-RLK) CERK1 is a major chitin-binding protein in Arabidopsis thaliana and subject to chitin-induced phosphorylation. *J. Biol. Chem.*, **285**, 28902–28911.
- Pfaffl, M.W.** (2001) A new mathematical model for relative quantification in real-time RT-PCR. *Nucleic Acids Res.*, **29**, e45.
- Pfister, A., Barberon, M., Alassimone, J., et al.** (2014) A receptor-like kinase mutant with absent endodermal diffusion barrier displays selective nutrient homeostasis defects. *eLife*, **3**, e03115.
- Pieterse, C.M.J., Leon-Reyes, A., Van der Ent, S. and Van Wees, S.C.M.** (2009) Networking by small-molecule hormones in plant immunity. *Nat. Chem. Biol.*, **5**, 308–316.
- Pitaksaringkarn, W., Matsuoka, K., Asahina, M., et al.** (2014) XTH20 and XTH19 regulated by ANAC071 under auxin flow are involved in cell proliferation in incised Arabidopsis inflorescence stems. *Plant J. Cell Mol. Biol.*, **80**, 604–614.
- Pitzschke, A., Schikora, A. and Hirt, H.** (2009) MAPK cascade signalling networks in plant defence. *Curr. Opin. Plant Biol.*, **12**, 421–426.
- Pozo, M.J., Loon, L.C.V. and Pieterse, C.M.J.** (2004) Jasmonates—Signals in plant-microbe interactions. *J. Plant Growth Regul.*, **23**, 211–222.
- Prade, L., Engh, R.A., Girod, A., Kinzel, V., Huber, R. and Bossemeyer, D.** (1997) Staurosporine-induced conformational changes of cAMP-dependent protein kinase catalytic subunit explain inhibitory potential. *Struct. Lond. Engl.* 1993, **5**, 1627–1637.
- Quigley, F., Rosenberg, J.M., Shachar-Hill, Y. and Bohnert, H.J.** (2002) From genome to function: the Arabidopsis aquaporins. *Genome Biol.*, **3**, 1–17.
- Ralhan, A., Schöttle, S., Thurow, C., Iven, T., Feussner, I., Polle, A. and Gatz, C.** (2012) The vascular pathogen *Verticillium longisporum* requires a jasmonic acid-independent COI1 function in roots to elicit disease symptoms in Arabidopsis shoots. *Plant Physiol.*, **159**, 1192–1203.
- Ranf, S., Gisch, N., Schäffer, M., et al.** (2015) A lectin S-domain receptor kinase mediates lipopolysaccharide sensing in Arabidopsis thaliana. *Nat. Immunol.*, **16**, 426–433.
- Redkar, A., Hoser, R., Schilling, L., Zechmann, B., Krzymowska, M., Walbot, V. and Doehlemann, G.** (2015) A Secreted Effector Protein of *Ustilago maydis* Guides Maize Leaf Cells to Form Tumors. *Plant Cell*, **27**, 1332–1351.
- Redkar, A., Matei, A. and Doehlemann, G.** (2017) Insights into Host Cell Modulation and Induction of New Cells by the Corn Smut *Ustilago maydis*. *Front. Plant Sci.*, **8**, 899.
- Reeves, W.M., Lynch, T.J., Mobin, R. and Finkelstein, R.R.** (2011) Direct targets of the transcription factors ABA-Insensitive(ABI)4 and ABI5 reveal synergistic action by ABI4 and several bZIP ABA response factors. *Plant Mol. Biol.*, **75**, 347–363.
- Ren, D., Liu, Y., Yang, K.-Y., Han, L., Mao, G., Glazebrook, J. and Zhang, S.** (2008) A fungal-responsive MAPK cascade regulates phytoalexin biosynthesis in Arabidopsis. *Proc. Natl. Acad. Sci. U. S. A.*, **105**, 5638–5643.
- Reusche, M., Klásková, J., Thole, K., et al.** (2013) Stabilization of cytokinin levels enhances Arabidopsis resistance against *Verticillium longisporum*. *Mol. Plant-Microbe Interact. MPMI*, **26**, 850–860.
- Reusche, M., Thole, K., Janz, D., Truskina, J., Rindfleisch, S., Drübert, C., Polle, A., Lipka, V. and Teichmann, T.** (2012) *Verticillium* infection triggers VASCULAR-RELATED NAC DOMAIN7-dependent de novo xylem formation and enhances drought tolerance in Arabidopsis. *Plant Cell*, **24**, 3823–3837.
- Reusche, M., Truskina, J., Thole, K., et al.** (2014) Infections with the vascular pathogens *Verticillium longisporum* and *Verticillium dahliae* induce distinct disease symptoms and differentially affect drought stress tolerance of Arabidopsis thaliana. *Environ. Exp. Bot.*, **108**, 23–37.
- Robb, J., Brisson, J.D., Busch, L. and Lu, B.C.** (1979) Ultrastructure of wilt syndrome caused by *Verticillium dahliae*. VII. Correlated light and transmission electron microscope identification of vessel coatings and tyloses. *Can. J. Bot.*, **57**, 822–834.
- Robert-Seilantantz, A., Grant, M. and Jones, J.D.G.** (2011) Hormone crosstalk in plant disease and defense: more than just jasmonate-salicylate antagonism. *Annu. Rev. Phytopathol.*, **49**, 317–343.

- Roos, J., Bejai, S., Mozūraitis, R. and Dixelius, C.** (2015) Susceptibility to *Verticillium longisporum* is linked to monoterpene production by TPS23/27 in *Arabidopsis*. *Plant J. Cell Mol. Biol.*, **81**, 572–585.
- Roos, J., Bejai, S., Oide, S. and Dixelius, C.** (2014) RabGAP22 is required for defense to the vascular pathogen *Verticillium longisporum* and contributes to stomata immunity. *PLoS One*, **9**, e88187.
- Sakamoto, K., Kusaba, M. and Nishio, T.** (1998) Polymorphism of the S-locus glycoprotein gene (SLG) and the S-locus related gene (SLR1) in *Raphanus sativus* L. and self-incompatible ornamental plants in the Brassicaceae. *Mol. Gen. Genet. MGG*, **258**, 397–403.
- Sánchez-Vallet, A., López, G., Ramos, B., et al.** (2012) Disruption of abscisic acid signaling constitutively activates *Arabidopsis* resistance to the necrotrophic fungus *Plectosphaerella cucumerina*. *Plant Physiol.*, **160**, 2109–2124.
- Santner, A., Calderon-Villalobos, L.I.A. and Estelle, M.** (2009) Plant hormones are versatile chemical regulators of plant growth. *Nat. Chem. Biol.*, **5**, 301–307.
- Scarpella, E., Francis, P. and Berleth, T.** (2004) Stage-specific markers define early steps of procambium development in *Arabidopsis* leaves and correlate termination of vein formation with mesophyll differentiation. *Dev. Camb. Engl.*, **131**, 3445–3455.
- Schaller, A. and Stintzi, A.** (2009) Enzymes in jasmonate biosynthesis - structure, function, regulation. *Phytochemistry*, **70**, 1532–1538.
- Schmitz, J.** (2015) Analyse der Jasmonoyl-Isoleucin-unabhängigen Funktion des Jasmonat-Rezeptors CORONATINE INSENSITIVE1 in Wurzeln von *Arabidopsis thaliana* (PhD Thesis). Retrieved from <http://hdl.handle.net/11858/00-1735-0000-0022-6031-4>.
- Schnathorst, W.C.** (1981) Life cycle and epidemiology of *Verticillium*. Pages 81-111 in: Fungal Wilt Diseases of Plants. ed. Mace E, Bell AA, Beckman CH (eds). *Academic Press, NY*.
- Schroeder, J.I. and Hagiwara, S.** (1990) Repetitive increases in cytosolic Ca²⁺ of guard cells by abscisic acid activation of nonselective Ca²⁺ permeable channels. *Proc. Natl. Acad. Sci. U. S. A.*, **87**, 9305–9309.
- Schurch, N.J., Schofield, P., Gierliński, M., et al.** (2016) How many biological replicates are needed in an RNA-seq experiment and which differential expression tool should you use? *RNA N. Y. N.*, **22**, 839–851.
- Schwessinger, B., Roux, M., Kadota, Y., Ntoukakis, V., Sklenar, J., Jones, A. and Zipfel, C.** (2011) Phosphorylation-dependent differential regulation of plant growth, cell death, and innate immunity by the regulatory receptor-like kinase BAK1. *PLoS Genet.*, **7**, e1002046.
- Shcherban, T.Y., Shi, J., Durachko, D.M., Gultinan, M.J., McQueen-Mason, S.J., Shieh, M. and Cosgrove, D.J.** (1995) Molecular cloning and sequence analysis of expansins—a highly conserved, multigene family of proteins that mediate cell wall extension in plants. *Proc. Natl. Acad. Sci. U. S. A.*, **92**, 9245–9249.
- Shen, Q. and Ho, T.H.** (1995) Functional dissection of an abscisic acid (ABA)-inducible gene reveals two independent ABA-responsive complexes each containing a G-box and a novel cis-acting element. *Plant Cell*, **7**, 295–307.
- Shen, Q., Zhang, P. and Ho, T.H.** (1996) Modular nature of abscisic acid (ABA) response complexes: composite promoter units that are necessary and sufficient for ABA induction of gene expression in barley. *Plant Cell*, **8**, 1107–1119.
- Shen, Q.J., Casaretto, J.A., Zhang, P. and Ho, T.-H.D.** (2004) Functional definition of ABA-response complexes: the promoter units necessary and sufficient for ABA induction of gene expression in barley (*Hordeum vulgare* L.). *Plant Mol. Biol.*, **54**, 111–124.
- Sigrist, C.J.A., Castro, E. de, Cerutti, L., Cuche, B.A., Hulo, N., Bridge, A., Bougueleret, L. and Xenarios, I.** (2013) New and continuing developments at PROSITE. *Nucleic Acids Res.*, **41**, D344–347.
- Söderman, E., Mattsson, J. and Engström, P.** (1996) The *Arabidopsis* homeobox gene ATHB-7 is induced by water deficit and by abscisic acid. *Plant J. Cell Mol. Biol.*, **10**, 375–381.
- Somssich, M., Khan, G.A. and Persson, S.** (2016) Cell Wall Heterogeneity in Root Development of *Arabidopsis*. *Front. Plant Sci.*, **7**, 1242.
- Song, Y., Liu, L., Wang, Y., Valkenburg, D.-J., Zhang, X., Zhu, L. and Thomma, B.P.H.J.** (2018) Transfer of tomato immune receptor Ve1 confers Ave1-dependent *Verticillium* resistance in tobacco and cotton. *Plant Biotechnol. J.*, **16**, 638–648.
- Song, Y., Zhang, Z., Boshoven, J., et al.** (2017) Tomato immune receptor Ve1 recognizes surface-exposed co-localized N- and C-termini of *Verticillium dahliae* effector Ave1. *bioRxiv*, doi: 10.1101/103473 [Epub ahead of print].

- Spoel, S.H., Koornneef, A., Claessens, S.M.C., et al.** (2003) NPR1 modulates cross-talk between salicylate- and jasmonate-dependent defense pathways through a novel function in the cytosol. *Plant Cell*, **15**, 760–770.
- Stark, C.** (1961) Das Auftreten der Verticillium-Tracheomykosen in Hamburger Gartenbaukulturen. *Gartenbauwissenschaft*, **26**, 493–528.
- Stergiopoulos, I. and Wit, P.J.G.M. de** (2009) Fungal effector proteins. *Annu. Rev. Phytopathol.*, **47**, 233–263.
- Strawn, M.A., Marr, S.K., Inoue, K., Inada, N., Zubieta, C. and Wildermuth, M.C.** (2007) Arabidopsis isochorismate synthase functional in pathogen-induced salicylate biosynthesis exhibits properties consistent with a role in diverse stress responses. *J. Biol. Chem.*, **282**, 5919–5933.
- Suzuki, M., Shibuya, M., Shimada, H., et al.** (2016) Autophosphorylation of Specific Threonine and Tyrosine Residues in Arabidopsis CERK1 is Essential for the Activation of Chitin-Induced Immune Signaling. *Plant Cell Physiol.*, **57**, 2312–2322.
- Swamy, P.M. and Smith, B.N.** (1999) Role of abscisic acid in plant stress tolerance. *Curr. Sci.*, **76**, 1220–1227.
- Talboys, P.W.** (1958) Association of tylosis and hyperplasia of the xylem with vascular invasion of the hop by *Verticillium albo-atrum*. *Trans. Br. Mycol. Soc.*, **41**, 249–260.
- Tanaka, Y., Sano, T., Tamaoki, M., Nakajima, N., Kondo, N. and Hasezawa, S.** (2006) Cytokinin and auxin inhibit abscisic acid-induced stomatal closure by enhancing ethylene production in Arabidopsis. *J. Exp. Bot.*, **57**, 2259–2266.
- Tao, Y., Xie, Z., Chen, W., Glazebrook, J., Chang, H.-S., Han, B., Zhu, T., Zou, G. and Katagiri, F.** (2003) Quantitative nature of Arabidopsis responses during compatible and incompatible interactions with the bacterial pathogen *Pseudomonas syringae*. *Plant Cell*, **15**, 317–330.
- Tappe, H.** (2008) *Verticillium longisporum* induced gene expression in Arabidopsis thaliana (PhD Thesis). Retrieved from <http://hdl.handle.net/11858/00-1735-0000-0006-B643-B>.
- Thatcher, L.F., Gardiner, D.M., Kazan, K. and Manners, J.M.** (2012) A highly conserved effector in *Fusarium oxysporum* is required for full virulence on Arabidopsis. *Mol. Plant-Microbe Interact. MPMI*, **25**, 180–190.
- Thatcher, L.F., Manners, J.M. and Kazan, K.** (2009) *Fusarium oxysporum* hijacks COI1-mediated jasmonate signaling to promote disease development in Arabidopsis. *Plant J. Cell Mol. Biol.*, **58**, 927–939.
- Thatcher, L.F., Powell, J.J., Aitken, E.A.B., Kazan, K. and Manners, J.M.** (2012) The lateral organ boundaries domain transcription factor LBD20 functions in *Fusarium* wilt Susceptibility and jasmonate signaling in Arabidopsis. *Plant Physiol.*, **160**, 407–418.
- Thimm, O., Bläsing, O., Gibon, Y., et al.** (2004) MAPMAN: a user-driven tool to display genomics data sets onto diagrams of metabolic pathways and other biological processes. *Plant J. Cell Mol. Biol.*, **37**, 914–939.
- Thines, B., Katsir, L., Melotto, M., et al.** (2007) JAZ repressor proteins are targets of the SCF(COI1) complex during jasmonate signalling. *Nature*, **448**, 661–665.
- Thole, K.** (2016) Towards the identification of *Verticillium* effector molecules involved in host plant developmental reprogramming (PhD thesis). Retrieved from <http://hdl.handle.net/11858/00-1735-0000-0028-8762-5>.
- Thompson, J.D., Higgins, D.G. and Gibson, T.J.** (1994) CLUSTAL W: improving the sensitivity of progressive multiple sequence alignment through sequence weighting, position-specific gap penalties and weight matrix choice. *Nucleic Acids Res.*, **22**, 4673–4680.
- Tjamos, S.E., Flemetakis, E., Paplomatas, E.J. and Katinakis, P.** (2005) Induction of resistance to *Verticillium dahliae* in Arabidopsis thaliana by the biocontrol agent K-165 and pathogenesis-related proteins gene expression. *Mol. Plant-Microbe Interact. MPMI*, **18**, 555–561.
- Ton, J., Flors, V. and Mauch-Mani, B.** (2009) The multifaceted role of ABA in disease resistance. *Trends Plant Sci.*, **14**, 310–317.
- Tordai, H., Bányai, L. and Patthy, L.** (1999) The PAN module: the N-terminal domains of plasminogen and hepatocyte growth factor are homologous with the apple domains of the prekallikrein family and with a novel domain found in numerous nematode proteins. *FEBS Lett.*, **461**, 63–67.
- Torres Zabala, M. de, Bennett, M.H., Truman, W.H. and Grant, M.R.** (2009) Antagonism between salicylic acid and abscisic acid reflects early host-pathogen conflict and moulds plant defence responses. *Plant J. Cell Mol. Biol.*, **59**, 375–386.
- Torres-Zabala, M. de, Truman, W., Bennett, M.H., Lafforgue, G., Mansfield, J.W., Rodriguez Egea, P., Bögre, L. and Grant, M.** (2007) *Pseudomonas syringae* pv. tomato hijacks the Arabidopsis abscisic acid signalling pathway to cause disease. *EMBO J.*, **26**, 1434–1443.

- Toruño, T.Y., Stergiopoulos, I. and Coaker, G.** (2016) Plant-Pathogen Effectors: Cellular Probes Interfering with Plant Defenses in Spatial and Temporal Manners. *Annu. Rev. Phytopathol.*, **54**, 419–441.
- Toufighi, K., Brady, S.M., Austin, R., Ly, E. and Provart, N.J.** (2005) The Botany Array Resource: e-Northern, Expression Angling, and promoter analyses. *Plant J. Cell Mol. Biol.*, **43**, 153–163.
- Tripathi, V., Parasuraman, B., Laxmi, A. and Chattopadhyay, D.** (2009) CIPK6, a CBL-interacting protein kinase is required for development and salt tolerance in plants. *Plant J. Cell Mol. Biol.*, **58**, 778–790.
- Trusov, Y., Sewelam, N., Rookes, J.E., Kunkel, M., Nowak, E., Schenk, P.M. and Botella, J.R.** (2009) Heterotrimeric G proteins-mediated resistance to necrotrophic pathogens includes mechanisms independent of salicylic acid-, jasmonic acid/ethylene- and abscisic acid-mediated defense signaling. *Plant J. Cell Mol. Biol.*, **58**, 69–81.
- Tsou, P.-L., Lee, S.Y., Allen, N.S., Winter-Sederoff, H. and Robertson, D.** (2012) An ER-targeted calcium-binding peptide confers salt and drought tolerance mediated by CIPK6 in Arabidopsis. *Planta*, **235**, 539–552.
- Tuteja, N.** (2007) Abscisic Acid and Abiotic Stress Signaling. *Plant Signal. Behav.*, **2**, 135–138.
- Ulker, B., Peiter, E., Dixon, D.P., et al.** (2008) Getting the most out of publicly available T-DNA insertion lines. *Plant J. Cell Mol. Biol.*, **56**, 665–677.
- Umezawa, T., Nakashima, K., Miyakawa, T., Kuromori, T., Tanokura, M., Shinozaki, K. and Yamaguchi-Shinozaki, K.** (2010) Molecular basis of the core regulatory network in ABA responses: sensing, signaling and transport. *Plant Cell Physiol.*, **51**, 1821–1839.
- Umezawa, T., Sugiyama, N., Mizoguchi, M., Hayashi, S., Myouga, F., Yamaguchi-Shinozaki, K., Ishihama, Y., Hirayama, T. and Shinozaki, K.** (2009) Type 2C protein phosphatases directly regulate abscisic acid-activated protein kinases in Arabidopsis. *Proc. Natl. Acad. Sci. U. S. A.*, **106**, 17588–17593.
- Van Damme, E., Lannoo, N. and Peumans, W.** (2008) Plant lectins. *Adv. Bot. Res. Inc. Adv. PLANT Pathol.*, **48**, 107–209.
- VanderMolen, G.E., Labavitch, J.M. and DeVay, J.E.** (1986) Fusarium-induced vascular gels from banana roots — a partial chemical characterization. *Physiol. Plant.*, **66**, 298–302.
- VanderMolen, G.E., Labavitch, J.M., Strand, L.L. and DeVay, J.E.** (1983) Pathogen-induced vascular gels: Ethylene as a host intermediate. *Physiol. Plant.*, **59**, 573–580.
- Verberne, M.C., Verpoorte, R., Bol, J.F., Mercado-Blanco, J. and Linthorst, H.J.** (2000) Overproduction of salicylic acid in plants by bacterial transgenes enhances pathogen resistance. *Nat. Biotechnol.*, **18**, 779–783.
- Vilches-Barro, A. and Maizel, A.** (2015) Talking through walls: mechanisms of lateral root emergence in Arabidopsis thaliana. *Curr. Opin. Plant Biol.*, **23**, 31–38.
- Vlad, F., Rubio, S., Rodrigues, A., et al.** (2009) Protein phosphatases 2C regulate the activation of the Snf1-related kinase OST1 by abscisic acid in Arabidopsis. *Plant Cell*, **21**, 3170–3184.
- Vlot, A.C., Dempsey, D.A. and Klessig, D.F.** (2009) Salicylic Acid, a multifaceted hormone to combat disease. *Annu. Rev. Phytopathol.*, **47**, 177–206.
- Wan, J., Zhang, X.-C., Neece, D., Ramonell, K.M., Clough, S., Kim, S.-Y., Stacey, M.G. and Stacey, G.** (2008) A LysM receptor-like kinase plays a critical role in chitin signaling and fungal resistance in Arabidopsis. *Plant Cell*, **20**, 471–481.
- Wang, J.-Y., Cai, Y., Gou, J.-Y., Mao, Y.-B., Xu, Y.-H., Jiang, W.-H. and Chen, X.-Y.** (2004) VdNEP, an Elicitor from *Verticillium dahliae*, Induces Cotton Plant Wilting. *Appl. Environ. Microbiol.*, **70**, 4989–4995.
- Wang, Y.H.** (2008) How effective is T-DNA insertional mutagenesis in Arabidopsis? *J. Biochem. Tech.*, **1**, 11–20.
- Wasilewska, A., Vlad, F., Sirichandra, C., Redko, Y., Jammes, F., Valon, C., Frei dit Frey, N. and Leung, J.** (2008) An update on abscisic acid signaling in plants and more.. *Mol. Plant*, **1**, 198–217.
- Wiermer, M., Feys, B.J. and Parker, J.E.** (2005) Plant immunity: the EDS1 regulatory node. *Curr. Opin. Plant Biol.*, **8**, 383–389.
- Wiermer, M., Germain, H., Cheng, Y.T., García, A.V., Parker, J.E. and Li, X.** (2010) Nucleoporin MOS7/Nup88 contributes to plant immunity and nuclear accumulation of defense regulators. *Nucl. Austin Tex*, **1**, 332–336.
- Wiese, M.V. and Devay, J.E.** (1970) Growth Regulator Changes in Cotton Associated with Defoliation Caused by *Verticillium albo-atrum*1. *Plant Physiol.*, **45**, 304–309.
- Wildermuth, M.C., Dewdney, J., Wu, G. and Ausubel, F.M.** (2001) Isochorismate synthase is required to synthesize salicylic acid for plant defence. *Nature*, **414**, 562–565.

- Wilhelm, S.** (1955) Longevity of the *Verticillium* wilt fungus in the laboratory and field. *Phytopathology*, **45**, 180-181.
- Winter, D., Vinegar, B., Nahal, H., Ammar, R., Wilson, G.V. and Provart, N.J.** (2007) An “Electronic Fluorescent Pictograph” Browser for Exploring and Analyzing Large-Scale Biological Data Sets. *PLoS ONE*, **2**, e718.
- Wulff, B.B.H., Chakrabarti, A. and Jones, D.A.** (2009) Recognition specificity and evolution in the tomato-*Cladosporium fulvum* pathosystem. *Mol. Plant-Microbe Interact. MPMI*, **22**, 1191–1202.
- Xie, M., He, Y. and Gan, S.** (2001) Bidirectionalization of polar promoters in plants. *Nat. Biotechnol.*, **19**, 677-679.
- Xiong, L., Schumaker, K.S. and Zhu, J.-K.** (2002) Cell signaling during cold, drought, and salt stress. *Plant Cell*, **14**, 165-183.
- Xu, J., Wang, G., Wang, J., Li, Y., Tian, L., Wang, X. and Guo, W.** (2017) The lysin motif-containing proteins, Lyp1, Lyk7 and LysMe3, play important roles in chitin perception and defense against *Verticillium dahliae* in cotton. *BMC Plant Biol.*, **17**, 148.
- Xu, Y., Hu, W., Liu, J., Zhang, J., Jia, C., Miao, H., Xu, B. and Jin, Z.** (2014) A banana aquaporin gene, MaPIP1;1, is involved in tolerance to drought and salt stresses. *BMC Plant Biol.*, **14**, 59.
- Yadeta, K.A. and J Thomma, B.P.H.** (2013) The xylem as battleground for plant hosts and vascular wilt pathogens. *Front. Plant Sci.*, **4**, 97.
- Yamaguchi-Shinozaki, K. and Shinozaki, K.** (1993) Characterization of the expression of a desiccation-responsive rd29 gene of *Arabidopsis thaliana* and analysis of its promoter in transgenic plants. *Mol. Gen. Genet. MGG*, **236**, 331–340.
- Yang, B., Sugio, A. and White, F.F.** (2006) Os8N3 is a host disease-susceptibility gene for bacterial blight of rice. *Proc. Natl. Acad. Sci. U. S. A.*, **103**, 10503–10508.
- Yang, Y., Costa, A., Leonhardt, N., Siegel, R.S. and Schroeder, J.I.** (2008) Isolation of a strong *Arabidopsis* guard cell promoter and its potential as a research tool. *Plant Methods*, **4**, 6.
- Yasuda, M., Ishikawa, A., Jikumaru, Y., et al.** (2008) Antagonistic interaction between systemic acquired resistance and the abscisic acid-mediated abiotic stress response in *Arabidopsis*. *Plant Cell*, **20**, 1678–1692.
- Zander, M., Chen, S., Imkampe, J., Thurow, C. and Gatz, C.** (2012) Repression of the *Arabidopsis thaliana* jasmonic acid/ethylene-induced defense pathway by TGA-interacting glutaredoxins depends on their C-terminal ALWL motif. *Mol. Plant*, **5**, 831–840.
- Zhang, Y., Goritschnig, S., Dong, X. and Li, X.** (2003) A gain-of-function mutation in a plant disease resistance gene leads to constitutive activation of downstream signal transduction pathways in suppressor of npr1-1, constitutive 1. *Plant Cell*, **15**, 2636–2646.
- Zhou, B.-J., Jia, P.-S., Gao, F. and Guo, H.-S.** (2012) Molecular characterization and functional analysis of a necrosis- and ethylene-inducing, protein-encoding gene family from *Verticillium dahliae*. *Mol. Plant-Microbe Interact. MPMI*, **25**, 964–975.
- Zhou, S., Hu, W., Deng, X., et al.** (2012) Overexpression of the wheat aquaporin gene, TaAQP7, enhances drought tolerance in transgenic tobacco. *PloS One*, **7**, e52439.
- Zhuang, L., Liu, M., Yuan, X., Yang, Z. and Huang, B.** (2015) Physiological Effects of Aquaporin in Regulating Drought Tolerance through Overexpressing of *Festuca arundinacea* Aquaporin Gene FaPIP2;1. *J. Am. Soc. Hortic. Sci.*, **140**, 404–412.
- Zipfel, C.** (2009) Early molecular events in PAMP-triggered immunity. *Curr. Opin. Plant Biol.*, **12**, 414–420.
- Zipfel, C., Kunze, G., Chinchilla, D., Caniard, A., Jones, J.D.G., Boller, T. and Felix, G.** (2006) Perception of the bacterial PAMP EF-Tu by the receptor EFR restricts *Agrobacterium*-mediated transformation. *Cell*, **125**, 749–760.

6. Supplemental Material

Table S1. Significantly transcriptionally regulated *Arabidopsis thaliana* (At) genes 4 days post infection (dpi) with *Verticillium* isolates of the chlorosis group. Differential gene expression was analysed using RobiNA v1.2.4 (Lohse *et al.*, 2012) and the DESeq analysis method (Anders and Huber, 2010) between samples of the chlorosis group versus wilting group and mock treatment. Raw P-values were adjusted using the False Discovery Rate algorithm (Benjamini and Hochberg, 1995). Only differentially expressed genes below a cut-off of $FDR \leq 0.05$ and a \log_2 fold (L2F) change in expression $\geq +1$ and ≤ -1 at 4 dpi are shown.

At gene ID	4 dpi (At)	Description	Functions in
At2g37180	1.6	PIP2;3 (PLASMA MEMBRANE INTRINSIC PROTEIN 2C)	transport (water)
At2g38465	-1.3	UNKNOWN PROTEIN	unknown

Table S2. Significantly transcriptionally regulated *Arabidopsis thaliana* (At) genes 4 days post infection (dpi) with *Verticillium* isolates of the wilting group. Differential gene expression was analysed using RobiNA v1.2.4 (Lohse *et al.*, 2012) and the DESeq analysis method (Anders and Huber, 2010) between samples of the wilting group versus chlorosis group and mock treatment. Raw P-values were adjusted using the False Discovery Rate algorithm (Benjamini and Hochberg, 1995). Only differentially expressed genes below a cut-off of $FDR \leq 0.05$ and a \log_2 fold (L2F) change in expression ≥ 1 and ≤ -1 at 4 dpi are shown.

At gene ID	4 dpi (At)	Description	Functions in
At2g23030	2.2	SNRK2.9 (SNF1-RELATED PROTEIN KINASE 2.9), osmotic stress response	drought response
At2g36270	1.3	ABI5 (ABA INSENSITIVE 5), transcription factor involved in ABA signal transduction	hormone-aba
At5g64940	-2.3	OSA1 (OXIDATIVE STRESS-RELATED ABC1-LIKE PROTEIN 1)	lipid (transport)
At2g30660	1.5	ATP-DEPENDENT CASEINOLYTIC (CLP) PROTEASE/CROTONASE FAMILY PROTEIN	protease
At3g24310	2.1	MYB305 (MYB DOMAIN PROTEIN 305)	transcription factor
At3g26740	1.8	CCL (CCR-LIKE)	unknown
At4g11211	-1.1	UNKNOWN PROTEIN	unknown

Table S3. Significantly transcriptionally regulated *Nicotiana benthamiana* (Nb) genes 8 days post infection (dpi) with *Verticillium* isolates of the chlorosis group. Differential gene expression was analysed using RobiNA v1.2.4 (Lohse *et al.*, 2012) and the DESeq analysis method (Anders and Huber, 2010) between samples of the chlorosis group versus wilting group and mock treatment. Raw P-values were adjusted using the False Discovery Rate algorithm (Benjamini and Hochberg, 1995). Only differentially expressed genes below a cut-off of $FDR \leq 0.05$ and a \log_2 fold (L2F) change in expression ≥ 1 at 8 dpi are shown. L2F change in expression at 4, 12 and 16 dpi is included.

Nb gene ID	At homolog	4 dpi (At)	8 dpi (Nb)	12 dpi (Nb)	16 dpi (Nb)	Description of At homolog	Functions in
NbS00023022g0012	At1g02460	0.6	6.0	5.6	4.1	POLYGALACTURONASE (PECTINASE) FAMILY PROTEIN	cell wall
NbS00016770g0012	At1g02460	0.6	5.5	6.3	4.0	POLYGALACTURONASE (PECTINASE) FAMILY PROTEIN	cell wall
NbS00032620g0003	At5g05340	0.2	4.7	4.7	4.3	PEROXIDASE (LIGNIN BIOSYNTHESIS)	cell wall/lignin
NbS00045980g0002	At3g03480	#N/A	3.7	3.7	3.0	CHAT (ACETYL COA:(Z)-3-HEXEN-1-OL ACETYLTRANSFERASE)	defence (mechanical and herbivore damage)
NbS00002591g0012	At1g08800	0.2	2.6	2.3	2.2	MYOB1 (MYOSIN BINDING PROTEIN 1)	defence
NbS00007540g0014	At5g55540	0.0	1.8	1.8	2.0	TRN1 (TORNADO 1)	development
NbS00030850g0009	At1g65800	-0.4	1.6	1.4	1.2	ARK2 (A. THALIANA RECEPTOR KINASE 2)	development
NbS00003501g0001	At3g14080	-0.1	4.1	3.5	3.6	LSM1B, SMALL NUCLEAR RIBONUCLEOPROTEIN FAMILY PROTEIN	drought / salt / low temperature
NbC25873455g0003	At1g20440	-0.3	5.5	5.6	5.5	RD17; COR47 (COLD-REGULATED 47) (DEHYDRIN)	drought response
NbS00012878g0008	At2g20880	0.6	2.4	2.4	2.0	ERF53, AP2 DOMAIN-CONTAINING TRANSCRIPTION FACTOR	drought response
NbS00058252g0004	At1g20510	0.2	1.6	2.2	1.5	OPCL1 (OPC-8:0 COA LIGASE1)	hormone-ja biosynthesis
NbS00023610g0002	At3g12120	-0.2	1.9	1.7	1.4	FAD2 (FATTY ACID DESATURASE 2), SYNTHESIS OF 18:2 FATTY ACIDS	lipid
NbS00002660g0010	At5g24080	1.6	4.0	4.8	5.4	PROTEIN KINASE FAMILY PROTEIN	signalling
NbS00017948g0005	At1g71930	0.0	2.7	2.8	1.9	VND7 (VASCULAR RELATED NAC-DOMAIN PROTEIN 7)	transdifferentiation
NbS00043163g0001	At4g23030	0.1	3.7	4.8	2.6	MATE EFFLUX PROTEIN-RELATED	transport
NbS00022345g0006	At1g59740	0.7	2.8	2.5	2.0	PROTON-DEPENDENT OLIGOPEPTIDE TRANSPORT (POT) FAMILY PROTEIN	transport (peptide)
NbS00007456g0005	At3g53420	0.4	4.7	5.7	4.7	PIP2;1 (PLASMA MEMBRANE INTRINSIC PROTEIN 2A)	transport (water)
NbS00018173g0011	At3g53420	0.4	4.7	5.2	4.9	PIP2;1 (PLASMA MEMBRANE INTRINSIC PROTEIN 2A)	transport (water)
NbS00041805g0002	At4g17340	-0.1	4.3	5.1	4.9	TIP2;2 (TONOPLAST INTRINSIC PROTEIN 2;2)	transport (water)
NbS00014942g0007	At4g01470	0.1	3.5	3.5	3.0	TIP1;3 (TONOPLAST INTRINSIC PROTEIN 1;3)	transport (water)
NbS00002057g0008	At4g01470	0.1	3.4	3.7	3.4	TIP1;3 (TONOPLAST INTRINSIC PROTEIN 1;3)	transport (water)
NbS00046028g0001	At2g37170	0.4	2.0	2.0	2.1	PIP2;2 (PLASMA MEMBRANE INTRINSIC PROTEIN 2)	transport (water)
NbS00031588g0009	At2g38640	0.4	3.3	3.3	3.0	UNKNOWN PROTEIN	unknown
NbS00028121g0001	At3g52820	0.0	2.4	2.2	2.7	PAP22 (PURPLE ACID PHOSPHATASE 22), METALLO-PHOSPHOESTERASE	unknown

Table S4. Significantly transcriptionally regulated *Nicotiana benthamiana* (Nb) genes 12 days post infection (dpi) with *Verticillium* isolates of the chlorosis group. Differential gene expression was analysed using RobiNA v1.2.4 (Lohse *et al.*, 2012) and the DESeq analysis method (Anders and Huber, 2010) between samples of the chlorosis group versus wilting group and mock treatment. Raw P-values were adjusted using the False Discovery Rate algorithm (Benjamini and Hochberg, 1995). Only differentially expressed genes below a cut-off of FDR \leq 0.05 and a log₂ fold (L2F) change in expression \geq 1 at 12 dpi are shown. L2F change in expression at 4, 8 and 16 dpi is included.

Nb gene ID	At homolog	4 dpi (At)	8 dpi (Nb)	12 dpi (Nb)	16 dpi (Nb)	Description of At homolog	Functions in
NbS00022106g0001	At5g40390	0.6	2.8	5.0	4.9	SIP1 (SEED IMBIBITION 1-LIKE), GALACTINOL-SUCROSE GALACTOSYLTRANSFERASE/ HYDROLASE, hydrolyses O-glycosyl compounds	cold stress
NbS00009480g0003	At5g36970	0.3	3.2	5.0	6.2	NHL25 (NDR1/HIN1-LIKE 25)	defence
NbS00061891g0005	At1g68290	0.2	3.4	3.9	4.4	ENDO 2 (ENDONUCLEASE 2), cleaves RNA, ssDNA, and dsDNA, with a substrate preference for ssDNA and RNA	endonuclease
NbS00057548g0005	At1g69850	-0.2	2.1	3.4	2.4	ATNRT1:2 (ARABIDOPSIS THALIANA NITRATE TRANSPORTER 1:2), also acts as an ABA importer	hormone-aba
NbS00042717g0004	At1g17140	-0.1	1.0	1.6	2.1	ICR1, Small GTPase ROP interactor and polarity regulator scaffold protein	hormone-auxin
NbS00054082g0004	At3g22600	0.1	4.7	8.1	11.5	LTPG5, GLYCOSYLPHOSPHATIDYLINOSITOL-ANCHORED LIPID PROTEIN TRANSFER 5,	lipid
NbS00002660g0010	At5g24080	1.6	4.0	4.8	5.4	PROTEIN KINASE FAMILY PROTEIN	signalling
NbS00034147g0011	At4g17980	0.2	2.7	3.8	2.3	ANAC071 (ARABIDOPSIS NAC DOMAIN CONTAINING PROTEIN 71)	transdifferentiation (tissue reunion)
NbS00018173g0011	At3g53420	0.4	4.7	5.2	4.9	PIP2;1 (PLASMA MEMBRANE INTRINSIC PROTEIN 2A)	transport (water)

Table S5. Significantly transcriptionally regulated *Nicotiana benthamiana* (*Nb*) genes 12 days post infection (dpi) with *Verticillium* isolates of the **wilting group.** Differential gene expression was analysed using *RobiNA* v1.2.4 (Lohse *et al.*, 2012) and the DESeq analysis method (Anders and Huber, 2010) between samples of the **wilting** group versus **chlorosis** group and **mock** treatment. Raw P-values were adjusted using the False Discovery Rate algorithm (Benjamini and Hochberg, 1995). Only differentially expressed genes below a cut-off of $FDR \leq 0.05$ and a \log_2 fold (L2F) change in expression ≥ 1 at 12 dpi are shown. L2F change in expression at 4, 8 and 16 dpi is included.

<i>Nb</i> gene ID	<i>At</i> homolog	4 dpi (<i>At</i>)	8 dpi (<i>Nb</i>)	12 dpi (<i>Nb</i>)	16 dpi (<i>Nb</i>)	Description of <i>At</i> homolog	Functions in
<i>NbS00002008g0007</i>	<i>At4g17030</i>	0.5	2.9	2.9	2.6	ATEXLB1 (ARABIDOPSIS THALIANA EXPANSIN-LIKE B1)	cell wall
<i>NbS00044506g0005</i>	<i>At4g17030</i>	0.5	3.8	2.6	1.7	ATEXLB1 (ARABIDOPSIS THALIANA EXPANSIN-LIKE B1)	cell wall
<i>NbS00032861g0003</i>	<i>At5g19040</i>	-0.2	3.4	4.2	3.1	IPT5 (ISOPENTENYLTRANSFERASE 5), cytokinin biosynthesis	hormone-cytokinin
<i>NbS00032364g0006</i>	<i>At5g12840</i>	-0.1	3.1	3.9	1.3	NF-YA1 (NUCLEAR FACTOR Y, SUBUNIT A1)	hormone-ABA
<i>NbS00032479g0003</i>	<i>At2g46680</i>	0.4	5.6	3.7	3.8	ATHB-7 (ARABIDOPSIS THALIANA HOMEBOX 7)	hormone-ABA
<i>NbS00056128g0003</i>	<i>At1g15740</i>	0.0	3.8	3.9	2.0	LEUCINE-RICH REPEAT FAMILY PROTEIN	LRR
<i>NbS00028352g0006</i>	<i>At2g47770</i>	-2.0	5.0	4.3	3.3	TSPO (OUTER MEMBRANE TRYPTOPHAN-RICH SENSORY PROTEIN)-RELATED	stress response
<i>NbS00037398g0011</i>	<i>At2g03590</i>	-0.2	3.5	4.4	1.8	ATUPS1 (ARABIDOPSIS THALIANA UREIDE PERMEASE 1)	transport (nucleotide)
<i>NbS00023055g0006</i>	<i>At5g53190</i>	Inf	1.9	2.5	2.2	SWEET3, bidirectional sugar transporter, phloem loading	transport (sugar)

Table S6. Significantly transcriptionally regulated *Nicotiana benthamiana* (Nb) genes 16 days post infection (dpi) with *Verticillium* isolates of the chlorosis group. Differential gene expression was analysed using RobiNA v1.2.4 (Lohse *et al.*, 2012) and the DESeq analysis method (Anders and Huber, 2010) between samples of the chlorosis group versus wilting group and mock treatment. Raw P-values were adjusted using the False Discovery Rate algorithm (Benjamini and Hochberg, 1995). Only differentially expressed genes below a cut-off of FDR \leq 0.05 and a log2 fold (L2F) change in expression \geq +4 and \leq -1 at 16 dpi are shown. L2F change in expression at 4, 8 and 12 dpi is included.

Nb gene ID	At homolog	4 dpi (At)	8 dpi (Nb)	12 dpi (Nb)	16 dpi (Nb)	Description of At homolog	Function
NbS00058524g0002	At5g41040	-0.2	2.7	5.4	6.8	RWP1, Encodes a feruloyl-CoA transferase required for suberin synthesis	casparian strip
NbS00032044g0012	At5g41040	-0.2	1.5	4.1	6.0	RWP1, Encodes a feruloyl-CoA transferase required for suberin synthesis	casparian strip
NbS00019447g0006	At4g03540	0.1	2.3	5.5	6.7	CASPIAN STRIP MEMBRANE DOMAIN PROTEIN (CASP) -LIKE PROTEIN	casparian strip
NbS00015813g0014	At5g44550	0.0	1.4	6.4	6.6	CASPIAN STRIP MEMBRANE DOMAIN PROTEIN (CASP) -LIKE PROTEIN	casparian strip
NbS00043958g0005	At3g18400	-0.1	1.3	4.9	6.4	ANAC058 (ARABIDOPSIS NAC DOMAIN CONTAINING PROTEIN 58)	casparian strip
NbS00002771g0004	At3g11430	0.0	1.3	4.3	6.3	GPAT5 (GLYCEROL-3-PHOSPHATE ACYLTRANSFERASE 5)	casparian strip
NbS00030724g0011	At2g39350	0.3	2.1	4.3	5.6	ABC TRANSPORTER FAMILY PROTEIN	casparian strip
NbS00026515g0010	At5g23190	-0.1	1.1	3.7	5.5	CYP86B1	casparian strip
NbS00017339g0006	At2g21610	-0.3	1.9	3.2	6.7	ATPE11, PECTINESTERASE FAMILY PROTEIN	cell wall
NbS00039987g0002	At5g64620	-0.2	-0.7	-1.6	-2.2	C/VIF2 (CELL WALL / VACUOLAR INHIBITOR OF FRUCTOSIDASE 2), repression leads higher levels of cellulose	cell wall
NbS00016770g0012	At1g02460	0.6	5.5	6.3	4.0	GLYCOSIDE HYDROLASE FAMILY 28 PROTEIN	cell wall/lignin
NbS00012729g0001	At1g50060	-0.6	0.0	-2.9	-4.8	PUTATIVE PATHOGENESIS-RELATED PROTEIN	defence
NbS00019641g0010	At5g09530	0.0	2.4	4.7	5.8	PELPK1, Positive regulator of germination	development
NbS00035999g0011	At1g14350	-0.1	-0.1	-0.4	-2.0	FLP (FOUR LIPS), MYB124	development
NbS00025091g0003	At4g37650	0.0	0.3	-0.9	-2.2	SHR (SHORT ROOT), SGR7	development
NbC25873455g0003	At1g20440	-0.3	5.5	5.6	5.5	RD17; COR47 (COLD-REGULATED 47) (dehydrin)	drought response
NbS00054082g0004	At3g22600	0.1	4.7	8.1	11.5	LTP, GLYCOSYLPHOSPHATIDYLINOSITOL-ANCHORED LIPID PROTEIN TRANSFER 5, LTPG5	lipid
NbS00054634g0001	At3g22600	0.1	7.5	8.9	11.1	LTP, GLYCOSYLPHOSPHATIDYLINOSITOL-ANCHORED LIPID PROTEIN TRANSFER 5, LTPG5	lipid
NbS00002528g0007	At3g22600	0.1	2.7	5.4	6.5	LTP, GLYCOSYLPHOSPHATIDYLINOSITOL-ANCHORED LIPID PROTEIN TRANSFER 5, LTPG5	lipid
NbS00007575g0012	At5g13900	0.0	3.4	6.2	7.2	LTP	lipid
NbS00011950g0007	At2g48140	0.0	2.9	5.1	6.4	LTP	lipid
NbS00031491g0009	At2g23540	-0.2	2.0	5.1	6.4	GDSL-MOTIF ESTERASE/ACYLTRANSFERASE/LIPASE	lipid
NbS00008258g0002	At4g33790	-0.2	2.2	4.6	6.5	CER4 (ECERIFERUM 4), G7, FAR3, fatty acyl-CoA reductase	lipid/cuticular wax

Table S6 continued.

<i>Nb</i> gene ID	<i>At</i> homolog	4 dpi (<i>At</i>)	8 dpi (<i>Nb</i>)	12 dpi (<i>Nb</i>)	16 dpi (<i>Nb</i>)	Description of <i>At</i> homolog	Functions in
<i>NbS00024104g0004</i>	<i>At5g19410</i>	0.0	1.6	4.1	6.4	ABC TRANSPORTER FAMILY PROTEIN	lipid (transport)
<i>NbS00026617g0028</i>	<i>At5g64330</i>	0.1	-0.5	-0.6	-1.2	NPH3 (NON-PHOTOTROPIC HYPOCOTYL 3)	phototropism
<i>NbS00011113g0005</i>	<i>At4g08950</i>	-0.1	-1.0	-0.7	-2.1	EXO (EXORDIUM), loss of function results in diminished leaf, root growth and reduced biomass	stunting
<i>NbS00000844g0011</i>	<i>At1g09850</i>	0.0	0.0	-0.3	-2.1	XBCP3 (XYLEM BARK CYSTEINE PEPTIDASE 3)	transdifferentiation
<i>NbS00018173g0011</i>	<i>At3g53420</i>	0.4	4.7	5.2	4.9	PIP2;1 (PLASMA MEMBRANE INTRINSIC PROTEIN 2A)	transport (water)

Table S7. Significantly transcriptionally regulated *Nicotiana benthamiana* (*Nb*) genes 16 days post infection (dpi) with *Verticillium* isolates of the wilting group. Differential gene expression was analysed using RobiNA v1.2.4 (Lohse *et al.*, 2012) and the DESeq analysis method (Anders and Huber, 2010) between samples of the wilting group versus chlorosis group and mock treatment. Raw P-values were adjusted using the False Discovery Rate algorithm (Benjamini and Hochberg, 1995). Only differentially expressed genes below a cut-off of $FDR \leq 0.05$ and a log₂ fold (L2F) change in expression ≥ 1 at 16 dpi are shown. L2F change in expression at 4, 8 and 12 dpi is included.

<i>Nb</i> gene ID	<i>At</i> homolog	4 dpi (<i>At</i>)	8 dpi (<i>Nb</i>)	12 dpi (<i>Nb</i>)	16 dpi (<i>Nb</i>)	Description of <i>At</i> homolog	Functions in
<i>NbS00002008g0007</i>	<i>At4g17030</i>	0.5	2.9	2.9	2.6	ATEXLB1 (ARABIDOPSIS THALIANA EXPANSIN-LIKE B1)	cell wall
<i>NbS00012729g0001</i>	<i>At1g50060</i>	-0.3	1.0	4.1	6.1	PUTATIVE PATHOGENESIS-RELATED PROTEIN	defence
<i>NbS00032479g0003</i>	<i>At2g46680</i>	0.4	5.6	3.7	3.8	ATHB-7 (ARABIDOPSIS THALIANA HOMEBOX 7)	hormone-ABA
<i>NbS00032861g0003</i>	<i>At5g19040</i>	-0.2	3.4	4.2	3.1	IPT5 (ISOPENTENYLTRANSFERASE 5), cytokinin biosynthesis	hormone-cytokinin

Table S8. Significantly transcriptionally regulated *Nicotiana benthamiana* (Nb) genes at 8, 12 and 16 days post infection (dpi) with *Verticillium* isolates of the chlorosis group. Raw RNA-read counts were of 8, 12 and 16 dpi samples were added. Subsequently, differential gene expression was analysed using RobiNA v1.2.4 (Lohse *et al.*, 2012) and the DESeq analysis method (Anders and Huber, 2010) between samples of the chlorosis group versus wilting group and mock treatment. Raw P-values were adjusted using the False Discovery Rate algorithm (Benjamini and Hochberg, 1995). Only differentially expressed genes below a cut-off of FDR \leq 0.05 and a log2 fold (L2F) change in expression \geq +4 and \leq -1 in 8+12+16 dpi dataset shown. L2F change in expression at 4, 8, 12 and 16 dpi is included.

Nb gene ID	At homolog	8+12+16 dpi (Nb)	4 dpi (At)	8 dpi (Nb)	12 dpi (Nb)	16 dpi (Nb)	Description of At homolog	Functions in
NbS00053231g0003	At5g25110	-1.3	-0.5	-1.3	-0.8	-1.7	CIPK25 (CBL-INTERACTING PROTEIN KINASE 25), SnRK3.25	abiotic stress (salt)
NbS00022544g0003	At2g39350	5.5	0.3	2.8	4.8	6.2	ABC TRANSPORTER FAMILY PROTEIN	casparian strip
NbS00030724g0011	At2g39350	4.7	0.3	2.1	4.3	5.6	ABC TRANSPORTER FAMILY PROTEIN	casparian strip
NbS00037868g0004	At2g39530	4.5	0.0	3.6	5.6	6.1	ABC TRANSPORTER FAMILY PROTEIN	casparian strip
NbS00012108g0005	At4g28110	6.2	0.6	3.0	6.2	7.1	ATMYB41 (MYB DOMAIN PROTEIN 41)	casparian strip
NbS00030442g0004	At4g28110	5.5	0.6	3.0	5.5	6.3	ATMYB41 (MYB DOMAIN PROTEIN 41)	casparian strip
NbS00026515g0010	At5g23190	4.3	-0.1	1.1	3.7	5.5	CYP86B1	casparian strip
NbS00058524g0002	At5g41040	5.7	-0.2	2.7	5.4	6.8	RWP1, Encodes a feruloyl-CoA transferase required for suberin synthesis	casparian strip
NbS00022478g0011	At5g42180	-1.3	-0.2	-0.9	-1.3	-2.2	PER64 (PEROXIDASE 64)	casparian strip
NbS00016770g0012	At1g02460	5.4	0.6	5.5	6.3	4.0	GLYCOSIDE HYDROLASE FAMILY 28 PROTEIN	cell wall
NbS00023022g0012	At1g02460	5.3	0.6	6.0	5.6	4.1	GLYCOSIDE HYDROLASE FAMILY 28 PROTEIN	cell wall
NbS00060283g0006	At1g70370	-1.3	0.2	-0.6	-1.4	-1.7	BURP DOMAIN-CONTAINING PROTEIN / POLYGALACTURONASE, PUTATIVE	cell wall
NbS00008570g0001	At4g10350	4.3	-0.4	3.4	5.1	Inf	ANAC070 (ARABIDOPSIS NAC DOMAIN CONTAINING PROTEIN 70)	cell wall (secondary cell wall synthesis)
NbS00018998g0013	At5g05340	4.3	0.2	3.8	4.1	4.5	PRX52 (PEROXIDASE 52)	cell wall/lignin
NbS00034132g0002	At4g13810	6.9	-0.2	Inf	Inf	6.5	ATRLP47 (RECEPTOR LIKE PROTEIN 47)	defence
NbS00036208g0008	At4g21440	5.8	0.5	4.9	5.1	6.9	ATMYB102 (ARABIDOPSIS MYB-LIKE 102)	defence
NbS00009480g0003	At5g36970	5.6	0.3	3.2	5.0	6.2	NHL25 (NDR1/HIN1-LIKE 25)	defence
NbS00028343g0022	At1g06520	6.1	0.5	3.3	5.7	7.0	GPAT1 (GLYCEROL-3-PHOSPHATE ACYLTRANSFERASE 1)	development
NbS00024799g0001	At3g09290	6.1	0.0	Inf	5.1	6.6	TAC1 (TELOMERASE ACTIVATOR1)	development
NbS00019641g0010	At5g09530	5.0	0.0	2.4	4.7	5.8	PELPK1, Positive regulator of germination	development
NbC25873455g0003	At1g20440	5.5	-0.3	5.5	5.6	5.5	RD17; COR47 (COLD-REGULATED 47) (dehydrin)	drought response
NbS00009681g0002	At1g54540	5.4	0.1	2.6	5.2	5.9	NHL11, LATE EMBRYOGENESIS ABUNDANT (LEA)	drought response
NbS00046588g0003	At2g26560	6.7	0.0	Inf	Inf	5.0	PLA2A (PHOSPHOLIPASE A 2A)	drought response

Table S8 continued.

<i>Nb</i> gene ID	<i>At</i> homolog	8+12+16 dpi (<i>Nb</i>)	4 dpi (<i>At</i>)	8 dpi (<i>Nb</i>)	12 dpi (<i>Nb</i>)	16 dpi (<i>Nb</i>)	Description of <i>At</i> homolog	Functions in
<i>NbS00011950g0007</i>	<i>At2g48140</i>	5.6	0.0	2.9	5.1	6.4	LTP	lipid
<i>NbS00054634g0001</i>	<i>At3g22600</i>	10.7	0.1	7.5	8.9	11.1	LTP, GLYCOSYLPHOSPHATIDYLINOSITOL-ANCHORED LIPID PROTEIN TRANSFER 5, LTPG5	lipid
<i>NbS00054082g0004</i>	<i>At3g22600</i>	9.4	0.1	4.7	8.1	11.5	LTP, GLYCOSYLPHOSPHATIDYLINOSITOL-ANCHORED LIPID PROTEIN TRANSFER 5, LTPG5	lipid
<i>NbS00002528g0007</i>	<i>At3g22600</i>	5.5	0.1	2.7	5.4	6.5	LTP, GLYCOSYLPHOSPHATIDYLINOSITOL-ANCHORED LIPID PROTEIN TRANSFER 5, LTPG5	lipid
<i>NbS00007575g0012</i>	<i>At5g13900</i>	6.4	0.0	3.4	6.2	7.2	LTP	lipid
<i>NbS00008258g0002</i>	<i>At4g33790</i>	5.4	-0.2	2.2	4.6	6.5	CER4 (ECERIFERUM 4), G7, FAR3, FATTY ACYL-COA REDUCTASE	lipid/cuticular wax
<i>NbS00002660g0010</i>	<i>At5g24080</i>	5.1	1.6	4.0	4.8	5.4	PROTEIN KINASE FAMILY PROTEIN	signalling
<i>NbS00021305g0003</i>	<i>At1g54820</i>	-1.3	0.4	-1.1	-1.0	-1.6	PROTEIN SERINE/THREONINE KINASE	signaling
<i>NbS00045132g0002</i>	<i>At3g28857</i>	-1.5	-1.1	-1.0	-1.4	-2.1	PRE5, BASIC HELIX-LOOP-HELIX (BHLHS) TF	transcription factor
<i>NbS00024319g0013</i>	<i>At3g58120</i>	-1.5	-0.1	-1.2	-1.2	-1.8	BZIP61	transcription factor
<i>NbS00034903g0004</i>	<i>At5g19530</i>	-1.3	-0.1	-0.9	-1.0	-1.9	ACL5 (ACAULIS 5), SPERMINE SYNTHASE/ THERMOSPERMINE SYNTHASE	transdifferentiation
<i>NbS00024340g0007</i>	<i>At3g11710</i>	4.3	0.0	4.3	4.3	4.3	ATKRS-1 (ARABIDOPSIS THALIANA LYSYL-TRNA SYNTHETASE 1)	translation
<i>NbS00030682g0008</i>	<i>At1g59740</i>	-1.2	0.7	-1.0	-0.9	-1.8	PROTON-DEPENDENT OLIGOPEPTIDE TRANSPORT (POT) FAMILY PROTEIN	transport (peptide)
<i>NbS00015341g0006</i>	<i>At4g10310</i>	-1.3	0.7	-0.8	-1.5	-1.9	HKT1 (HIGH-AFFINITY K ⁺ TRANSPORTER 1), sodium ion transmembrane transporter	transport (sodium)
<i>NbS00007456g0005</i>	<i>At3g53420</i>	5.0	0.4	4.7	5.7	4.7	PIP2;1 (PLASMA MEMBRANE INTRINSIC PROTEIN 2A)	transport (water)
<i>NbS00018173g0011</i>	<i>At3g53420</i>	5.0	0.4	4.7	5.2	4.9	PIP2;1 (PLASMA MEMBRANE INTRINSIC PROTEIN 2A)	transport (water)
<i>NbS00024338g0007</i>	<i>At3g53420</i>	4.9	0.4	6.2	4.8	3.6	PIP2;1 (PLASMA MEMBRANE INTRINSIC PROTEIN 2A)	transport (water)
<i>NbS00041805g0002</i>	<i>At4g17340</i>	4.8	-0.1	4.3	5.1	4.9	TIP2;2 (TONOPLAST INTRINSIC PROTEIN 2;2)	transport (water)
<i>NbS00013195g0003</i>	<i>At1g69160</i>	-1.3	0.0	-0.7	-1.3	-1.8	UNKNOWN PROTEIN	unknown
<i>NbS00012229g0003</i>	<i>At2g23690</i>	-1.8	0.1	-1.6	-1.6	-2.1	UNKNOWN PROTEIN	unknown
<i>NbS00051277g0001</i>	<i>At2g27770</i>	-1.2	-0.1	-0.8	-1.0	-1.8	UNKNOWN PROTEIN	unknown
<i>NbS00058741g0004</i>	<i>At2g45360</i>	4.4	0.6	4.1	4.2	4.6	UNKNOWN PROTEIN	unknown
<i>NbS00023513g0010</i>	<i>At3g62730</i>	5.2	0.0	5.2	5.9	4.7	UNKNOWN PROTEIN	unknown
<i>NbS00004337g0001</i>	<i>At4g24130</i>	5.2	-0.1	3.0	4.8	5.7	UNKNOWN PROTEIN	unknown
<i>NbS00007435g0003</i>	<i>At4g34320</i>	5.6	-0.6	4.4	6.0	7.2	UNKNOWN PROTEIN	unknown
<i>NbS00015724g0005</i>	<i>At4g36610</i>	5.0	0.0	2.2	4.5	6.7	UNKNOWN PROTEIN	unknown
<i>NbS00031400g0005</i>	<i>At4g36610</i>	4.6	0.0	2.1	3.9	5.7	UNKNOWN PROTEIN	unknown
<i>NbS00021074g0003</i>	<i>At5g03050</i>	4.6	-0.2	2.8	4.1	5.5	UNKNOWN PROTEIN	unknown

Table S9. Significantly transcriptionally regulated *Nicotiana benthamiana* (*Nb*) genes at 8, 12 and 16 days post infection (dpi) with *Verticillium* isolates of the wilting group. Raw RNA-read counts were of 8, 12 and 16 dpi samples were added. Subsequently, differential gene expression was analysed using RobiNA v1.2.4 (Lohse *et al.*, 2012) and the DESeq analysis method (Anders and Huber, 2010) between samples of the wilting group versus chlorosis group and mock treatment. Raw P-values were adjusted using the False Discovery Rate algorithm (Benjamini and Hochberg, 1995). Only differentially expressed genes below a cut-off of FDR \leq 0.05 and a log2 fold (L2F) change in expression \geq +1 in 8+12+16 dpi dataset shown. L2F change in expression at 4, 8, 12 and 16 dpi is included.

<i>Nb</i> gene ID	<i>At</i> homolog	8+12+16 dpi (<i>Nb</i>)	4 dpi (<i>At</i>)	8 dpi (<i>Nb</i>)	12 dpi (<i>Nb</i>)	16 dpi (<i>Nb</i>)	Description of <i>At</i> homolog	Functions in
<i>NbS00000943g0017</i>	<i>At1g53540</i>	3.2	-0.1	5.5	4.3	2.0	HSP20-LIKE CHAPERONES SUPERFAMILY PROTEIN	abiotic stress
<i>NbS00002008g0007</i>	<i>At4g17030</i>	2.8	0.5	2.9	2.9	2.6	ATEXLB1 (ARABIDOPSIS THALIANA EXPANSIN-LIKE B1)	cell wall
<i>NbS00050006g0001</i>	<i>At5g01300</i>	3.4	0.1	4.3	4.7	2.3	PEBP (PHOSPHATIDYLETHANOLAMINE-BINDING PROTEIN)	development
<i>NbS00028352g0006</i>	<i>At2g47770</i>	4.0	-2.0	5.0	4.3	3.3	TSPO (OUTER MEMBRANE TRYPTOPHAN-RICH SENSORY PROTEIN)-RELATED	drought response
<i>NbS00006911g0001</i>	<i>At4g30960</i>	2.6	0.3	3.4	2.8	2.1	CBL-INTERACTING PROTEIN KINASE (CIPK6), SNRK3.14	drought response
<i>NbS00012361g0028</i>	<i>At5g52300</i>	2.5	-1.9	2.1	2.6	2.7	RD29B	drought response
<i>NbS00019713g0013</i>	<i>At2g46680</i>	3.2	0.4	4.9	3.1	2.5	ATHB-7 (ARABIDOPSIS THALIANA HOMEBOX 7)	hormone-ABA
<i>NbS00032479g0003</i>	<i>At2g46680</i>	4.6	0.4	5.6	3.7	3.8	ATHB-7 (ARABIDOPSIS THALIANA HOMEBOX 7)	hormone-ABA
<i>NbS00032364g0006</i>	<i>At5g12840</i>	2.7	-0.1	3.1	3.9	1.3	NF-YA1 (NUCLEAR FACTOR Y, SUBUNIT A1)	hormone-ABA
<i>NbS00022068g0005</i>	<i>At2g29380</i>	3.3	-0.4	5.7	5.4	1.7	HAI3 (HIGHLY ABA-INDUCED PP2C GENE 3)	hormone-ABA
<i>NbS00031747g0001</i>	<i>At2g31230</i>	2.6	0.4	2.4	2.5	2.7	ERF15 (ETHYLENE-RESPONSIVE ELEMENT BINDING FACTOR 15)	hormone-ABA
<i>NbS00032861g0003</i>	<i>At5g19040</i>	3.6	-0.2	3.4	4.2	3.1	IPT5 (ISOPENTENYLTRANSFERASE 5), cytokinin biosynthesis	hormone-cytokinin
<i>NbS00037398g0011</i>	<i>At2g03590</i>	2.9	-0.2	3.5	4.4	1.8	ATUPS1 (ARABIDOPSIS THALIANA UREIDE PERMEASE 1)	transport (nucleotide)
<i>NbS00023055g0006</i>	<i>At5g53190</i>	2.2	-Inf	1.9	2.5	2.2	SWEET3, bidirectional sugar transporter, phloem loading	transport (sugar)
<i>NbS00008139g0013</i>	<i>At2g16980</i>	2.4	-0.1	1.7	2.8	2.5	TETRACYCLINE RESISTANCE PROTEIN	transport (tetracyclin)
<i>NbS00009974g0006</i>	<i>At5g04000</i>	2.2	-0.5	2.6	2.4	1.6	UNKNOWN PROTEIN	unknown
<i>NbS00016185g0003</i>	<i>At5g50360</i>	1.7	-1.2	2.3	1.6	1.3	UNKNOWN PROTEIN	unknown

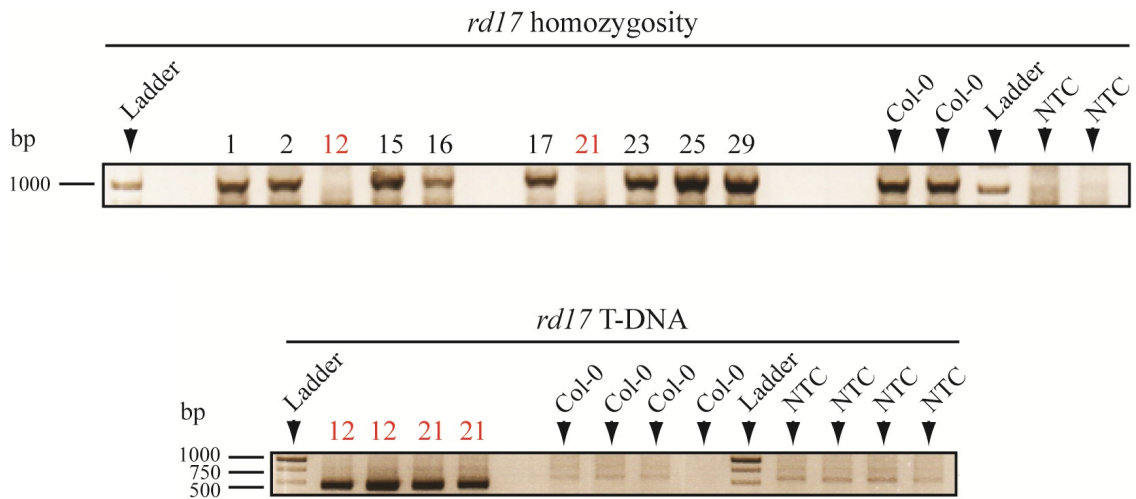


Figure S1. Identification of homozygous *A. thaliana* *rd17* T-DNA insertion mutants by PCR-based genotyping. Plants were tested for T-DNA insertion in SAIL_1295_D06 (*rd17*) (upper panel) using T-DNA insertion flanking primers as well as homozygosity of the T-DNA integration (lower panel) using the T-DNA left border primer and the respective T-DNA insertion flanking primer. Col-0 wild-type plants as well as a non-template control (NTC), containing only the PCR mix, were included. Note that an unspecific PCR product is present in NTC and Col-0 samples (runs at ca. 600 bp), which is however larger than the *rd17* T-DNA band (runs at ca. 450 bp). Homozygous T-DNA insertion lines are highlighted red.

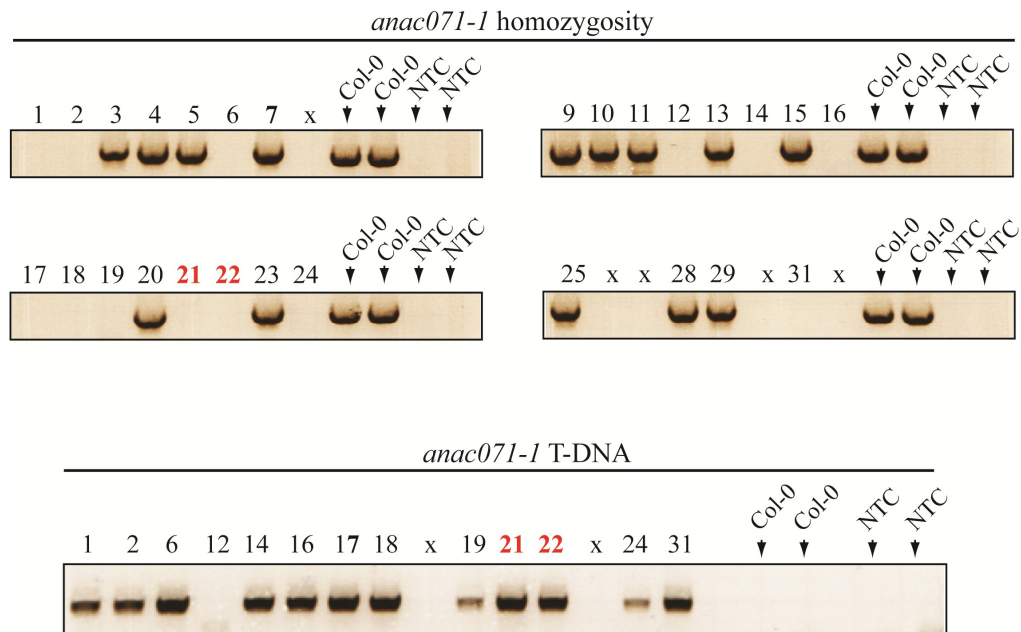


Figure S2. Identification of homozygous *A. thaliana anac071-1* T-DNA insertion mutants by PCR-based genotyping. Plants were tested for T-DNA insertion in SALK_012841 (*anac071-1*) (upper panel) using T-DNA insertion flanking primers as well as homozygosity of the T-DNA integration (lower panel) using the T-DNA left border primer and the respective T-DNA insertion flanking primer. Col-0 wild-type plants as well as a non-template control (NTC), containing only the PCR mix, were included. Homozygous T-DNA insertion lines highlighted red were selected for use in further experiments.

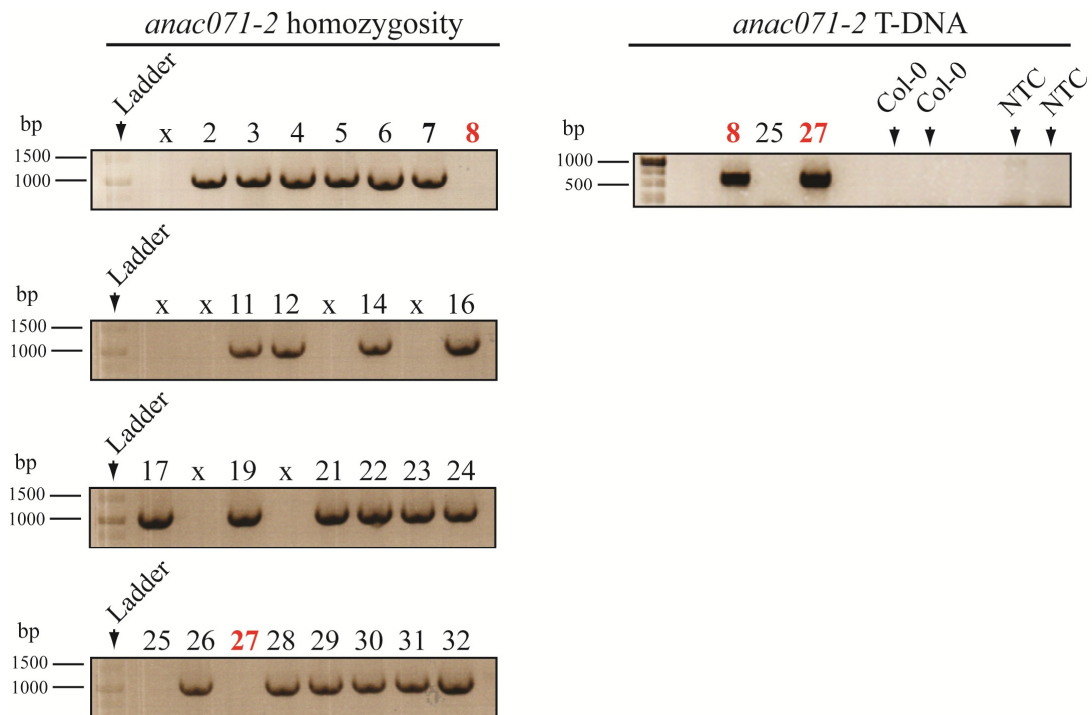


Figure S3. Identification of homozygous *A. thaliana anac071-2* T-DNA insertion mutants by PCR-based genotyping. Plants were tested for T-DNA insertion in SALK_105147 (*anac071-2*) (upper panel) using T-DNA insertion flanking primers (expected product size is 1104 kb) as well as homozygosity of the T-DNA integration (lower panel) using the T-DNA left border primer and the respective T-DNA insertion flanking primer (product expected in the 497-797 bp range). Col-0 wild-type plants as well as a non-template control (NTC), containing only the PCR mix, were included in case of the *anac071-1* T-DNA PCR. Homozygous T-DNA insertion lines are highlighted red.

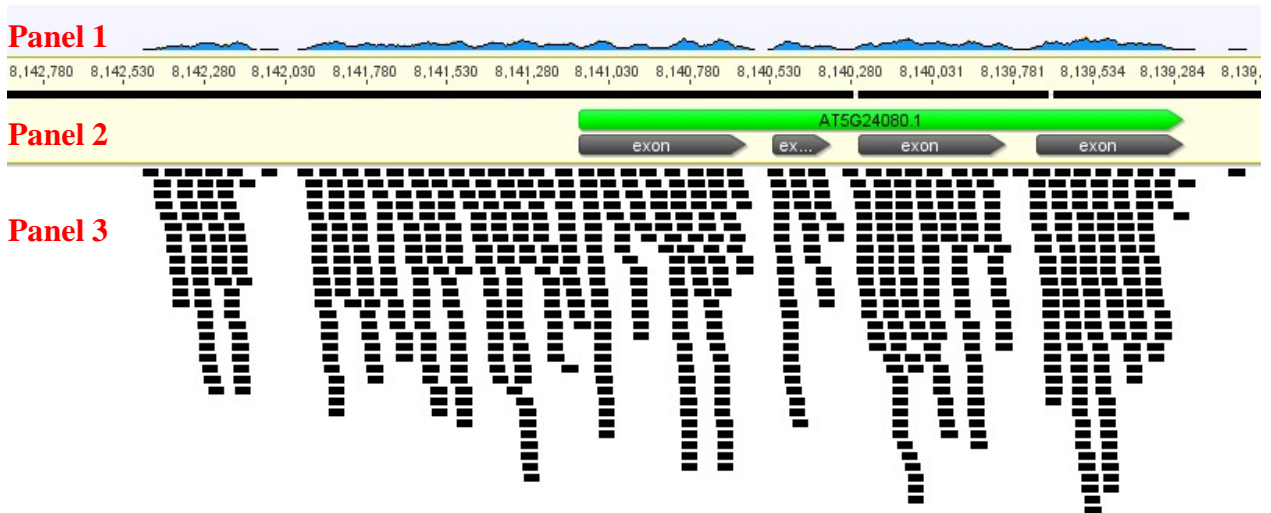


Figure S4. RNA sequencing reads mapping to the *At5g24080* genomic sequence. *At5g24080* genomic sequence was obtained from The Arabidopsis Information Resource (TAIR) TAIR10 genome release (Berardini *et al.*, 2015). Panel 1 shows the RNA sequencing read coverage, panel 2 shows the TAIR 10 genome release annotation whereas panel 3 represents the mapped RNA sequencing reads.

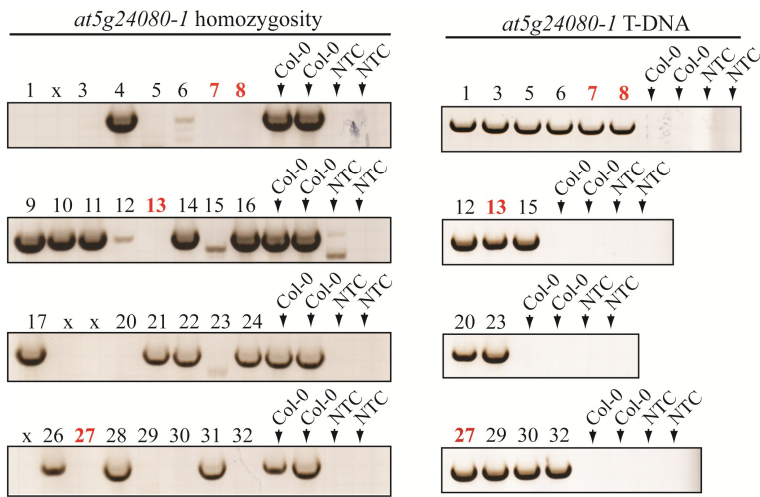


Figure S5. Identification of homozygous *A. thaliana at5g24080-1* T-DNA insertion mutants by PCR-based genotyping. Plants were tested for T-DNA insertion in SALK_086625 (*at5g24080-1*) (left panel) using T-DNA insertion flanking primers as well as homozygosity of the T-DNA integration (right panel) using the T-DNA left border primer and the respective T-DNA insertion flanking primer. Col-0 wild-type plants as well as a non-template control (NTC), containing only the PCR mix, were included. Homozygous T-DNA insertion lines highlighted red were selected for use in further experiments.

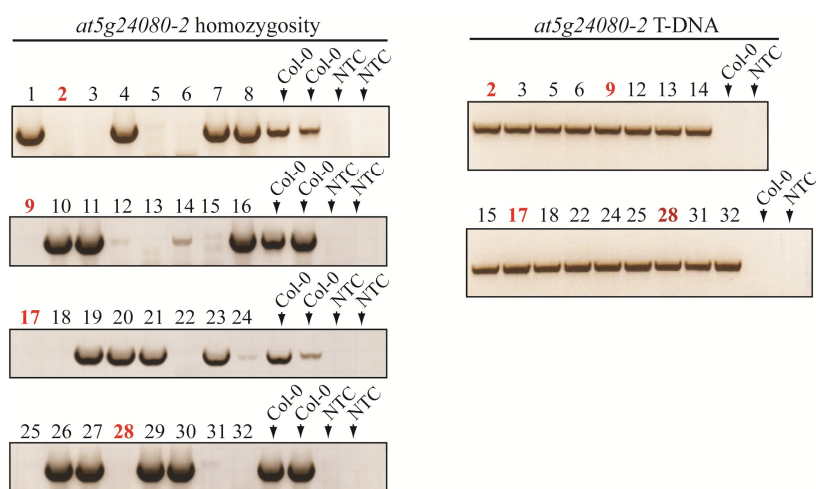


Figure S6. Identification of homozygous *A. thaliana* at5g24080-2 T-DNA insertion mutants by PCR-based genotyping. Plants were tested for T-DNA insertion in SALK_147104 (*at5g24080-2*) (left panel) using T-DNA insertion flanking primers as well as homozygosity of the T-DNA integration (right panel) using the T-DNA left border primer and the respective T-DNA insertion

flanking primer. Col-0 wild-type plants as well as a non-template control (NTC), containing only the PCR mix, were included. Homozygous T-DNA insertion lines highlighted red were selected for use in further experiments.

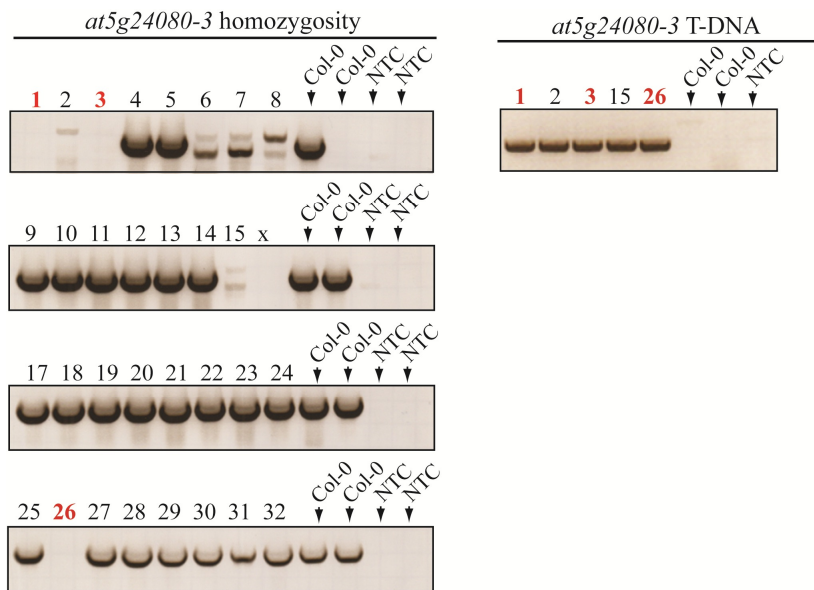


Figure S7. Identification of homozygous *A. thaliana* at5g24080-3 T-DNA insertion mutants by PCR-based genotyping. Plants were tested for T-DNA insertion in SAIL_551_D12 (*at5g24080-3*) (left panel) using T-DNA insertion flanking primers as well as homozygosity of the T-DNA integration (right panel) using the T-DNA left border primer and the respective T-DNA insertion flanking primer. Col-0 wild-type plants as well as a

non-template control (NTC), containing only the PCR mix, were included. Homozygous T-DNA insertion lines highlighted red were selected for use in further experiments.

At5g24080 1 ATGCTCTTCATTTCAATTTTATTTTCCTTCTGTTGGTCTCTTCTCATTCTTTTGCTTCTTCTTAGTTAGCT
at5g24080-1 1 ATGCTCTTCATTTCAATTTTATTTTCCTTCTGTTGGTCTCTTCTCATTCTTTTGCTTCTTCTTAGTTAGCT
at5g24080-2 1 ATGCTCTTCATTTCAATTTTATTTTCCTTCTGTTGGTCTCTTCTCATTCTTTTGCTTCTTCTTAGTTAGCT
at5g24080-3 1 ATGCTCTTCATTTCAATTTTATTTTCCTTCTGTTGGTCTCTTCTCATTCTTTTGCTTCTTCTTAGTTAGCT

At5g24080 71 TGGCCACTGAACCGCACATCGGTTTGGGTTCAAAGCTAAAAGCTAGTGAACCGAACCGGGCATGGGTTTC
at5g24080-1 71 TGGCCACTGAACCGCACATCGGTTTGGGTTCAAAGCTAAAAGCTAGTGAACCGAACCGGGCATGGGTTTC
at5g24080-2 71 TGGCCACTGAACCGCACATCGGTTTGGGTTCAAAGCTAAAAGCTAGTGAACCGAACCGGGCATGGGTTTC
at5g24080-3 71 TGGCCACTGAACCGCACATCGGTTTGGGTTCAAAGCTAAAAGCTAGTGAACCGAACCGGGCATGGGTTTC

At5g24080 141 TGCTAACGGTACTTTTGCAATCGGGTTTACTCGGTTTAAAGCCAACCGACCGATTCTTACTGAGCATTGGG
at5g24080-1 141 TGCTAACGGTACTTTTGCAATCGGGTTTACTCGGTTTAAAGCCAACCGACCGATTCTTACTGAGCATTGGG
at5g24080-2 141 TGCTAACGGTACTTTTGCAATCGGGTTTACTCGGTTTAAAGCCAACCGACCGATTCTTACTGAGCATTGGG
at5g24080-3 141 TGCTAACGGTACTTTTGCAATCGGGTTTACTCGGTTTAAAGCCAACCGACCGATTCTTACTGAGCATTGGG

At5g24080 211 TTCGCACAACCTTCTGGTGATCCAACCATCGTCTGGTCTCCCAACAGGTACACATAATCCTTTGATATTT
at5g24080-1 211 TTCGCACAACCTTCTGGTGATCCAACCATCGTCTGGTCTCCCAACAGGTACACATAATCCTTTGATATTT
at5g24080-2 211 TTCGCACAACCTTCTGGTGATCCAACCATCGTCTGGTCTCCCAACAGGTACACATAATCCTTTGATATTT
at5g24080-3 211 TTCGCACAACCTTCTGGTGATCCAACCATCGTCTGGTCTCCCAACAGGTACACATAATCCTTTGATATTT

At5g24080 281 AGTTATTGAAGCAATCTATATTAGTAGTAAATATATACAAATTTTATGTTAAGCTCAAATAAATTTCTTTA
at5g24080-1 281 AGTTATTGAAGCAATCTATATTAGTAGTAAATATATACAAATTTTATGTTAAGCTCAAATAAATTTCTTTA
at5g24080-2 281 AGTTATTGAAGCAATCTATATTAGTAGTAAATATATACAAATTTTATGTTAAGCTCAAATAAATTTCTTTA
at5g24080-3 281 AGTTATTGAAGCAATCTATATTAGTAGTAAATATATACAAATTTTATGTTAAGCTCAAATAAATTTCTTTA

At5g24080 351 GTACCAACGTTTGTATTTCCCTATGATCAGAAATTTCCACATTATTTTACTCAAAAATATAAATATCTA
at5g24080-1 351 GTACCAACGTTTGTATTTCCCTATGATCAGAAATTTCCACATTATTTTACTCAAAAATATAAATATCTA
at5g24080-2 351 GTACCAACGTTTGTATTTCCCTATGATCAGAAATTTCCACATTATTTTACTCAAAAATATAAATATCTA
at5g24080-3 351 GTACCAACGTTTGTATTTCCCTATGATCAGAAATTTCCACATTATTTTACTCAAAAATATAAATATCTA

At5g24080 421 AAATATAGAAACTCCCCAGTCACAAAAGAAGCCGTTGGAGCTAGAAGCCACGGGAAACCTCGTACTCT
at5g24080-1 421 AAATATAGAAACTCCCCAGTCACAAAAGAAGCCGTTGGAGCTAGAAGCCACGGGAAACCTCGTACTCT
at5g24080-2 421 AAATATAGAAACTCCCCAGTCACAAAAGAAGCCGTTGGAGCTAGAAGCCACGGGAAACCTCGTACTCT
at5g24080-3 421 AAATATAGAAACTCCCCAGTCACAAAAGAAGCCGTTGGAGCTAGAAGCCACGGGAAACCTCGTACTCT

At5g24080 491 CCGACCAAAACACTGTCGCTGGACCTCAAACACGTCAAACCATGGTGTGAATCAGCGGTTATGTCCGA
at5g24080-1 491 CCGACCAAAACACTGTCGCTGGACCTCAAACACGTCAAACCATGGTGTGAATCAGCGGTTATGTCCGA
at5g24080-2 491 CCGACCAAAACACTGTCGCTGGACCTCAAACACGTCAAACCATGGTGTGAATCAGCGGTTATGTCCGA
at5g24080-3 491 CCGACCAAAACACTGTCGCTGGACCTCAAACACGTCAAACCATGGTGTGAATCAGCGGTTATGTCCGA

At5g24080 561 ATCTGGAAACTTCTCCTCCTTGGAACAGAAGTTACTGCTGGTCCAACCATTTGGCAAAGCTTTTCGCAA
at5g24080-1 561 ATCTGGAAACTTCTCCTCCTTGGAACAGAAGTTACTGCTGGTCCAACCATTTGGCAAAGCTTTTCGCAA
at5g24080-2 561 ATCTGGAAACTTCTCCTCCTTGGAACAGAAGTTACTGCTGGTCCAACCATTTGGCAAAGCTTTTCGCAA
at5g24080-3 561 ATCTGGAAACTTCTCCTCCTTGGAACAGAAGTTACTGCTGGTCCAACCATTTGGCAAAGCTTTTCGCAA

At5g24080 631 CCTTCCGACACTCTCCTCCCAAAACCAACCTTAAACCGTTTCTTAGAATAACCTCTAACCCCTCACCGT
at5g24080-1 631 CCTTCCGACACTCTCCTCCCAAAACCAACCTTAAACCGTTTCTTAGAATAACCTCTAACCCCTCACCGT
at5g24080-2 631 CCTTCCGACACTCTCCTCCCAAAACCAACCTTAAACCGTTTCTTAGAATAACCTCTAACCCCTCACCGT
at5g24080-3 631 CCTTCCGACACTCTCCTCCCAAAACCAACCTTAAACCGTTTCTTAGAATAACCTCTAACCCCTCACCGT

At5g24080 701 CGCGCCATGGCCATTACTCCCTGAAAATGCTGCAGCAACACACTTCACCTTAGCCTCGGCCTAACCTACAA
at5g24080-1 701 CGCGCCATGGCCATTACTCCCTGAAAATGCTGCAGCAACACACTTCACCTTAGCCTCGGCCTAACCTACAA
at5g24080-2 701 CGCGCCATGGCCATTACTCCCTGAAAATGCTGCAGCAACACACTTCACCTTAGCCTCGGCCTAACCTACAA
at5g24080-3 701 CGCGCCATGGCCATTACTCCCTGAAAATGCTGCAGCAACACACTTCACCTTAGCCTCGGCCTAACCTACAA

At5g24080 771 CATCAATCTTGACCCTCAGCAAACCTACTCGTACTGGTCCGGACCAGATATATCTAATGTTACAGGAGAT
at5g24080-1 771 CATCAATCTTGACCCTCAGCAAACCTACTCGTACTGGTCCGGACCAGATATATCTAATGTTACAGGAGAT
at5g24080-2 771 CATCAATCTTGACCCTCAGCAAACCTACTCGTACTGGTCCGGACCAGATATATCTAATGTTACAGGAGAT
at5g24080-3 771 CATCAATCTTGACCCTCAGCAAACCTACTCGTACTGGTCCGGACCAGATATATCTAATGTTACAGGAGAT

At5g24080 841 GTTACCGCAGTTCTTGACGATACCGGAAGCTTCAAGATCGTTTATGGAGAATCCTCAATAGGAGCAGTGT
at5g24080-1 841 GTTACCGCAGTTCTTGACGATACCGGAAGCTTCAAGATCGTTTATGGAGAATCCTCAATAGGAGCAGTGT
at5g24080-2 841 GTTACCGCAGTTCTTGACGATACCGGAAGCTTCAAGATCGTTTATGGAGAATCCTCAATAGGAGCAGTGT
at5g24080-3 841 GTTACCGCAGTTCTTGACGATACCGGAAGCTTCAAGATCGTTTATGGAGAATCCTCAATAGGAGCAGTGT

At5g24080 911 ACGTCTACAAGAACC CGGTAGATGATAACCGGAATTACAACAACAGTAGTAATTTAGGGTTAACAAAAA
at5g24080-1 911 ACGTCTACAAGAACC CGGTAGATGATAACCGGAATTACAACAACAGTAGTAATTTAGGGTTAACAAAAA
at5g24080-2 911 ACGTCTACAAGAACC CGGTAGATGATAACCGGAATTACAACAACAGTAGTAATTTAGGGTTAACAAAAA
at5g24080-3 911 ACGTCTACAAGAACC CGGTAGATGATAACCGGAATTACAACAACAGTAGTAATTTAGGGTTAACAAAAA

At5g24080 981 TCCGGTTCTGCGGAGATTGGTATTAGAGAACAACGGTAATCTCCGGTTATACCGATGGGACAACGACATG
at5g24080-1 981 TGA-----
at5g24080-2 981 TCCGGTTCTGCGGAGATTGGTATTAGAGAACAACGGTAATCTCCGGTTATACCGATGGGACAACGACATG
at5g24080-3 981 TCCGGTTCTGCGGAGATTGGTATTAGAGAACAACGGTAATCTCCGGTTATACCGATGGGACAACGACATG

At5g24080 1051 AACGGTTCAAGCCAATGGGTCCTGGAATGGGCAGCTGTATCAAACCCGTGTGACATAGCTGGGATTTGCC
at5g24080-1 -----
at5g24080-2 1051 AACGGTTCAAGCCAATGGGTCCTGGAATGGGCAGCTGTATCAAACCCGTGTGACATAGCTGGGATTTGCC
at5g24080-3 1051 AACGGTTCAAGCCAATGGGTCCTGGAATGGGCAGCTGTATCAAACCCGTGTGACATAGCTGGGATTTGCC

At5g24080 1121 GTAACGGAGTTTGAATTTGGACCGAACCAAGAAAAACGCTGACTGTTTATGTTTGCCCGGTTTCGGTCAA
at5g24080-1
at5g24080-2 1121 GTAACGGAGTTTGAATTTGGACCGAACCAAGAAAAACGCTGACTGTTTATGTTTGCCCGGTTTCGGTCAA
at5g24080-3 1121 GTAACGGAGTTTGAATTTGGACCGAACCAAGAAAAACGCTGACTGTTTATGTTTGCCCGGTTTCGGTCAA

At5g24080 1191 ACTTCCTGATCAAGAAAACGCTAAACTCTGTTTCAGACAACCTCATCTTTGGTCCAAGAATGTGAAAGCAAC
at5g24080-1
at5g24080-2 1191 ACTTCCTGATCAAGAAAACGCTAAACTCTGTTTCAGACAACCTCATCTTTGGTCCAAGAATGTGAAAGCAAC
at5g24080-3 1191 ACTTCCTGATCAAGAAAACGCTAAACTCTGTTTCAGACAACCTCATCTTTGGTGTAA

At5g24080 1261 ATTAATCGTAACGGTAGCTTCAAGATCTCGACGGTCCAAGAGACCAACTACTATTTTTCAGAACGTTCTG
at5g24080-1
at5g24080-2 1261 ATTAATCGTAACGGTAGCTTCAAGATCTCGACGGTCCAAGAGACCAACTACTATTTTTCAGAACGTTCTG
at5g24080-3

At5g24080 1331 TCATCGAAAAATATCAGCGATATCAGCAACGTGAGGAAATGCGGTGAGATGTGTTTGTTCAGATTGCAAGTG
at5g24080-1
at5g24080-2 1331 TCATCGAAAAATATCAGCGATATCAGCAACGTGAGGAAATGCGGTGAGATGTGTTTGTTCAGATTGCAAGTG
at5g24080-3

At5g24080 1401 GTAGCTTCAGTTTATGTTTATGATGATGAGAAGCCTTATTGTTGGATTTTAAAGAGTCTGAATTTTGGC
at5g24080-1
at5g24080-2 1401 GTAGCTTCAGTTTATGTTTATGATGATGAGAAGCCTTATTGTTGGATTTTAAAGAGTCTGAATTTTGGC
at5g24080-3

At5g24080 1471 GGGTTTCGAGATCCTGGCTCAACCCCTTTTCGTGAAGACTAGAGCTAATGAATCTTATCCCTCAAATTCGA
at5g24080-1
at5g24080-2 1471 GGGTTTCGAGATCCTGGCTCAACCCCTTTTCGTGAAGACTAGAGCTAATGAATCTTATCCCTCAAATTCGA
at5g24080-3

At5g24080 1541 ATAATAATGATTCTAAATCGCGTAAGAGCCACGGATTAAGACAAAAGGTTCTGGTGATTCTATAGTTGT
at5g24080-1
at5g24080-2 1541 ATAATAATGATTCTAAATCGCGTAAGAGCCACGGATTAAGACAAAAGGTTCTGGTGATTCTATAGTTGT
at5g24080-3

At5g24080 1611 GGGGATGCTTGTGCTTGTGGCACTACTTGGGATGTTGTTATACTATAATTTAGATAGGAAGAGAACACTA
at5g24080-1
at5g24080-2 1611 GGGGATGCTTGTGCTTGTGGCACTACTTGGGATGTTGTTATACTATAATTTAGATAGGAAGAGAACACTA
at5g24080-3

At5g24080 1681 AAGAGAGCCGCAAGAAGCTCTTATCCTTTGTGACTCTCCTGTGAGTTTCACTTACCGGATCTCCAGA
at5g24080-1
at5g24080-2 1681 AAGAGAGCCGCAAGAAGCTCTTATCCTTTGTGACTCTCCTGTGAGTTTCACTTACCGGATCTCCAGA
at5g24080-3

At5g24080 1751 ACTGTACCAACAACCTTCTCCCAACTTCTTGGATCAGGTCAGAATCAACAATCATCATATAACAAGTTTTA
at5g24080-1
at5g24080-2 1751 ACTGTACCAACAACCTTCTCCCAACTTCTTGGATCAGGTCAGAATCAACAATCATCATATAACAAGTTTTA
at5g24080-3

At5g24080 1821 ACTTAGAAGTGTTCAAATCTTATTTCTTTGTTTATGATGTGGTAGGTGGATTGGGACAGTATACAA
at5g24080-1
at5g24080-2 1821 ACTTAGAAGTGTTCAAATCTTATTTCTTTGTTTATGATGTGGTAGGTGGATTGGGACAGTATACAA
at5g24080-3

At5g24080 1891 AGGAACAGTAGCGGGTGAACCGCTAGTCGCGGTGAAGAGATTAGACAGAGCATTATCTCATGGCGAGAGA
at5g24080-1
at5g24080-2 1891 AGGAACAGTAGCGGGTGAACCGCTAGTCGCGGTGAAGAGATTAGACAGAGCATTATCTCATGGCGAGAGA
at5g24080-3

At5g24080 1961 GAGTTCATCACTGAAGTCAATACCATGGTTCAATGCATCACATGAACCTTGTTCGCTTGTGTGGTTACT
at5g24080-1
at5g24080-2 1961 GAGTTCATCACTGAAGTCAATACCATGGTTCAATGCATCACATGAACCTTGTTCGCTTGTGTGGTTACT
at5g24080-3

At5g24080 2031 GCTCGGAAGACTCACACCGGTATGACTTAGAAGACTTTTACAAAACATTTACTCTGTTTCAAGCAAAC
at5g24080-1
at5g24080-2 2031 GCTCGGAAGACTCACACCGGTATGACTTAGAAGACTTTTACAAAACATTTACTCTGTTTCAAGCAAAC
at5g24080-3

At5g24080 2101 AGATTTGAATAAATGTTTTTTTTGGTGACATTACAGGCTTCTAGTTTATGAGTACATGATAAATGGGTCGT
at5g24080-1
at5g24080-2 2101 AGATTTGAATAAATGTTTTTTTTGGTGACATTACAGGCTTCTAGTTTATGAGTACATGATAAATGGGTCGT
at5g24080-3

At5g24080 2171 TAGACAAATGGATATTCTCTTCAGAACAGACAGCTAATCTACTTGATTGGCGAACACGTTTGAATAGC
at5g24080-1
at5g24080-2 2171 TAGACAAATGGATATTCTCTTCAGAACAGACAGCTAATCTACTTGATTGGCGAACACGTTTGAATAGC
at5g24080-3

At5g24080	2241	GGTTGCGACTGCACAAGGAATCGCATATTTTCATGAGCAGTGTGCGAAACAGGATTATACATTGCGACATT
at5g24080-1		-----
at5g24080-2	2241	GGTTGCGACTGCACAAGGAATCGCATATTTTCATGAGCAGTGTGCGAAACAGGATTATACATTGCGACATT
at5g24080-3		-----
At5g24080	2311	AAACCTGAAAACATCTTGTGGATGATAATTTTGTCCCTAAGGTATCAGATTTTGGGCTAGCCAAGATGA
at5g24080-1		-----
at5g24080-2	2311	AAACCTGAAAACATCTTGTGGATGATAATTTTGTCCCTAAGGTATCAGATTTTGGGCTAGCCAAGATGA
at5g24080-3		-----
At5g24080	2381	TGGGGAGAGAGCATTTCGCATGTGGTTACGATGATTAGAGGGACGAGAGGGTATCTAGCGCCCGAATGGGT
at5g24080-1		-----
at5g24080-2	2381	TGGGGAGAGAGCATTTCGCATGTGGTTACGATGATTAGAGGGACGAGAGGGTATCTAGCGCCCGAATGGGT
at5g24080-3		-----
At5g24080	2451	GAGTAACCGCCCGATCACGGTGAAGGCCGATGTGTATAGTTATGGAATGCTTCTTCTAGAGATCGTAGGT
at5g24080-1		-----
at5g24080-2	2451	GAGTAACCGCCCGATCACGGTGAAGGCCGATGTGTATAGTTATGGAATGCTTCTTCTAGAGATCGTAGGT
at5g24080-3		-----
At5g24080	2521	GGTAGGAGAAATCTTGATATGTCCTATGACGCTGAGGATTTCTTTTACCCTGGATGGGCCTACAAGGTAA
at5g24080-1		-----
at5g24080-2	2521	GGTAGGAGAAATCTTGATATGTCCTATGACGCTGAGGATTTCTTTTACCCTGGATGGGCCTACAAGGTAA
at5g24080-3		-----
At5g24080	2591	ATTTAGACGATTCTTAAAATATAAAAGAAAGGGCTTAAATTAGTTATAAAACATAAAAGATTATAACGTCCTA
at5g24080-1		-----
at5g24080-2	2591	ATTTAGACGATTCTTAAAATATAAAAGAAAGGGCTTAAATTAGTTATAAAACATAAAAGATTATAACGTCCTA
at5g24080-3		-----
At5g24080	2661	ACGAGTTTTTGAAAATAAATGAATAGGAACTAACGAATGGGACATCTTTGAAAGCTGTGGATAAAAGGCT
at5g24080-1		-----
at5g24080-2	2661	ACGAGTTTTTGAAAATAAATGAATAGGAACTAACGAATGGGACATCTTTGAAAGCTGTGGATAAAAGGCT
at5g24080-3		-----
At5g24080	2731	ACAAGGAGTAGCAGAGGAAGAAGAAGTAGTGAAGGCTCTTAAAGTGGCTTTCTGGTGCATACAAGACGAA
at5g24080-1		-----
at5g24080-2	2731	ACAAGGAGTAGCAGAGGAAGAAGAAGTAGTGAAGGCTCTTAAAGTGGCTTTCTGGTGCATACAAGACGAA
at5g24080-3		-----
At5g24080	2801	GTATCGATGAGGCCGTCGATGGGTGAGGTGGTTAAGCTTTTAGAAGGCACTTCGGATGAGATAAACTGCG
at5g24080-1		-----
at5g24080-2	2801	GTATCGATGAGGCCGTCGATGGGTGAGGTGGTTAAGCTTTTAGAAGGCACTTCGGATGAGATAAACTGCG
at5g24080-3		-----
At5g24080	2871	CACCGATGCCACAGACGATTCTAGAACTTATAGAGGAAGGATTGGAGGATGTGTATAGAGCGATGAGGAG
at5g24080-1		-----
at5g24080-2	2871	CACCGATGCCACAGACGATTCTAGAACTTATAGAGGAAGGATTGGAGGATGTGTATAGAGCGATGAGGAG
at5g24080-3		-----
At5g24080	2941	AGAGTTCAATAATCAGCTTAGCTCTTTGACTGTTAATACAATCACAACCTCTCAGAGTTATCGTTCCTCC
at5g24080-1		-----
at5g24080-2	2941	AGAGTTCAATAATCAGCTTAGCTCTTTGACTGTTAATACAATCACAACCTCTCAGAGTTATCAAACACTG
at5g24080-3		-----
At5g24080	3011	TCTCGGTCTCATGCTACTTGTAGTTATTCTTCAATGTCTCCTAGGTAG
at5g24080-1		-----
at5g24080-2	3011	ATAGTTTAA
at5g24080-3		-----

Figure S8. Genomic sequence alignment of *At5g24080* wild-type, *at5g24080-1*, *at5g24080-2* and *at5g24080-3* Open Reading Frames (ORF). The alignment was produced in using the CLUSTAL W algorithm (Thompson *et al.*, 1994). Aligning sequences are highlighted in mint green. Sequences introduced by the T-DNA insertion in *At5g24080-1*, *At5g24080-2* and *At5g24080-3* are underlined in red. Introns are underlined in yellow. Splice site prediction was carried out using the NetGene2 Server (Hebsgaard *et al.*, 1996). Start codons are depicted in green, whereas stop codons are shown in yellow.

AT5G24080	1	MSSPFHYFPPSVGLFSFFCFLLVSLATEPHIGLGSKCLKASEPNRAWVSANG
AT5G24080-1	1	MSSPFHYFPPSVGLFSFFCFLLVSLATEPHIGLGSKCLKASEPNRAWVSANG
AT5G24080-2	1	MSSPFHYFPPSVGLFSFFCFLLVSLATEPHIGLGSKCLKASEPNRAWVSANG
AT5G24080-3	1	MSSPFHYFPPSVGLFSFFCFLLVSLATEPHIGLGSKCLKASEPNRAWVSANG
AT5G24080	51	TFAIGFTRFKPTDRFLLSIWFAQLPGDPTIVWSPNRRNSPVTK EAVLELEA
AT5G24080-1	51	TFAIGFTRFKPTDRFLLSIWFAQLPGDPTIVWSPNRRNSPVTK EAVLELEA
AT5G24080-2	51	TFAIGFTRFKPTDRFLLSIWFAQLPGDPTIVWSPNRRNSPVTK EAVLELEA
AT5G24080-3	51	TFAIGFTRFKPTDRFLLSIWFAQLPGDPTIVWSPNRRNSPVTK EAVLELEA
AT5G24080	101	TGNLVLSQDQNTVVWTSNTSNHGVE SAVMSESGNFLLLGTEVTAGPTIIWQS
AT5G24080-1	101	TGNLVLSQDQNTVVWTSNTSNHGVE SAVMSESGNFLLLGTEVTAGPTIIWQS
AT5G24080-2	101	TGNLVLSQDQNTVVWTSNTSNHGVE SAVMSESGNFLLLGTEVTAGPTIIWQS
AT5G24080-3	101	TGNLVLSQDQNTVVWTSNTSNHGVE SAVMSESGNFLLLGTEVTAGPTIIWQS
AT5G24080	151	FSQPSDTLLPNQPLTVSLELTSNPSPSRHGHYSKLMQQHTSLSLGLTYN
AT5G24080-1	151	FSQPSDTLLPNQPLTVSLELTSNPSPSRHGHYSKLMQQHTSLSLGLTYN
AT5G24080-2	151	FSQPSDTLLPNQPLTVSLELTSNPSPSRHGHYSKLMQQHTSLSLGLTYN
AT5G24080-3	151	FSQPSDTLLPNQPLTVSLELTSNPSPSRHGHYSKLMQQHTSLSLGLTYN
AT5G24080	201	INLDPHANYSYWGGPDISNVTGDVAVLDDTGSFKIVYGESSIGAVVYVK
AT5G24080-1	201	INLDPHANYSYWGGPDISNVTGDVAVLDDTGSFKIVYGESSIGAVVYVK
AT5G24080-2	201	INLDPHANYSYWGGPDISNVTGDVAVLDDTGSFKIVYGESSIGAVVYVK
AT5G24080-3	201	INLDPHANYSYWGGPDISNVTGDVAVLDDTGSFKIVYGESSIGAVVYVK
AT5G24080	251	NPVDDNRNYNNSNLGLTKNPVLRRLVLENNGNRLRYRDNDMNGSSQWV
AT5G24080-1	251	NPVDDNRNYNNSNLGLTKNPVLRRLVLENNGNRLRYRDNDMNGSSQWV
AT5G24080-2	251	NPVDDNRNYNNSNLGLTKNPVLRRLVLENNGNRLRYRDNDMNGSSQWV
AT5G24080-3	251	NPVDDNRNYNNSNLGLTKNPVLRRLVLENNGNRLRYRDNDMNGSSQWV
AT5G24080	301	PEWAAVSNPCDIAGICGNGVCNLDRTKKNADCLCLPGSVKLPDQENAKLC
AT5G24080-1	301	PEWAAVSNPCDIAGICGNGVCNLDRTKKNADCLCLPGSVKLPDQENAKLC
AT5G24080-2	301	PEWAAVSNPCDIAGICGNGVCNLDRTKKNADCLCLPGSVKLPDQENAKLC
AT5G24080-3	301	PEWAAVSNPCDIAGICGNGVCNLDRTKKNADCLCLPGSVKLPDQENAKLC
AT5G24080	351	SDNSSLVQECESNINRNGSFKISTVQETNYYSERSVNIENISDISNVRKC
AT5G24080-1	351	SDNSSLVQECESNINRNGSFKISTVQETNYYSERSVNIENISDISNVRKC
AT5G24080-2	351	SDNSSLVQECESNINRNGSFKISTVQETNYYSERSVNIENISDISNVRKC
AT5G24080-3	351	SDNSSLVQECESNINRNGSFKISTVQETNYYSERSVNIENISDISNVRKC
AT5G24080	401	GEMCLSDCKCVASVYGLDDEKPYCWILKSLNFGGFRDPGSTLFVKTRANE
AT5G24080-1	401	GEMCLSDCKCVASVYGLDDEKPYCWILKSLNFGGFRDPGSTLFVKTRANE
AT5G24080-2	401	GEMCLSDCKCVASVYGLDDEKPYCWILKSLNFGGFRDPGSTLFVKTRANE
AT5G24080-3	401	GEMCLSDCKCVASVYGLDDEKPYCWILKSLNFGGFRDPGSTLFVKTRANE
AT5G24080	451	SYPSNSNNNDKSRKSHGLRQKVLVPIVVVGMVLVALLGMLLYYNLDRK
AT5G24080-1	451	SYPSNSNNNDKSRKSHGLRQKVLVPIVVVGMVLVALLGMLLYYNLDRK
AT5G24080-2	451	SYPSNSNNNDKSRKSHGLRQKVLVPIVVVGMVLVALLGMLLYYNLDRK
AT5G24080-3	451	SYPSNSNNNDKSRKSHGLRQKVLVPIVVVGMVLVALLGMLLYYNLDRK
AT5G24080	501	RTLKRAAKNSLILCDSPVSFYRDLQNCTNNSQLLGGSGGFVTYKGTVA
AT5G24080-1	501	RTLKRAAKNSLILCDSPVSFYRDLQNCTNNSQLLGGSGGFVTYKGTVA
AT5G24080-2	501	RTLKRAAKNSLILCDSPVSFYRDLQNCTNNSQLLGGSGGFVTYKGTVA
AT5G24080-3	501	RTLKRAAKNSLILCDSPVSFYRDLQNCTNNSQLLGGSGGFVTYKGTVA
AT5G24080	551	GETLVAVKRLDRALSHGEREFITEVNTIGSMHHMNLVRLCGYCSEDSHRL
AT5G24080-1	551	GETLVAVKRLDRALSHGEREFITEVNTIGSMHHMNLVRLCGYCSEDSHRL
AT5G24080-2	551	GETLVAVKRLDRALSHGEREFITEVNTIGSMHHMNLVRLCGYCSEDSHRL
AT5G24080-3	551	GETLVAVKRLDRALSHGEREFITEVNTIGSMHHMNLVRLCGYCSEDSHRL
AT5G24080	601	LVYEYMINGSLDKWIFSSSQTANLLDWRTRFEIAVATAQGIAYPHEQCRN
AT5G24080-1	601	LVYEYMINGSLDKWIFSSSQTANLLDWRTRFEIAVATAQGIAYPHEQCRN
AT5G24080-2	601	LVYEYMINGSLDKWIFSSSQTANLLDWRTRFEIAVATAQGIAYPHEQCRN
AT5G24080-3	601	LVYEYMINGSLDKWIFSSSQTANLLDWRTRFEIAVATAQGIAYPHEQCRN
AT5G24080	651	RIIHCDIKPENILLDDNFCPKVSDPFLAKMMGREHSHVVTMIRGTRGYLA
AT5G24080-1	651	RIIHCDIKPENILLDDNFCPKVSDPFLAKMMGREHSHVVTMIRGTRGYLA
AT5G24080-2	651	RIIHCDIKPENILLDDNFCPKVSDPFLAKMMGREHSHVVTMIRGTRGYLA
AT5G24080-3	651	RIIHCDIKPENILLDDNFCPKVSDPFLAKMMGREHSHVVTMIRGTRGYLA
AT5G24080	701	PEWVSNRPI TVKADVSYGMLLLEIVGGRRNLDMSYDAEDFFYPGWAYKE
AT5G24080-1	701	PEWVSNRPI TVKADVSYGMLLLEIVGGRRNLDMSYDAEDFFYPGWAYKE
AT5G24080-2	701	PEWVSNRPI TVKADVSYGMLLLEIVGGRRNLDMSYDAEDFFYPGWAYKE
AT5G24080-3	701	PEWVSNRPI TVKADVSYGMLLLEIVGGRRNLDMSYDAEDFFYPGWAYKE
AT5G24080	751	LTNGTSLKAVDKRLQGVAE EEEVVKALKVAFWCIQDEVSMRPPSMGEVVKL
AT5G24080-1	751	LTNGTSLKAVDKRLQGVAE EEEVVKALKVAFWCIQDEVSMRPPSMGEVVKL
AT5G24080-2	751	LTNGTSLKAVDKRLQGVAE EEEVVKALKVAFWCIQDEVSMRPPSMGEVVKL
AT5G24080-3	751	LTNGTSLKAVDKRLQGVAE EEEVVKALKVAFWCIQDEVSMRPPSMGEVVKL
AT5G24080	801	LEGTSD E INLPPMPQTILELIEEGLEDVYRAMRREFNNQLS SLTVNTITT
AT5G24080-1	801	LEGTSD E INLPPMPQTILELIEEGLEDVYRAMRREFNNQLS SLTVNTITT
AT5G24080-2	801	LEGTSD E INLPPMPQTILELIEEGLEDVYRAMRREFNNQLS SLTVNTITT
AT5G24080-3	801	LEGTSD E INLPPMPQTILELIEEGLEDVYRAMRREFNNQLS SLTVNTITT
AT5G24080	851	SQSYRSSSRSHATCSYSSMSPR
AT5G24080-1	851	SQSYOTLIV
AT5G24080-2	851	SQSYOTLIV
AT5G24080-3	851	SQSYOTLIV

Figure S9. Amino acid sequence alignment of *At5g24080* wild-type, *at5g24080-1*, *at5g24080-2* and *at5g24080-3* Open Reading Frames (ORF). The N-terminal signal peptide is marked in purple, the bulb-type lectin domain is shown in turquoise, S-locus glycoprotein domain in dark green, the PAN-like domain in grey, transmembrane domain is depicted in orange and the serine/threonine protein kinase domain in yellow. Sequences resulting from the T-DNA insertion in *At5g24080-1*, *At5g24080-2* and *At5g24080-3* as determined experimentally by Sanger sequencing of homozygous mutants are underlined in red. Moreover, the introduced premature stops are highlighted red. N-terminal signal peptide prediction was carried out using SignalP 4.1 (Petersen *et al.*, 2011). The bulb-type lectin domain, S-locus glycoprotein domain, PAN-like domain as well as the serine/threonine protein kinase domain were predicted by PROSITE release 20.16 (Sigrist *et al.*, 2013). Prediction of the transmembrane domain was carried out using DAS-TMfilter (Cserzö *et al.*, 2002). The alignment was produced in using the CLUSTAL W algorithm (Thompson *et al.*, 1994).

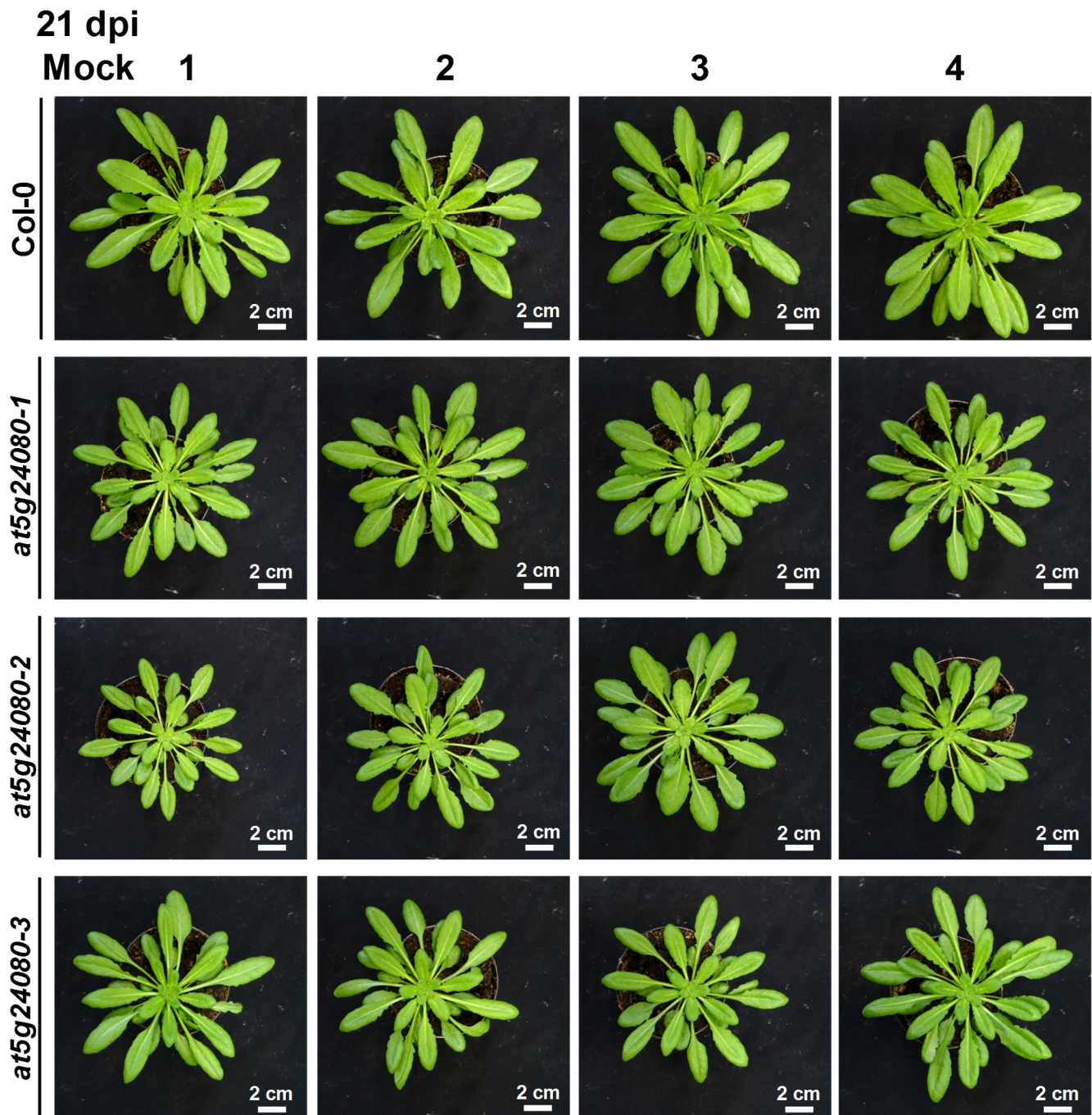


Figure S10. Phenotypes of *A. thaliana* Col-0 wild-type and *at5g24080* mutants 21 days after mock treatment. Four representative plants per genotype are shown.

21 dpi

c-VL43

1

2

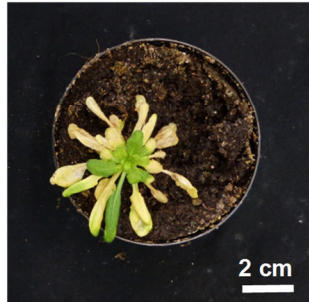
3

4

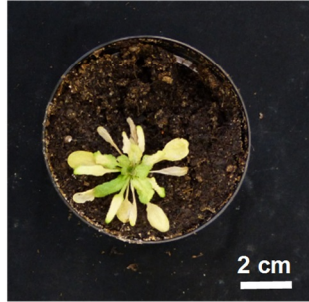
Col-0



at5g24080-1



at5g24080-2



at5g24080-3

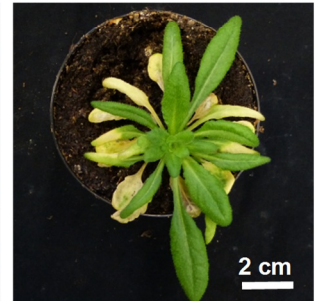
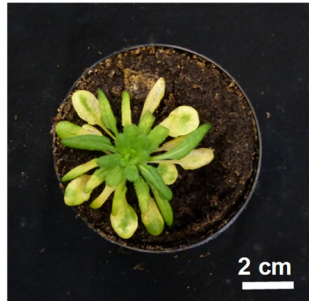


Figure S11. Disease phenotypes of *A. thaliana* Col-0 wild-type and *at5g24080* mutants 21 days post infection (dpi) with the chlorosis-inducing *V. longisporum* isolate c-VL43. Four representative plants per genotype are shown.

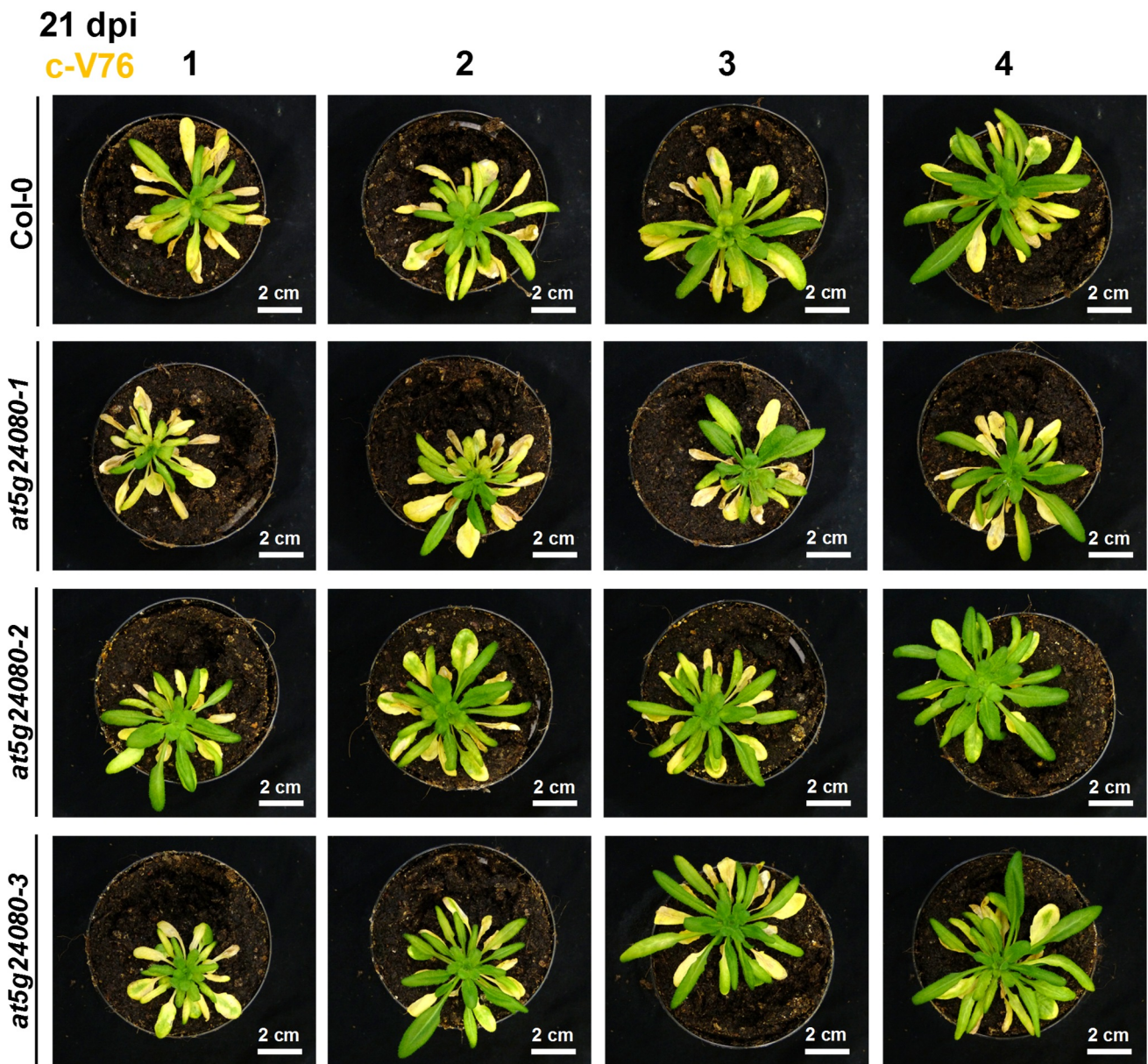


Figure S12. Disease phenotypes of *A. thaliana* Col-0 wild-type and *at5g24080* mutants 21 days post infection (dpi) with the chlorosis-inducing *V. dahliae* isolate c-V76. Four representative plants per genotype are shown.

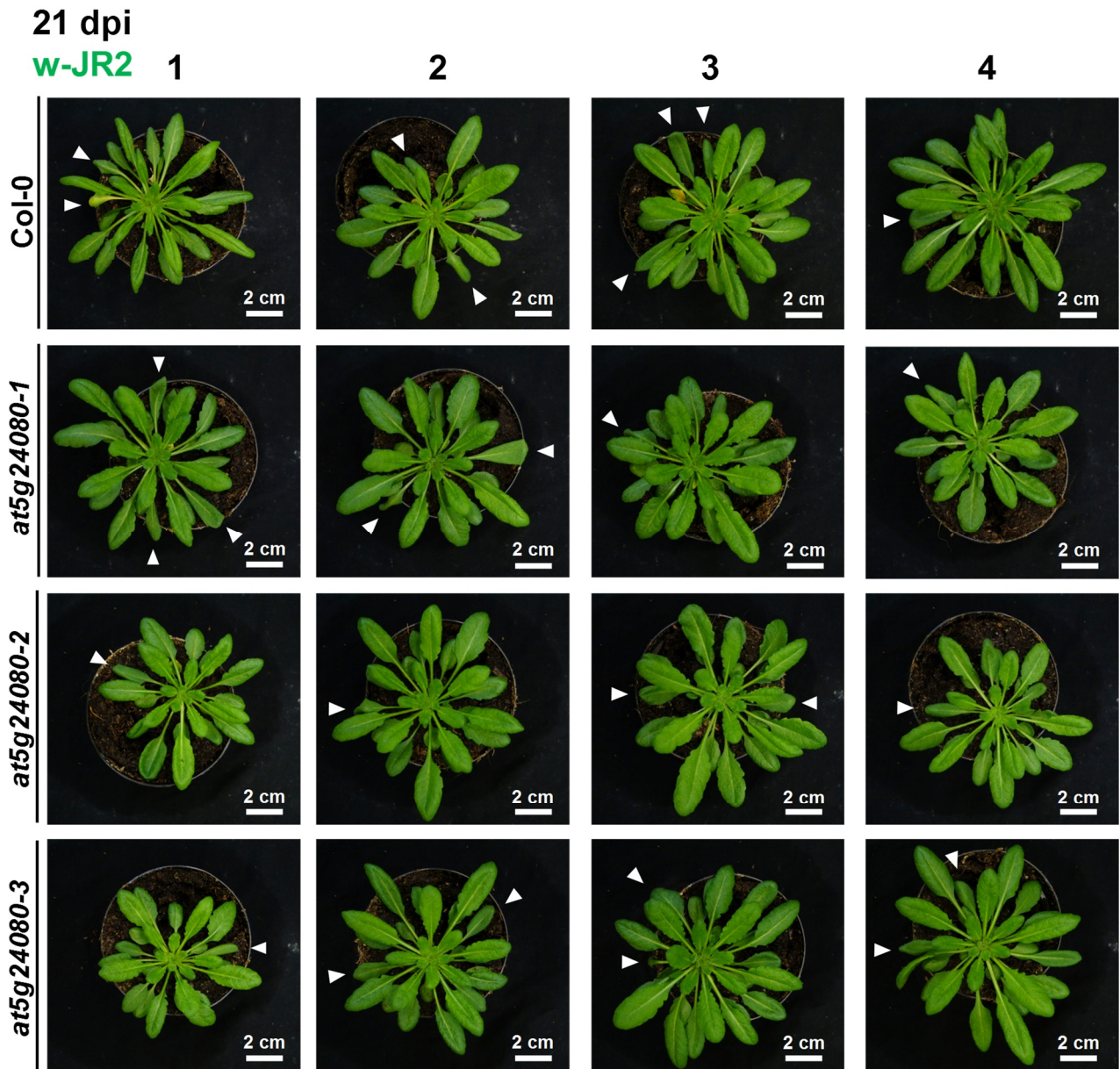


Figure S13. Disease phenotypes of *A. thaliana* Col-0 wild-type and *at5g24080* mutants 21 days post infection (dpi) with the wilting-inducing *V. dahliae* isolate w-JR2. Four representative plants per genotype are shown. Arrowheads indicate wilting leaves.

Table S10. Top 50 *At5g24080* co-regulated genes according to ATTED II *Arabidopsis thaliana* microarray database (Ath-m version c6.0). Co-regulon analysis was performed using the ATTED II web interface version 8.0 (<http://atted.jp>, Aoki *et al.*, 2016). Expression data after 10 μ M ABA treatment was retrieved using the TRABAS web interface (Choudhury and Lahiri, 2008) as log₂ fold change in expression from the ME00333 microarray dataset. *At5g24080* is included (top row).

At gene ID	Description	Significantly regulated by chlorosis isolates	10 μ M ABA		
			30 min	1 h	3 h
<i>At5g24080</i>	LecRLK	yes	-0.8	0.1	3.3
<i>At1g52690</i>	LEA7	no	-1.5	0.6	6.0
<i>At2g47770</i>	TSPO	no	-1.2	0.5	5.2
<i>At3g02480</i>	LEA	no	-1.2	0.0	5.1
<i>At3g17520</i>	LEA	no	-0.9	-0.8	5.0
<i>At5g06760</i>	LEA4-5	no	-0.8	0.9	4.8
<i>At5g52300</i>	RD29B	no	-0.7	-0.7	4.2
<i>At5g59220</i>	SAG113	no	-0.6	2.0	4.2
<i>At2g41190</i>	transporter	no	-1.0	0.4	4.1
<i>At1g07430</i>	HAI2	no	-1.0	1.0	4.1
<i>At2g37870</i>	inhibitor	no	-0.7	-0.5	4.0
<i>At4g33905</i>	Mpv17/PMP22	no	-0.9	0.1	3.9
<i>At2g47780</i>	REF	no	-0.9	1.0	3.9
<i>At1g49450</i>	Transducin/WD40 repeat-like	no	-0.3	1.4	3.8
<i>At3g05640</i>	Protein phosphatase 2C	no	-0.9	-0.1	3.8
<i>At2g29380</i>	HAI3	no	-0.7	-0.1	3.5
<i>At3g55090</i>	ABCG16	no	-0.8	0.5	3.5
<i>At1g69260</i>	AFP1	no	-0.1	1.7	3.4
<i>At3g29575</i>	AFP3	no	-0.2	1.4	3.3
<i>At1g60190</i>	PUB19	no	0.0	1.5	3.3
<i>At5g11110</i>	SPSA2	no	-0.3	1.7	3.2
<i>At5g57050</i>	ABI2	no	-0.1	1.8	3.1
<i>At4g05100</i>	MYB74	no	-0.3	1.5	3.1
<i>At5g05220</i>	unknown protein	no	-0.7	-0.4	2.9
<i>At1g69480</i>	ERD1/XPR1/SYG1	no	-0.5	-0.2	2.9
<i>At5g15190</i>	unknown protein	no	-0.5	0.1	2.8
<i>At1g05100</i>	MAPKKK18	no	-0.5	0.8	2.7
<i>At1g24600</i>	unknown protein	no	-0.4	0.2	2.7
<i>At3g48510</i>	unknown protein	no	-0.4	0.1	2.5
<i>At5g04250</i>	Cysteineases	no	-0.5	0.2	2.5
<i>At1g19970</i>	ER lumen retaining receptor	no	-0.4	0.0	2.4
<i>At4g28110</i>	MYB41	yes	-0.3	1.0	2.4
<i>At3g11410</i>	PP2CA	no	0.7	1.5	2.2
<i>At1g80110</i>	PP2-B11	no	-0.2	0.6	2.1
<i>At2g45570</i>	CYP76C2	no	-0.4	-0.5	2.0
<i>At4g21440</i>	MYB102	yes	-0.4	-0.2	2.0
<i>At5g53710</i>	unknown protein	no	-0.2	-0.2	1.5
<i>At3g57540</i>	Remorin	no	0.1	1.2	1.5
<i>At2g34610</i>	unknown protein	no	0.0	0.3	1.5
<i>At3g63060</i>	EDL3	no	-0.2	0.5	1.4
<i>At5g50360</i>	unknown protein	no	-0.2	-0.2	1.3
<i>At2g32510</i>	MAPKKK17	no	-0.1	0.4	1.1
<i>At1g64380</i>	DNA-binding	no	-0.2	0.8	1.0
<i>At1g79900</i>	BAC2	no	-0.1	-0.3	1.0
<i>At3g02940</i>	MYB107	no	-0.1	-0.1	0.9
<i>At1g66830</i>	kinase	no	0.0	0.0	0.5
<i>At4g37990</i>	ELI3-2	no	-0.1	-0.1	0.3
<i>At3g61450</i>	SYP73	no	0.0	-0.1	0.3
<i>At2g33080</i>	RLP28	no	0.1	-0.1	0.1
<i>At2g20880</i>	ERF53	yes	0.1	0.6	0.1
<i>At4g28140</i>	DNA-binding	no	0.2	0.0	-0.1

Table S11. Top 50 *At5g24080* co-regulated genes according to ATTED II *Arabidopsis thaliana* RNAseq database (Ath-r version c2.0). Co-regulon analysis was performed using the ATTED II web interface version 8.0 (<http://atted.jp>, Aoki *et al.*, 2016). Expression data after 10 μ M ABA treatment was retrieved using the TRABAS web interface (Choudhury and Lahiri, 2008) as log₂ fold change in expression from the ME00333 microarray dataset. *At5g24080* is included (top row).

At gene ID	Description	Significantly regulated by chlorosis isolates	10 μ M ABA		
			30 min	1 h	3 h
<i>At5g24080</i>	LecRLK	yes	-0,8	0,1	3,3
<i>At1g52690</i>	LEA7	no	-1,5	0,6	6,0
<i>At3g17520</i>	LEA	no	-0,9	-0,8	5,0
<i>At5g06760</i>	LEA4-5	no	-0,8	0,9	4,8
<i>At5g13170</i>	SWEET15	no	-1,0	-0,5	4,7
<i>At5g59320</i>	LTP3	no	-1,4	-0,4	4,7
<i>At5g52300</i>	RD29B	no	-0,7	-0,7	4,2
<i>At5g59220</i>	SAG113	no	-0,6	2,0	4,2
<i>At2g41190</i>	transporter	no	-1,0	0,4	4,1
<i>At1g07430</i>	HAI2	no	-1,0	1,0	4,1
<i>At4g33905</i>	Mpv17/PMP22	no	-0,9	0,1	3,9
<i>At2g47780</i>	REF	no	-0,9	1,0	3,9
<i>At1g49450</i>	Transducin/WD40 repeat-like	no	-0,3	1,4	3,8
<i>At1g69260</i>	AFP1	no	-0,1	1,7	3,4
<i>At1g60190</i>	PUB19	no	0,0	1,5	3,3
<i>At4g05100</i>	MYB74	no	-0,3	1,5	3,1
<i>At5g05220</i>	unknown protein	no	-0,7	-0,4	2,9
<i>At1g69480</i>	ERD1/XPR1/SYG1	no	-0,5	-0,2	2,9
<i>At1g04220</i>	KCS2	no	-0,8	0,5	2,9
<i>At3g48510</i>	unknown protein	no	-0,4	0,1	2,5
<i>At2g19900</i>	NADP-ME1	no	-0,4	-0,3	2,5
<i>At4g28110</i>	MYB41	no	-0,3	1,0	2,4
<i>At5g61820</i>	unknown protein	no	-0,5	0,9	2,4
<i>At4g24960</i>	HVA22D	no	-0,5	1,1	2,3
<i>At2g17680</i>	DUF241	no	-0,4	-0,3	2,3
<i>At3g11410</i>	PP2CA	no	0,7	1,5	2,2
<i>At5g41040</i>	RWP1	yes	-0,7	0,0	2,2
<i>At4g21440</i>	MYB102	no	-0,4	-0,2	2,0
<i>At5g43840</i>	HSFA6A	no	-0,4	-0,4	1,9
<i>At5g09530</i>	PRP10	no	-0,6	-0,1	1,9
<i>At5g04380</i>	transferase	no	-0,3	-0,3	1,7
<i>At2g23120</i>	Late embryogenesis abundant	no	-0,3	0,5	1,6
<i>At3g30210</i>	MYB121	no	-0,4	-0,2	1,5
<i>At5g53710</i>	unknown protein	no	-0,2	-0,2	1,5
<i>At5g05390</i>	LAC12	no	-0,2	-0,3	1,4
<i>At5g50360</i>	unknown protein	no	-0,2	-0,2	1,3
<i>At5g54300</i>	DUF761	no	-0,2	0,2	1,3
<i>At3g20500</i>	PAP18	no	-0,2	0,0	0,8
<i>At4g27530</i>	unknown protein	no	-0,1	-0,1	0,6
<i>At2g40170</i>	GEA6	no	0,0	-0,1	0,4
<i>At1g50960</i>	GA2OX7	no	-0,2	0,3	0,4
<i>At2g37180</i>	RD28	no	-0,1	0,3	0,2
<i>At1g69470</i>	unknown protein	no	0,0	-0,1	0,0
<i>At2g44810</i>	DAD1	no	-0,1	-0,1	0,0
<i>At5g63350</i>	unknown protein	no	n.a	n.a.	n.a.
<i>At3g62990</i>	unknown protein	no	n.a	n.a.	n.a.
<i>At5g46610</i>	transporter	no	n.a	n.a.	n.a.
<i>At4g01985</i>	unknown protein	no	n.a	n.a.	n.a.
<i>At3g03341</i>	unknown protein	no	n.a	n.a.	n.a.
<i>At5g40790</i>	unknown protein	no	n.a	n.a.	n.a.

not available (n.a.)

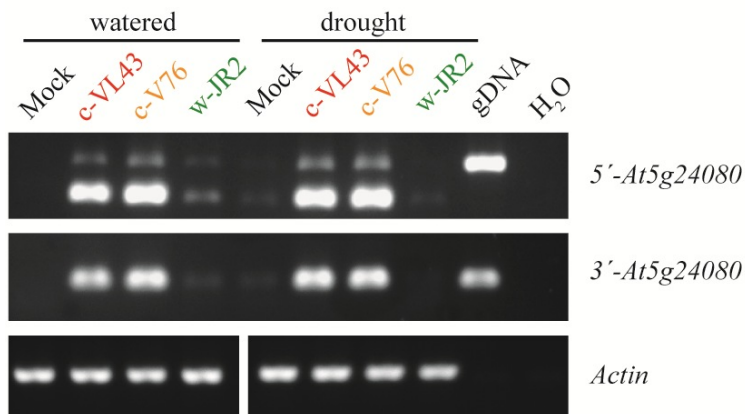
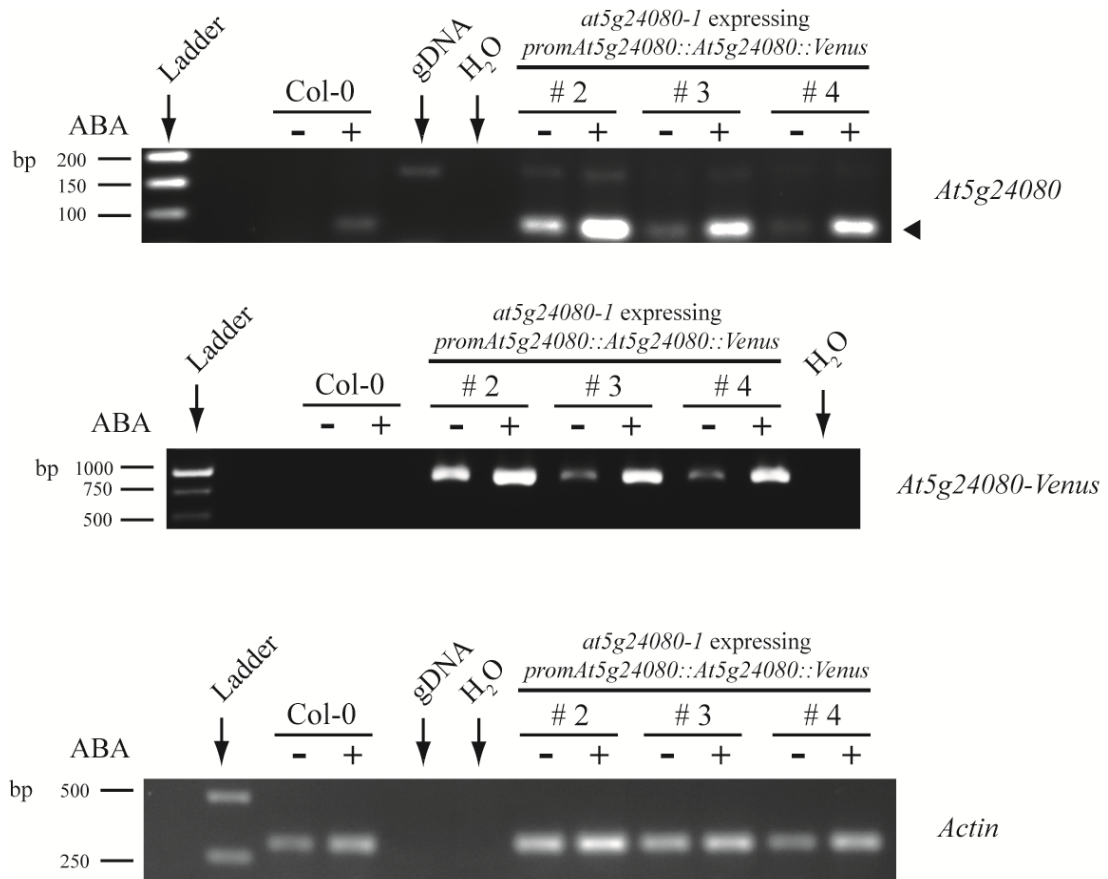


Figure S14. Semi-quantitative RT-PCR analysis of *At5g24080* expression during *V. longisporum* isolate c-VL43 as well as *V. dahliae* c-V76 and w-JR2 infection under normal water supply and drought stress conditions. Pools of 4 rosettes per sample were harvested 36 days post infection (dpi) and subjected to RNA extraction. The housekeeping gene *Actin* was amplified as control. A genomic DNA (gDNA) control was included to monitor potential

contamination by gDNA. A reverse primer which binds two exon borders and spans an intron sequence was used in case of the *Actin* gene to exclude gDNA amplification. The 3'-*At5g24080* primer combination does not span an intron. Consequently, the 3'-*At5g24080* gDNA PCR product size corresponds to the size of the cDNA product. The experiment was performed once.

A



B

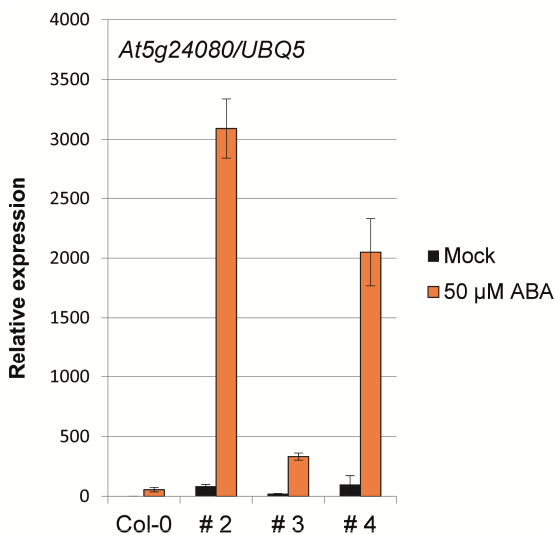
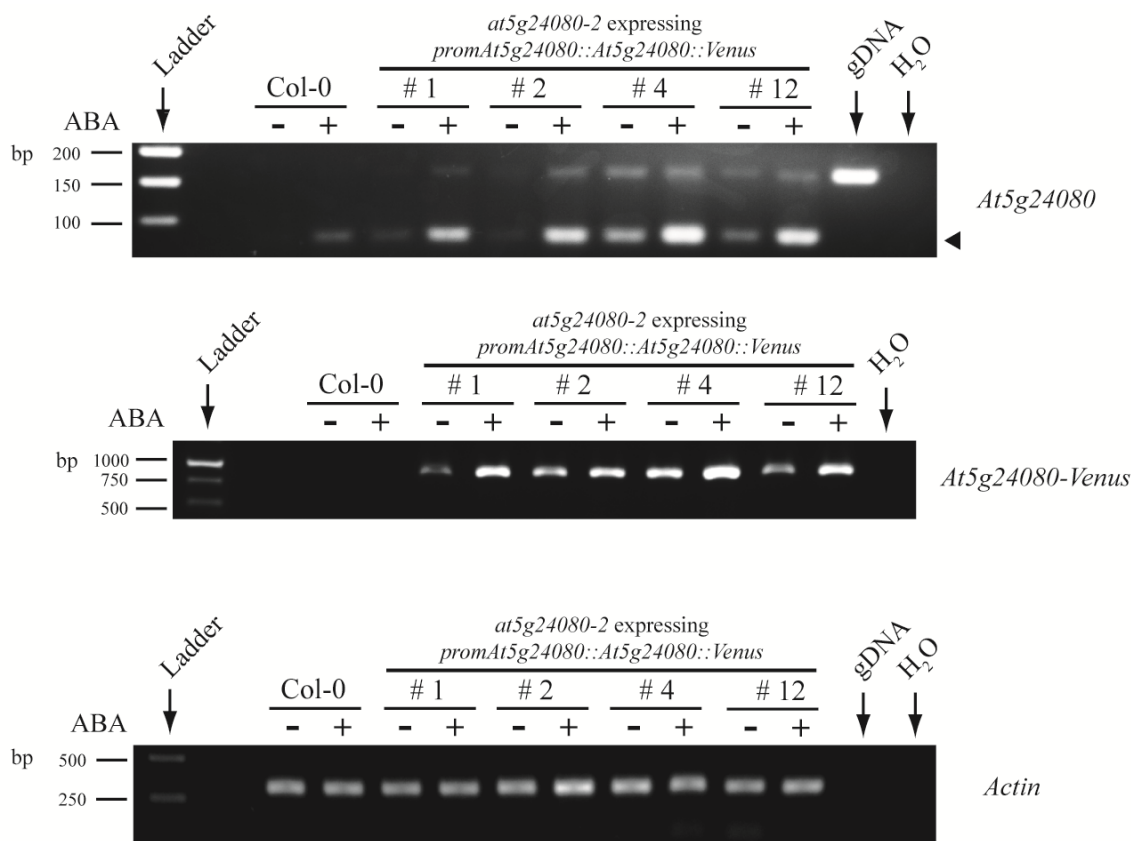


Figure S15. Expression of *At5g24080* in leaf discs of 11-week-old *A. thaliana* Col-0 and transgenic *Arabidopsis thaliana* T₁ lines stably expressing *At5g24080* in the *at5g24080-1* background under the control of its native promoter after treatment with 50 μM ABA overnight. 8 leaf discs per sample were used for RNA extraction. (A) Semi-quantitative RT-PCR analysis of *At5g24080* and *At5g24080-Venus* expression. “+” indicates samples collected from ABA treated leaf discs, whereas “-” represents the mock treated control. The housekeeping gene *Actin* was amplified as control. A genomic DNA (gDNA) control was included in case of *At5g24080* to monitor potential contamination by gDNA. A reverse primer which binds two exon borders and spans an intron sequence was used in case of the *Actin* gene to exclude gDNA amplification. The *Actin* cDNA PCR product

corresponds to 302 bp. Expected sizes of *At5g24080* PCR products are 79 bp cDNA and 161 bp gDNA. Size of *At5g24080-Venus* PCR product is 840 bp. The arrowhead indicates *At5g24080* cDNA bands. (B) qPCR analysis of *At5g24080* expression. 15 ng cDNA were amplified in qPCR. Bars represent mean gene expression ± standard deviation in arbitrary units from 3 technical replicates, normalized to the expression of *UBQ5*. The experiment was performed once.

A



B

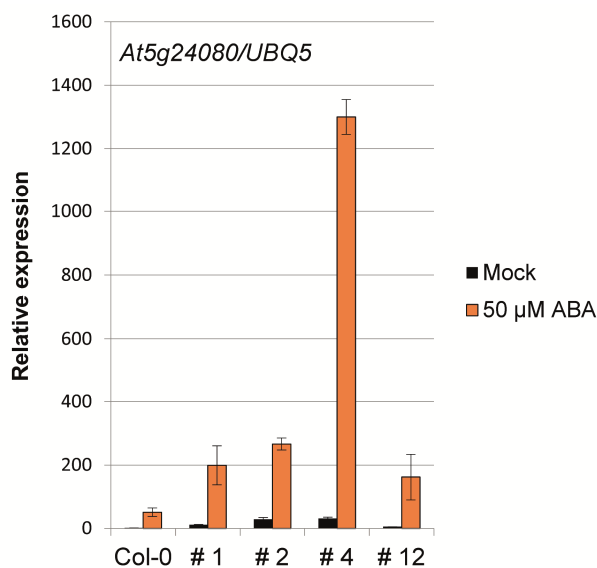


Figure S16. Expression of *At5g24080* in leaf discs of 11-week-old *A. thaliana* Col-0 and transgenic *Arabidopsis thaliana* T₁ lines stably expressing *At5g24080* in the *at5g24080-2* background under the control of its native promoter after treatment with 50 μM ABA overnight. 8 leaf discs per sample were used for RNA extraction. (A) Semi-quantitative RT-PCR analysis of *At5g24080* and *At5g24080-Venus* expression. “+” indicates samples collected from ABA treated leaf discs, whereas “-” represents the mock treated control. The housekeeping gene *Actin* was amplified as control. A genomic DNA (gDNA) control was included in case of *At5g24080* to monitor potential contamination by gDNA. A reverse primer which binds two exon

borders and spans an intron sequence was used in case of the *Actin* gene to exclude gDNA amplification. The *Actin* cDNA PCR product corresponds to 302 bp. Expected sizes of *At5g24080* PCR products are 79 bp cDNA and 161 bp gDNA. Size of *At5g24080-Venus* PCR product is 840 bp. The arrowhead indicates *At5g24080* cDNA bands. (B) qPCR analysis of *At5g24080* expression. 15 ng cDNA were amplified in qPCR. Bars represent mean gene expression ± standard deviation in arbitrary units from 3 technical replicates, normalized to the expression of *UBQ5*. The experiment was performed once

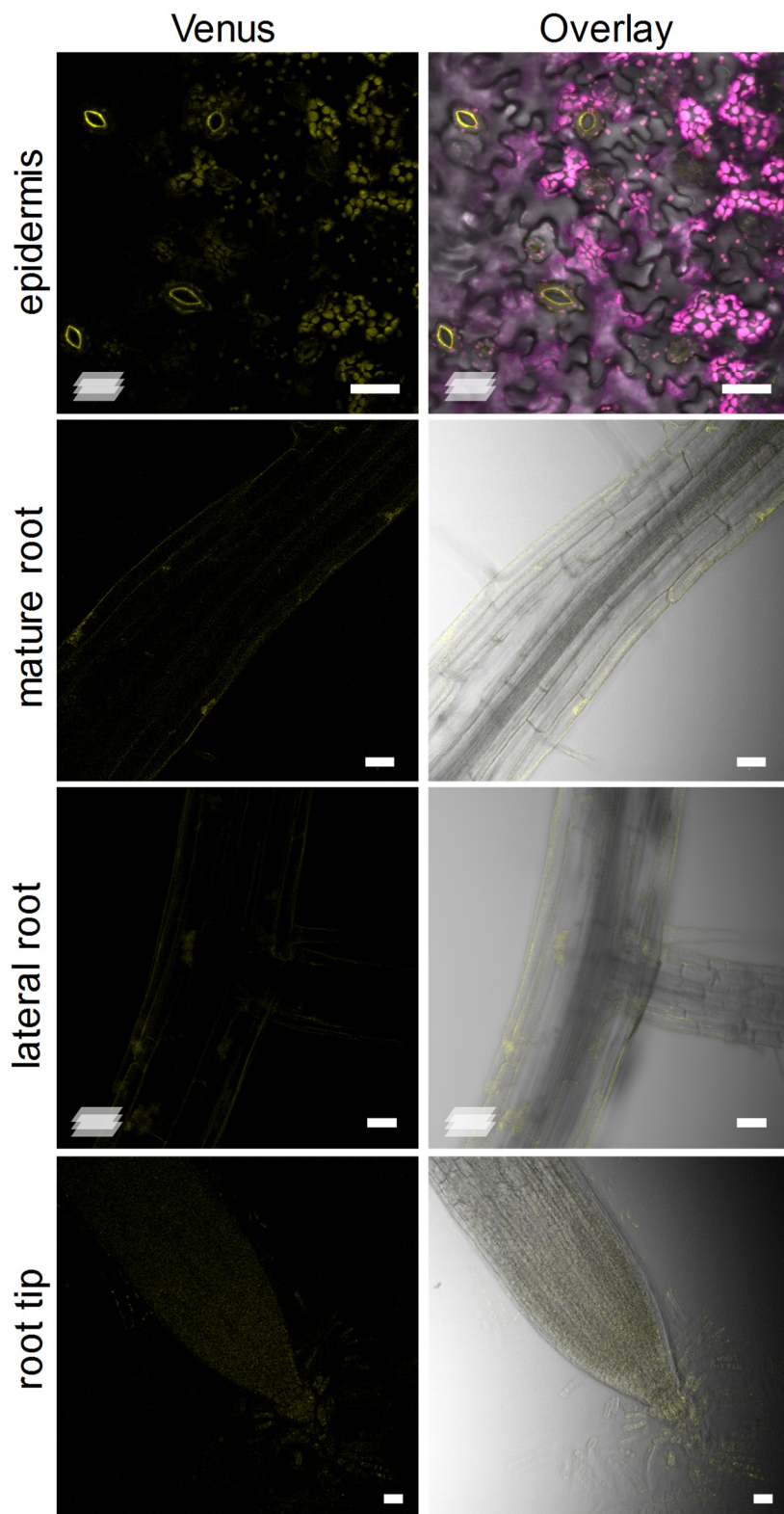


Figure S17. Confocal Laser Scanning Microscopy of 12-day-old *A. thaliana* Col-0 wild-type *in vitro* seedlings as a control for auto-fluorescence in the Venus channel. Images show Venus fluorescence (yellow) as well as overlays of the Venus fluorescence with the chloroplast autofluorescence (magenta) and the bright field channel (grey). Maximum projection images are indicated by a stack symbol in the left lower corner. Scale bar = 30 μ m.

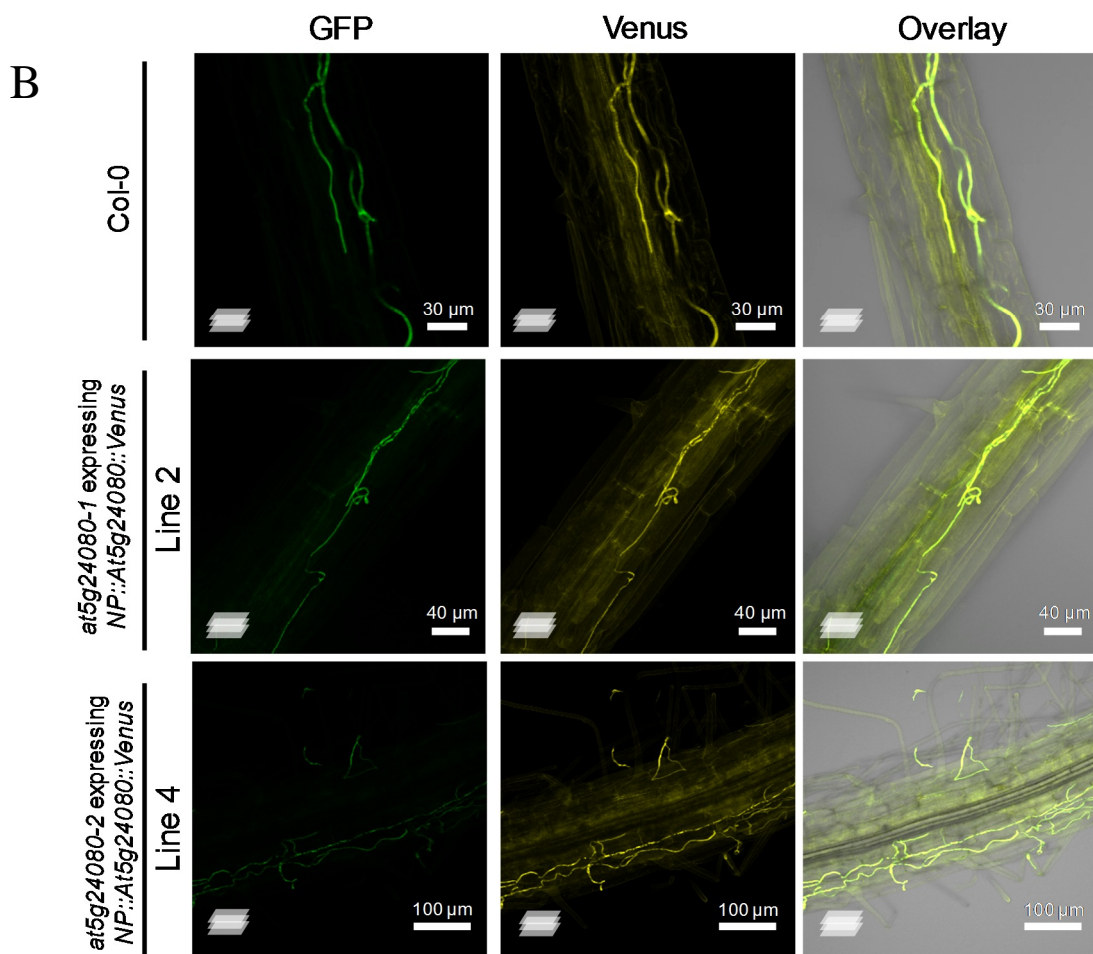
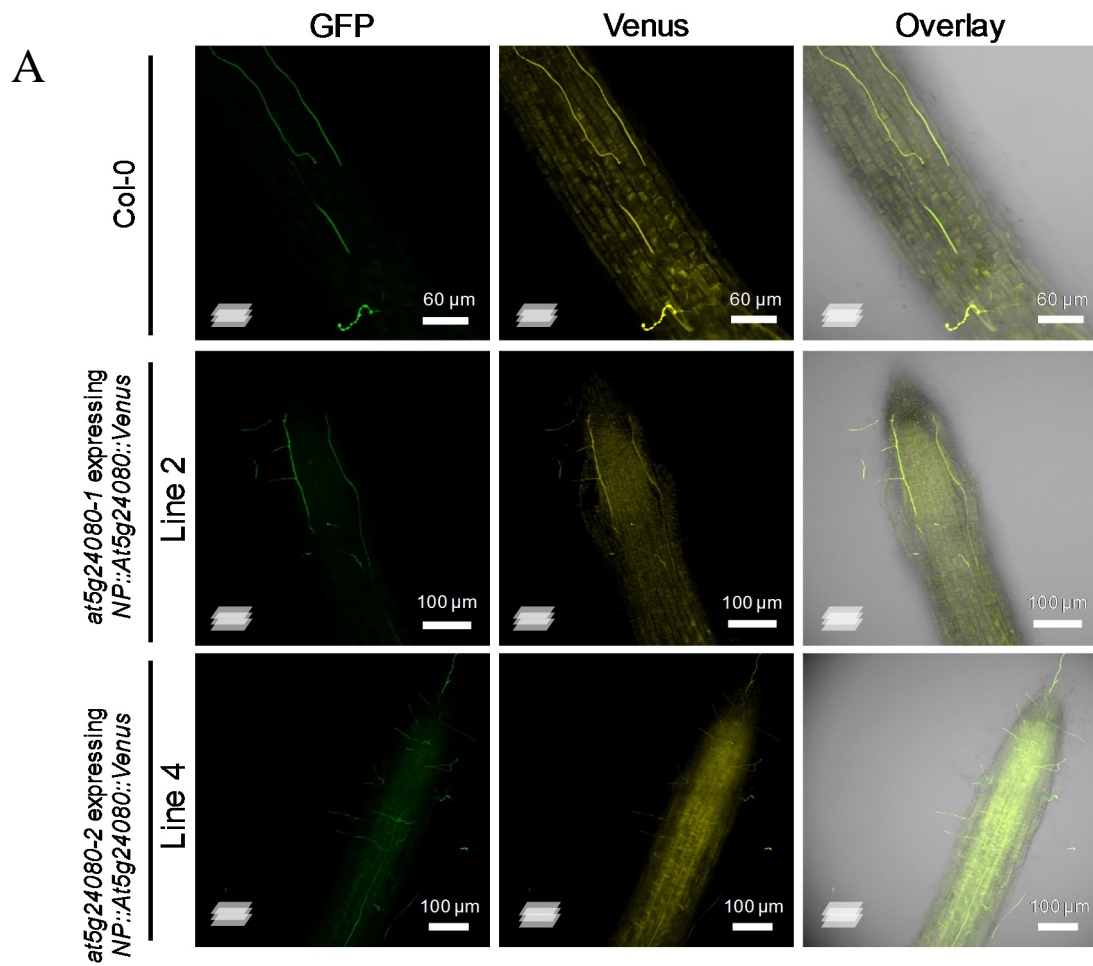


Figure S18. Confocal Laser Scanning Microscopy (CLSM) of independent transgenic *A. thaliana* T₂ lines stably expressing *At5g24080::Venus* under the control of its native promoter after infection with a GFP-tagged *V. longisporum* VL43 line. The root system of 2 ½-week-old *in vitro* grown seedlings was spray inoculated with a spore suspension of $1 \cdot 10^5$ spores per ml and subjected to CLSM at 2 days post infection (dpi). Figure shows maximum projection images of GFP fluorescence, Venus fluorescence (yellow) as well as an overlay of the GFP and Venus fluorescence with the bright field channel (grey). Note that GFP-tagged fungal hyphae are visible in the Venus channel, since the emission spectra of GFP and Venus fluorophores overlap. **(A)** Fungal colonisation of the root tip. **(B)** Fungal growth in the mature root. NP: prom*At5g24080*.



Figure S19. Disease phenotypes of *A. thaliana aba1-101* 21 days post infection (dpi) with the *V. dahliae* isolate c-V76.

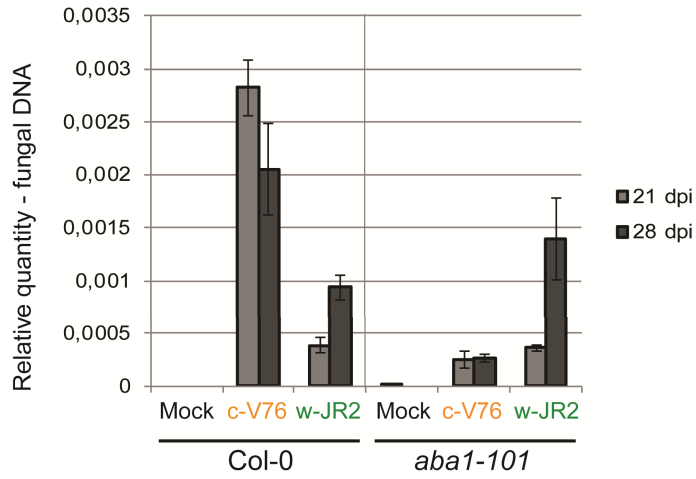
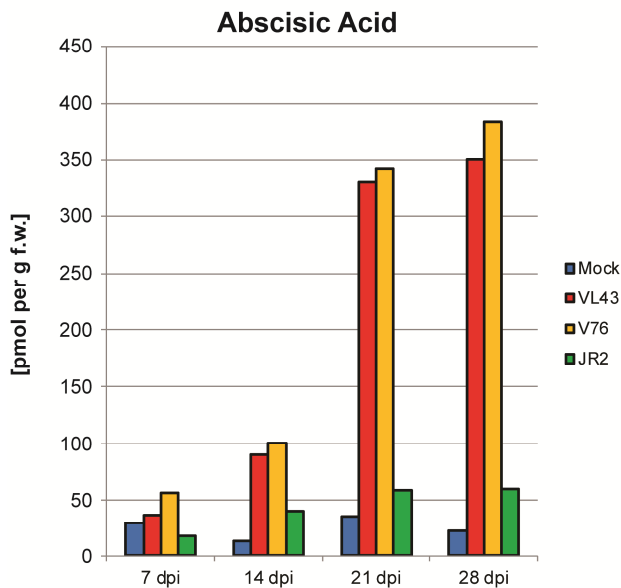


Figure S20. Proliferation of *V. dahliae* isolate c-V76 and w-JR2 in *A. thaliana* Col-0 wild-type and *aba1-101* ABA biosynthesis mutant. Results of an independent repetition of the infection experiment presented in Fig. 33 are shown. Pools of 4 plants per sample were used for genomic DNA (gDNA) extraction. Bars represent quantity of *Verticillium beta-Tubulin* \pm standard deviation in arbitrary units from 3 technical replicates, normalized to the expression of *A. thaliana UBG5*.

A



B

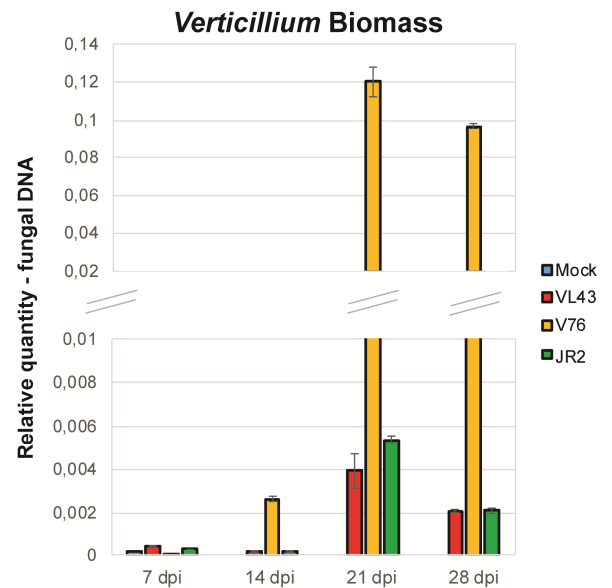


Figure S21. Abscisic Acid (ABA) and fungal biomass content and in *A. thaliana* Col-0 wild-type during *V. longisporum* isolate c-VL43 as well as *V. dahliae* isolate c-V76 and w-JR2 infection. The experiment was repeated with similar results. **(A)** ABA levels in the course of c-VL43, c-V76 and w-JR2 infection. Bars represent ABA content in pmol per g fresh weight (f.w.). Pools of 4 rosettes per sample were subjected to HPLC-MS/MS analysis. **(B)** Proliferation of c-VL43, c-V76 and w-JR2 in course of infection shown in (A). Pools of 4 rosettes per sample were used for genomic DNA (gDNA) extraction. 40 ng gDNA were amplified in qPCR. Bars represent quantity of *Verticillium beta-Tubulin* \pm standard deviation in arbitrary units from 2 technical replicates, normalized to the expression of *A. thaliana UBQ5*.

7. Deposition of transcriptome data

A. thaliana and *N. benthamiana* transcriptome data used in this PhD Thesis was deposited at the Department of Plant Cell Biology, Georg August University Göttingen, Germany. For access please contact PD Dr. Thomas Teichmann (Thomas.Teichmann@biologie.uni-goettingen.de).

Danksagung

Ich bedanke mich bei allen, die mich während der Arbeit an meiner Dissertation begleitet und unterstützt haben.

Zunächst möchte ich mich herzlich bei Prof. Dr. Volker Lipka dafür bedanken, dass er mir die Möglichkeit gegeben hat meine Dissertation in seiner Abteilung anzufertigen. Ferner möchte ich mich für das interessante Thema der Dissertation bedanken und die von ihm gewährte Freiheit Fragestellungen innerhalb des Projekts nach eigenen Vorstellungen zu bearbeiten. Seine konstruktive Kritik und Anregungen während regelmäßiger Besprechungen und Seminare sowie seine Hilfsbereitschaft trugen zum Gelingen von Posterpräsentationen, zahlreicher Vorträge und dieser Dissertation bei. Zudem sorgten die von ihm initiierten, betrieblichen Freizeitaktivitäten für ein positives Arbeitsklima in der Abteilung. Ich möchte mich bei Prof. Dr. Volker Lipka auch für seine Funktion als Erstbetreuer und Referent sowie die Begutachtung dieser Dissertation bedanken.

Ich bedanke mich bei PD Dr. Thomas Teichmann für die Übernahme des Korreferates und seine Funktion als Zweitbetreuer dieser Dissertation. Des Weiteren möchte ich mich bei ihm für viele Anregungen und konstruktive Diskussionen bezüglich meines Projekts bedanken.

Meinen Erst- und Zweitbetreuern sowie Prof. Dr. Gerhard Braus, Prof. Dr. Andrea Polle, Jun.-Prof. Dr. Kai Heimel und Dr. Martin Fulda danke ich für die Bereitschaft die Prüfungskommission dieses Promotionsvorhabens zu bilden.

Ich möchte mich ganz herzlich bei Dr. Marcel Wiermer, Dr. Hassan Ghareeb und Dr. Elena Petutschnig für das Bereitstellen von *Arabidopsis thaliana* Mutanten-Saatgut, Pathogenstämmen und Chemikalien bedanken, sowie ihre Unterstützung beim Erlernen neuer Labormethoden.

Ich danke Karin für ihre Unterstützung und Hilfsbereitschaft, die sie mir am Anfang meiner Dissertation bei fachlichen Fragen sowie Problemen bezüglich der Arbeit mit *Verticillium* und der bioinformatischen Software zur Auswertung der RNA-Sequenzierungsanalyse entgegengebracht hat. Ich bedanke mich auch bei Charlotte, Yvonne, Christopher, Jan und Sabine W., die mir immer eine große Hilfe bei labormethodischen Fragen und Problemen waren.

Des Weiteren danke ich Prof. Dr. Ivo Feußner und Dr. Krzysztof Zienkiewicz für die Bereitschaft die HPLC-MS/MS Analysen durchzuführen und auszuwerten.

Ein weiterer Dank geht an die Gärtnerinnen Feli, Susanne und an Herrn Wedemeyer für das Anfertigen der großen Mengen Erdtöpfe, die während der gesamten Zeit dieser Dissertation verbraucht wurden und auch für ihre Bereitschaft spontane Bestellungen und Sonderwünsche zu erledigen. Ich bedanke mich auch bei Anja und Gabi für das Abfertigen der Bestellungen von Chemikalien und Dingen des Laborbedarfs sowie ihre administrativen Aufgaben.

Ich danke Karin, Sabine L., Leonie, Sina und Mohamed für die gute Atmosphäre in den beiden Laboren und dem Büro und dafür, dass wir auch in schwierigeren Zeiten immer einen Witz auf Lager hatten. Ihnen, aber auch Charlotte, Yvonne und der Kickertruppe danke ich für die kurzweiligen Mittagspausen.

Ein großer Dank geht an unsere technische Angestellte Melanie, die mich gegen Ende meines Promotionsvorhabens bei vielen molekularbiologischen Arbeiten unterstützt hat und dafür auch Überstunden in Kauf genommen hat. Vor allem aber auch danke für die tatkräftige Unterstützung beim Mörsern des zahlreichen Pflanzenmaterials.

Zu guter Letzt möchte ich mich bei meiner Freundin bedanken, die mich über die gesamte Zeit meines Promotionsvorhabens unterstützt und mir für das Gelingen aller Präsentationen und Vorträge die Daumen gedrückt hat.

Lebenslauf

Persönliche Daten

Name: Dimitri Stepanets
Anschrift: Schlagemühlenweg 9
37081 Göttingen
Geburtsdatum/-ort: 12.11.1988 in Shitomir, Ukraine
Nationalität: Deutsch

Studium

08.2014 - Heute
Georg-August-Universität Göttingen,
Promotion

am Albrecht-von-Haller-Institut für Pflanzenwissenschaften,
Abteilung Zellbiologie der Pflanze,
Leitung: Prof. Dr. Volker Lipka

10.2011 - 03.2014
Georg-August-Universität Göttingen,
Masterstudiengang „Microbiology and Biochemistry“
Gesamtnote: 1,3 (mit Auszeichnung)

Masterarbeit mit dem Titel:
„Analysis of the role of *Arabidopsis* Nup107-160 complex
members Nup160, MOS3/Nup96 and Seh1 in resistance to
Botrytis cinerea and in *Agrobacterium*-mediated plant
transformation”

Abteilung Zellbiologie der Pflanze

10.2007 - 04.2011
Georg-August-Universität Göttingen,
Bachelorstudiengang „Biologie“
Gesamtnote: 2,2

Bachelorarbeit mit dem Titel:
„Untersuchungen zum Kern-Zytoplasma Transport während
pflanzlicher Immunantworten und der
Etablierung pilzlicher Pathogenität“

Abteilung Zellbiologie der Pflanze

Schulische Ausbildung

08.2004 - 07.2007

Berufliches Gymnasium Witzenhausen
Fachrichtung: Biologietechnik

Abschluss: Allgemeine Hochschulreife

Praktika und Nebentätigkeiten

11.2013 - 03.2014

Georg-August-Universität Göttingen,
Abteilung Zellbiologie der Pflanze

Studentische Hilfskraft

- § Betreuung einer Bachelor-Abschlussarbeit
- § Vermittlung von Methodenkenntnissen
- § Arbeitspläne erstellen
- § Weiterführung des Masterarbeitsprojekts
- § Präsentation der Ergebnisse

02.2012 - 04.2012,
08.2009,
03.2009 - 04.2009

Alfred Zindel AG, Witzenhausen,

Werkstudent im Qualitätsmanagement

- § Stichprobentest in der Lebensmittelproduktion
- § Mikrobiologische Abklatschtests
- § Wareneingangskontrollen
- § Anfertigung von Artikelspezifikationen
- § Erstellung von Reklamationsstatistiken

06.2006 - 07.2006

Universität Kassel,
Fachbereich Ökologische Agrarwissenschaften,
Praktikum im Fachgebiet Umweltchemie

Sprachkenntnisse

Russisch: Muttersprache

Deutsch: verhandlungssicher

Englisch: fließend (C1-Niveau)

Ukrainisch: sehr gut (B2-Niveau)

Weitere Kenntnisse

MS Office:	Microsoft Word, Excel, PowerPoint
Bildbearbeitung:	Adobe Photoshop und Illustrator
Bioinformatik:	Clone Manager, Geneious, RobiNA
Führerschein:	Klasse B

Referenzen

Prof. Dr. Volker Lipka¹
Abteilungsleiter
Tel. 0551 / 39-177800
E-Mail: Volker.Lipka@biologie.uni-goettingen.de

PD Dr. Thomas Teichmann¹
Forschungsgruppenleiter
Tel. 0551 / 39-177802
E-Mail: Thomas.Teichmann@biologie.uni-goettingen.de

Dr. Marcel Wiermer²
Forschungsgruppenleiter
Tel. 0551 / 39-177846
E-Mail: wiermer@uni-goettingen.de

¹Adresse: Georg-August-Universität Göttingen,
Albrecht-von-Haller-Institut für Pflanzenwissenschaften,
Abteilung Zellbiologie der Pflanze,
Julia-Lermontowa-Weg 3, 37077 Göttingen

²Adresse: Georg-August-Universität Göttingen,
Albrecht-von-Haller-Institut für Pflanzenwissenschaften,
Abteilung Molekularbiologie der Pflanze-Mikroben-Interaktionen,
Julia-Lermontowa-Weg 3, 37077 Göttingen

Göttingen, 8 Februar 2018